Green Fluorescent Protein as a Tool to Study Glut4 Trafficking

By

Lachlan Clive Campbell

Thesis submitted in accordance with the requirements of the University of Glasgow for the degree of Doctor of Philosophy

Research conducted within the Division of Biochemistry and Molecular Biology at Glasgow University

December 1999

ProQuest LLC.
789 East Eisenhower Parkway
P.O. Box 1346
Ann Arbor, MI 48106 – 1346

Abstract

Glut4 is the principal glucose transporter expressed in the peripheral tissues. In response to insulin, Glut4 moves from an intracellular compartment to the plasma membrane in a process called translocation. Once at the cell surface, Glut4 transports glucose across the plasma membrane into the cell and thus regulates whole body glucose homeostasis. At the molecular level we tagged Glut4 with Green Fluorescent Protein (GFP) in order to glean further insight into the translocation process. The native fluorescence of GFP then allowed us to analyse the trafficking of GFP-tagged Glut4 chimeras in real time using confocal microscopy. Glut4-GFP expressed in 3T3-L1 fibroblasts or fully differentiated adipocytes, displayed an intracellular distribution that only partially overlapped with the early endosomal compartment. However, Glut4-GFP constructs that carried mutations in N- and C- terminus targeting motifs were localised to the plasma mebrane. Time lapse confocal analysis revealed the dynamic nature of Glut4-GFP-containing vesicles in the basal state. When Glut4-GFP-expressing adipocytes were treated with insulin, Glut4-GFP translocated to the plasma membrane. Translocation was rapid, analogous to endogenous Glut4 translocation in 3T3-L1 adipocytes. However, upon insulin removal, Glut4-GFP failed to reinternalise. We suggest that this failure to reinternalise, while recycling normally in the basal state, reflects a Glut4-specific reinternalisation mechanism following insulin-stimulated translocation. Glut4-GFP exhibited a similar intracellular distribution when expressed in L6 muscle cells. Nitric oxide (NO) donors stimulate glucose uptake into L6 muscle cells. Using inhibitors of the nitric-oxide signalling pathway and Glut4-GFP we investigated the mechanism by which NO-donors increase glucose transport into L6 cells. Recent research has also implicated ADP-Ribosylation Factors (ARFs) in insulin-stimulated Glut4 trasnlcoation. ARFs are small molecular weight GTPases. By site-directed mutagenesis we endeavoured to change the specificity of the ARF5 and ARF6 isoforms from GTP to XTP. These mutations would allow us to control ARF5/6 function in stable 3T3-L1 cell lines. Our goal is then to analyse the contribution of ARF5 and ARF6 to insulin stimulated Glut4-GFP translocation.

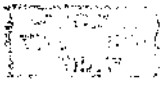

Acknowledgements

I would firstly like to thank my supervisor, Professor Gwyn Gould, for giving me the opportunity to conduct this research and for his support over the past few years. In addition I would like to thank all the members of Lab C36, past and present, for their camaraderie while working in the laboratory. In particular I would like to thank Dr. D. Cope for her help with the molecular biological aspects of this thesis and Dr. K. Powell for her help with the confocal microscope. Finally, I thank the members of Lab C218 for their friendly advice and Dr. E. M. Gibbs for his supervision during the part of my Ph.D. training spent at Pfizer Central Research, Groton, Connecticut.

Table of Contents

Chapter 1

Chapter 2

List of Tables

List of Figures

Chapter 1

1.0.0 Introduction

1.1.0 *Physiological background*

Energy balance is of critical importance to all organisms. Ingested food in the form of carbohydrate, protein or fat is broken down into a usable form for metabolism or is stored for future use. Clearly any imbalance in the organism's ability to control its energy reserves would be detrimental to survival. Therefore sophisticated methods have evolved to fine tune the availability of energy-bearing molecules within the bloodstream.

Carbohydrate forms the bulk of the human diet. Enzymes in the gastro-intestinal tract, amylase and maltase, break down ingested carbohydrate into their constitutive monosaccharides; glucose, fructose and galactose [1]. These sugars are then transported by a distinct class of proteins from the gastro-intestinal tract into the bloodstream. The principal sugar used by multi-cellular organisms to carry chemical energy throughout the body is glucose. Other sugars are metabolised through the glucose pathways. Once glucose is available in the bloodstream the initial step of glucose metabolism is the transport of the hexose across the cell membrane down a normally large concentration gradient from the extracellular fluid into the cell cytoplasm. This process is called facilitated diffusion and is carried out by a family of at least five glucose transport proteins. However, this apparently straight-forward mechanism must fulfill a range of criteria to achieve effective glucose homeostasis.

Basal plasma glucose levels must be held steady at an average concentration of 4.5 mM, typically with a range of 3.4 to 6.5 mM [2]. The brain has an absolute requirement for glucose. If glucose concentrations fall much below these values, central nervous system function is impaired and death may ensue. However, the pool of circulating blood glucose is only sufficient to maintain brain oxidation for three hours, even if all other glucose use ceased [2]. Therefore, in the fasting state the body requires its glucose homestatic mechanisms to mobilise glucose stored as glycogen principally in the liver and skeletal muscle. The whole body control of blood glucose levels is facilitated by coordinated secretion of the pancreatic island hormones insulin and glucagon.

Together, insulin and glucagon play a crucial role in the control of metabolic processes. Secretion of glucagon is coordinated to control the availability of metabolic substrate molecules; free fatty acids, amino acids, glucose, when required for exercise. The dominant effect of glucagon is in the liver. Glucagon binds to its cognate receptor in the plasma membrane of hepatic cells and signal transduction is via a stimulatory G-protein, adenyl cyclase and cAMP as a second messenger. cAMP-activated protein kinase A initiates a cascade of phosphorylations that activates glycogenolysis to release glucose into the bloodstream from glycogen stores. Furthermore, glucagon also activates gluconeogenesis to stimulate glucose synthesis by the hepatic extraction of amino acids [3].

Conversely, insulin coordinates the storage of post-prandial nutrients for future metabolic requirements and in almost all respects the actions of insulin are exactly opposite to those of glucagon [3]. However, insulin does not only antagonise the action of glucagon by promoting glycogen synthesis and inhibiting gluconeogenesis. Insulin also has an effect on glucose disposal into the peripheral tissues, adipose tissue and skeletal muscle. Furthermore, in the long term insulin acts as a growth factor and anabolic agent.

Historically, insulin has long been a biomolecule of interest to research scientists. Insulin was the first hormone isolated from an animal source in a pure enough form to be administered therapeutically, the first protein to be sequenced at the amino acid level and the first protein to have its three dimensional structure solved. It was also the first peptide hormone for which a mechanism of action at the cell membrane was demonstrated and the first protein measured by radioimmunoassay [3]. Finally, and perhaps most importantly, insulin was the first peptide hormone whose biosynthesis was achieved by recombinant DNA technology [4]. The precise mechanism by which insulin exerts its effects on target tissues is currently the area of intense research area around the world by both academic and pharmaceutical laboratories.

There is already a wealth of literature that describes the known actions of insulin in the context of glucose homeostasis [5-7]. The insulin-secreting β cells of the pancreas have their own glucose sensing mechanism that controls the secretion of insulin into the bloodstream. In simple terms, glucose is transported into the islet cell by facilitative diffusion whereupon glucose is phosphorylated by glucokinase to form glucose-6-phosphate. Metabolism of glucose-6-phosphate raises ATP and NAD(P)H levels that in

turn cause potassium channels to close and calcium channels to open. The influx of calcium into the cell then triggers the exocytosis of insulin granules [8]. Once released into the circulation, insulin travels to its target tissues.

1.2.0 *The Glut family of glucose transporters*

As already mentioned, insulin has a profound effect on glucose utilisation by the peripheral tissues as well as the liver. The principal means by which insulin lowers blood glucose is by stimulating glucose uptake into muscle and fat tissue. It has been established that there are at least 5 distinct glucose transporter isoforms representing a family of facilitative glucose transporters expressed by distinct genes. The members of the glucose transporter family, termed the Gluts, have unique patterns of tissue distribution and substrate binding properties (Table 1) that define their role in whole body glucose homeostasis. Glut1 (the erythrocyte-type glucose transporter) was the first glucose transporter to be purified [9]. The isolation of this protein from red blood cell membranes enabled the study of its kinetic parameters and the generation of antibody probes [10-13]. These antibodies together with the partial amino acid sequence of the transporter allowed for the cloning of Glut1 cDNA [14, 15].

The cloning of the Glut1 cDNA was the breakthrough that allowed the identification of the other members of the Glut family. Using low stringency Glut1 cDNA probes Thorens *et al.* were able to isolate Glut2 cDNA from a hepatocyte library [16]. Expression of this transporter isoform in *Xenopus* oocytes allowed further studies of its kinetic properties [17]. Gould *et al.* showed that Glut2 exhibited a supraphysiological K_m for glucose, an observation that fits well with Glut2's physiological requirement to transport glucose out of the hepatocyte following gluconeogenesis.

In an attempt to clone a novel glucose transporter cDNA from skeletal muscle, Kayano *et al.* screened a human foetal muscle library using the low-stringency hybridisation approach [18]. A unique transporter was successfully cloned and called Glut3. However, Northern blot analysis revealed that barely any Glut3 mRNA was detectable in adult skeletal muscle. Instead, Glut3 was very highly expressed in the brain and nerve tissues. Colville *at al.* expressed Glut3 in *Xenopus* oocytes and found that Glut3 has a much lower K_m for glucose than either Glut1 or Glut2. These properties of Glut3 suggest that the brain is able to transport glucose across its plasma membrane

under hypoglycaemic conditions when blood glucose is at a relatively low value and thereby satisfying the brain's high demand for glucose [19].

Following the successes of cloning Glut2 and Glut3 using the low-stringency hybridisation approach, it was hoped that another novel glucose transporter may account for the unique insulin-regulatable transport activity observed in muscle and adipose tissues. The cDNA sequence of Glut4 was soon forthcoming [20-24] and this new isoform was found to be expressed in the muscle, adipose and heart [25]. Insulin stimulation of rat adipose tissue results in an approximate 20-30 fold increase in glucose transport [26]. Furthermore, kinetic analysis reveals that an elevation in the V_{max} for the glucose transport rate is responsible for this increase [27] with no significant effect on the substrate affinity constant K_m. The now widely accepted model by which insulin elicits this effect on glucose transport is by increasing the number of Glut4 molecules at the plasma membrane [28, 29]. Unlike the other glucose transporter isoforms, Glut4 has an intracellular distribution. However, upon insulin binding to its cognate receptor on the plasma membrane, a signalling cascade is triggered within the cell that results in the movement of Glut4 from its basal intracellular location to the plasma membrane, in process called 'translocation' [30]. Glut4 displays a relatively low K_m value for glucose and therefore once recruited to the plasma membrane works near its maximal rate to transport blood glucose into the peripheral tissues [27]. Subsequent to blood glucose normalisation and insulin withdrawl, Glut4 is reinternalised [31-33].

Hexose transport in the small intestine is evidently a prerequisite to glucose availability in the bloodstream. The transport of glucose from the lumen of the gastro-intestinal tract into the epithelial cells is mediated predominantly by the unrelated Na^+-dependent glucose transporter [34]. However, another facilitative glucose transporter, Glut5 was cloned from human small intestine [18]. This apparent anomaly in the normal boundary separating glucose transporter expression between the small intestine and the other tissues was explained when Burant *et al.* demonstrated that Glut5 is in fact a dedicated fructose transporter [35]. Northern blot analysis has since revealed that Glut5 is expressed in a range of tissue, including muscle, adipose and brain [36]. This observation suggests that Glut5 serves to transport dietary fructose across the gastrointestinal tract epithelium and furthermore allows peripheral tissues to metabolise blood fructose.

An outline of the Glut family tissue distribution and kinetic properties is shown in the table below [37].

Isoform	Tissues	K_m (mM) for the non-metabolisable glucose analogue 2-deoxyglucose
Glut1	Placenta; brain; blood-tissue barrier; adipose and muscle tissue (low levels); tissue culture cells; transfromed cells	6.9±1.5
Glut2	Liver; pancreatic β-cell; kidney proximal tubule	11.2±1.1
Glut3	Brain and nerve cells	1.4±0.06
Glut4	Muscle, heart and adipose tissue	4.6±0.3
Glut5	Small intestine; brain, muscle and adipose tissue at low levels	Not Applicable

Table 1 Tissue distribution of the Glut isoforms

1.2.1 *Glucose transporter structure*

Based on their amino acid sequence, all members of the Glut family are predicted to contain twelve membrane spanning amphiphatic helical domains (figure 1.0) [37]. The glucose transporter essentially consists of two "halves", encompassing helices 1-6 and 7-12, a conformation that may have evolved following an ancestral gene duplication event [38]. The two halves are linked by a large intracellular loop. Another large loop is present on the extracellular domain of the transporter between helices 1 and 2 and contains an N-linked glycosylation site. Both the N- and C- terminals of the Gluts are positioned on the cytoplasmic side of the membrane. The intracellular location of the N- and C- termini has been confirmed using antibodies raised against the extreme ends of the Glut1 that react only when the inner surface of the plasma membrane is exposed [39]. The question of which areas or specific amino acids endow particular glucose transporters with their unique properties has been addressed in a number of studies. Injection of glucose transporter mRNA into *Xenopus* oocytes and subsequent kinetic analysis has revealed the importance of a conserved QLS motif in transmembrane helix 7 for substrate specificity [40]. A similar study identified an asparagine residue in helix VIII of Glut3 important for the efficient transport of glucose [41]

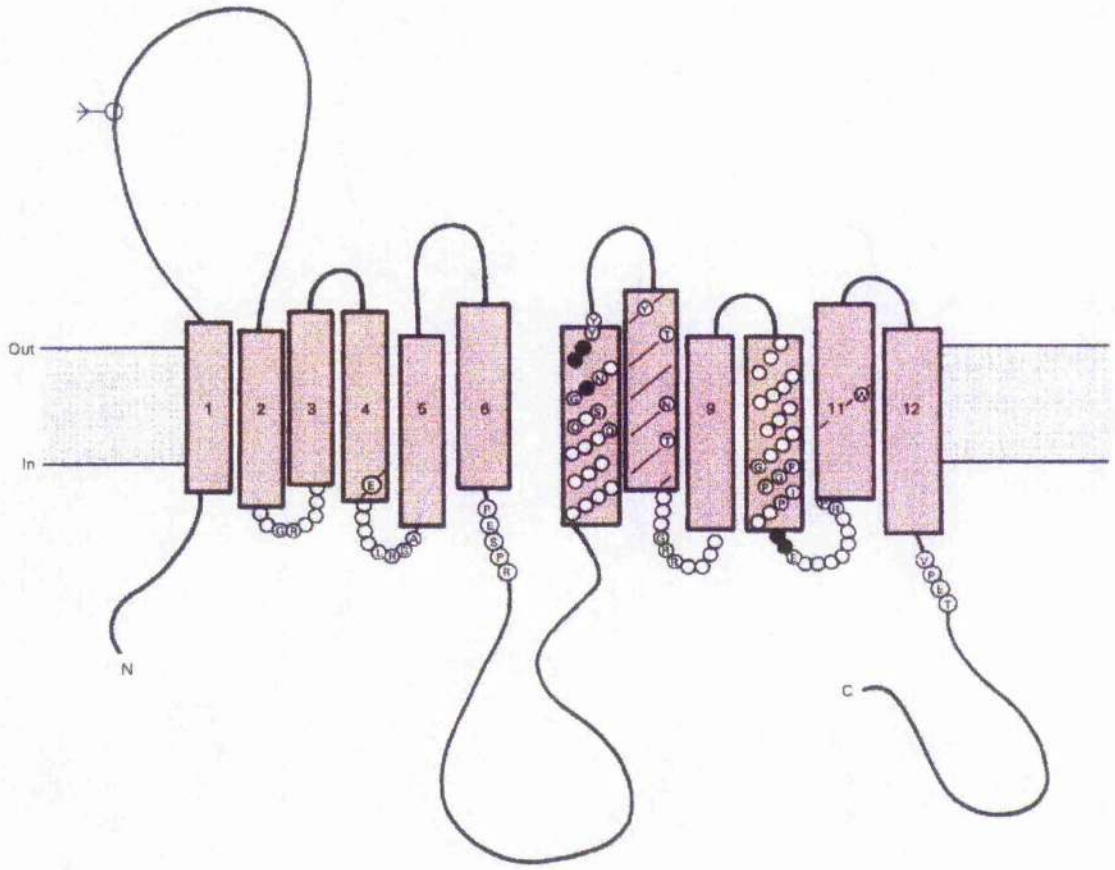

Figure 1.1 Hypothetical model for the structure of the glucose transporters

The protein is predicted to contain 12 transmembrane helices (1-12), with both the N- and C-termini intracellularly disposed. N-linked glycosylation can occur in the extracellular loop between helices 1 and 2 as shown. Conserved amino acids are indicated by the appropriate single-letter code; filled circles indicate conservative substitutions. Note that not all conserved amino acids are shown. (Figure taken with permission from Review Gould, G. W., and Holman, G. D. 1993).

Ligand binding and labeling studies suggest that the glucose transporters have separate internal and external substrate binding sites. For example the photolabel ATB-BMPA is specific for the exofacial site [42] whereas cytochalasin B is specific for the internal binding site [43]. These observations suggest that the glucose transporter is capable of a conformational change in order to transfer a glucose molecule across the membrane. Indeed, a C- terminal truncation of Glut1 when expressed in Chinese Hamster Ovary (CHO) cells locks the transporter into an inward-facing form without transport activity [44]. Similarly, substitution of tyrosine 293 locks Glut1 into an outward-facing

conformation when analysed in CHO cells, as indicated by a reduction in cytochalasin B affinity [45]. These studies emphasise the importance of understanding glucose transporters as dynamic molecules rather than merely simple pores to allow the passage of glucose. As with other membrane proteins, this area of Glut research is hampered by the absence of any 3D crystal. Nevertheless, the detailed and careful studies described shed much light on the nature of facillatative glucose transport.

1.3.0 *Signalling pathways leading to glucose uptake*

1.3.1 *Insulin signalling*

As mentioned previously, insulin stimulates fat and muscle cells to increase their rate of glucose transport principally by recruiting Glut4 to the plasma membrane. Therefore, some mechanism must carry the signal from the insulin receptor to the intracellular Glut4 compartment. The insulin receptor itself is a tetrameric protein composed of two α–subunits and two β–subunits [46, 47]. Furthermore, the insulin receptor is also a tyrosine kinase [48]. Insulin binding to the α–subunit induces a conformational change that stimulates the kinase activity of the β–subunit [49]. The β–subunit in turn catalyses the transfer of a phosphate group onto tyrosine residues within the insulin receptor itself and intracellular substrate proteins [50]. Substrate phosphorylation by the insulin receptor tyrosine kinase appears to involve the binding of phosphorylated receptor tyrosine 960 to phosphotyrosine-binding (PTB) domains of substrate proteins [51]. The substrate proteins of insulin receptor tyrosine kinase include members of the Insulin Receptor Substrate (IRS) family [51]. Phosphorylation of IRS enables the recruitment of signalling proteins through their Src homology 2 (SH2) or PTB domains to phosphotyrosine sites on the insulin receptor/IRS1 complex. These signalling proteins include the p110 subunit of phosphatidyl-inositol 3-kinase (PI3K) that is recruited to the complex via the SH-2 domain of the p85 PI3K regulatory subunit [52]. They also include the phosphotyrosine phosphatase SHPTP2 that has the potential to dephosphorylate IRS and the insulin receptor thus turning off the insulin signal [53]. Also, GRB2 an adaptor protein that links insulin signalling into the Ras pathway [54] and Rho-associated protein serine/threonine kinase ROKα [55] that may alter processes under the control of the small GTPase Rho such as actin assembly and mitogenisis. Clearly with such a complicated array of signalling proteins associated with the insulin

receptor and IRS, there is considerable scope for cross talk between signalling pathways. This complexity makes it difficult to predict the final out come of inhibition of any one of the individual signalling elements. A simplified view of the insulin receptor, IRS and some of the potential downstream effector molecules is shown in the figure below.

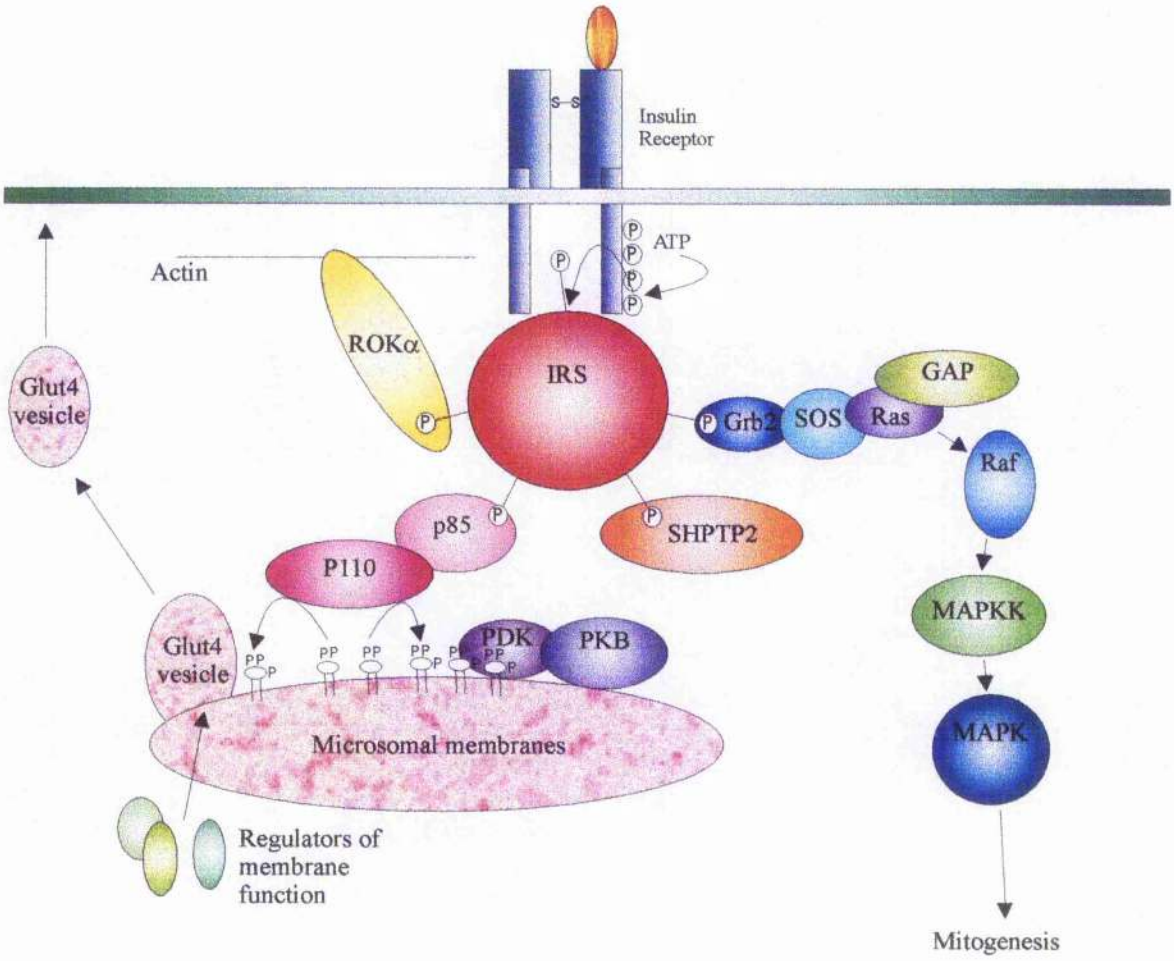

Figure 1.2 Signalling elements downstream of $p21^{ras}$ and phosphatidyl-inositol 3-kinase products regulated by insulin

SOS, Son Of Sevenless (the Ras guanine nucleotide exchange factor); GAP, Ras GTPase activating protein; MAPK, mitogen activated protein kinase: MAPKK, mitogen activated protein kinase kinase; PDK, kinase responsible for phosphorylating Thr308 of PKB; PKB, protein kinase B.

As shown in the figure above, clearly two of the major signalling pathways activated by insulin are the PI3-K and the $p21^{ras}$ cascades. Furthermore, recent research is starting to

establish a link between PI3-K activation and membrane fusion events. Some of these regulators of membrane fusion include ADP-Ribosylation Factors (ARF) [56], the early-endosomal autoantigen (EEA1) [57] and the ARF binding site opener (ARNO) [58] and will be discussed in greater depth later in this chapter.

A great deal of effort has been expended in establishing which particular signalling elements are responsible for the acute phase of the insulin response and Glut4 translocation. Expression of the Raf-1 protein kinase in 3T3-L1 adipocytes has no effect on insulin-stimulated glucose uptake whereas basal uptake is increases 40-fold [59]. In addition, microinjection of oncogenic $p21^{ras}$ into 3T3-L1 adipocytes has no effect on insulin-stimulated Glut4 translocation but does induce c-Fos protein expression, a downstream component of the MAPK mitogenic pathway [60]. These data suggest that the $p21^{ras}$ pathway communicates the long-term mitogenic signal from insulin to transcription factors within the nucleus of the cell.

However, a large amount of data now indicates that PI3-K plays a crucial role in acute phase insulin signalling and Glut4 trabslocation [52]. Specific inhibitors of PI3-K, such as wortmannin and LY29004, completely abrogate the short term actions of insulin [31, 61], as does expression of dominant inhibitory constructs of the p85 regulatory subunit of PI3-K [62]. An analogous experiment whereby a constitutively active form of the catalytic p110 subunit of PI3-K is injected into 3T3-L1 adipocytes demonstrates that expression of p110 is sufficient to cause translocation of Glut4 to the plasma membrane [63]. All of these studies support the hypothesis that the PI3-K rather than the $p21^{ras}$ pathway mediates insulin-stimulated Glut4 translocation. However, more recent data suggests that a further insulin-specific signalling pathway in conjunction with PI3-K activity is necessary to communicate the biological effects of insulin. Jiang *et al.* synthesised a cell-permeable analogue of the PI3-K product $PI(3,4,5)P_3$ that was unable on its own to cause Glut4 translocation in 3T3-L1 adipocytes [64]. However, the PIP_3 analogue was capable of rescuing insulin-stimulated hexose transport into adipocytes pretreated with wortmannin. Such data argues that PI3-K activation is indeed necessary but not sufficient for short-term insulin action. The nature of this additional PI3-K-independent signalling event that contributes to insulin-stimulated glucose uptake in the presence of wortmannin remains unknown.

1.3.2 *Exercise stimulated glucose transport*

Of course glucose uptake into peripheral tissues does not only occur in the post-prandial state. During exercise skeletal muscle requires an increased level of glucose transport influx to fuel the metabolic processes required for ATP generation and muscle contraction. However, it is now known that there are distinct intracellular signalling mechanisms that lead to exercise- and insulin-stimulated glucose transport in skeletal muscle [65]. In skeletal muscle tissue the effects of contraction and insulin on glucose transport are additive, yet only the effect of the latter is blocked by wortmannin [66]. Similarly, insulin but not contraction stimulates the activity PI3-K and the downstream serine/threonine kinases PDK and PKB (figure 1.2) [67].

During exercise, ATP levels decrease within the muscle cell whereas AMP levels increase. The muscle cell uses this high AMP signal to stimulate more glucose uptake via the 5′-AMP-activated protein kinase (AMPK). Rat hind limb contraction but not insulin has been shown to stimulate AMPK activity [68]. The cell permeable 5′-AMP analogue 5-aminoimidazole-4-carboximide ribonucleoside furthermore mimics the effects of contraction by stimulating glucose uptake into skeletal muscle in a wortmannin-insensitive manner [68, 69]. These data indicate that like PI3-K in insulin-stimulated glucose uptake, AMPK may be the key molecular switch mediating exercise-stimulated hexose transport.

The effects of the nitric oxide (NO) signalling pathway on glucose transport in muscle cells has also been keenly investigated over recent years. Nitric oxide stimulates guanylate cyclase to produce cGMP that has three known possible fates within the cell. The cGMP may be broken down by phosphodiesterases, although cGMP is also known to inhibit cAMP-dependent phosphodiesterases, or open a cyclic nucleotide-gated ion channel [70], or stimulate cGMP-dependent protein kinase G (PKG) [71] (figure 1.3).

Contraction-stimulation is known to increase levels of NO from incubated skeletal muscle preparations [72]. However, practical limitations arise when trying to study the effects of muscle contractions and endogenous NO production on cells grown in culture. Therefore NO-donors, such as sodium nitroprusside (SNP), have been widely used to study the effects of an exogenous source of NO on various biological effects [73]. In skeletal muscle SNP is known to stimulate glucose transport and raise intracellular cGMP levels [74]. In agreement with these studies, the nitric oxide synthase inhibitor L-

NAME blocks exercise-stimulated glucose transport in rat skeletal muscle but has no effect on insulin-stimulated glucose transport [75].

Clearly, like AMPK, NO appears to play a crucial part in exercise-stimulated glucose transport separate and removed from the effects of insulin. An intriguing hypothesis is that AMPK and NO are in fact two halves of the same puzzle. One may conjecture that as AMP levels rise within the cell during exercise, AMPK is stimulated, which in turn phosphorylates and activates nitric oxide synthase (NOS), leading to increased cGMP levels and elevated glucose transport through an as yet undefined downstream signalling pathway (figure 1.3). Evidence in support of this hypothesis is provided by a recent study showing that AMPK can phosphorylate and activate cardiac endothelial NO synthase (eNOS) *in vitro* [76].

1.3.3 *G-Protein-coupled signalling pathways and glucose transport*

Adrenergic receptor agonists are also known to have a stimulatory effect on glucose uptake. From a physiological point of view this would make sense since skeletal muscle requires an enhanced supply of glucose to energise a "fight or flight" response. Adrenergic receptor agonists couple to glucose transport via heterotrimeric G-proteins [77], adenylate cyclase activation [78], cAMP production and stimulation of protein kinase A (PKA) activity [79]. The β–adrenergic agonist noradrenaline in both skeletal muscle [80] and 3T3-L1 adipocytes [81] has been shown to increase glucose transport. Furthermore, the effects of insulin and noradrenaline on glucose uptake are additive [82]. This result infers that noradrenaline and insulin stimulate different signalling pathways. In support of this hypothesis the effects of noradrenaline are not inhibited by wortmannin [82]. Clearly, glucose transport is mediated by a number of stimuli providing great potential for cross talk control between different intracellular signalling mechanisms. For example the reported effect of adenosine to potentiate the stimulation by insulin of glucose uptake in brown fat cells from 15- to 30-fold [83]. This evidence does indeed suggest that the G protein-coupled signal triggered by adenosine can regulate the insulin-stimulated pathway.

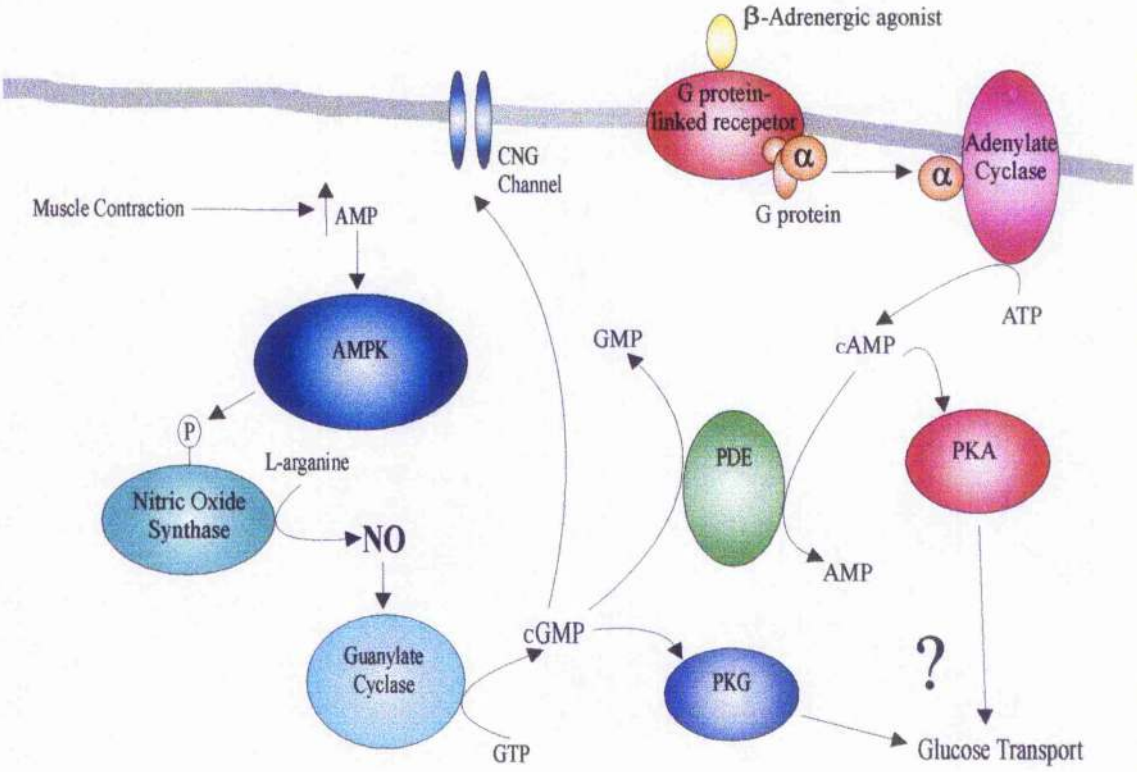

Figure 1.3 Outline of the muscle contraction-, nitric oxide- (NO) and G protein-linked receptor agonist-stimulated glucose transport pathways

AMPK, 5′-AMP-activated protein kinase; PDE, phosphodiesterase; PKG, protein kinase G; PKA, protein kinase A; CNG channel, cyclic nucleotide-gated ion channel.

1.4.0 *Glut4 trafficking*

1.4.1 *Glut4 subcellular distribution*

Almost twenty years have passed since glucose transporter translocation was proposed as the mechanism by which insulin mediates enhanced glucose transport into muscle and adipose tissue [30, 84]. Since then the precise mechanism by which the glucose transporter trafficks to the plasma membrane has proven elusive to researchers. Glut4 is considered to be the key glucose transporter isoform that mediates glucose uptake in

peripheral tissues and is highly expressed in adipose tissue and striated muscle [85], whereas Glut1 is expressed at significantly lower levels in the same tissue [85]. In both the basal and insulin-stimulated state [29, 32, 86] Glut4 slowly recycles between the plasma membrane and one or more intracellular compartments. However, the overwhelming majority of Glut4 resides within intracellular vesicles in the basal state, making the distribution of Glut4 unique amongst the glucose transporter isoforms. Kinetic analysis of Glut4 trafficking has revealed that the increase in Glut4 observed at the plasma membrane in response to insulin is primarily the result of a large increase in the rate of Glut4 vesicle exocytosis and a smaller decrease in the rate of internalisation by endocytosis [86, 87]. PI3-K appears to play a crucial part in Glut4 translocation since treatment of cells with low nanomolar concentrations of wortmannin completely abolishes the recruitment of Glut4 to the cell surface [88, 89]. Furthermore, insulin mediates the targeting of IRS/PI3-K complexes to microsomes with a concomitant rise in PI3-P, PI 3,4-P_2 and PI 3,4,5-P_3 levels within the vesicle membrane. These data are consistent with the hypothesis that that PI3-K is involved in the insulin-regulated movement of Glut4 to the plasma membrane.

The elements downstream of PI3-K in the insulin-stimulated signalling pathways regulating Glut4 translocation are poorly understood. However, the involvement of serine/thronine kinases is suggested by the ability of inhibitors of serine phosphatases to stimulate Glut4 translocation in the presence of wortmannin [88]. This result is supported by the claim that insulin also causes the recruitment of PKB to Glut4-containing vesicles [90] in a wortmannin-dependent manner. In concert with this result, constitutively active PKB results in up-regulation of glucose transport and redistribution of Glut4 to the plasma membrane [91]. To further complicate matters, stable transfection of the protein kinase C isoform PKC-ζ into 3T3-L1 adipocytes also leads to Glut4 translocation [92]. Whether such studies truly reflect a complicated serine/threonine kinase cascade downstream of PI3-K *in vivo*, or merely represent an artifact of kinase overexpression remains to be seen.

It is well established that integral membrane proteins traffic to and from the plasma membrane through an endosomal recycling membrane system [93]. Immunoelectron microscopy has revealed that Glut4 is distributed to a number of different classes of intracellular vesicles. To date the consensus of research suggests that the majority of intracellular Glut4 protein is localised to small vesicles and

tubulovesicular structures throughout the cytosol, with relatively smaller amounts associated with the endosomal system and the *trans* Golgi network (TGN) [94-96]. Each of these intracellular organelles represent complex, discontinuous membrane structures. Therefore, differentiating between these structures even at the resolution afforded by the electron microscope is difficult. Nevertheless, several observations suggest that a large fraction of the Glut4 population resides within a unique Glut4 storage compartment separate from the other elements of the constitutive recycling pathway. For example, internalisation of transferrin conjugated to horse-radish peroxidase in adipocytes and its subsequent ablation using diamino benzidine chemistry has shown that endosomal recycling proteins such as the transferrin receptor and Glut1 can be specifically ablated whereas a large fraction of Glut4 cannot in 3T3-L1 adipocytes [97, 98].

Using immunofluorescence and immunoelectron microscopy, Ralston *et al.* examined the distribution of Glut4 in skeletal myotubes [99]. In this study the researchers used a panel of antibodies as markers of the Golgi complex, of the TGN, and of early and late endosomes to define the position of these subcellular compartments relative to Glut4. They observed segregation of Glut4 and TfR both by immunofluorescence and by immunogold electron microscopy. By immunofluorescence alone Glut4 was found primarily around the nuclei, in a pattern suggesting an association with the Golgi complex. Similarly, immunoelectron microscopy showed that most of the Glut4 was associated with Golgi complexes. To test that Glut4 was indeed localised to the TGN the researchers treated the cells with the fungal metabolite Brefeldin A (BfA) that causes the Golgi complex, the endosomes and the TGN to disperse. However, in Bfa-treated cells Glut4 no longer colocalised with the TGN marker TGN38. Therefore, they were forced to conclude that if Glut4 is stored in the TGN in muscle myotubes, it must be a subcompartment that does not contain TGN38. Alternatively, the Glut4 storage compartment represents a population of vesicles geographically close to yet separate from the TGN. This latter suggestion is supported by immunofluorescence analysis of 3T3-L1 adipocytes where no colocalisation between Glut4 and TGN38 is observed [100]. Moreover, in the same study, no TGN38 was detected in immunoabsorbed Glut4-containing vesicles when immunoblotted with a TGN-38 specific antiserum. In the analogous experiment with immunoabsorbed TGN-38-containing vesicles, only 5-10% of the total low-density membrane Glut4 colocalised with TGN-38.

Together, these data paint a complex picture of Glut4 distribution with subpopulations of Glut4 colocalising with various markers of the endosomal system or TGN to greater or lesser extents. However, none of the subcellular markers described previously fully mimic the distribution of the intracellular Glut4 pool. Nevertheless, there appears to be other proteins that do share a considerable degree of colocalisation with Glut4. Unlike the transferrin receptor endosomal marker or TGN38 the TGN marker, the v-SNARE Vesicle Associated Membrane Protein 2 (VAMP2) colocalises with Glut4 [97]. Another protein, the aminopeptidase vp165 (IRAP) has also been found to colocalise identically with Glut4 in adipocytes and cardiomyocytes [101]. Although the exact biological function of vp165 is as yet unknown, injection of 3T3-L1 adipocytes with a GST-IRAP or a fusion protein containing only 28 amino acids from IRAP was as effective as 100 nM insulin in increasing cell surface Glut4 when analysed by immunofluorescence [102]. These observations therefore suggest the presence of a distinct vesicle population enriched in VAMP2 and Glut4. This unique compartment may account for the ability of insulin to stimulate 2-4-fold plasma membrane increases of recycling proteins, for example Glut1 and transferrin receptor, whereas plasma membrane Glut4 content can increase 10-20 fold [86].

1.4.2 *Glut4 trafficking and the SNARE hypothesis*

From studies in the mammalian synapse, it has been revealed that the membrane proteins referred to as v-SNAREs, located in transport vesicles, bind to t-SNAREs located in the target membrane [103]. The high affinity and specificity of this interaction ensures that transport vesicles dock and fuse with their correct target membrane. The SNARE hypothesis thereby proposes that for all membrane trafficking events, a high-affinity match between a ligand in a transport/secretory vesicle (v-SNARE) and a receptor in the target membrane (t-SNARE) would be required to complete a docking and fusion reaction [93].

The v-SNARE Vesicle-Associated Membrane Protein 2 (VAMP2) is expressed in adipocytes [104]. This was a significant finding because like the mammalian synapse, adipocytes also possess a regulated secretory system that translocates Glut4 to the plasma membrane. Unlike the transferrin receptor endosomal marker or TGN38 the TGN marker, VAMP2 colocalises with Glut4 and translocates to the plasma membrane in response to insulin [97]. It was subsequently shown that adipocytes also express an additional v-SNARE called cellubrevin that, based on subcellular fractionation, also

appears to colocalise with Glut4 in adipocytes [105]. However, the use of the transferrin-conjugated horseradish peroxidase endosome ablation technique proposed a more specific role for VAMP2 in Glut4 trafficking than cellubrevin [97]. Whereas the majority of cellubrevin was targeted to endosomes, a large fraction of VAMP2 was targeted to the Glut4 storage compartment [97].

More recently several other studies have implicated a role for VAMP2 in Glut4 translocation. Vaccinia virus-mediated expression of the cytoplasmic domain of VAMP2 in adipocytes or the introduction of VAMP2-GST fusion proteins into permabilised adipocytes results in the inhibition of insulin-stimulated Glut4 translocation [106, 107]. Likewise, introduction of the cytoplasmic domain of syntaxin 4, the VAMP2 t-SNARE, also resulted in an inhibition of insulin-stimulated Glut4 but not Glut1 translocation to the plasma membrane [106]. Finally, microinjection of tetanus toxin and botulinum D toxin which cleave members of the VAMP family block insulin-stimulated Glut4 translocation in 3T3-L1 adipocytes [108]. In combination these data suggest a model whereby VAMP2 is a constituent of Glut4-containing vesicles and regulates the insulin-induced fusion of these vesicles to the plasma membrane during translocation. On the other hand, cellubrevin, classified as an endosomal v-SNARE in previous studies [109], only colocalises with the fraction of Glut4 that is distributed to the recycling endosomes, and mediates the constitutive endosomal trafficking of Glut4 [110].

We have already mentioned that Syntaxin 4 is a likely t-SNARE for VAMP2 [106]. Using the technique of Far Western blotting, membrane fractions from 3T3-L1 adipocytes have been probed with the cytosolic portion of VAMP2 fused to GST [111]. Two plasma membrane-enriched proteins were specifically labeled with this probe, identified as Syntaxin 4 and Syndet, a murine homologue of a previously described t-SNARE SNAP-25. These proteins were further shown to form an SDS resistant ternary complex and microinjection of anti-Syndet antibodies into 3T3-L1 adipocytes inhibited insulin-stimulated Glut4 translocation by 40% [111]. A model now begins to take shape in which Syntaxin 4/Syndet form the t-SNARE for VAMP2 that provides the specificity for insulin-induced fusion of Glut4-containing vesicles with the plasma membrane. However, until recently the accessory molecules that presumably must be required to control this fusion event remained unidentified.

In the case of synaptic transmission there are several modulators of v- and t-SNARE interactions, in particular the Munc18 proteins [112]. The Munc18a isoform is

predominantly expressed in neurons where it inhibits the association of v-SNARES VAMP1 and SNAP25 with the t-SNARE syntaxin 1 [113]. However, Tellman *et al.* successfully isolated three distinct Munc18 isoforms from a 3T3-L1 adipocytes cDNA library by screening with a rat brain Munc18 DNA probe [114]. Munc18a, previously identified in neuronal tissue, and two novel isoforms, Munc18b and Munc18c were cloned from the adipocytes cDNA library.

To continue the analogy between synaptic vesicles, the role of Munc18c in insulin-stimulated Glut4 translocation in 3T3-L1 adipocytes was examined [112]. Using yeast two-hybrid analyses, Munc18c was shown to specifically compete for VAMP2 binding to syntaxin 4 and plasma membrane lawn assays revealed that over expression of FLAG epitope tagged Munc18c in 3T3-L1 adipocytes inhibited insulin-stimulated translocation of Glut4 [112]. Furthermore, Munc18c was transfected into Chinese Hamster Ovary (CHO) cells to examine its function as a regulatory target of insulin signal transduction [112]. Although CHO cells are not a *bonafide* insulin-responsive cell line, they were used in this experiment since these cells contain very low endogenous levels of Munc18. Immunoprecipitation of endogenous syntaxin 4 demonstrated the co-immunoprecipitation of the expressed FLAG-Munc18c protein. However, insulin stimulation resulted in a decreased amount of FLAG-Munc18c that was co-immunoprecipitated with syntaxin 4. Hence, this data suggests that Munc18 inhibits the interaction between VAMP2 and syntaxin 4 in the basal state by binding tightly to the latter protein at the plasma membrane. Insulin then relieves this inhibition by inducing the dissociation of Munc18c from syntaxin 4.

In addition to v-SNAREs and t-SNAREs, multiple membrane fusion events involving the Golgi, endoplasmic reticulum and plasma membrane depend on the *N*-ethylmaleimide-sensitive factor (NSF) [115]. Although NSF is widely recognised as an essential factor in multiple transport events this protein's exact function is still unknown. However, membrane association of NSF does require the accessory proteins termed α–, β–, and γ–SNAPs (soluble NSF attachment proteins) [93]. *In vitro* biochemical studies have demonstrated that NSF, SNAPs and SNAREs form a 20 S complex that is proposed to function in vesicle fusion [103]. However, to form a stable 20 S particle, a nonhydrolysable analogue of ATP, for example ATPγS is required. NSF has an intrinsic ATPase activity that in the presence of ATP results in the disassembly of the 20 S complex into its constitutive parts [103]. Interpretation of this finding is

difficult, however it seems likely that the hydrolysis of ATP by NSF causes a conformational change in the SNARE proteins that plays some part in the vesicle fusion sequence of events. Furthermore, such *in vitro* studies using recombinant proteins may force interactions not that are not replicated *in vivo*. More recent studies have in fact placed the function of NSF earlier in the sequence of vesicle fusion events before vesicle docking [115-117]. If this scenario proves the same in Glut4-containing vesicles, then NSF and α–SNAP would function to prime v- and t-SNAREs into a docking competent state (figure 1.4).

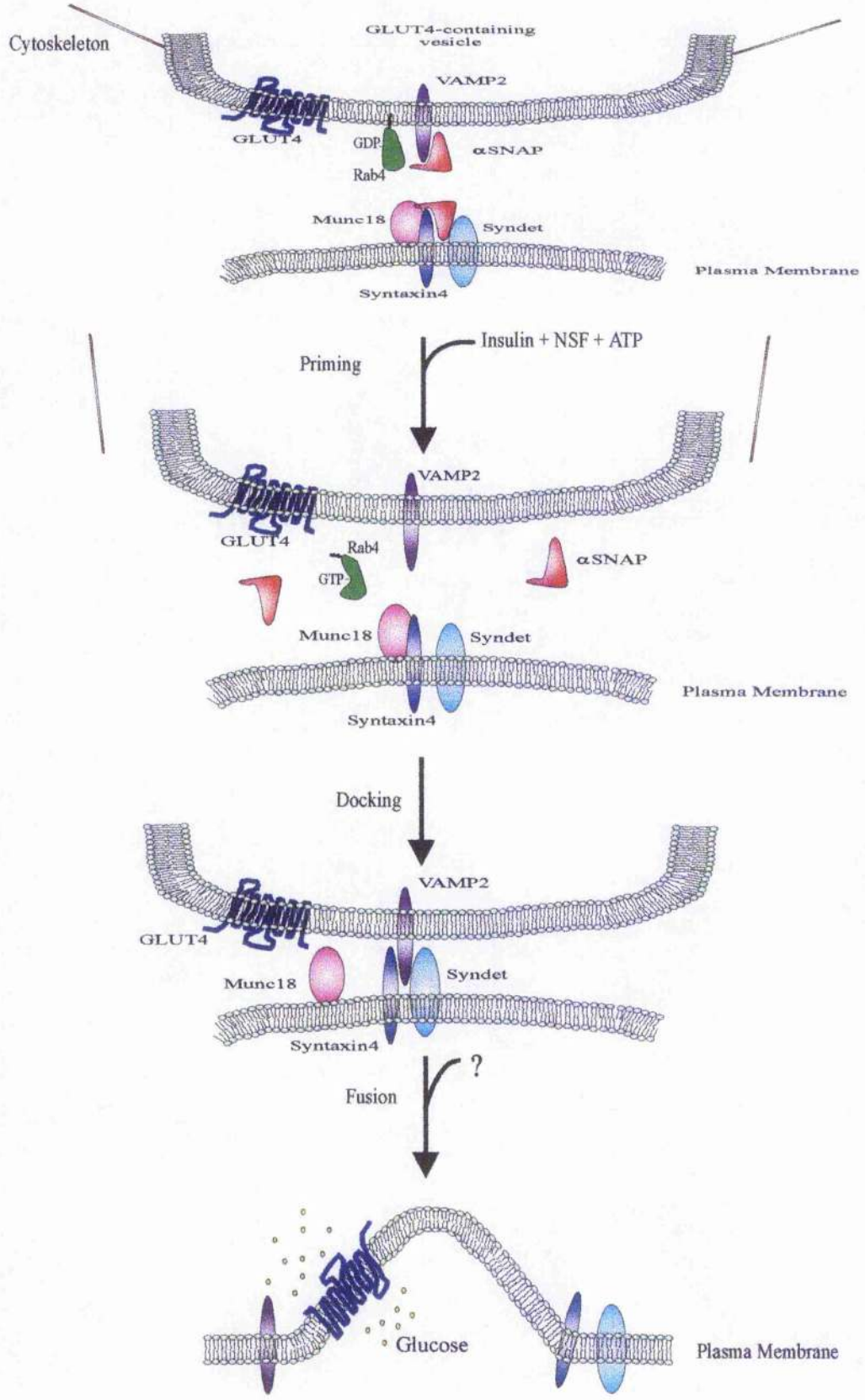

Figure 1.4 Sequence of events involving the SNARE proteins that function in Glut4 trafficking

1.4.3 *The role of small molecular weight GTPases in Glut4 trafficking*

The Rab family of small GTP-binding proteins is also known to play an important role in vesicle trafficking. To date more than 30 different Rab proteins have been identified with each one specialised towards a particular membrane fusion event [118]. By analogy with research examining the trafficking of membrane proteins to the yeast vacuole, Rab proteins are thought to catalyse the membrane fusion event subsequent to SNARE priming by NSF and α–SNAP [117]. Rab 4 was proposed to play a specific role in insulin sensitive cells when it was discovered that Rab 4 colocalises with the Glut4-enriched membrane fraction and with vesicles immunopurified with an anti-Glut4 antibody in 3T3-L1 adipocytes [119]. After insulin treatment, a 50% decrease in the Rab4 content of the low density microsomal fraction was observed, concomitantly with a departure of Glut4 to the plasma membrane. Insulin redistributed Rab4 to the cytosol and its movement was reversed by insulin withdrawl. It therefore appears that Rab4 cycles between the cytosol and Glut4-containing vesicles depending upon the presence or absence of insulin respectively. In a more recent study, a synthetic peptide corresponding to the Rab 4 hypervariable carboxyl-terminal domain was successfully transferred into rat adipocytes by electroporation and inhibited insulin-stimulated glucose transport by 50% without affecting the basal transport activity [120]. The researchers also showed that the exocytotic recruitment of Glut4 by insulin to the plasma membrane was inhibited by the Rab4 peptide. Another study by Shibata *et al.* showed that insulin stimulated the binding of a radiolabeled non-hydrolysable GTP analogue [^{35}S]GTPγS to Rab4 in a wortmannin-dependent manner [121]. Furthermore, dissociation of Rab4 from microsomes to the cytosol was also inhibited by wortmannin. This result suggests that insulin stimulates the guanine nucleotide exchange on Rab4 via a PI3-K-dependent signalling pathway. The accepted interpretation of this data is that Rab4 is therefore an essential component of the translocation machinery (figure 1.5).

1.4.4 *The possible role of "velcro factors" and guanine nucleotide exchange proteins in Glut4 vesicle fusion*

The pieces of the molecular jigsaw that link signalling via PI3-K and membrane fusion events mediated by SNAREs were discovered only recently. The PI3-K product PI(3)P binds the early-endosomal autoantigen (EEA1) through a FYVE finger domain within

the protein, in the context of the early endosomal membrane [57]. This interaction is inhibited by wortmannin such that endosome fusion no longer can take place [57]. Crucially, this interaction is stabilised by the presence of GTP-bound Rab5 since EEA1 contains two GTP-Rab5 binding sites, at the N- and C- termini [57]. Therefore, EEA1 is hypothesised to function as a 'velcro factor' in the initial docking between endosomal membranes, by virtue of the dual interaction of its C-terminus with PI3P and Rab5 and of its N-terminus with Rab 5. EEA1 may also dimerize owing to an extensive coiled-coil domain [93]. This dimerization would allow interaction with PI(3)P at both membranes and perhaps also allow an interaction with SNARE molecules, based on the ability of EEA1 to promote membrane fusion events [57]. To date, other than EEA1, the FYVE finger domain has been identified in the yeast Sec1p family of proteins that interact with SNAREs [93]. It would be of great interest to know if any variants of the FYVE finger domain proteins capable of binding $PI(3,4,5)_3$ are expressed in insulin-responsive cells.

EEA1 is not the only identified 'velcro factor'. Another, Rabaptin-5 that also interacts with Rab5 was identified using a yeast two-hybrid screen [122]. In addition, rabaptin-5 is complexed with Rabex-5 that acts as a rab5 GTP nucleotide-exchange factor (GEF) [123]. But intriguingly, while Rabaptin-5 can interact with Rab5 at its C-terminus, it can also interact with GTP-bound rab4 at a distinct N-terminal site [124]. This presents the tantalising possibility that Rabaptin-5 could act as a molecular linker between rab4, rab5 and a FYVE finger domain protein, possibly mediating an interaction between Glut-4 containing vesicles (Rab4) and the plasma membrane (Rab5) [125] in response to insulin. This, as yet untested link, is outlined in the figure below.

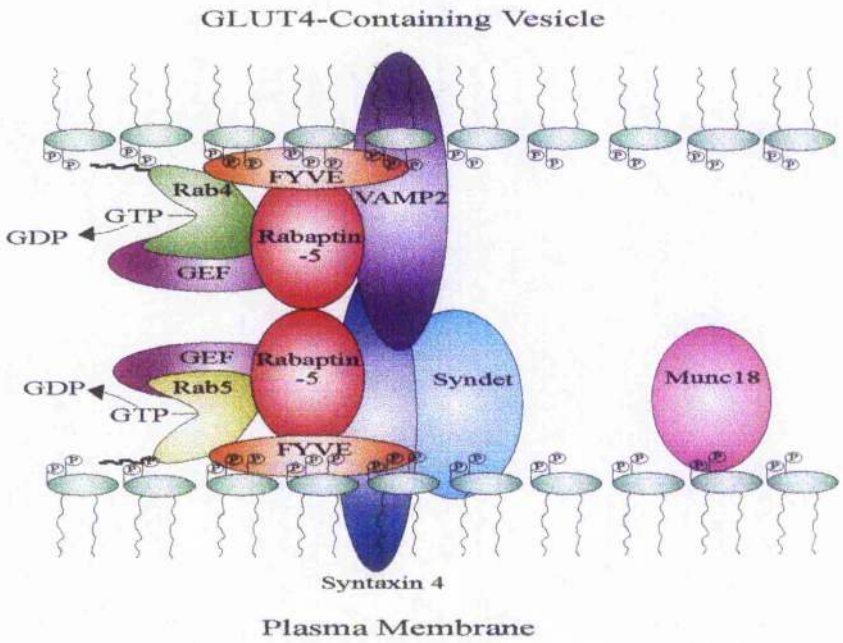

Figure 1.5 Putative transient docking step in the fusion of Glut4-containing vesicles with the plasma membrane

Subsequent to priming by NSF, SNAP, ATP and stimulation of PI3-K activity by insulin, a putative FYVE finger domain-containing protein binds $PI(3,4,5)P_3$ in the membranes. We hypothesise that a FYVE finger protein (for example a yeast Sec1p homologue) could then recruit rabaptin-5 to the complex and acts as an adaptor between Rab4 and Rab5 containing membranes. Rabaptin-5 is also associated with a guanine nucleotide exchange factor (GEF), that catalyses the exchange of GDP for GTP on Rab proteins. The GTP-bound Rabs then stabilise the interactions between $PI(3,4,5)P_3$, the FYVE finger protein, rabaptin-5 and the SNAREs long enough for membrane fusion to occur.

Another class of GEFs that includes GRP1 [126], ARNO [127] and cytohesin-1 [128] contain a pleckstrin homology domain (PH) that has the ability to bind $PI(3,4,5)P_3$ with high affinity. Furthermore, these GEFs also contains a Sec7 domain that catalyses the exchange of GDP for GTP on ADP-Ribosylation Factors (ARFs). The relationship between ARF proteins, small GTPases known to modulate membrane transport events, and Glut4 trafficking is discussed in detail in Chapter 4. However, it is clear that this further class of GEFs that binds directly to PI3-kinase products and regulates guanine nucleotide exchange on ARFs represents another rich vein for prospectors investigating signalling and membrane trafficking.

1.4.5 *Glut4 endocytosis*

So far in this chapter we have only discussed trafficking events that lead to Glut4 exocytosis. The exocytotic arm of Glut4 trafficking is emphasised because kinetic analysis has indicated that insulin increases the rate of Glut4 exocytosis 10-20 fold with only a 2-3-fold decrease in the rate of endocytosis [129]. Whereas PI3-K activity is necessary to increase the rate of Glut4 exocytosis, wortmannin has no effect on the rate of Glut4 endocytosis [130]. Instead, Glut4 endocytosis is mediated by clathrin-coated pits [131]. Electron microscopy of plasma membrane fragments indicates that in the non-stimulated state Glut4 is primarily localised to clathrin lattices. Following insulin treatment, Glut4 labeling of clathrin lattices is only slightly increased, whereas the labeling of uncoated regions is markedly increased [131]. This suggests that Glut4 recycles from the plasma membrane both in the presence and absence of insulin. This interpretation of the data is confirmed by the finding that disruption of clathrin lattices by potassium depletion increases levels of cell surface Glut4 in the basal state [132].

The clathrin-coated vesicles comprise of a clathrin coat linked to the endocytosed membrane protein via a heterotetrameric adaptin complex (AP-2) [93]. A tyrosine-based targeting motif at the N-terminus of Glut4 is suggested to interact with AP-2 [133], providing further evidence that Glut4 recycles from the plasma membrane via clathrin-coated vesicles (CCVs). The initial localisation of AP-2 to the plasma membrane is thought to be provided by interaction with the membrane receptor synaptotagmin 1 [134]. However, the CCVs that bud from the plasma membrane are distinct from those which bud from the TGN and incorporate a different adaptor complex (AP-1) [93].

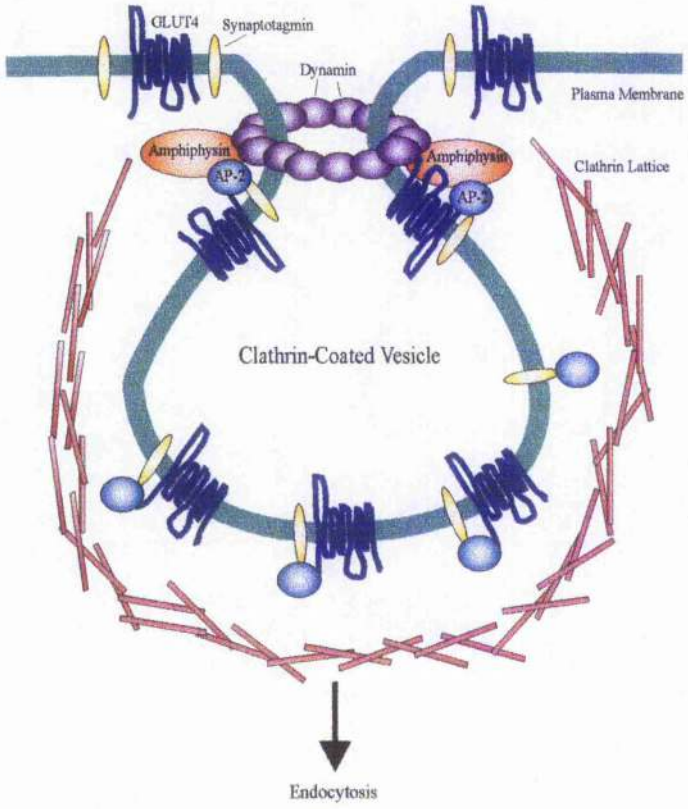

Figure 1.6 The internalisation of Glut4 is thought to occur through a dynamin-dependent mechanism

Subsequent to insulin-stimulated Glut4 translocation, Glut4 accumulates in clathrin-coated invaginations of the plasma membrane. Endocytosis is mediated by interactions between AP-2, synaptotagmin, amphiphysin and the N-terminus of Glut4. Dynamin is recruited to the clathrin-coated vesicle via an interaction with the SH-3 domain of amphiphysin. Insulin may modulate the interaction between dynamin and amphiphysin, thereby inhibiting clathrin-coated vesicle formation and reducing the rate of Glut4 endocytosis from the plasma membrane. Once internalised the vesicles lose their clathrin coat and are then stored at an intracellular site or undergo another round of translocation.

One other essential molecule implicated in CCV formation is the GTPase dynamin [135]. In addition to a GTPase domain, dynamin also contains a pleckstrin homology domain that can interact with inositol phospholipids [136], and a proline rich domain that binds a specific subset of SH3 domain-containing proteins, for example amphiphysin [137]. Furthermore, insulin induces the tyrosine phosphorylation of dynamin [138], providing a possible mechanism whereby insulin causes a two fold reduction in the rate of Glut4 endocytosis [129]. In support of a role for dynamin in endocytosis Al-Hasani *et al.* showed that expression of a GTPase-negative mutant in rat adipose cells increased the amount of cell surface HA-tagged Glut4 in both the basal and insulin-stimulated states. In contrast overexpression of dynamin wild type

decreased the amount of cell surface HA-Glut4 in both the basal and insulin-stimulated states. In addition, microinjection of a dynamin peptide encompassing the amphiphysin binding sites prevents Glut4 endocytosis and results in Glut4 accumulation at the plasma membrane [139]. Amphiphysin is also known to interact with AP-2 [137, 140]. Therefore we can hypothesise that insulin-induced phosphorylation of dynamin may inhibit the interaction between amphiphysin, dynamin and AP-2 hence reducing the rate of Glut4 endocytosis (figure 1.6).

1.5.0 *Transgenic/Knockout mice as new investigative tools*

The emerging field of genetic engineering has allowed researchers to examine the function of individual genes in the context of the whole animal. By introducing null mutations into a particular gene we can then observe the phenotypic consequences. Furthermore, a knockout mouse may expose a molecular redundancy that allows an engineered animal to compensate for the disruption of a particular gene.

Homologous recombination is the most commonly used technique for generating a knockout animal. Following sequence analysis of the gene of interest a targeting vector is designed. This vector contains a selection gene, for example the neomycin phosphotransferase gene (*neo*) flanked by sequence corresponding to the gene of interest. An embryonic stem cell suspension is then microinjected or electroporated with the targeting vector. Once within the nucleus of the stem cells, the targeting vector is designed to take advantage of homologous recombination between the chromosomes during mitosis. With luck, the *neo* gene is then inserted into an exon of the gene to be disrupted. After 5-7 days, the G418-resistant clones are isolated and subjected to screening for homologous recombination by PCR. Clones in which the gene of interest has been successfully targeted are then implanted into the host animal. The phenotypes of the viable embryos are then analysed after birth [141]. The same strategy of homologous recombination can also be used to overexpress the product of a gene. In transgenic mice, a transgene construct with its own promoter will normally be expressed in all tissues where the gene is normally expressed, while it can be targeted to selected tissues by the choice of an appropriate promoter.[141].

A brief outline of the effects of manipulating insulin signalling or Glut4 trafficking in knockout mice is given in the table below.

Gene Knockout	Viable	Diabetes	Phenotype	Reference
Insulin	No	Yes	Growth retardation	[142]
Insulin Receptor	No	Yes	Growth retardation	[143]
IRS-1	Yes	No	Growth retardation and mild insulin resistance	[144]
IRS-2	Yes	Yes	Growth retardation and hyperinsulinaemia	[145]
Glut4	Yes	No	Growth retardation and hyperinsulinaemia	[146]
PI3-K(p85α)	Yes	No	Hypoglycaemia	[147]

Table 2 Gene knockouts and their physiological consequence in mice

Perhaps not surprisingly insulin or insulin receptor knockout mice are not viable. Homozygous insulin receptor knockouts were viable for less than a week, [143] and in that time display marked hyperglycaemia that led to hyperinsulinaemia. The absence of insulin signalling in the liver and adipose tissue also resulted in reduced hepatic glycogen content and decreased fat cell content respectively. This data highlights the crucial nature of insulin in regulating whole body glucose homeostasis and therefore the survival of the animal itself.

A more recent muscle-specific IR gene knockout was achieved using the Cre/loxP system [148]. The resultant muscle-specific IR gene knockout mice displayed a 95% reduction in IR expression in skeletal muscle. These animals remained phenotypically normal despite having greatly impaired insulin-stimulated glucose uptake into skeletal muscle. This was a surprising finding since skeletal muscle is generally considered to be the principal tissue of insulin-stimulated glucose disposal. This result may signify that compensatory measures exist in mice to maintain glucose homeostasis.

Another good example of functional redundancy and compensatory measures in insulin signalling is provided by the IRS-1 gene knockout. Four members of the IRS family have now been identified (IRS-1, 2, 3, and 4) [52]. IRS-1 and IRS-2 are widely distributed, although the relative expression levels are different between tissues. Unlike the IR mutants IRS-1 homozygous null mutants do not present with any major metabolic abnormalities [144], although a mild degree of insulin resistance was observed. This result suggested that another mechanism was substituting for IRS-1

deletion. To address this possibility, insulin signalling and action were further studied in muscle from IRS-1 knockout mice. A 144% increase in IRS-2-associated PI3-K activity compared to controls was found in muscle form IRS-$1^{-/-}$ mice [149]. This data thus provided evidence for an IRS-1-independent pathway of insulin signalling.

In turn IRS-2 was inactivated in knockout mice and the phenotype observed markedly different from the IRS-$1^{-/-}$ mouse [145]. As the animals grew older, mild insulin resistance had developed into severe diabetes by 10 weeks. The IRS-2 deficiency was found to contribute not only to peripheral insulin resistance, similar to an IRS-1 deficiency, but also prevented adequate pancreatic β-cell compensation. Both of these abnormalities are found in human type 2 diabetic patients [150]. In contrast with the significant enhancement of insulin-stimulated PI3-kinase associated with IRS-2 seen in the IRS-$1^{-/-}$ mice, insulin stimulated PI3-kinase activity associated with IRS-1 in muscle was reduced by more than 50%. Therefore, IRS-1 cannot compensate for an IRS-2 deficiency in the same way that IRS-2 can compensate for an IRS-1 deficiency. This may explain the more severe diabetic phenotype observed in IRS-$2^{-/-}$ mice.

Studies using inhibitors suggest that PI3-K is a crucial enzyme in insulin signalling [31, 89]. This observation was tested further in mice homozygous for a targeted disruption in the p85α regulatory subunit of PI3-kinase [147]. In this mutant expression of the full-length p85α gene is blocked while the ability to express a truncated p85α splice variant is retained. These mice are viable, indicating that the other PI3-kinase adaptor/regulatory subunits may compensate for the loss of p85α. These animals are in fact hyper-responsive to insulin and present with hypoglycaemia. This observation is explained by upregulation of the p50α alternative splicing isoform that overcompensates for the loss of p85α in insulin-sensitive tissues.

We have already discussed the structure, function and trafficking of Glut4 in some detail. Glut4 is the principal glucose transporter isoform responsible for glucose disposal into insulin-responsive tissues [151, 152]. Therefore one might expect that disruption of Glut4 would result in insulin resistance. Application of the gene-targeting approach to the Glut4 gene has produced mice carrying a null mutation in this gene [146]. The targeted disruption was achieved by inserting a *neo* cassette into exon 10 of the Glut4 gene. Surprisingly, homozygous Glut4 null mice did not show an overtly diabetic phenotype. However, Glut4$^{-/-}$ mice were insulin resistant, indicated by a 5-6-fold higher postprandial hyperinsulinaemia. A compensatory increase of Glut2 and

Glut1 were detected in the liver and heart respectively. Nevertheless, increased expression of other glucose isoforms was not detected in skeletal muscle. This finding brought speculation that as yet unidentified glucose transporter isoform may be expressed in skeletal muscle that can compensate for null mutation in the Glut4 gene. The phenotype of the Glut4 null mouse is even more surprising when compared to transgenic mice that have elevated levels of Glut4 expression [153]. Liu *et al.* found that increased expression of the human Glut4 gene *in vivo* results in a constitutively high level of cell surface Glut4 protein expression and more efficient control over fluctuations in plasma glucose concentrations. Clearly there is a dichotomy between these two observations, where Glut4 null mice have essentially normal blood glucose control whereas mice that overexpress Glut4 show enhanced glucose control.

In light of the data from the Glut4 null mouse, a Glut2 null mouse may also be expected to show evidence of a mechanism to compensate for Glut2 ablation. Targeted disruption of the Glut2 gene has been achieved in mice by replacing exons 5, 6, and 7 by a *neo* cassette [154]. However, in contrast to Glut4 null mice, Glut2 null mice were diabetic and died within 2-3 weeks of birth. We speculate that the unexpectedly mild phenotype of the Glut4 null mice may be a result of the method used to disrupt the Glut4 gene. Disruption of the Glut4 gene was achieved by targeting exon 10 only, whereas in the Glut2 null mouse 3 exons were disrupted. A situation may therefore arise where a partially disrupted Glut4 protein may still be capable of transporting glucose in response to insulin, hence maintaining a reasonable degree of blood glucose control. Furthermore, a partially mutated Glut4 protein may not necessarily be evident on a Western blot from Glut4$^{-/-}$ tissues due to altered electrophoretic properties.

Due to the redundancy between elements of the insulin signalling pathway it is difficult to make firm conclusions from null mutations in the context of the whole animal. Such studies do however highlight the complexity of insulin signalling and Glut4 trafficking. In addition targeted gene disruptions shed some light on the pathogenesis of diabetes.

Diabetes itself is a major health problem being responsible for a great deal of morbidity and mortality in the western world [6, 150]. The disease is also becoming more widespread throughout Asia as more cultures develop a taste for a western lifestyle and high fat foods. The majority of diabetic patients suffer from non-insulin-dependent diabetes mellitus (NIDDM), characterised by hyperglycaemia in the presence of normal or elevated levels of circulating insulin. This insulin resistance could in

theory arise from any defect in the insulin signalling and Glut trafficking pathways distal to the binding of the hormone to its plasma membrane receptor. Research in humans with NIDDM has tried to address whether there are any genetic predispositions towards this disease.

Mutations found in patients with genetic forms of extreme insulin resistance confirm that the tyrosine kinase activity of the insulin receptor plays a crucial role in insulin signalling [155]. However, mutations in the insulin receptor gene are not responsible for the majority of cases of NIDDM. Similarly, mutations in the insulin gene itself, or the glucokinase gene (glucose is phosphorylated by glucokinase to form glucose 6-phosphate as the initial step in glucose metabolism) are rarely found in cases of NIDDM [156, 157]. Several polymorphisms have been identified in the amino acid sequence of human IRS-1 and studies have reported that some of the variant sequences are increased in prevelance among patients with NIDDM [158, 159]. However, when mutant forms of IRS-1 were expressed in COS-7 cells, the mutations did not alter the level of expression or the extent of insulin receptor-mediated tyrosine phosphorylation of recombinant IRS-1 [160]. Nor did the mutations disrupt the association of recombinant IRS-1 with PI3-K. Therefore, this biochemical study does not lend support to the hypothesis that mutations in IRS-1 contribute to NIDDM. Perhaps this is not surprising since mouse IRS-1 deletion mutants only present with mild diabetes [144].

Knockout studies in mice suggest that IRS-2 may play a more significant role in insulin signalling [145] Therefore mutations in IRS-2 may be more likely to contribute to an NIDDM predisposition. Bektas *et al.* investigated whether variability at the IRS-2 locus plays a role in the etiology of early-onset autosomal dominant type 2 diabetes [161]. They evaluated the genetic linkage between diabetes and two polymorphic markers located in the region of the IRS-2 gene in 29 families with early-onset autosomal dominant type 2 diabetes. However, no mutations segregating with diabetes could be found in these families, indicating that IRS-2 is not a major gene in this disease. Mutations in the p85α subunit of PI3-kinase that contribute to insulin resistance have also been identified in some small populations [162, 163], but no biochemical characterisation of these p85 variants has yet been performed.

1.6.0 *The role of Glut4 in Non-Insulin Dependent Diabetes Mellitus*

Clearly there is a lack of convincing evidence that mutations in elements of the insulin signalling cascade as we understand it contribute to the development of NIDDM. Since the translocation of Glut4 in response to insulin in peripheral tissues is considered the key event in maintaining glycaemic control, perhaps mutations in the Glut4 gene would more readily account for the development of NIDDM. Point mutations in Glut4 have been noted, however these too occur in too small a proportion of cases to be considered an important aetiological factor in insulin resistance [164, 165].

Again, gene defects cannot account for the functional impairment of insulin-stimulated glucose transport in NIDDM. Instead, a functional impairment is the most likely cause of insulin resistance. The principal types of functional defects that may arise can be divided into two groups. Firstly, insulin resistance may arise due to inadequate expression of glucose transporters in peripheral tissues, and secondly, Glut4 may be expressed at sufficiently high levels but does not translocate efficiently to the plasma membrane.

Pretranslational suppression of Glut4 protein is documented as causing insulin resistance in adipocytes from patients with NIDDM and obesity [166]. Hence, lower than normal levels of Glut4 mRNA are detected in adipocytes from these subjects. Glut4 translocation has also been shown to be defective in adipocytes obtained from obese and type 2 diabetic patients [167]. Similarly, transgenic mice expressing the human Glut4 gene specifically in adipose tissue display a marked increase in basal glucose disposal and insulin-sensitive glucose uptake [168].

In skeletal muscle the situation has proven to be different. Most studies have shown no change in muscle cellular Glut4 expression in insulin resistant patients [169, 170]. However, plasma membrane-associated levels of Glut4 were lower, suggesting an impairment of translocation in response to insulin. Therefore, the defect causing insulin resistance in skeletal muscle may lie on the pathway of insulin signalling or transporter translocation. Nevertheless, the pharmacological manipulation of Glut4 expression may be a useful strategy to alleviate insulin resistance. This notion is supported by research in transgenic mice. Leturque *et al.* created transgenic mice that had a 3-fold increase in Glut4 glucose transporter level in skeletal muscle and heart [171]. This increase was sufficient to significantly improve insulin action and to reduce basal glucose levels in transgenic streptozotocin-induced diabetic mice.

The molecular basis for regulation of Glut4 gene expression in states of relative insulin deficiency *in vivo* has been difficult to solve. However it is well established that physical exercise has an up-regulatory effect on muscle Glut4 content [172]. This increase in Glut4 expression explains the improvement in insulin sensitivity observed in exercise trained subjects [173].

In a more recent study, a perfectly conserved myocyte enhancer factor 2 (MEF2)-binding domain was identified in the promoter regulatory region of the Glut4 gene [174]. This domain was necessary, but not sufficient, to support tissue-specific expression of a chloramphenicol acetyltransferase (CAT) reporter gene in heart, skeletal muscle and brown adipose tissue of transgenic mice. Gel shift assays of nuclear extracts from the major Glut4-expressing tissues had significant MEF2 binding activity. In addition, MEF2 DNA binding activity was substantially reduced in nuclear extracts isolated from the skeletal muscle of diabetic mice, which correlated with decreased transcription of the Glut4 gene. However, this decrease was fully restored by insulin treatment. This observation is analogous to the established view that in states of insulin deficiency there is marked reduction in Glut4 expression due to a decrease in Glut4 gene transcription which can be restored upon insulin treatment [175]. Taken together these data support a role for MEF2 in the regulation of Glut4 expression in the principal tissues of glucose disposal, therefore agents with the potential to upregulate MEF2 expression or activity may prove effective antidiabetic agents.

Clearly a better understanding of Glut4 expression and in particular Glut4 translocation may open the doorway to designing more effective treatments for insulin resistance. It was with this background in mind that a strategy to study Glut4 translocation using green fluorescent protein was proposed.

1.7.0 *Green Fluorescent Protein*

Green fluorescent protein (GFP) was discovered by Shimomura *et al.* as a companion protein to aequorin, a chemiluminescent protein from *Aequorea* jellyfish [176]. The same group then published the emission spectrum of GFP which peaked at 508 nm [177]. However, the emission spectrum of purified aequorin was blue and peaked near 470 nm, the approximate value of one of the excitation peaks of GFP. These data implied that the GFP converted the blue light emitted from aequorin into green fluorescence in intact cells. The GFP chromophore was later identified by Shimomura *et*

al. as 4-(*p*-hydroxybenzylidene)imidazolidin-5-one attached to the peptide backbone of GFP [178]. The GFP gene was cloned by Prasher *et al.* [179] and subsequently shown to retain its fluorescent properties when expressed in other organisms [180]. Therefore, the gene alone contains all the information necessary for the posttranslational synthesis of the chromophore, and no jellyfish-specific enzymes are required. This research heralded the application of GFP to cellular biology.

In due course, the three dimensional structure of GFP was solved in 1996 [181]. GFP is an 11-stranded β-barrel threaded by an α–helix running up the axis of the cylinder. The chromophore is attached to the α–helix and situated in the center of the β–barrel [181] (figure 1.7).

The GFP protein used in our study of Glut4 trafficking was a triple mutant (GFP3) (a gift from Dr. J. Pines, Wellcome/CRC Institute, Cambridge, U.K.). The first is a benign mutation, Q80R, common in most cDNA constructs derived from the original sequence and is probably the result of a PCR error [182]. The second mutation, V163A, is proposed to improve 37°C-folding, reduce aggregation at high concentrations and increase the diffusibility of the protein inside cells [183]. The third mutation S65T improves the brightness of GFP and shifts the excitation peak of GFP slightly from 470 to 489 nm [184].

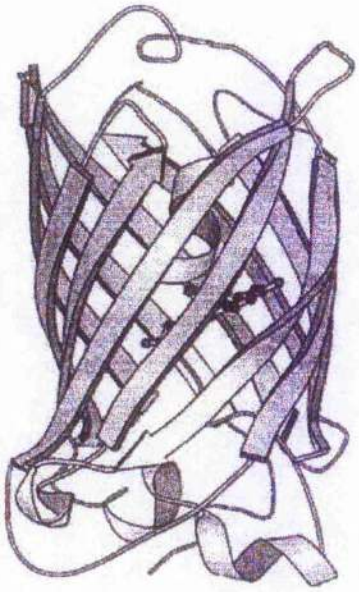

Figure 1.7 Three-dimensional structure of GFP. Image taken from Tsien *et al.* 1998 [182]

The cell biological applications of GFP fall into two main groups. GFP can be used as a reporter gene, or alternatively, as a molecular tag. When used as a reporter gene, GFP expression reflects the strength of the promoter to which the GFP cDNA is linked [180]. In tagging studies however, GFP fluorescence reflects levels of gene expression or subcellular localisations caused by targeting domains or host proteins to which GFP is fused. The application of this technique to research in cellular biology are numerous including, GFP-tagged TGN38 to study membrane traffic pathways, [185], visualisation of protein transport along the secretory pathway, [186] and real time visualisation of internalisation of the thyrotropin-releasing hormone receptor [187].

The use of GFP to tag proteins at the molecular level has several advantages over conventional fluorescent techniques. Principally, GFP fluorescence can be observed in living rather than chemically-fixed cells, and consequently allows the real time visualisation of GFP-tagged proteins. In this study we hoped to make use of these advantages to improve our understanding of Glut4 trafficking.

1.8.0 *Summary of our work*

We begin Chapter 2 of this thesis by describing general materials and methods molecular biology behind the construction of the Glut4-GFP cDNAs. These constructs were then transfected into 3T3-L1 fibroblasts, Chapter 3, in order to investigate wild

type and mutant Glut4-GFP distribution in a fibroblastic background. The localisation of Glut4-GFP was also compared to Texas Red Transferrin, an early endosomal marker. Finally we examined the effects of cytoskeleton-disrupting agents in Glut4-GFP-transfected cells. Comparisons between our own results and those of other groups using conventional immunofluorescence techniques to examine Glut4 distribution are made in the discussion.

In Chapter 4 we examined wild type and Glut4-GFP distribution and translocation in 3T3-L1 adipocytes, an insulin-responsive cell line. Again we compared Glut4-GFP and endosomal marker distribution. Furthermore, we investigated the movement of Glut4-GFP to the cell surface in response to insulin and describe what we believe to be a Glut4-specific reinternalisation mechanism following insulin-induced translocation. The implications of this Glut4-specific recycling mechanism are later discussed within the context of known Glut4 trafficking parameters.

Chapter 5 describes the molecular biology and biochemistry used to construct and analyse ADP Ribosylation Factor (ARF) XTPases. Following recent research that suggests a role for ARFs 5 and 6 in insulin-induced Glut4 translocation we endeavored to make XTP-specific ARF5/6 in order to control ARF function in permeabilised adipocytes [56]. Site directed mutagenisis was used to convert the nucleotide specificity of ARFs 5 and 6 from GTP to XTP. Successfully mutated and epitope tagged ARF cDNA constructs were then expressed in HEK293 cells and analysed by immunoblotting. The long term goal of the ARF XTPases remains to examine the role ARFs 5 and 6 may play in Glut4-GFP translocation.

Finally, in Chapter 6 we move on from insulin-induced Glut4-GFP translocation to study Nitric Oxide-induced glucose uptake and translocation in L6 muscle cells. We examine the effects of nitric oxide donors and inhibitors of the nitric oxide signalling pathway on deoxyglucose uptake and cGMP levels within the cell. We suggest that nitric oxide-induced cGMP levels are closely linked to the rate of deoxyglucose uptake in L6 cells. However, we observed no effects of a nitric oxide donor on GFP-Glut4 translocation.

In closing, we propose that GFP-tagged Glut4 provides a novel means to study Glut4 trafficking in real time. Visualisation of Glut4-GFP in live cells gives us an insight into the dynamics of Glut4 movement not possible using conventional techniques. The ability to examine the subcellular distribution of Glut4 in live cells and in real time therefore represents a step forward in our understanding of Glut4 trafficking.

Chapter 2

2.0.0 General Materials and Methods

2.1.0 *Materials.*

Nocodazole, Cytochalasin D, Chloroquine and Wortmannin were from Sigma, U.K. Texas red transferrin and Lysotracker-Red® were from Molecular Probes (Leiden, The Netherlands). LY294002 was generously provided by Dr Simon Cook (BBSRC Babraham Institute, Cambridge, UK).

2.2.0 *Molecular sub-cloning of GFP3 by Polymerase Chain Reaction (PCR)*

Two oligonucleotide primers (P10 and P11) were designed corresponding respectively to the 5′ and 3′ ends of the GFP3 cDNA. Primers were synthesised and supplied by Genosys. The P10 primer removed the start codon from GFP3 and introduced in its place a BamH I restriction site, whereas the P11 primer introduced an Xba I restriction site and a 'myc' epitope tag.

P10 and P11 oligonucleotide sequences

Sense Primer P10

5′ T T T T G G A T C C A G T A A A G G A G A A G A A 3′

BamH I GFP3 coding sequence

Anti-Sense Primer P11

5′ T T T T T C T A G A T C A C T T C A G G T C C T C C T C C G A G A T C A G C T T C T G C T C C A T T T T G T A T A G T T C A T C 3′

P11 Sense

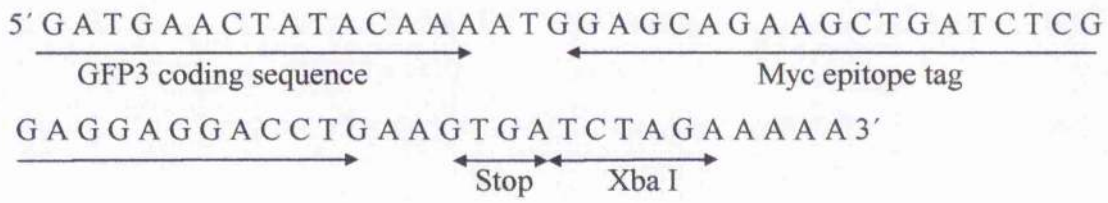

The GFP3 cDNA was then amplified by PCR using *Taq* DNA polymerase and subcloned into an expression vector using the Eukaryotic TA Cloning® kit from Invitrogen. *Taq* polymerase has a nontemplate-dependent activity which adds a single deoxy-adenosine (A) to the 3′ ends of duplex molecules. The linearised vector supplied with the Invitrogen kit has single 3′ deoxythymidine (T) residues. This allows PCR inserts to ligate efficiently with the vector.

2.2.1 *Insertion of Taq-amplified PCR products into pCR3.1 vector*

The pCR3.1 vector DNA is T-tailed to allow for efficient ligation to the *Taq*-amplified and A-tailed PCR product. However, the pCR3.1 vector also carries a eukaryotic cytomegalovirus promoter that allows for expression in a cellular background of any suitable cDNA subcloned into the multiple cloning site of pCR3.1.

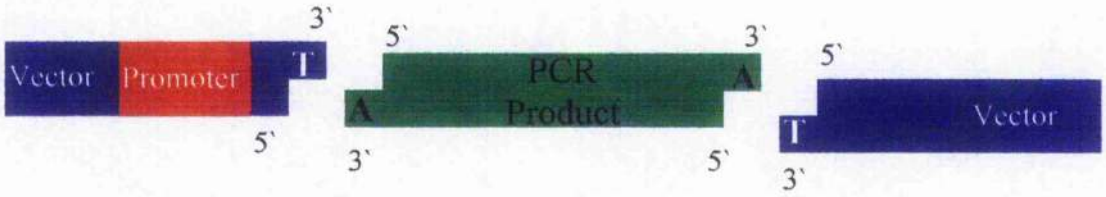

Figure 2.1 A-tailed PCR products generated by *Taq* DNA polymerase were ligated into the T-tailed eukaryotic expression vector pCR3.1

2.2.2 *GFP cDNA PCR Protocol*

1.0 µl of GFP3/pcDNA3 template DNA (50 ng/ µl)

2.5 µl P10 primer (50 µM)

2.5 µl P11 primer (50 µM)

5.0 µl 10x PCR Buffer

0.5 µl 100mM dNTPs

37.5 µl sterile H_2O

1.0 µl *Taq* DNA polymerase

PCR cycle parameters

10 minutes 94°C

1 minute 94°C
1 minute 55°C
3 minutes 72°C
) 30 cycles

10 minutes 72°C

2.2.3 *Agarose gel analysis of GFP cDNA PCR product*

Following completion of the PCR, the DNA was purified with the Wizard PCR clean-up kit and re-suspended in 50 µl TE buffer (pH 7.6) (10 mM Tris.Cl, 1 mM EDTA). 5 µl of the resultant DNA (lane A, figure) solution was then checked by gel electrophoresis [188] on a 1% agarose TBE (0.09 M Tris Borate, 0.002 M EDTA) gel to verify the DNA product size against a Lambda DNA-*Bst*E II Digest molecular weight standard (lane B, figure 2.2). The GFP3 cDNA migrated through the gel at a rate corresponding to its predicted molecular size of 700 base pairs.

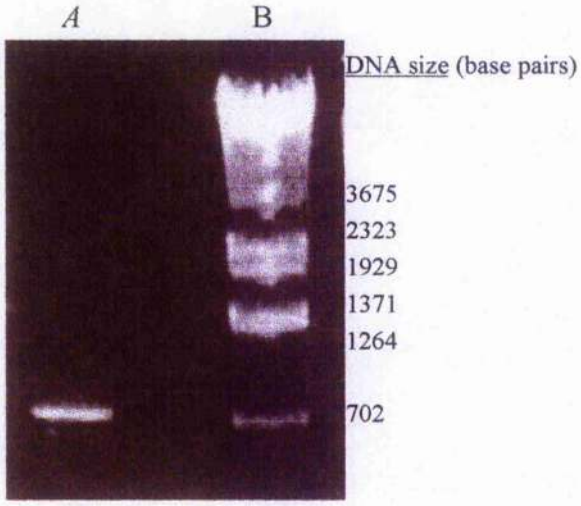

Figure 2.2 The GFP3 cDNA PCR product was analysed by TBE agarose gel electrophoresis

The distance migrated by the GFP3 cDNA (Lane A) was then compared to a Lambda DNA-*Bst*E II Digest molecular weight standard (Lane B).

The DNA was then quantified by measuring its absorbance in TE solution at 260nm [188]. The GFP3 DNA A-tailed PCR product was then ligated into the Invitrogen pCR3.1 expression vector.

2.2.4 *Ligation of GFP cDNA into pCR3.1 vector*

To estimate the amount of PCR product needed to ligate with 60 ng of pCR3.1 vector, the formula shown below was used.

$$\text{Xng PCR product} = \frac{(\text{Y bp PCR product: 600})(\text{60 ng pCR3.1 vector})}{(\text{size in bp of the pCR3.1 vector: 5044})}$$

Where "X" ng is the amount of PCR product of "Y" base pairs to be ligated for a 1:1 (vector:insert) molar ratio. However, it is recommended that a 1:2 (vector:insert) ratio be used, so "X" was multiplied by 2 to calculate the amount needed for ligation.

Control Ligation	GFP3/pCR3.1 Ligation
1 µl 10x ligation buffer	1 µl of 14 ng/µl GFP3 PCR DNA
2 µl pCR3.1 vector (30 ng/µl)	1 µl of 10x ligation buffer
2 µl pCR3.1 vector (30 ng/µl)	2 µl pCR3.1 vector (30 ng/µl)
6 µl sterile H_2O	2 µl pCR3.1 vector (30 ng/µl)
	5 µl sterile H_2O

Ligation reactions were incubated overnight at 14°C

2.2.5 *Bacterial Transformation*

Subsequently, 2 µl of each ligation reaction was transformed into One Shot™ TOP10F' competent cells as described in the Invitrogen TA Cloning Kit. Transformed cells were spread onto agar plates containing 50 µg/µl ampicillin and grown overnight at 37°C. Colonies were then picked from the GFP3/pCR3.1 agar plate and grown overnight in 3 ml LB medium containing 50 µg/µl ampicillin at 37°C in a rotary shaking incubator at 225 rpm. Putative GFP3/pCR3.1 DNA was extracted from the resultant cultures by the alkaline lysis method of small-scale preparations of plasmid DNA [188].

2.2.6 *Restriction enzyme analysis of putative GFP3/pCR3.1 clones*

DNA from the putative GFP3/pCR3.1 clones was cut with BamH I and Xba I restriction enzymes with the rationale that these enzymes would cut at the newly created BamH I and Xba I restriction sites if the GFP3 PCR product had been successfully sub-cloned into the pCR3.1 vector.

The following restriction digest was performed for each of the 18 putative GFP3/pCR3.1 clones:

5.0 µl putative GFP3/pCR3.1 DNA
1.0 µl 10x multi-core buffer
4.0 µl sterile H_2O
0.5 µl BamH I
0.5 µl Xba I

Each of the digests was incubated for 2 hours in a 37°C water bath and then analysed by gel electophoresis on a 1 % agarose TBE gel.

Two of the eighteen putative clones yielded a DNA fragment, estimated at 700 base pairs in length when compared to the DNA molecular weight marker, corresponding to the GFP3 cDNA positioned between the BamH I and Xba I restriction sites. The bacterial cultures corresponding to GFP3/pCR3.1 clones 1 and 2 were frozen at -80°C (600 µl culture volume: 800 µl sterile 50% glycerol) so that cultures could be regrown and fresh DNA extracted at a later date.

However, the directionality of the GFP3 insert within these two clones remained to be established. The nature of the TA Cloning Kit allows for the DNA PCR product to insert into the pCR3.1 vector in either the sense or antisense orientation. Therefore, a single BamH I digest run alongside a BamH I, Xba I double digest, was performed to establish the orientation of the insert. DNA restriction digests were carried out as described above.

Correct Orientation

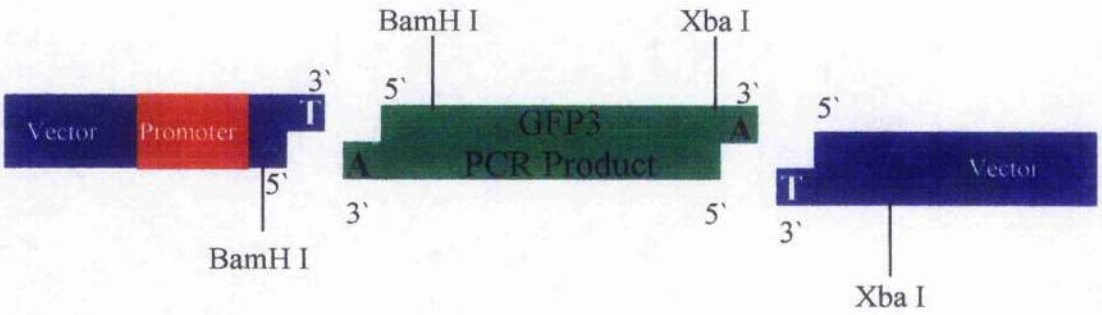

Incorrect Orientation

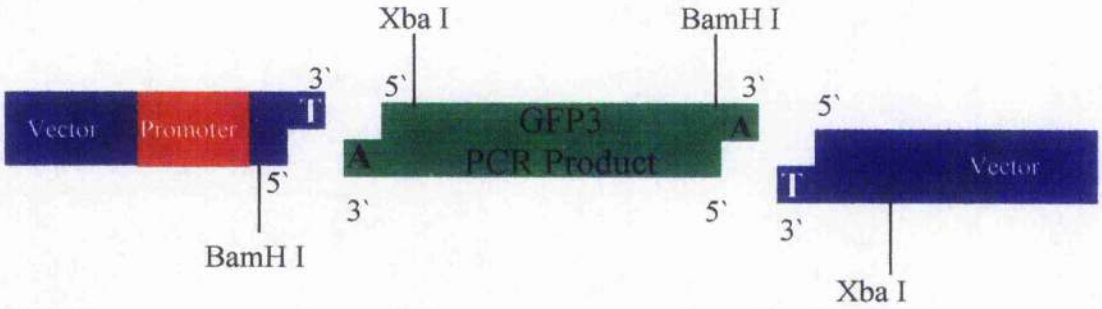

Figure 2.3 The two possible alignments of the GFP3 cDNA within the pCR3.1 vector and the relative positions of restriction sites used to determine GFP3 cDNA orientation within clones

Following analysis on a 1% agarose TBE gel (figure 2.4) it was established that one of the two clones, Clone 1, contained the GFP3 insert in the correct orientation. The DNA sequence of this construct, GFP3/pCR3.1 was then verified by automated sequencing and found to contain no random mutations.

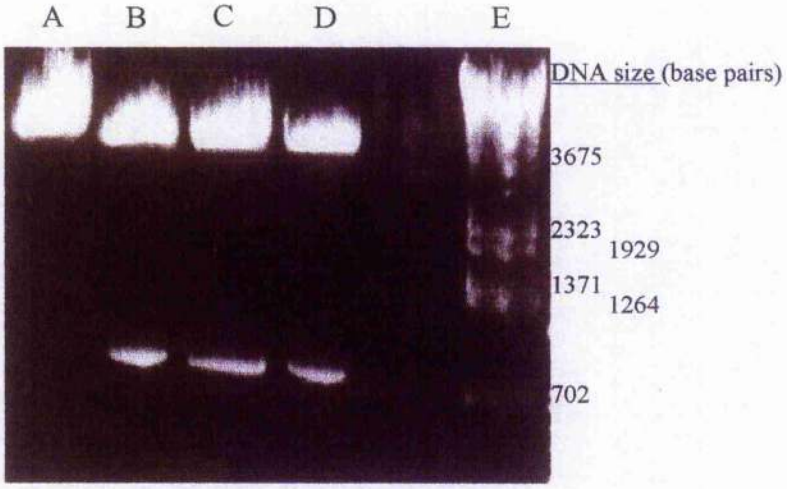

Figure 2.4 Orientation analysis of the GFP3 cDNA PCR product within the pCR3.1 vector

Orientation was analysed by restriction digests with BamH I and BamH I/Xba I, followed by agarose gel electrophoresis. GFP3/pCR3.1 clones in which the GFP3 cDNA was correctly inserted into the vector backbone yielded no visible band when digested with BamH I (Lane A) and a 750 bp band when digested with BamH I/Xba I (Lane B). Resultant DNA bands were compared to a cDNA molecular weight marker (Lane E). Clones in which the GFP3 cDNA was incorrectly inserted into the vector backbone yielded 750 bp bands when digested with Bam HI (Lane C) or BamH I/Xba I (Lane D).

2.2.7 *PCR amplification and sub-cloning of wild type and mutant Glut4 into GFP3/pCR3.1*

cDNA in plasmid vectors for wild type rat Glut4 and each of the four Glut4 mutants used in this study (FAG, SAG, DAG and LAG) were supplied by Dr. D. James, University of Queensland. Two single stranded oligonucleotide DNA primers, P1 and P9, corresponding to the 5′ and 3′ ends respectively of the Glut4 cDNA were designed. Primers were synthesised and supplied by Genosys. The P1 primer introduced a Hind III restriction site immediately upstream of the Glut4 start site, whereas the P9 primer introduced a BamH I site in place of the Glut4 'stop' codon. This BamH I site corresponds to the BamH I site introduced into the 5′ end of the GFP3 cDNA by PCR and therefore allows an 'in-frame' fusion of the Glut4 and GFP3 cDNA to be constructed.

P1 and P9 oligonucleotide sequences

Sense Primer P1

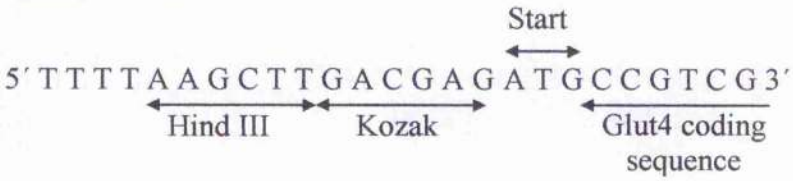

Antisense Primer P9

5′ T T T T G G A T C C G T C G T T C T C A T C T G G 3′

P9 Sense

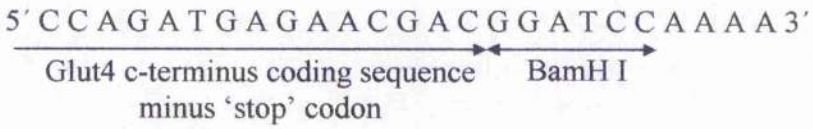

Schematic diagram of Glut4 and GFP3 cDNA fusion

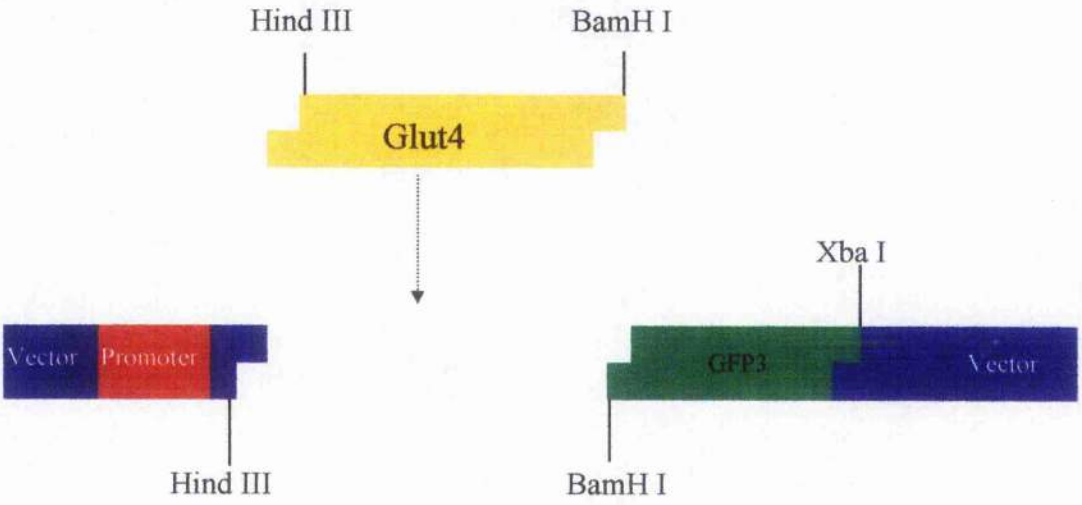

Figure 2.5 Overview of Glut4 cDNA ligation into the Hind III and BamH I sites of GFP3/pCR3.1.

The cDNA corresponding to wild type and mutant Glut4 was amplified by PCR using the P1 and P9 primers under the conditions and parameters already described for the PCR amplification of the GFP3 cDNA. Similarly, the wild type and mutant Glut4 PCR

amplified cDNA fragments were A-tail subcloned into the Invitrogen pCR3.1 vector as previously described. Following mini-prep DNA extraction, the putative Glut4/pCR3.1 DNA clones were double digested with BamH I and Xba I restriction enzymes. Putative Glut4/pCR3.1 clones containing the correct insert yielded a DNA band corresponding to the Glut4 or Glut4 mutant cDNA upon a BamH I/Hind III double digest and agarose gel electrophoresis.

The wild type and mutant Glut4 cDNAs that yielded an insert upon restriction digests with BamH I and Hind III were sequenced as previously described and the corresponding bacterial cultures made into glycerol stocks and stored at -80°C. Once the sequence of the wild-type and mutant Glut4/pCR3.1 and the GFP3/pCR3.1 cDNAs had been verified, the corresponding glycerol stocks were thawed and used to inoculate 100 ml LB (+ 50 μg/ml ampicillin). These bacterial cultures were grown overnight in an orbital shaker (225 rpm) incubator at 37°C. Plasmid DNA was then extracted from the bacterial cultures using the 'Qiagen' Maxi-Prep kit which works by the same alkaline lysis principal as that described for the 'mini-preps'. The plasmid DNA thus obtained was quantified by measuring its optical density at 260 nm.

2.3.0 *Sub-cloning of wild type and mutant Glut4 cDNA into the GFP3/pCR3.1 vector*

First the GFP3/pCR3.1, wild type Glut4/pCR3.1 and Glut4 mutant/pCR3.1 plasmid vectors were cut with the BamH I and Hind III restriction enzymes as shown:

8 μl (5 μg) GFP3/pCR3.1	5 μl (5 μg) wt Glut4/pCR3.1
4 μl 10x Multi-Core buffer	or
24 μl H_2O	5 μl (5 μg) mutant Glut4/pCR3.1
2 μl Hind III	2 μl 10x Multi-Core buffer
2 μl BamH I	11 μl H_2O
40 μl total *	1 μl Hind III
	1 μl BamH I
	20 μl total

Reaction mixes incubated at 37°C for 2 hours.

The 40 μl total * volume of the GFP3/pCR3.1 reaction mix was then treated with calf intestinal phosphatase (CIP). CIP treatment removes the exposed 5' phosphate group

from the plasmid vector DNA molecule, thus reducing the likelihood that the DNA vector will religate with itself rather than the chosen DNA insert;

40 µl GFP3/pCR3.1 reaction mix

20 µl 10x CIP buffer

130 µl H_2O

10 µl CIP enzyme

200 µl total volume

Tube incubated at 37°C for 2 hours.

The 200 µl CIP-treated DNA solution was then phenol/chloroform extracted [188] to remove enzyme proteins and ethanol precipitated to remove the buffer, before resuspension in 10 µl T.E.

2.3.1 *Agarose gel purification of linearised, CIP-treated GFP3/pCR3.1 vector and wild-type/mutant Glut4 cDNA fragments*

Each of the DNA samples was loaded onto a 1% agarose TAE gel and separated by electrophoresis. The appropriate DNA bands were cut from the gel with a clean razor blade and the DNA purified using the Wizard PCR Preps DNA Purification System. The samples were then resuspended in 50 µl H_2O and 5 µl quantitated visually on another 1% TAE agarose gel.

2.3.2 *Ligation of wild-type and mutant Glut4 cDNA into GFP3/pCR3.1*

Each of the wild type and mutant Glut4 cDNA fragments were ligated into the GFP3/pCR3.1 vector and transformed into One Shot™ TOP10F' competent cells by means of the protocols previously described. Similarly, DNA was 'mini-prep' extracted from putative bacterial clones and restriction digested as shown before with BamH 1 and Hind III. DNA clones in which the Glut4 cDNA had successfully ligated into the GFP3/pCR3.1 vector yielded a 1500 base pair fragment, corresponding to the wild type or mutant Glut4 cDNA.

The plasmid DNA from the wild type or mutant Glut4-GFP3/pCR3.1 clones was sequenced as previously described to check for random mutations. Frozen glycerol stocks of the bacterial clones expressing the wild type or mutant Glut4-GFP3/pCR3.1

construct were made as before and used to inoculate LB culture media prior to large scale 'Maxi-Prep' extraction of plasmid DNA.

2.4.0 *Sub-cloning of GFP-Glut4 cDNA into pNOT.NOT*

A plasmid vector expressing GFP3-Glut4 was supplied by Dr. C. Livingstone, GFP3G4/pcDNA1. The following subcloning strategy was designed to transfer the GFP3G4 cDNA from pcDNA1 (Invitrogen) into the pOP13.aP2 expression vector, via the pNOT.NOT shunt vector: The pOP13.aP2 expresion vector was chosen because the aP2 element represents a fat-specific promoter. Therefore, our GFP-Glut4 construct when subcloned into pOP13.aP2 would be under the control of the aP2 element and therefore only expressed in fully differentiated 3T3-L1 adipocytes. It was hoped that limiting the expression of GFP-Glut4 to an adipocyte background would overcome any potential problems arising from GFP-Glut4 expression while the cells remained preadipocytes.

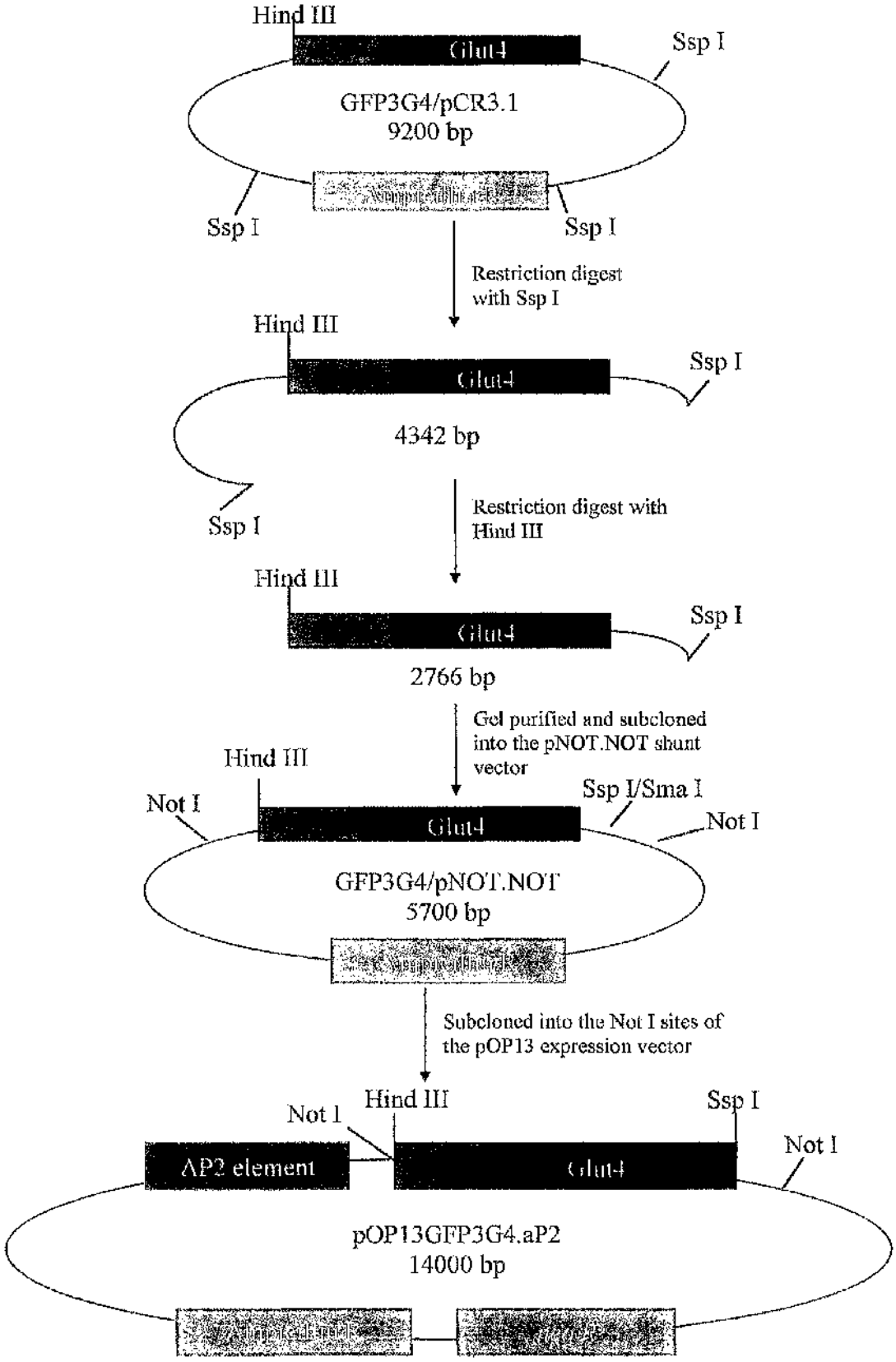

Figure 2.6 Outline of the process used to subclone GFP-Glut4 DNA into the shunt vector pNOT.NOT. and thereafter into the fat specific expression vector pOP13.aP2.

Once the subcloning steps were complete, the nucleotide sequence of pOP13GFP3G4.aP2 was checked by automated sequencing, and the plasmid amplified using the Qiagen Maxi-Prep kit. The pOP13GFP3G4.aP2 was then transfected into 3T3-L1 fibroblasts as described below and stable cell lines selected.

2.5.0 *Tissue culture*

3T3-L1 fibroblasts were grown on polylysine-coated glass coverslips, with one coverslip in each well of a six-well tissue culture plate. Coverslips were dipped in polylysine solution for 10 minutes, dried off in a drying oven, then rinsed with distilled water and autoclaved before being placed in 6-well plates. Cells were then seeded into the tissue culture plates and maintained in Dulbecco's modified Eagle's medium high glucose supplemented with 10% calf serum and 1% penicillin/streptomycin, at 37 °C and 10 CO_2.

Fibroblasts which were later to be differentiated into adipocytes were grown on collagen-coated coverslips. Collagen solution (Sigma, Type I Collagen) was applied to each well, swirled and then removed. The plates were dried with the lid off in the cell culture hood under an ultraviolet lamp and then washed with serum-free Dulbecco's modified Eagle's medium. Once the 3T3-L1 fibroblasts were four days post-confluency, differentiation into adipocytes was initiated. Throughout the differentiation process the same type of medium was used as that used to grow the fibroblasts, but with the calf serum replaced by 10% foetal calf serum. On the first day of the differentiation process the medium was supplemented with isobutylmethylxanthine (500 μM), dexamethasone (25 μM), and insulin (4 μg/ml). After 2 days the medium was replaced, supplemented with insulin (4 μg/ml) only. 2 days later and every 2 days thereafter, medium containing no supplements was used to feed the cells.

2.5.1 *Stable cell line selection*

The pOP13GFP3G4.aP2 DNA plasmid contains a *neo* R gene. Therefore, following transfection, any cell that stably incorporates the pOP13GFP3G4.aP2 DNA into its own chromosomal DNA will also express the *neo* resistance gene and become resistant to the drug G418. The pOP13GFP3G4.aP2 plasmid was transfected into 3T3-L1 fibroblasts grown to 30% confluency in 10 cm tissue culture plates. The following day, transfected cells, and untransfected control cells were treated with 500 μg/ml G418 to kill any cells

not carrying the *neo* R gene. After 7 days of G418 treatment all the untransfected control cells were dead, and G418 resistant colonies, that had incorporated the pOP13GFP3G4.aP2 plasmid into their genome, were visible on the plates with transfected cells. These colonies were selected by placing cloning rings sealed with sterile Vaseline onto the base of the base of aspirated tissue culture plates and adding 200 µl trypsin to each ring. Trypsinised cells from each individual cloning ring were then grown in separate 25 cm^2 tissue culture flasks in medium supplemented with 300 µg/ml G418,and then split into 5x 75 cm^2 flasks. Once the clonal cells grown in 75 cm^2 flasks approached confluency, they were frozen down [188] and stored in liquid nitrogen.

2.6.0 *Cell microinjection*

3T3-L1 adipocytes were grown on glass coverslips and injected at days 7 to 10 post-differentiation using an Eppendorf microinjector system fitted on a Zeiss Axiovert microscope. A heated stage was adjusted to provide a temperature of 37°C in the bathing medium (DMEM supplemented with 10% foetal bovine serum, penicillin/streptomycin and 20 mM Hepes pH 7.4) which was pre-equilibrated in a CO_2 incubator prior to use. Prior to injection, plasmid DNA diluted to a concentration of ~200µg/ml in either dH_2O or TE buffer was microfuged for 15 minutes to separate out any particulate matter and the supernatant DNA solution transferred to a fresh tube. For each coverslip, around 100 cells were injected into the nucleus with plasmid DNA at a pressure of ~ 20 hpa. Following injection, cells were washed twice with DMEM containing 10% foetal bovine serum and incubated in DMEM/foetal bovine serum overnight in a CO_2 incubator at 37°C.

2.7.0 *Confocal microscopy*

All of the GFP images described in this work were taken by confocal microscopy. We used this method rather than conventional fluorescent microscopy because confocal microscopy produces blur-free, crisp images of cells at various depths. Confocal imaging rejects the out-of-focus information by placing a pinhole in front of the detector, so that only the region of the specimen that is in focus is detected. Confocal imaging can only be performed by pointwise illumination and detection, hence a laser is used as a light source in laser scanning microscopy.

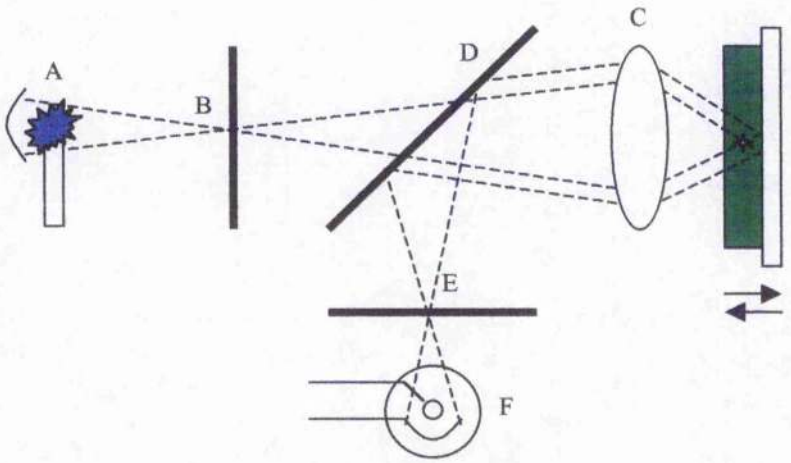

Figure 2.7 Optical design of a confocal microscope

Light at a wavelength of 488nm is emitted from laser (A) and passes through a small pinhole (B) and expands to fill the entrance pupil of the microscope objective lens. The objective lens focuses the light to a small spot on the specimen, green oblong, at the focal plane of the objective lens. Light reflected back from the illuminated spot on the cell is partially reflected by a beamsplitter (D) and directed at a pinhole (E) placed in front of the detector (F). The position of this pinhole (F) is what gives the system its confocal property, by blocking light that did not originate from the focal plane of the microscope objective. The ability to reject light from above or below the focal plane enables the confocal microscope to detect light emitting from just one depth within the specimen cell. A true 3D image can be processed by taking a series of confocal images at successive planes into the specimen and assembling them in computer memory.

This description shows how the confocal microscope detects light from one point in the cell, corresponding to one pixel in the image. The brightness of the pixel depends on the intensity of the light measured from that point in the cell. In order to collect an image of the whole area of interest the laser beam is moved with scanning mirrors to move the focused spot through the cell. The image is assembled pixel by pixel as the scan proceeds.

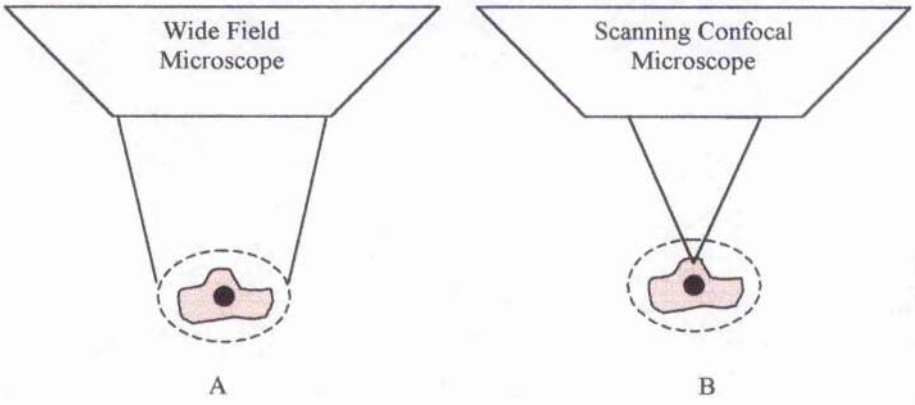

Figure 2.8 The confocal microscope obtains an image in a different way from a conventional microscope

Most confocal microscopes scan a diffraction-limited spot over a cell in order to generate a confocal image. However, figure 2.8, illustrates how a wide-field microscope obtains an image all at once by illuminating the entire cell. This form of imaging is inherently an analogue process and requires the use of a CCD camera to convert it to a digital image. Scanning beam confocal microscopy on the other hand is a digital process as shown in figure 2.8. Therefore, by illuminating one point at a time, the scanning microscope gains a tremendous increase in light intensity when compared to a wide-field microscope.

2.7.1 *Image capture and analysis*

Cover-slips of injected cells were imaged using a Zeiss 4 Laser Scanning Confocal microscope operating in confocal mode using either 40X, 63X or 100X Plan-APOCHROMAT 1.4 NA oil-immersion objectives, with samples on a heated stage adjusted so as to provide a temperature of 37°C in the bathing medium. Images were collected using either (or both) of 488 nm or 543 nm lasers with appropriate filter sets for collection of the GFP signal (band-pass 505-520 nm) or 'red' signals (long-pass 590 nm). Data files were saved in .TIF format and analysed using MetaMorph software (Universal Imaging, CA). In order to quantitate the extent of GFP-Glut4 translocation to the plasma membrane, we employed MetaMorph software to isolate a region of interest which corresponded to a defined area just above and just below the plane of the plasma

membrane in a given confocal image. Fluorescence intensity in this area was expressed as a percentage of the total cellular GFP-Glut4 fluorescence. Such analysis corrects for variations in cell morphology and for expression level of GFP-Glut4 within individual cells and between separate experiments

2.7.2 *3-Dimensional reconstructions and time-lapse movies*

Z-sections of Glut4-GFP-transfected cells were made by taking confocal slices at 0.5 μm intervals through the body of the cell. On average 25-30 such sections were taken through each cell, corresponding to an approximate cell height of 12-15 μm. Three-dimensional reconstructions of z-sections through Glut4-GFP-transfected cells were then built in computer memory using Metamorph software. Time-lapse movies were made by taking a confocal slice through the same section of a Glut4-GFP-transfected cell once every 30 seconds. On average, the time-lapse movies contain 30 frames, corresponding to 15 minutes of real time. The 3-d reconstructions and time-lapse movies were saved in .TIF format and then converted into Quicktime files for writing to CD-ROM. For best results we recommend copying 3-d reconstruction and time lapse files from the CD-ROM onto a computer hard drive before viewing.

2.8.0 *Use of fluorescently labelled markers for intracellular organelles.*

3T3-L1 fibroblasts or adipocytes expressing GFP-Glut4 were incubated with Texas Red Transferrin (20μg/ml) or Lysotracker-Red® (50 nM) for 30 minutes at 37°C in serum-free DMEM in the incubator. Thereafter, cells were washed in KRP/glucose, transferred to the heated microscope stage at 37°C and images collected as outlined above.

2.9.0 *2-Deoxyglucose uptake assay*

All uptake assays were performed in triplicate on fully differentiated adipocytes grown in 6-well tissue culture plates. Following the approprate treatment, cells were washed once with 2 ml of Krebs Ringer Phosphate (KRP) buffer pH.7.4, then incubated for 20 minutes in radioactive 50 μM 2-deoxyglucose (14C 2-deoxyglucose 0.1 μCi/ml). Uptake was stopped by three washes with ice cold phosphate buffered saline (PBS) pH. 7.4 and the plates left to air dry. Thereafter, cells were then solubilized by incubation in 1% Triton X-100 on an orbital shaker and the radioactivity associated with the cells determined by scintillation counting. Uptake values were corrected for the non-specific

association of sugars with the cells by substracting the uptake in the presence of 10 μM cytochalasin B, a potent inhibitor of transport.

Chapter 3

3.0.0 Distribution of wild-type and mutant Glut4-GFP in a 3T3-L1 fibroblast background

3.1.0 Introduction

Fat and muscle are insulin-responsive tissues that redistribute Glut4 from an intracellular location to the plasma membrane upon insulin binding to its cell surface receptor [30, 189]. In the absence of insulin, when fat and muscle cells are analysed by immunoelectron microscopy, Glut4 is found to reside within small intracellular vesicles [95] [96]. Similarly, when transfected into Chinese Hamster Ovary (CHO) cells or fibroblasts, Glut4 is distributed to punctate structures in the cell interior [190] [191] identified by immunoelectron microscopy as small vesicles [192]. Regardless of cell background, Glut1 [193, 194], Glut2 [195] and Glut3 [196] are targeted preferentially to the plasma membrane. These observations suggest that of all the glucose transporter isoforms, only Glut4 is targeted to an intracellular compartment in a number of different cell types. In adipocytes and skeletal muscle, distribution of Glut4 to this unique compartment may provide the basis for its specialised function as the insulin-regulatable glucose transporter.

Upon further examination in CHO cells, intracellular Glut4 was located within endocytic structures distinct from early recycling endosomes defined by the presence of the transferrin receptor (TfR) [190]. In the same study, another marker TGN38 which labels the *trans*-Golgi network, also did not significantly colocalise with Glut4-containing vesicles. A similar study in the neuroendocrine cell line PC12 also found little overlap between Glut4 and TfR [197]. Furthermore, Herman *et al.* saw little colocalisation between Glut4 and the unique synaptic-vesicle-specific protein synaptophysin, and the polymeric immunoglobulin receptor (pIgR), a marker of transcytotic and endocytotic pathways when Glut4 was expressed in PC12 cells. Taken together, these data indicate that following transfection of non-insulin responsive cells, a distinct subpopulation of Glut4 storage vesicle is observed. The function of this compartment within cells not normally associated with post-prandial glucose disposal may reflect a widespread ability of various cell types to modulate the cellular distribution of certain plasma membrane proteins.

Targeting motifs within the N- and C- termini confer upon Glut4 its discrete intracellular location [191, 192, 198-200]. Piper *et al.* showed that an aromatic-based motif found in the N-terminus of Glut4 (FQQI) is crucial for the intracellular location of Glut4 in CHO cells. The mutation F5A resulted in the redistribution of Glut4 to the cell surface. Moreover, Verhey *et al.* observed that mutation of a dileucine motif in the C-terminus of Glut4 is sufficient to alter the subcellular sorting of the transporter from its normal intracellular location to the cell surface in NIH3T3 cells. A dileucine pair has also been implicated in the internalisation and lysosomal sorting of other plasma membrane proteins that include the T cell surface antigen CD4 [201] and the Mannose-6-Phosphate receptor [202]. Interestingly, the dileucine motif lies adjacent to the principal phosphorylation site in Glut4, serine 488 [203]. This serine residue is phosphorylated by cAMP-dependent protein kinase [203]. Mutation of this residue impairs the internalisation of Glut4 when expressed in CHO cells [199] and therefore serine 488 phosphorylation may also play a significant part in the subcellular distribution of Glut4. All of the observed targeting motifs and phosphorylation states of Glut4 may in combination explain some of the unique properties of the insulin-regulatable glucose transporter.

Chloroquine is an acidotrophic drug that accumulates within acidic vesicles neutralising the pH. [204]. In insulin signalling, termination of signal transduction is achieved by endosomal insulin degradation following dissociation of insulin from its receptor as the intralumenal environment of the endosome acidifies [205]. Thus Bevan *at al.* showed that treatment of rats with chloroquine extends the lifetime of the activated insulin receptor complex in endosomes thereby enhancing the positive effects of insulin on glucose transport and glycogen synthesis. Presumably by the same mechanism in a clinical context, chloroquine has been shown to reduce insulin resistance in type II diabetes [206]. If a portion of the intracellular pool of Glut4 resides within acidic endosomes, chloroquine treatment may also be expected to have an effect on the normal subcellular distribution of Glut4.

Over the years our understanding of the cytoskeleton and the part it plays in cell function has changed from a position whereby the cytoskeleton plays merely a structural role. More recent studies have led to the realisation that elements of the cytoskeleton play a crucial role in cell movement, signalling and intracellular tafficking [207]. Both microtubules and actin filaments are implicated in the postendocytotic trafficking of the polymeric immunoglobulin receptor in MDCK cells [208]. Therefore microtubules and

actin filaments may also be expected to play a role in the efficient trafficking of other plasma membrane proteins that recycle through endosomes, for example TfR and glucose transporters. Indeed, Jin *et al.* found that nocodazole, a microtubule depolymerising agent, does affect TfR recycling from the cell surface to endosomes in cultured human leukemia cells [209]. Furthermore, Tsakiridis *et al.* showed that in L6 muscle cells disruption of the actin cytoskeleton using Cytochalasin D, a widely used inhibitor of actin filament formation [210], prevented the recruitment of glucose transporters to the plasma membrane and inhibited the insulin-dependent stimulation of glucose transport [211]. In a similar study in 3T3-L1 adipocytes, Wang *et al.* implicated actin-dependent phosphatidylinositol 3-kinase (PI3-K) relocalisation to glucose transporter storage vesicles as a prerequisite to insulin-stimulated glucose transport [212]. Although Clark *et al.* also put forward a role for actin in PI3K localisation in adipocytes they failed, along with another study [213], to show any effect on insulin action of agents known to disrupt the cytoskeleton. Clearly, there are grounds for further research to explore the relationship between cytoskeletal elements and components of the insulin-stimulated glucose transport machinery.

In the work described in this chapter we used GFP-tagged Glut4 to resolve in a fibroblast background some of the questions outlined above. There are several advantages of using GFP-tagged protein chimeras to study aspects of Glut4 targeting distribution. Firstly, the native fluorescence of GFP allows visualisation of GFP-tagged molecules in living cells, eliminating any artifacts encountered in traditional immunofluorescence studies produced by the fixation process. Furthermore, since GFP allows us to visualise proteins in living cells, we can follow the trafficking of GFP-tagged molecules in real time. Using confocal microscopy we looked at the basal distribution of GFP-tagged wild type Glut4 in the 3T3-L1 fibroblasts. Then, we examined the relative importance of known targeting motifs within Glut4. Using molecular techniques GFP-tagged Glut4 mutants were made and their cellular distribution compared to wild type. Furthermore, colocalisation studies showed the degree of overlap between wild type or mutant Glut4-GFP and Texas-Red Transferrin, a marker for the endosomal recycling compartment. Finally, using the cytoskeleton-disrupting agents nocodazole and cytochalasin D we examined the relative contributions of microtubules and actin respectively on basal Glut4-GFP distribution.

We propose that even in a non-physiological background, Glut4-GFP displays a distinct pattern of distribution similar to that of native Glut4 in muscle and fat cells. In

addition, we suggest that the localisation of Glut4-GFP is intimately tied to the microtubule network of fibroblast cells.

3.2.0 Materials and Methods

3.2.1 *Phallotoxin/Rhodamine staining of actin filaments*

3T3-L1 fibroblasts were grown to 80 % confluency on polylysine-coated coverslips and given any appropriate drug treatment. Cells were then washed 3 times with PBS pH. 7.4 at 37°C and fixed in 3.7% formaldehyde in PBS for 10 minutes at room temperature. Next the cells were washed 3 times with warm PBS and then permeabilised in PBS + 0.1% Triton X-100 for 5 minutes. Following another 3 washes with PBS, non-specific binding sites were blocked by incubating the cells in PBS + 1% Bovine Serum Albumin (BSA) for 30 minutes. The cells were then incubated in room temperature in phallotoxin/rhodamine, diluted 1:40 in PBS + 1% BSA, and kept covered to prevent evaporation and photodegradation. Finally, cells were washed 3 times with PBS and the coverslips mounted on microscope slides with 'Immu-mount' (Shandon)

3.2.2 *Immunofluorescence staining of microtubules*

3T3-L1 fibroblasts grown to 80% confluency on glass coverslips were washed 3 times with PBS pH.7.4 at 37°C and then fixed with 3.7% formaldehyde in PBS for 10 minutes at room temperature. The cells were then washed 3 times with PBS and permeabilised in PBS + 0.1% Triton X-100 for 5 minutes. Next, the cells were washed 3 more times in PBS before incubation in PBS + 1% BSA for 60 minutes to block non-specific binding sites. Mouse anti-tubulin primary antibody diluted 1:3200 in PBS + 1% BSA was added to the cells and incubated for 2 hours at room temperature. Subsequently, cells were washed 5 times in PBS before incubation with anti-mouse Texas-Red conjugated secondary antibody, diluted 1:200 in PBS + 1% BSA, for 2 hours. Cells were then washed 3 times in PBS and the coverslips mounted on microscope slides with Immu-mount.

3.2.3 *Image capture and analysis of actin and microtubules*

Actin and microtubules were labeled as described above and visualised under fluorescent light on a Zeiss inverted microscope using a 40X Plan-APOCHROMAT 1.4 NA oil-immersion objective. Images were collected using a Charged Coupled Device (CCD) camera and data files saved in .TIF format and analysed using MetaMorph software (Universal Imaging, CA) on a desktop PC.

3.3.0 Results

3.3.1 *Transient expression of Glut4-GFP chimeras in 3T3-L1 fibroblasts*

A eukaryotic expression vector containing the cDNA that encodes Enhanced Green Fluorescent Protein (EGFP) was purchased from Clontech. This plasmid was used as a control when investigating the cellular distribution of Glut4-GFP chimeras in 3T3-L1 fibroblasts. At the molecular level, GFP cDNA was tagged to the N-terminus (GFP-Glut4/pcDNA1) or the C-terminus (Glut4-GFP/pCR3.1) of Glut4 in a suitable eukaryotic expression vector. These GFP-tagged Glut4 DNA constructs were then transfected into 3T3-L1 fibroblasts and their cellular localisation examined by LSM as described. The GFP-Glut4 and the Glut4-GFP chimeras were found to have a similar pattern of distribution within the cell. Regardless of whether Glut 4 was tagged with GFP at the N- or C- termini, the pattern of green fluorescence associated with Glut4 within the cell was the same. Both GFP-Glut4 and Glut4-GFP were distributed to a perinuclear compartment and discrete punctate structures spread throughout the cytoplasm when transiently expressed in 3T3-L1 fibrobalsts (figure 3.2.2). However, when the EGFP control plasmid was transfected into fibroblasts, green fluorescence from EGFP was seen evenly dispersed throughout the cytoplasm and nucleus (figure 3.2.1). This suggests that the pattern of distribution seen when the Glut4-GFP chimeras are expressed in cells is a function of Glut4 targeting.

3.3.2 *Transient expression of GFP-tagged Glut4 mutants in 3T3-L1 fibroblasts*

Previous studies have shown that targeting motifs at both the N- and C- termini of Glut4 are important for normal Glut4 targeting within the cell. The FAG, SAG, DAG and LAG Glut4 mutants that carry mutations within these targeting motifs were tagged with GFP at the C-terminus using molecular methods and subcloned into the eukaryotic expression vector pCR3.1. Following transfection into 3T3-L1 fibroblasts, the cellular distribution of the GFP-tagged Glut4 mutants was examined by LSM and compared to that of GFP-tagged wild type Glut4 (figure 3.2.2).

3.3.3 *FAGGFP distribution in 3T3-L1 fibroblasts*

The Glut4 'FAG' mutant carries a phenylalanine to alanine mutation at position 5 of a putative phenylalanine targeting motif in the N-terminus of Glut4. Following transient

expression of GFP-tagged FAG in 3T3-L1 fibroblasts, the distribution of green fluorescence associated with the FAGGFP chimera was noticeably different to that seen when GFP-tagged wild type Glut4 was transfected into the same cell type (figure 3.2.2). Whereas almost all wild type Glut4-GFP fluorescence was intracellular, the FAGGFP chimera was predominantly located at the plasma membrane. Furthermore, the perinuclear compartment visible in wild type Glut4-GFP-transfected cells was less noticeable in cells expressing FAGGFP. This suggests that the phenylalanine residue at position 5 may be important for the intracellular retention of Glut4 in a fibroblast background.

3.3.4 *Distribution of SAGGFP and DAGGFP in 3T3-L1 fibroblasts*

The C-terminus of Glut4 contains a serine phosphorylation site at position 488. We speculated that this phosphorylation site adajacent to a dileucine motif at positions 489/490 may be important in Glut4 trafficking. Therefore two mutant Glut4 GFP chimeras were constructed that carry a mutation at this phosphorylation site. SAGGFP contains a serine 488 to alanine mutation, while DAGGFP carries a serine 488 to aspartate mutation. With the DAG mutant we hoped to simulate a phosphorylated serine 488 by substitution with a negatively charged aspartate residue. However, when SAGGFP/pCR3.1 and DAGGFP/pCR3.1 were transiently expressed in 3T3-L1 fibroblasts the subcellular organisation of green fluoresence seen under LSM was not noticeably different to that seen in cells transfected with wild type GFP-tagged Glut4 (figure 3.2.2). This was illustrated by a perinuclear and punctate pattern of distribution within the cell. This leads us to conclude that the serine phosphorylation site at position 488 of Glut 4 is not crucial to the intracellular distribution of wild type Glut4 when expressed in 3T3-L1 fibroblasts.

3.3.5 *Transient expression of LAGGFP in 3T3-L1 fibroblasts*

Glut4 cDNA encoding leucine to alanine mutations within the C-terminal dileucine motif of Glut4 (LAG) was ligated into the GFP3/pCR3.1 expression vector and transfected into 3T3-L1 fibroblasts. When visualised by LSM, the subcellular distribution of LAGGFP appeared to alter depending on the level of chimera expression. In cells that appeared to express a high level of LAGGFP, judged by the total amount of fluorescence seen in the cell by LSM, a significant amount of LAGGFP was located at the plasma membrane (figure 3.2.2). However, in cells that showed a lesser degree of

expression, the LAGGFP fusion protein did not appear to accumulate at the cell surface (figure 3.5). These results suggest that when expressed at high levels, LAGGFP may saturate a component the cell's recycling mechanism and therefore accumulates at the plasma membrane. This observation therefore implies that the C-terminal dileucine motif is important in mediating the distribution of wild type Glut4 in a fibroblast background.

3.3.6 *Colocalisation studies of Glut4-GFP and Texas Red Transferrin*

Texas Red Transferrin is a commonly used cellular marker for the early endosomal recycling compartment. In order to establish whether our wild type Glut4-GFP and mutant Glut4-GFP species were occupying this endosomal compartment in 3T3-L1 fibroblasts, Texas Red Transferrin (TRT) was added to Glut4-GFP-transfected cells in culture. The degree of colocalisation between the green and red channels, corresponding to GFP and Texas Red respectively, was examined by dual wavelength confocal microscopy. In areas where the colocalisation between the green and the red channels is complete the colours merge to yellow.

Figure 3.3A shows the colocalisation between GFP-Glut4 and TRT, whereas figure 3.3B shows the overlap between Glut4-GFP and TRT in 3T3-L1 fibroblasts. The yellow areas in both of the merged images from figures 3.4A and 3.4B suggest that at least a portion of the GFP-tagged Glut4 resides in an endosomal compartment. However, there are also areas within the cell where the green and red channels do not overlap, indicating that there is another GFP-Glut4 pool out with the early endosomal recycling compartment.

GFP and TRT colocalisation experiments were also performed using the mutant Glut4-GFP constructs. SAGGFP (figure 3.4A) and DAGGFP (figure 3.4B) showed a degree of overlap with TRT similar to that seen when using wild type Glut4-GFP, suggesting that the serine 488 phosphorylation site is not involved in Glut4 sequestration from the endosomal recycling compartment in 3T3-L1 fibroblasts. However, the extent of colocalisation between TRT and FAGGFP (figure 3.5A) did appear different when compared to wild type Glut4-GFP and TRT. Most of the FAGGFP containing regions seen in figure 3.5A have direct Texas Red Transferrin counterparts, hence the large degree of yellow overlap seen in the merged images. Therefore substitution of the phenylalanine residue at position 5 may cause the majority of Glut4-GFP to become trapped in endosomal recycling compartment and accumulate

at the plasma membrane. Furthermore, the overlap observed between LAGFP and TRT (figure 3.5B) was also somewhat different to that seen with wild type Glut4. A large portion of the LAGGFP chimera was located within the perinuclear compartment of 3T3-L1 fibroblasts, with few corresponding areas seen in cells labeled with TRT. This suggests that the dileucine motif in the C-terminal portion of Glut4 may be important for Glut 4 entry into the recycling endosomal compartment. Therefore, LAGGFP is restricted to a non-endosomal pool in 3T3-L1 fibroblasts and will accumulate at the plasma membrane if expressed at high levels.

3.3.7 *Effect of disruption of the cell cytoskeleton on Glut4-GFP distribution*

Nocodazole is a known inhibitor of microtubule polymerisation, whereas cytochalasin D disrupts the formation of actin filaments. To test the effectiveness of nocodazole in 3T3-L1 fibroblasts, cells were incubated with 10 μg/ml nocodazole for 60 minutes, fixed in 3.7% formaldehyde and the microtubules immunolabeled as described. Untreated cells displayed a reticular network of microtubules that was particularly dense around one side of the nucleus (figure 3.6A). This dense area of microtubules was taken to be the microtubule organising center (MTOC). The MTOC in 3T3-L1 fibroblasts broadly matched in terms of size and localisation the perinuclear compartment seen in Glut4-GFP transfected cell. However, in nocodazole-treated cells the microtubules were disorganised and the MTOC dispersed (figure 3.6B).

To investigate whether disruption of microtubules could alter the distribution of Glut4-GFP in 3T3-L1 fibroblasts, transfected cells were incubated at 37°C in the presence of nocodazole. Live cells were then visualised by confocal microscopy (figure 3.7). In Glut4-GFP-transfected cells treated with nocodazole, the perinuclear compartment seen in untreated cells had dispersed. Furthermore, the discrete, punctate vesicles visible in the cytoplasm of untreated Glut4-GFP-transfected cells were more poorly defined. Incubation with nocodazole caused a similar pattern of GFP fluorescence in cells transfected with GFP-Glut4 or Glut4 mutant GFP species. These data are taken to imply that in a fibroblast background Glut4-GFP distribution is dependent upon an intact microtubule network, particularly in the region of the MTOC.

The ability of cytochalsin D to disrupt actin filaments in 3T3-L1 fibroblasts was verified by incubating cells in the presence of 25 μg/ml cytochalsin for 30 minutes and immuno-staining with phalloidin-rhodamine. Fluorescence microscopy of untreated

cells showed linear actin filaments stretched across the body of the cell (figure 3.6C). However, in cytochalasin D treated cells the characteristically straight actin filaments were absent (figure 3.6D). Fibroblasts transfected with Glut4-GFP were also treated with 25 μg/ml cytochalasin D and the live cells analysed by confocal microscopy. In contrast to nocodazole-treated cells, the Glut4-GFP-transfected cells incubated with an effective concentration of 25 μg/ml cytochalasin D looked no different to untreated cells (figure 3.8). Hence, an intact actin cytoskeleton does not appear to be a prerequisite for the distinctive distribution pattern of Glut4-GFP in transfected 3T3-L1 fibroblasts.

3.3.8 *Chloroquine treatment of Glut4-GFP-transfected 3T3-L1 fibroblasts*

Chloroquine is known to increase the pH. of endosomes when added to cells in culture and to inhibit recycling through the early endosomal compartment. The images from our colocalisation studies suggest that at least a portion of the GFP-Glut4 population in transfected 3T3-L1 fibroblasts is located within the early endosomes. Therefore, we treated GFP-Glut4-transfected cells growing in normal medium with 200 μM chloroquine for 2 hours and examined the pattern of GFP-associated fluorescence by LSM. Transfected cells treated with chloroquine displayed a portion of GFP-Glut4 at the plasma membrane and another fraction of GFP-Glut4 residing within abnormally large cytoplasmic endosomes (figure 3.9). This data lends further weight to the argument that part of the GFP-Glut4 population in transfected 3T3-L1 fibroblasts resides within the endosomal compartment. Moreover, inhibition of normal endosomal function by treatment with chloroquine leads to the accumulation of GFP-Glut4 at the plasma membrane of transfected cells.

3.3.9 *GFP-Glut4-expressing 3T3-L1 stable cell lines*

Stable cells lines that express GFP-Glut4 in a differentiation-dependent manner were transfected and selected as described in materials and methods. However, upon analysis by confocal microscopy, none of the clonal G418-resistant 3T3-L1 cells lines displayed any green fluorescence associated with GFP-Glut4 expression. A few cells amongst a mixed population of G418-resistant 3T3-L1's showed some green fluorescence when examined at day 6 of the differentiation process (figure 3.1). However, even that small population of fluorescent cells disappeared as differentiation continued. Following unsuccessful attempts to make stable cell lines with GFP-Glut4 expression under the

control of either a constitutive or 'fat dependent' (ap2) promoter, no further efforts in the pursuit of this goal were made.

Figure 3.1 GFP-Glut4 is not amenable to the creation of a stable adipocyte cell line.
A selection of cells stably expressing GFP-Glut4 from a mixed population of 3T3-L1 adipocytes at day 6 post-differentiation.

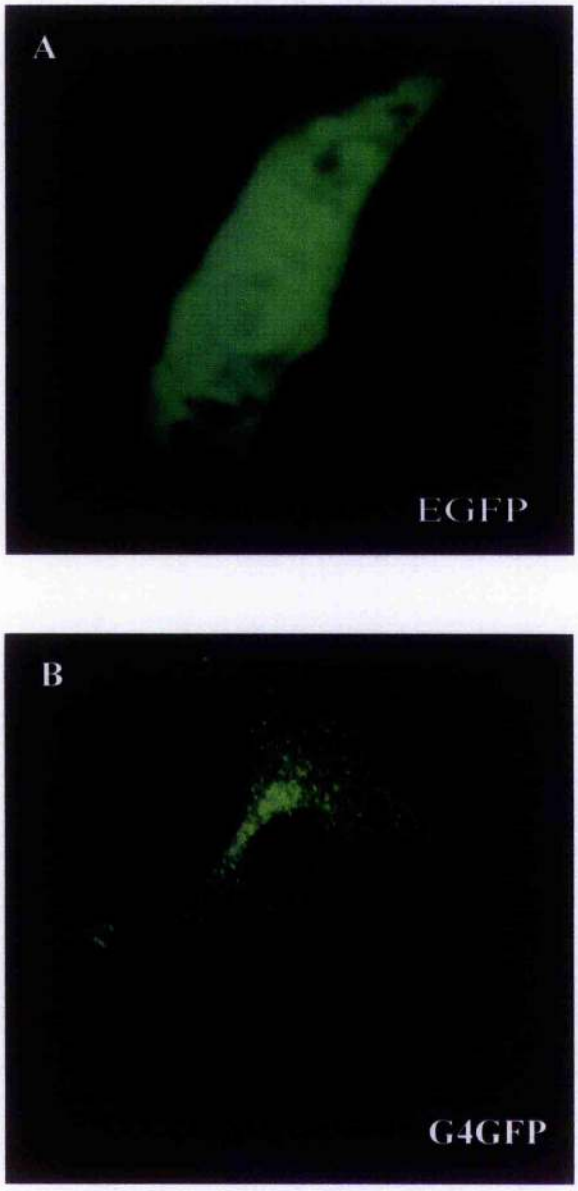

Figure 3.2.1 Comparison of EGFP and Glut4-GFP expression in 3T3-L1 fibroblasts

The control plasmid pEGFP (Clontech) was transfected into 3T3-L1 fibrobalsts (A) and the pattern of GFP-associated fluorescence compared with Glut4-GFP (B). Glut4-GFP was distributed to discrete intracellular vesicles, whereas EGFP was evenly dispersed throughout the cytoplasm.

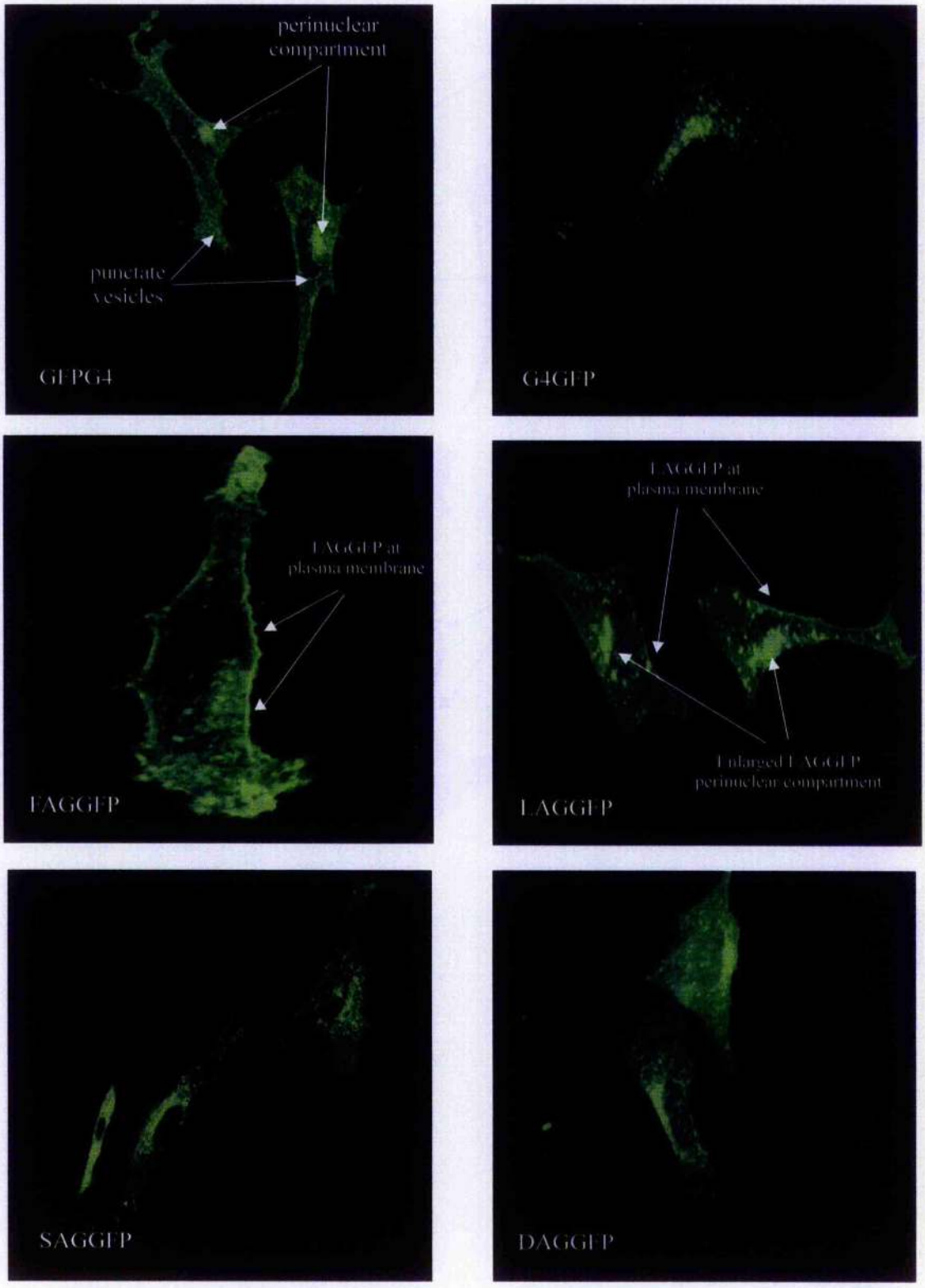

Figure 3.2.2 Basal distribution of wild-type amd mutant Glut4-GFP chimeras in 3T3-L1 fibroblasts 3T3-L1 fibroblasts were grown to 50% confluency on poly-Lysine-coated coverslips and then transfected with wild type or mutant Glut4 cDNAs tagged with GFP. The cells were then analysed by confocal microscopy 24 hours after transfection.

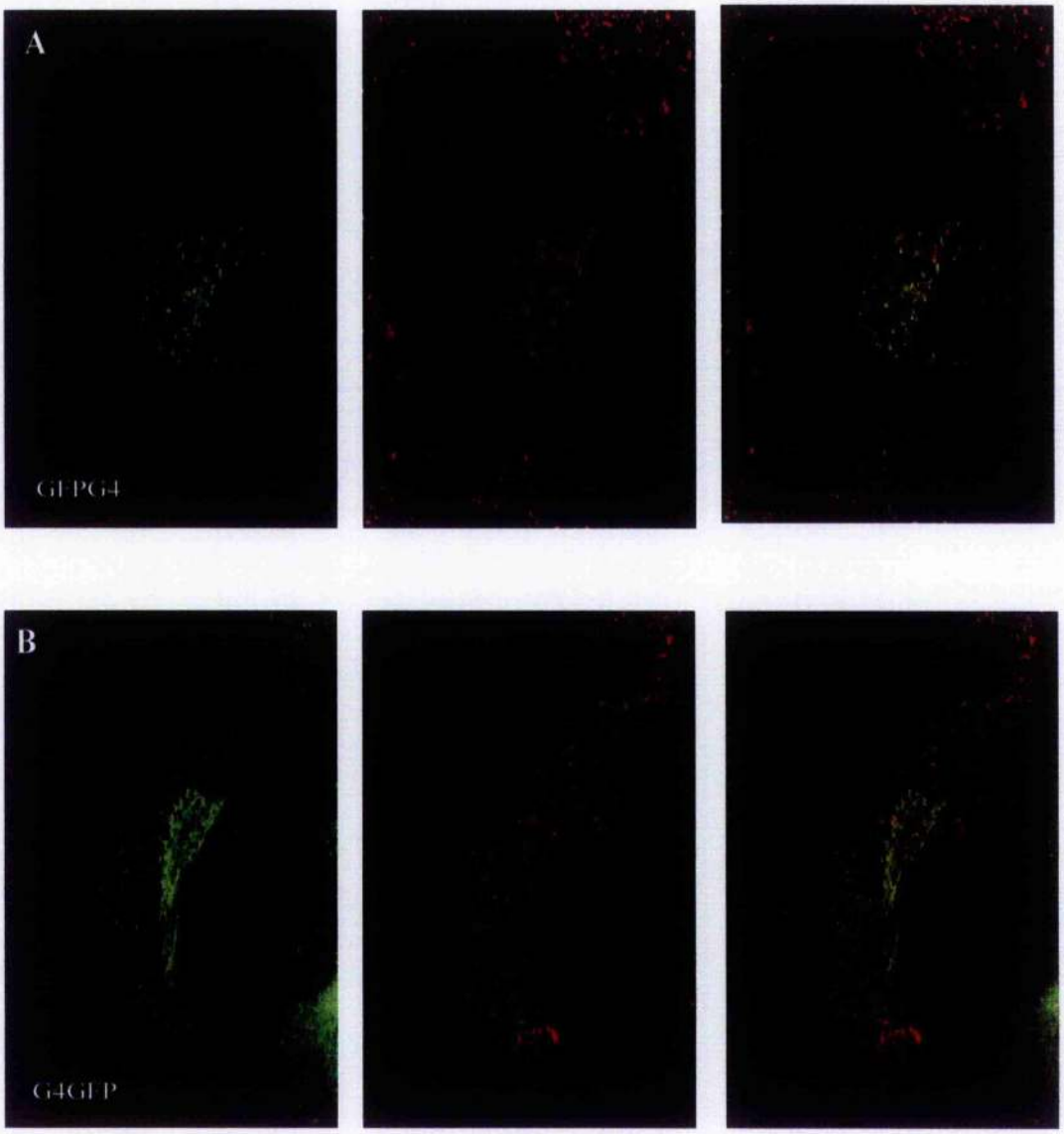

Figure 3.3 Colocalisation between Glut4-GFP and the endosomal marker Texas Red Transferrin Glut4 tagged with GFP at either the N- or C- terminus (figures A and B respectively) were transfected into 3T3-L1fibroblasts and their subcellular distributions compared with the early endosomal marker Texas Red Transferrin (TRT). The green left hand panel represents GFP-associated fluorescence, while the red centre panel shows the TRT marker. The merged right hand panel shows the overlap between GFP and TRT in the same cell. Regions where the colocalisation between GFP and TRT are greatest show as yellow on the merged image.

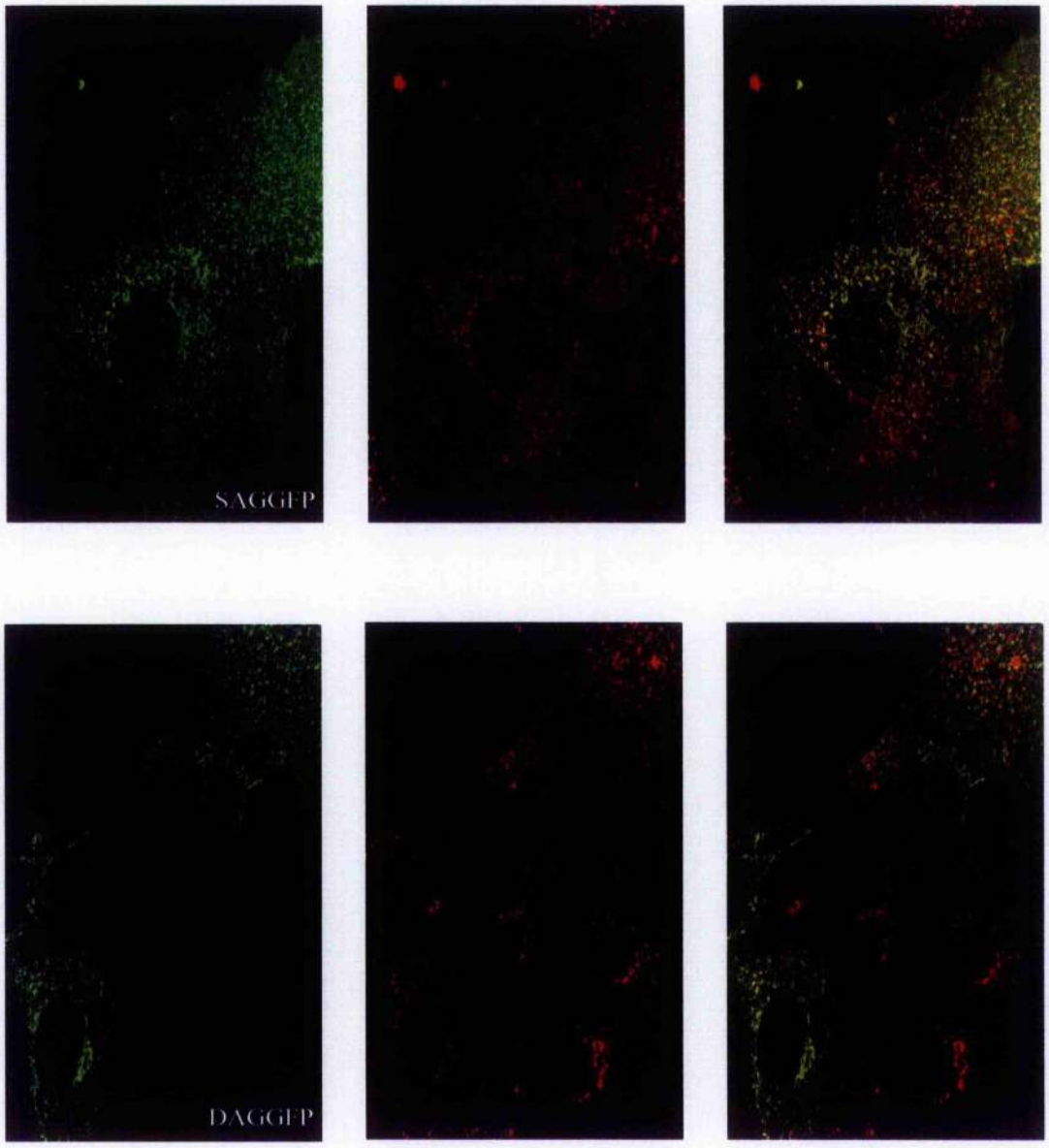

Figure 3.4 Colocalisation of SAG- and DAG-GFP with Texas Red Transferrin in 3T3-L1 fibroblasts SAGGFP (A) and DAGGFP (B) were transfected into 3T3-L1 fibroblasts and their subcellular distributions compared with the early endosomal marker Texas Red Transferrin (TRT). The green left hand panel represents GFP-associated fluorescence, while the red centre panel shows the TRT marker. The merged right hand panel shows the overlap between GFP and TRT in the same cell. Regions where the colocalisation between GFP and TRT are greatest show as yellow on the merged image.

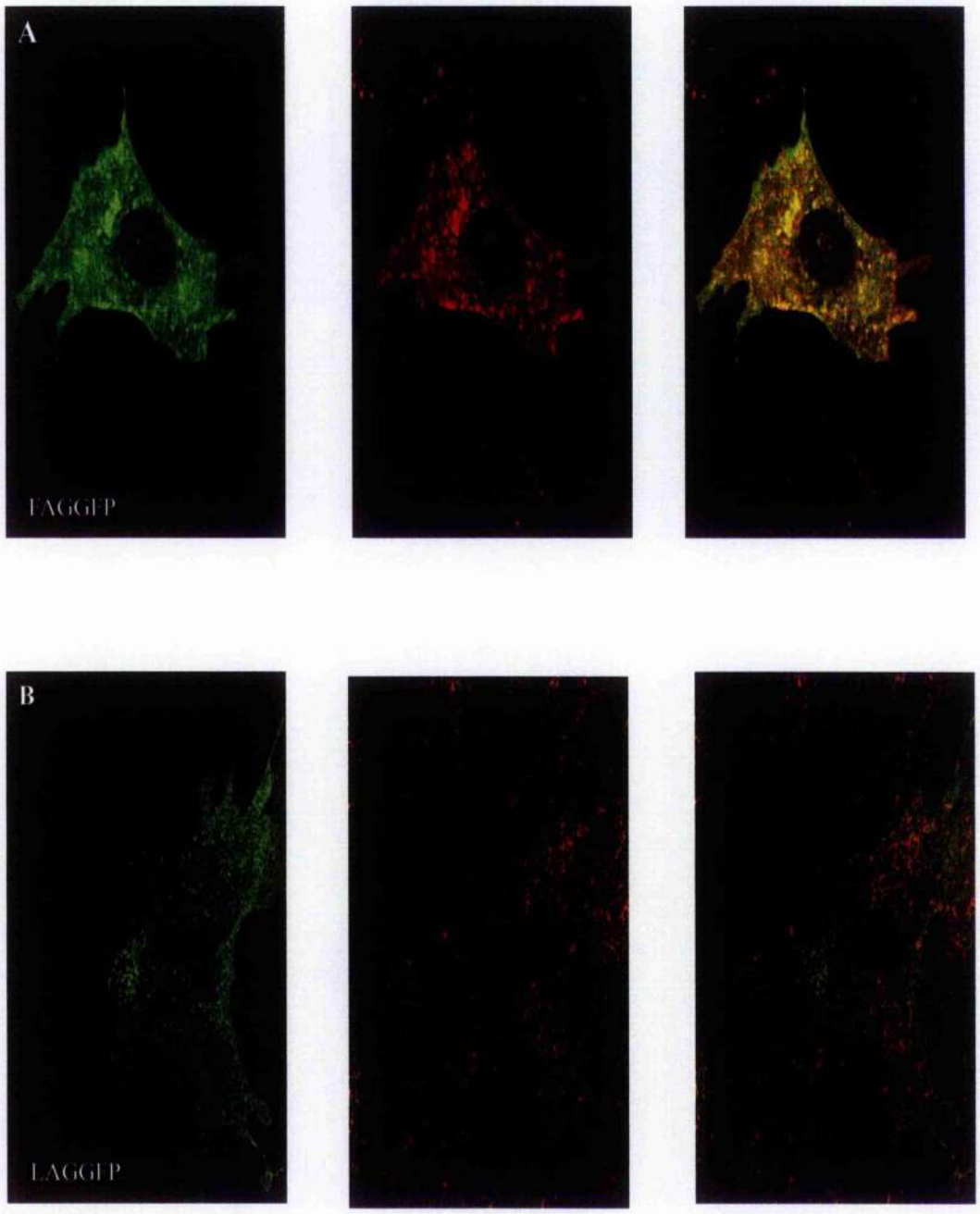

Figure 3.5 Colocalisation of FAG- and LAG-GFP with Texas Red Transferrin in 3T3-L1 fibroblasts
FAGGFP (A) and LAGGFP (B) were transfected into 3T3-L1 fibroblasts and their subcellular distributions compared with the early endosomal marker Texas Red Transferrin (TRT). The green left hand panel represents GFP-associated fluorescence, while the red centre panel shows the TRT marker. The merged right hand panel shows the overlap between GFP and TRT in the same cell. Regions where the colocalisation between GFP and TRT are greatest ahow as yellow on the merged image.

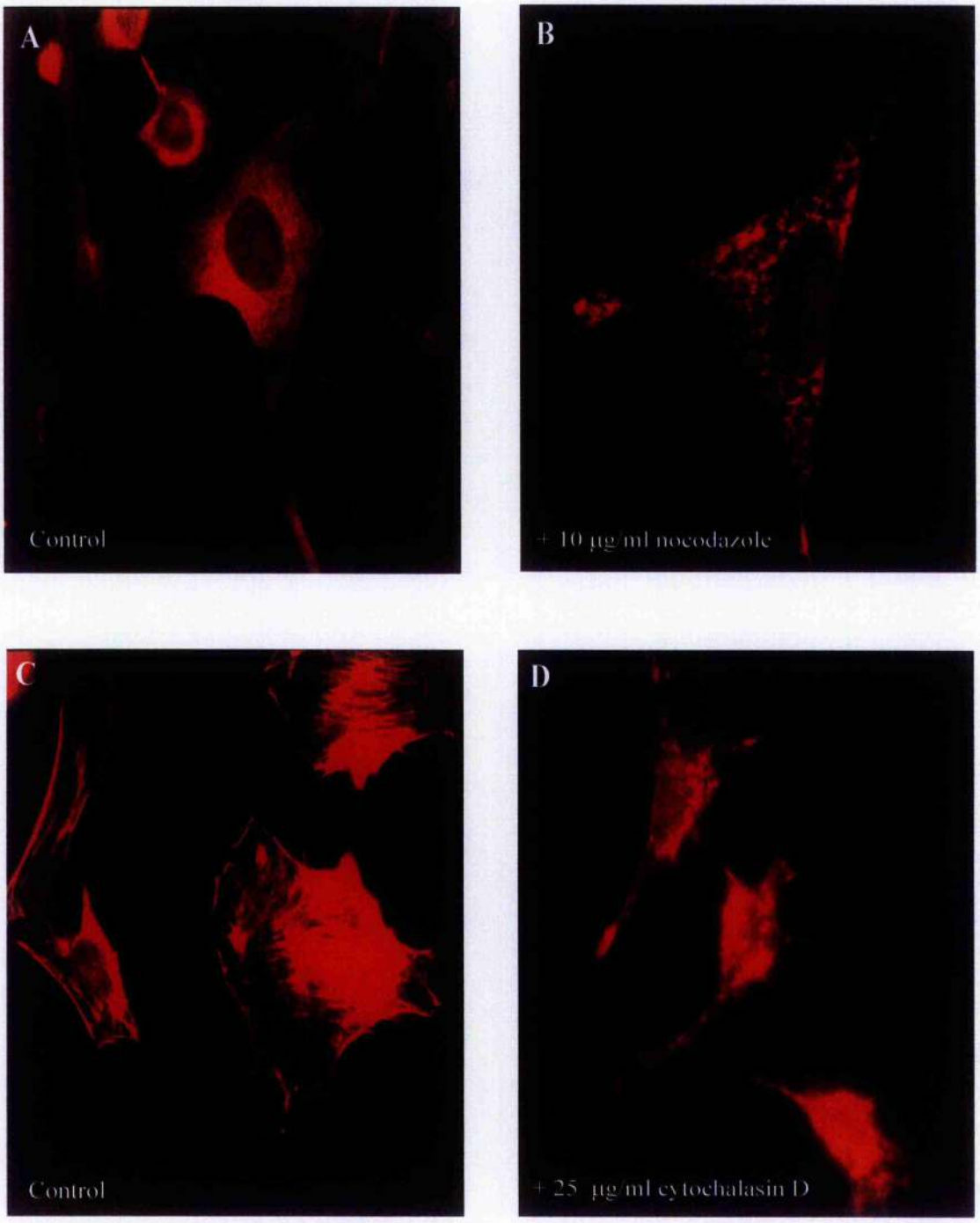

Figure 3.6 Effect of the drugs nocodazole and cytochalasin D on the microtubules and actin filaments respectively in 3T3-L1 fibroblasts

3T3-L1 fibroblasts were treated with 10 µg/ml nocodazole for 60 minutes (B), or 25 µg/ml cytochalasin D for 30 minutes (D), or left untreated (A and C). Cells were then fixed and the microtubules stained, (A and B) or the actin filaments stained (C and D), as described in materials and methods. Images were captured using a CCD camera and saved onto a PC.

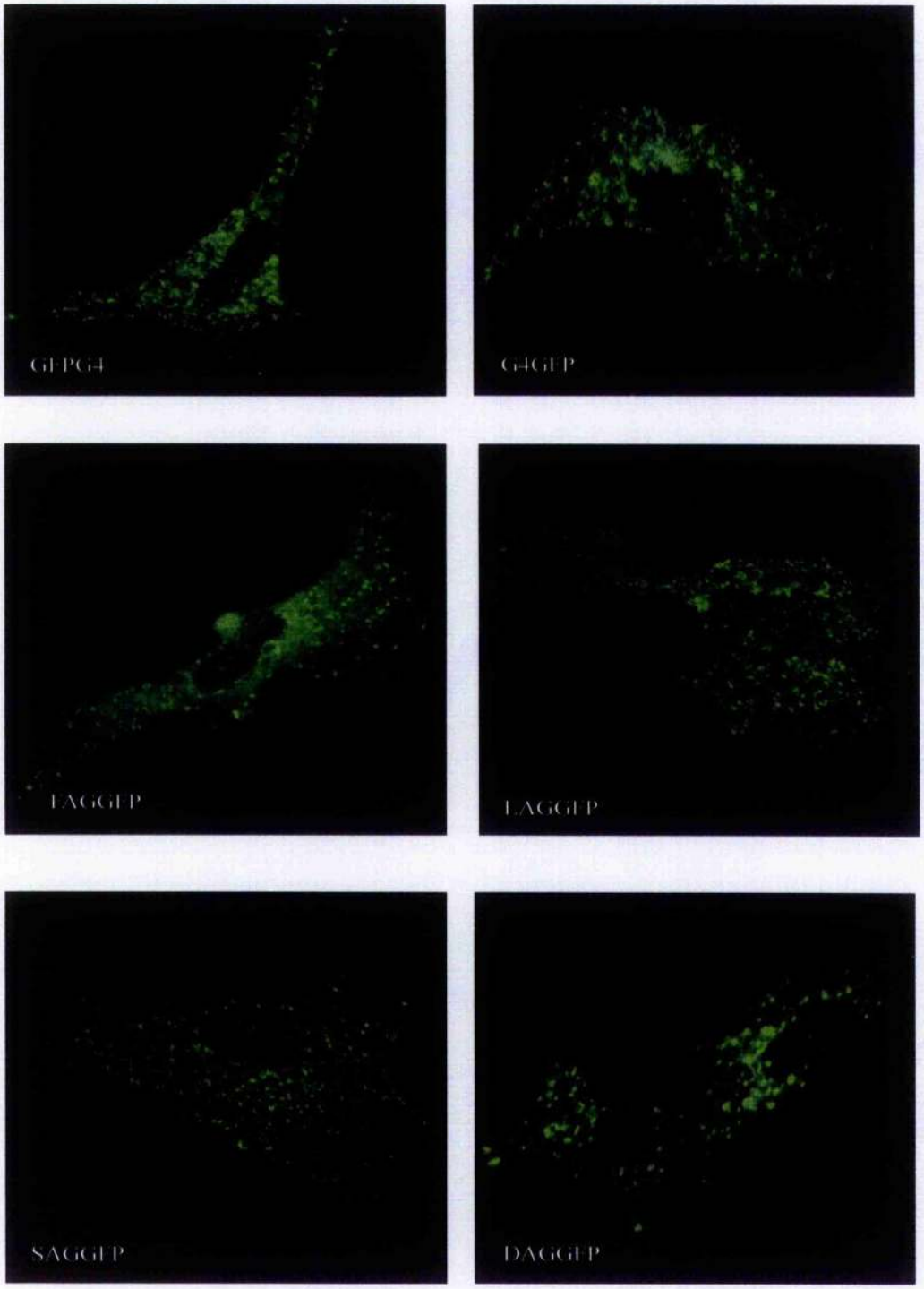

Figure 3.7 Wild-type and mutant Glut4-GFP distribution in nocodazole-treated cells 3T3-L1 fibroblasts were transfected with wild type or mutant GFP-tagged Glut4 and then treated for 60 minutes with 10 μg/ml nocodazole, an agent that inhibits microtubule formation. The cells were then analysed by confocal microscopy. Changes in the distribution of Glut4-GFP and mutant Glut4-GFP in the presence of nocodazole are evident when compared to untreated cells (figure3.2.2).

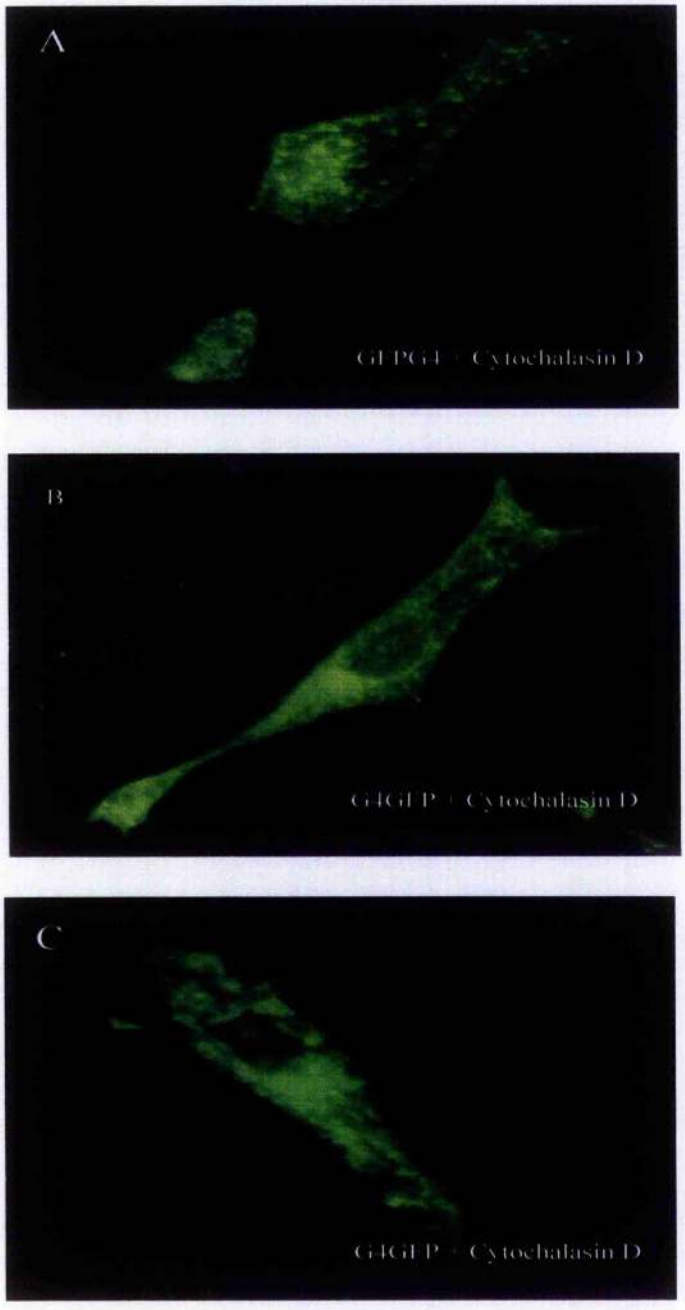

Figure 3.8 Distribution of GFP-Glut4 in cytochalasin D-treated 3T3-L1 fibroblasts GFP-Glut4-transfected cells were treated for 30 minutes with 25 µg/ml cytochalasin D (A, B and C), an inhibitor of actin filament formation. The distribution of GFP-Glut4 was then anaysed by confocal microscopy and compared to GFP-Glut4 localisation in untreated cells (figure 3.2.2).

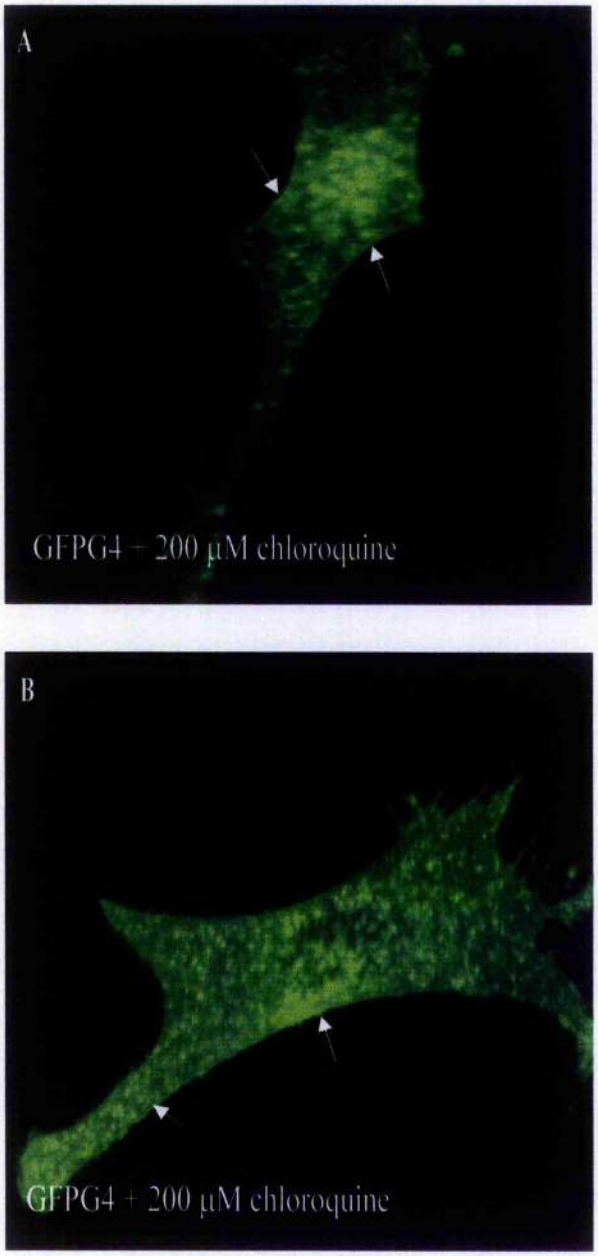

Figure 3.9 Distribution of GFP-Glut4 in chloroquine-treated 3T3-L1 fibroblasts
GFP-Glut4-transfected 3T3-L1 fibroblasts were treated with 200 μM of the acidotrophic agent chloroquine (A and B). Following a two hour incubation with chloroquine,the distribution of GFP-Glut4 was analysed by confocal microscopy. Chloroquine was observed to cause the swelling of GF-PGlut4-containing vesicles and to redistribute some of the GFP-Glut4 population to the plasma membrane (see arrows).

3.4.0 Discussion

3.4.1 *Wild-type Glut4-GFP*

Using molecular techniques we made GFP-tagged wild type Glut4 cDNAs. The Glut4-GFP cDNAs were then subcloned into eukaryotic expression vectors and transfected into 3T3-L1 fibroblasts. Following transient expression of the plasmid vectors, Glut4 associated GFP fluorescence was analysed by confocal microscopy. We found that GFP-tagged Glut4, with GFP present at either the N- or C- terminal of Glut4, occupied two distinct locations within the cell. One location represented a large perinuclear compartment, within which the majority of the Glut4-GFP fluorescence resided. The other compartment comprised the many punctate Glut4-GFP vesicles present throughout the cytoplasm of the cell. At this level of resolution there were no differences in the pattern of distribution between Glut4 chimeras tagged at either the N- or C-terminus.

Texas-Red Transferrin is an early endosomal marker that we used in conjunction with Glut4-GFP to establish the compartment within which Glut4-GFP resides when transfected into 3T3-L1 fibroblasts. The unmerged red images of fibroblasts incubated with TRT show that the early endosomal system within these cells comprises punctate vesicles spread throughout the cytoplasm. Figure shows that when expressed in 3T3-L1 fibroblasts, at least some of the total wild type Glut4-GFP population is present in the early endosomal system, identified by the yellow overlap signal seen in the merged images. However, clearly there are populations of Glut4-GFP, around the perinuclear compartment and within cytoplasmic vesicles that do not colocalise with Texas-Red transferrin. Again, within the limits of our image resolution, there were no apparent differences in the degree of over lap between either C- or N- terminus tagged Glut4-GFP and TRT.

This pattern of Glut4 distribution in a fibroblast background broadly matches the findings of other researchers [192, 193]. We therefore conclude that our GFP-tagged Glut4 chimeras localise to an intracellular compartment that is at least morphologically similar to that occupied by untagged Glut4 when expressed in fibroblasts. This further implies that the large unwieldy GFP molecule tacked on to either the N- or C- terminus of Glut4 does not appear to interfere with Glut4 trafficking and distribution in fibroblast cells. The nature of this Glut4-GFP positive, Texas Red Transferrin negative

compartment within 3T3-L1 fibroblasts remains to be elucidated. This compartment may represent a unique organelle within 3T3-L1 fibroblasts, the formation of which is stimulated by the expression of Glut4. If this were true, expression of endogenous Glut4 during 3T3-L1 adipocyte differentiation would allow for the formation of a unique organelle around which the cellular translocation machinery could be organised as differentiation progressed. However, we cannot exclude the possibility that the intracellular Glut4-GFP-containing vesicles correspond to a sub-compartment of an organelle such as the *trans*-Golgi reticulum (TGN). Fibroblasts transfected with Glut4-GFP showed no discernable translocation of Glut4-GFP in response to insulin (data not shown), despite evidence that 3T3-L1 fibroblasts do express insulin receptors [214]. Therefore, we suggest that factors in addition to Glut4 expression within a discrete intracellular compartment and the presence of cell surface insulin receptors are required for Glut4 translocation.

The pattern of overlap observed between Glut4-GFP and Texas Red Transferrin in 3T3-L1 fibroblasts is in agreement to reports by other groups performing similar immunofluorescent studies in CHO and PC12 cells [190, 197]. Wei *et al.* distinguished between Glut4 and transferrin containing compartments in CHO cells by double-labeling immunofluorescence assays. In these experiments Wei *et al.* showed that Glut4 and TfR did appear to be colocalised to some extent in the perinuclear region. However, in the periphery of the cell, many structures enriched for Glut4 but not for the TfR were apparent. Similarly, work by Herman *et al.* in the neuroendocrine cell line PC12 showed that Glut4 immunoreactivity was detected in punctate structures throughout the cytoplasm and enriched in the perinuclear region. Furthermore, Herman *et al.* found the majority of Glut4 did not codistribute with TfR, although a small amount of overlap was observed primarily in the perinuclear region.

In addition our colocalisation data is similar to results obtained in fully differentiated 3T3-L1 adipocytes [98]. Livingstone *et al.* showed that endosomal compartment ablation only caused a 40 % reduction in Glut4 translocation to the cell surface in response to insulin, suggesting that there is also a non-endosomal pool of insulin-responsive Glut4 within 3T3-L1 adipocytes. However, it is unlikely that a similar non-endosomal pool of Glut4 in 3T3-L1 fibroblasts would move to the cell surface in response to insulin as essential components of the translocation machinery, for example VAMP2 [107] may not be expressed in 3T3-L1 cells until differentiation into adipocytes is complete. Indeed, El-Jack *et al.* have recently shown that expression

of the transcription factors CCAAT/enhancer-binding protein α (C/EBPα) and peroxisome proliferator-activated receptor γ (PPARγ) are prerequisites for adipogenesis and the establishment of insulin-sensitive glucose transport in a variety of murine fibroblast cell lines [215].

To review, we transfected GFP-tagged Glut4 into 3T3-L1 fibroblasts and saw no difference in the pattern of distribution of Glut4 with the GFP attached to either the N- or C- terminus. When expressed in fibroblasts, Glut4-GFP was localised to a perinuclear compartment and discrete punctate vesicles throughout the cytoplasm. Colocalisation studies with the endosomal marker Texas Red Transferrin showed only a partial overlap with Glut4-GFP. This data, in terms of Glut4 distribution and overlap with the endosomal marker TRT is largely in agreement with other work performed in a variety of both insulin-responsive and non-insulin responsive cell lines. This suggests that Glut4 is targeted to a class of vesicle present in a wide range of cell types. Herman *et al.* proposed that this may be a distinct organelle involved in transient cell surface modification without *de novo* synthesis of membrane protein. Based on our data we propose that GFP represents a novel means by which to study in real time Glut4 trafficking through this distinct class of vesicles.

3.4.2 *Distribution of Glut4-GFP mutants in 3T3-L1 fibroblasts*

In addition to wild type, Glut4 cDNA carrying mutations in either an N-terminal phenylalanine motif (FAG), a C-terminal dileucine motif (LAG) or a serine phosphorylation site (SAG or DAG) were linked to GFP and transiently expressed in 3T3-L1 fibroblasts. In common with the findings of Piper *et al.* 1993, FAGGFP was found to distribute predominantly to the plasma membrane, with an apparent concomitant decrease in the amount of GFP fluorescence emanating from the perinuclear compartment. This suggests that the phenylalanine residue at position 5 of Glut4 is important for Glut4 recycling between the interior of the cell and the plasma membrane. Similarly, in agreement with other studies [191, 216], we also found that when expressed at high levels, LAGGFP accumulated at the plasma membrane (Figure 3.2.2). However, unlike FAGGFP, LAGGFP displayed a particularly well defined perinuclear compartment. Serine 488 is the principal phosphorylation site in Glut4 and there is some evidence that this residue plays a part in Glut4 distribution in CHO cells [199]. Two mutant Glut4-GFP constructs were made; SAGGFP carried a serine 488 to

alanine mutation, whereas DAGGFP carried a serine 488 to aspartate residue to mimic a charged phosphate group. We found no difference in the intracellular distribution of SAG and DAG compared to wild type Glut4 when tagged with GFP and transiently expressed in 3T3-L1 fibroblasts (figure 3.2.2).

That mutation of a phenylalanine or dileucine motif should result in the aberrant targeting of Glut4-GFP is perhaps not surprising. Within the secretory pathway of mammalian cells, selected membrane proteins are sorted from the TGN through the endosomal pathway to the major hydrolytic compartment, the lysosomes [217]. This sorting process is directed by tyrosine-based and dileucine-based targeting signals [218]. These targeting motifs can interact with clathrin adaptors 1 and 2 (AP-1 and AP-2) [133, 218]. AP-1 and AP-2 co-assemble with clathrin into a coat that drives vesicle budding at the TGN and plasma membrane respectively prior to trafficking through the endosomal system [133, 218]. Therefore any plasma membrane protein bearing a mutation in these tyrosine or dileucine-based targeting motifs (FAG/LAG) may not be correctly sorted from the TGN or plasma membrane. Such a mechanism could explain the accumulation of FAGGFP at the cell surface if the mutation of phenylalanine to alanine prevented Glut4 interaction with AP-2. Similarly, a dileucine motif mutation may hinder the interaction between Glut4 and AP-1 at the TGN, and AP-2 at the plasma membrane, thereby causing an accumulation of LAGGFP at a perinuclear TGN compartment and at the cell surface.

Regarding the significance of serine 488 in Glut4 targeting, our results are somewhat different to those described in the literature. Garripa *et al.* characterised the trafficking motifs contained in the carboxyl terminus of Glut4 by constructing a chimera in which the carboxyl-terminal 30 amino acids of Glut4 were substituted for the amino-terminal cytoplasmic domain of the transferrin receptor. The distribution of this chimera was then analysed in CHO cells. In agreement with our results, the distribution of Glut4/TfR chimeras in which the dileucine motif of the carboxyl domain of Glut4 was mutated to a di-alanine sequence was shifted towards the cell surface. However, Garripa *et al.* also found a similar shift to the cell surface when the serine 488 phosphorylation site of the Glut4 carboxyl terminus was mutated to alanine or aspartate. We suggest that the fibroblast cell background in our experiments may explain the difference between our own results concerning the importance of the Glut4 serine phosphorylation site at position 488 and those of Garippa *et al.* Furthermore, it is not unreasonable to suppose that the serine phosphorylation site may work in conjunction with another targeting

element within the structure of Glut4, for example the intracellular loop between helixes 6 & 7. Therefore, when studying the C-terminal tail of Glut4 in isolation from the rest of the transporter as Garripa *et al.* have done, subtleties in targeting based upon intramolecular interactions may be overlooked.

Furthermore, we transiently expressed mutant Glut4-GFP constructs in 3T3-L1 fibroblasts and colocalised with Texas-Red Transferrin. The degree of overlap between the serine 488 mutants (SAGGFP and DAGGFP) and TRT was similar to the extent of colocalisation between wild type Glut4-GFP and TRT (figure 3.4). This suggests that phosphorylation of serine 488 in Glut4-GFP is not essential for sorting between an early endosomal and a non-endosomal compartment in 3T3-L1 fibroblasts. However LAGGFP, carrying mutations in the dileucine motif of Glut4 did appear to show somewhat less overlap with TRT (figure 3.5B), particularly in the perinuclear region. This may represent an accumulation of LAGGFP within the TGN or a unique non-endosomal Glut4 pool due to a compromised interaction between the mutant Glut4 transporter and AP-1. Notwithstanding, FAGGFP showed a more complete pattern of overlap with TRT when compared with wild type Glut4-GFP and TRT (figure 3.5A), suggesting that a large proportion of FAGGFP is trapped within the early endosomal system of the cell as well as at the plasma membrane (figure 3.2.2). This result is in agreement with studies in 3T3-L1 adipocytes [219]. Using endosomal ablation Melvin *et al.* showed that in a 3T3-L1 adipocyte cell line stably expressing an F5A (FAG) Glut4 mutant, the majority of the FAG was localised to the recycling endosomal pathway. In combination, these results suggest that the amino terminal FQQI motif functions in trafficking Glut4 from early endosomes.

In conclusion, we made mutant Glut4-GFP cDNA chimeras and transfected them into 3T3-L1 fibroblasts. Mutants containing a phenylalanine to alanine substitution at position 5 (FAG) were predominantly located at the cell surface. Similarly, cells that expressed high levels of Glut4-GFP with leucine to alanine mutations at positions 489 and 490 (LAG), also displayed Glut4 associated GFP fluorescence at the plasma membrane. In contrast, when Glut4-GFP chimeras carrying a serine to alanine mutation at position 488 of the transporter (SAG and DAG) were transfected into fibroblast cells, the pattern of mutant Glut4-GFP fluorescence appeared no different to wild type. Furthermore, we examined the degree of overlap between our mutant Glut4-GFP chimeras and the endosomal marker TRT. The extent of colocalisation between FAGGFP and TRT was substantial when compared to wild type, suggesting that the

majority of intracellular FAGGFP was located within the endosomal system. In contrast there appeared to be very little of the LAGGFP mutant distributed to the endosomal system. These data imply that phenylalanine 5 is crucial to the correct intracellular distribution of Glut4-GFP and the effective trafficking of Glut4 from the endosomal system to a discrete intracellular Glut4 pool in a fibroblast background. Furthermore, when expressed at high levels the dileucine motif of Glut4 also becomes important for the correct intracellular distribution of Glut4. The colocalisation data indicates that the C-terminal dileucine may also be involved in the trafficking of Glut4 away from a unique intracellular vesicle back into the endosomal system. In addition, we found that serine 488 appears to play no part in the extent of distribution of Glut4-GFP into the endosomal system of 3T3-L1 fibroblasts. In common with the results obtained expressing wild type Glut4-GFP, we found that mutant Glut4-GFP when transfected into 3T3-L1 fibroblasts behaves in a similar manner to that seen when expressed in other cell types. This suggests that the cellular machinery required for the typical pattern of wild type or mutant Glut4 distribution is a common feature of many cell types. The components of this cellular machinery that guide Glut4 distribution remain to be identified. Nevertheless, GFP-tagged Glut4 transporters would allow us to study in real time the downstream effects on trafficking of disruption of any one of these components.

3.4.3 *Effect of the acidotrophic agent chloroquine on Glut4-GFP distribution in 3T3-L1 fibroblasts*

The acidotrophic agent chloroquine neutralises the pH. of acidic endosomes when applied to cultured cells. In figure 3.9 we show that chloroquine disrupts the normal pattern of Glut4-GFP distribution in 3T3-L1 fibroblasts with the formation of large intracellular vesicles and Glut4-GFP accumulation at the plasma membrane. This result also lends weight to the suggestion that a portion of the total Glut4-GFP population in 3T3-L1 fibroblasts resides within the acidic endosomal system. On the basis of this result we also speculate on the lowering of blood glucose seen in response to chloroquine in a clinical context [206]. In addition to the prolonged activated insulin receptor complex described by Bevan *et al.*, chloroquine treatment may further improve glucose transport into the cell by impairment of the endosomal recycling pathway and hence cause an increase in glucose transporter levels at the plasma membrane.

3.4.4 *Role of the cytoskeleton in Glut4-GFP distribution in 3T3-L1 fibroblasts*

The role of the cytoskeleton in Glut4-GFP localisation in 3T3-L1 fibroblasts was examined using cytochalasin D, an inhibitor of actin filament assembly [210], and nocodazole [209] to depolymerise microtubules. In figure 3.6 we showed that cytochalasin D and nocodazole are effective at the concentrations used throughout the study. Figure 3.7 shows that incubation of Glut4-GFP-transfected 3T3-L1 fibroblasts in 10 μg/ml nocodazole prior to visualisation causes disruption of the perinuclear compartment in cells expressing either wild type or mutant Glut4-GFP. We therefore conclude that microtubules are needed to maintain the integrity of the perinuclear compartment seen when Glut4-GFP is expressed in 3T3-L1 fibroblasts. Furthermore, there is no longer any evidence of FAGGFP accumulation at the plasma membrane in nocodazole-treated cells, suggesting that microtubules also play a part in FAGGFP displacement to the plasma membrane or to retain the mutant transporter at the cell surface.

3.4.5 *Summary*

To summarise, in this chapter we have shown that Glut4-GFP chimeras are efficiently expressed in 3T3-L1 fibroblasts and display a distinctive pattern of distribution within the cell. The importance of N- and C- terminal targeting motifs to Glut4-GFP localisation and their contribution to sorting within the endosomal system was established. Furthermore, we show conclusive evidence from cells imaged in real time that there are at least two pools of Glut4-GFP within 3T3-L1 fibroblasts; a TRT-positive endosomal pool, and a TRT-negative non-endosomal pool. Finally, we showed that microtubules play an intimate part between Glut4-GFP and its discrete pattern of distribution within the cell. In the next chapter we used the now established power of GFP-based studies to explore Glut4 trafficking in an insulin-responsive cell line.

Chapter 4

4.0.0 Trafficking of GFP-Glut4 in adipocytes.

4.1.0 Introduction.

Insulin stimulates glucose transport in skeletal muscle and adipose tissue by virtue of the expression of the Glut4 glucose transporter isoform [151, 152]. In the absence of insulin, this transporter is predominantly localised to intracellular membranes associated with the endosomal system, the *trans* Golgi network (TGN)[1] and within tubular vesicular elements throughout the cytosol [94, 95, 220, 221]. In response to insulin, there is a rapid redistribution of Glut4 from these locations to the plasma membrane resulting in a dramatic increase in the rate of glucose transport into the cell [94, 95, 220, 221]. Studies using transporter-specific photolabels have shown that Glut4 undergoes continuous recycling between the plasma membrane and intracellular membrane compartments in both the presence and absence of insulin [26, 29, 32, 86, 87].

Green Fluorescent Protein (GFP) [179, 222] from the jellyfish *Aequoria victoria* has revolutionised cell biology, being widely used to 'tag' proteins of interest and study the dynamics of their subcellular trafficking in living cells in real time [222]. Many membrane/membrane associated proteins have been studied using this method, including TGN38 [185], G protein-coupled receptors [187, 223] and proteins which utilise the secretory pathway [186]. As such, GFP fusions allow detailed analysis of the dynamics of the behaviour of membrane proteins in a variety of different experimental circumstances. To that end, we have used a range of GFP-Glut4 chimeras to further study the trafficking of Glut4 in adipocytes.

Using these Glut4-GFP chimeras we aimed to study a number of aspects of Glut4 trafficking. Firstly, we wanted to establish that the distribution and response to insulin of our Glut4-GFP chimeras was the same as described for endogenous Glut4. Once satisfied that the distribution of Glut4-GFP mirrored that of native Glut4 we sought to characterise in real time wild type and mutant Glut4-GFP distribution and movement. Thirdly, we wanted to further characterise the intracellular Glut4 compartment by comparing the distribution of Glut4-GFP with markers for the endosomal, lysosomal system. Finally, we aimed to study the relationship between the Glut4-GFP-containing compartment and the cell cytoskeleton using agents that disrupt microtubule formation.

We show that two chimeras of GFP-Glut4 (GFP at either the N- or C- terminus) localise to intracellular membranes within 3T3-L1 adipocytes and exhibit insulin-dependent translocation to the plasma membrane with kinetics similar to that of the endogenous protein. These chimeras exhibit limited overlap with TfR, appear to recycle between the plasma membrane and intracellular compartment(s) in the absence of insulin, and are localised to compartments distinct from both late endosomes and lysosomes. In contrast to native Glut4, removal of the insulin stimulus or treatment of insulin-stimulated cells with PI3K inhibitors did not result in re-internalisation of either chimera from the plasma membrane, suggesting that the recycling properties of GFP-tagged Glut4 differs from the native Glut4 molecule. We suggest that the recycling pathway utilised by GFP-Glut4 in the absence of insulin is distinct from that used to internalise GFP-Glut4 from the plasma membrane after withdrawal of the insulin stimulus, which may in turn represent distinct pathways for internalisation of endogenous Glut4 in adipocytes.

4.2.0 Materials and Methods.

4.2.1 *Construction of Glut4-GFP chimeras*

The Glut4-GFP constructs used in this study were the same as those described in Chapter 3.

4.2.2 *Insulin-stimulation experiments.*

Prior to experiments, coverslips of microinjected cells were incubated in serum-free DMEM in a CO_2-incubator for 2h. After this time, either insulin (100 nM) or vehicle were added to duplicate plates and the incubation continued for times between 2 and 30 minutes in the incubator. Thereafter, cells were rapidly washed into KRP (130 mM NaCl, 5 mM KCl, 1.2 mM $MgSO_4$, 1.2 mM $CaCl_2$, 20 mM Hepes, 1.2 mM Na_2HPO_4, pH 7.4) containing 10 mM glucose at 37°C and viewed on a Zeiss Axiovert microscope as described below.

4.2.3 *Insulin reversal experiments.*

For analysis of insulin reversal, the following experimental conditions were employed. After stimulation with insulin for 30 minutes as outlined above, cells were washed once with serum-free DMEM at 37°C and then either (i) incubated with anti-insulin antibodies in DMEM exactly as outlined in [224], or (ii) washed repeatedly in KRM buffer (as KRP except the Hepes was replaced with 20 mM MES at pH 6.0) for the times indicated in the figure legends on a hot plate at 37°C prior to microscopic examination. In experiments using PI3K inhibitors, cells were washed in serum-free DMEM at 37°C then incubated in serum-free DMEM containing either wortmannin (50 - 250 nM) or LY294002 (10 μM) for the times indicated in a CO_2 incubator. In order to insure that these conditions effectively reversed insulin action, deGlc transport or Glut4 plasma membrane lawn assays were performed contemporaneously on parallel plates of cells using methods described [100, 107].

4.2.4 *Potassium-depletion experiments.*

Coverslips of cells expressing GFP-Glut4 were washed twice in either KRP or KRP in which the potassium chloride was replaced with sodium chloride, then incubated on a hot plate in 4 ml of the buffer for 2h prior to image capture, which was performed in the same buffer.

4.2.5 *Immunofluorescence analysis of endogenous Glut4.*

Endogenous Glut4 was localised in acetone fixed cells using an antibody against the C-terminus of Glut4. Treated cells grown on glass coverslips were washed with ice cold PBS and then fixed by incubation in ice cold acetone for 5 minutes. Next, fixed cells were washed 3 times with PBS and then washed a further 3 times over a period on 1 hour with PBS/5% goat serum, that served to block non-specific binding sites. Subsequently, coverslips were turned upside down and incubated on parafilm in 100 µl anti-Glut4 antibody diluted 1:200 in PBS/1% goat serum. The cells were then washed 3 times in PBS\1% BSA before incubation with FITC-conjugated secondary antibody, diluted 1:200 in PBS/2.5% goat serum, for 30 minutes. Finally, the cells were washed 3 more times with PBS before mounting onto microscope slides with 15 µl Mowiol. The mounted slides were left to dry overnight before imaging on the confocal microscope using the default FITC settings.

4.2.6 *Statistical Analysis*

Statistical analysis was performed using StatView 4 (Abacus, CA).

4.3.0 Results

4.3.1 *Expression of GFP-Glut4, Glut4-GFP and GFP-Glut1 in 3T3-L1 adipocytes by microinjection and the effects of insulin*

As described in Chapter 2 we were unsuccessful in our attempts to make a 3T3-L1 adipocytes cell line that stably expressed our GFP-Glut4 chimera. Therefore, we chose to express GFP-Glut4 in 3T3-L1 adipocytes transiently. To this end we employed a wide variety of chemical transient transfection strategies. However, each of the methods used gave little or no GFP-Glut4 expression. Consequently, we resorted to direct nucleus microinjection in order to express GFP-Glut4 in 3T3-L1 adipocytes. Although more successful than our attempts with transient transfection, the labour-intensive microinjection approach did somewhat limit the power of our system. As a consequence of the microinjection strategy we were unable to undertake quantitative biochemical experiments and were therefore limited to qualitative fluorescent analysis using the confocal microscope.

The N-terminal GFP Glut4 chimera (GFP-Glu4) and the C-terminal GFP Glut4 chimera (Glut4-GFP) cDNAs were the same as those described in Chapter 3. These cDNAs were microinjected in the nuclei of 3T3-L1 adipocytes and imaged by confocal analysis as described in *Materials and Methods*. In the absence of insulin, GFP-Glut4 and Glut4-GFP displayed a predominantly intracellular localisation (figure 4.1). Upon treatment with 1μM insulin, both GFP-Glut4 and Glut4-GFP translocated to the plasma membrane within a 15 minute time span.

The GFP-tagged Glut1 construct (GFP-Glut1) was made and generously supplied by J. Wakefield in our laboratory. When injected into 3T3-L1 adipocytes the distribution of Glut1-GFP was noticeably different from the GFP-tagged Glut4 chimeras (figure 4.1). In the basal state GFP-Glut1 was observed at both the plasma membrane and within intracellular structures. Upon treatment with insulin, there was little evidence of GFP-Glut1 translocation to the plasma membrane. Quantification of the extent of insulin-stimulated translocation of GFP-Glut4, Glut4-GFP and GFP-Glut1 is presented in figure 4.1.

4.3.2 *Effects of nocodazole and chloroquine on GFP-Glut4 distribution in 3T3-L1 adipocytes*

The microtubule-disrupting drug nocodazole was added directly to the media of Glut4-GFP-injected 3T3-L1 adipocytes at a concentration of 10 μg/ml. Following an hour-long incubation, nocodazole caused disruption of punctate Glut4-GFP-containing vesicles and dispersal of the Glut4-GFP positive perinuclear compartment (figure 4.2). In addition, some accumulation of Glut4-GFP at the plasma membrane was observed in nocodazole-treated cells. When the acidotrophic agent chloroquine was added to injected adipocytes, the intracellular Glut4-GFP vesicles appeared swollen and a portion of the Glut4-GFP population was observed to accumulate at the plasma membrane (figure 4.2).

4.3.3 *Colocalisation of GFP-Glut4 with Texas Red Transferrin or Lysotracker-Red®*

In order to further characterise the Glut4-GFP intracellular compartment we performed colocalisation experiments between Glut4-GFP and the early endosomal marker Texas Red Transferrin (TRT) or Lysotracker® to identify the late endosomes/lysosomes. Glut4-GFP-injected adipocytes were incubated with TRT or Lysotracker® and analysed by confocal microscopy (figure 4.3). In all experiments, only partial overlap between Glut4-GFP and the Texas Red Transferrin itinerary was observed. Even less colocalisation was evident when the Glut4-GFP pattern of distribution was compared with intracellular Lysotracker®.

4.3.4 *FAG-GFP and LAG-GFP exhibit distinct localisation*

3T3-L1 adipocytes were microinjected with plasmid DNA encoding either FAG-GFP or LAG-GFP and incubated for 24h prior to analysis. Shown are representative cells expressing FAG-GFP or LAG-GFP.(figure 4.4.1) The cells shown are representative of >10 experiments of this type. In all cells observed, FAG-GFP accumulated at the plasma membrane of 3T3-L1 adipocytes. Similarly, in LAG-GFP-injected cells, LAG-GFP accumulated at the plasma membrane in adipocytes displaying high levels of GFP chimera expression, as judged by the relative intensity of GFP-associated fluorescence. In addition, a pronounced LAG-GFP-containing perinuclear compartment was observed.

4.3.5 *DAG-GFP and SAG-GFP distribution and the effects of insulin*

The SAG-GFP and DAG-GFP constructs carry a mutation in the serine 488 phosphorylation site of Glut4. SAG carries an S488A and DAG a S488D mutation. When these chimeras were expressed in 3T3-L1 adipocytes, the pattern of intracellular distribution as analysed by confocal microscopy was indistinguishable from wild type Glut4-GFP (figure 4.4.1). Furthermore, upon stimulation with insulin at 37°C in a CO_2 incubator, both DAG-GFP and SAG-GFP were observed to translocate to the plasma membrane (figure 4.4.2). In each case the proportion of total DAG-GFP/SAG-GFP that translocated to the plasma membrane and the time course of movement was very similar to Glut4-GFP.

4.3.6 *Colocalisation of GFP-tagged FAG, LAG, DAG and SAG with Texas Red Transferrin*

Analogous to the experiments described with Glut4-GFP, GFP-tagged FAG, LAG, DAG and SAG were colocalised with Texas Red Transferrin (TRT). The degree of colocalisation between FAG-GFP and TRT was considerable (figure 4.5A), and the areas of overlap more extensive than between Glut4-GFP and TRT (figure 4.3). In contrast, the extent of colocalisation between LAG-GFP and TRT (figure 4.5B) appeared much less marked when compared to Glut4-GFP and TRT (figure 4.3), especially in the environs of the LAG-GFP perinuclear compartment. When the same type of experiment was performed using GFP-tagged DAG and SAG chimeras (figure 4.6), the extent of overlap with the TRT itinerary was indistinguishable from Glut4-GFP and TRT at this level of resolution.

4.3.7 *Reversal of insulin-stimulated glucose transport and Glut4 translocation in 3T3-L1 adipocytes by low pH washing or wortmannin treatment*

For comparison with Glut4-GFP internalisation following insulin treatment we examined the effctes of reversal of insulin-stimulated glucose transport and endogenous Glut4 translocation in 3T3-L1 adipocytes. Cells were treated with 100 nM insulin for 30 minutes and then assayed for glucose transport following a low pH wash or wortmannin treatment (figure 4.7). In addition plasma membrane lawn assays were performed under similar conditions to measure the extent of Glut4 translocation. As expected both of

these methods were shown to reverse insulin-stimulated glucose transport and Glut4 translocation in wild-type 3T3-L1 adipocytes.

4.3.8 *GFP-Glut4 is not internalised after insulin withdrawal*

3T3-L1 adipocytes were microinjected with DNA encoding GFP-Glut4 and incubated for 24 h. Cells were then incubated in serum-free DMEM for 2h, then insulin was added (100 nM) for a further 30 minutes to induce GFP-Glut4 translocation. To test the ability of GFP-Glut4 to reinternalise following insulin stimulation we then *either* (a) transferred cells to a hot-plate at 37°C and rapidly washed in KRM buffer, pH 6 for 0, 30 or 60 min. Or, (b) transferred to a hot plate and washed into KRP buffer ± 50 nM wortmannin and incubated for 60 min prior to image analysis (figure 4.8). The results show that following a low pH wash or wortmannin treatment, GFP-Glut4 is still not reinternalised from the plasma membrane to any significant extent.

4.3.9 *Potassium-depletion results in the accumulation of GFP-Glut4 at the plasma membrane.*

To examine whether GFP-Glut4 recycles between the intracellular Glut4-storage vesicle and the plasma membrane we incubated GFP-Glut4-injected adipocytes in K^+-depleted buffer. 3T3-L1 adipocytes expressing GFP-Glut4 were washed into KRP either with or without K^+. After a 2 hour incubation on a 37°C hot-plate the cells were imaged by confocal microscopy. Cells from each of the two conditions are shown in figure 4.9. Substantial increases in levels of plasma membrane-associated GFP-Glut4 fluorescence were observed in cells pre-incubated in the K^+-depleted buffer. To ensure that endogenous Glut4 also accumulates at the plasma membrane under the same conditions, 3T3-L1 adipocytes were incubated in K^+-depleted buffer and then analysed by whole cell immunofluorescence as described in *Materials and Methods*. Similar to our findings in GFP-Glut4 expressing cells, endogenous Glut4 also accumulated at the plasma membrane when incubated in a K^+-depleted buffer (figure 4.9).

4.4.0 *3-D reconstructions and time-lapse movies*

3-D reconstructions and time lapse movies of 3T3-L1 adipocytes injected with Glut4-GFP cDNAs are available on the accompanying CD-ROM. For a complete index of all files on the CD-ROM see the accompanying *Word* document.

Panel A

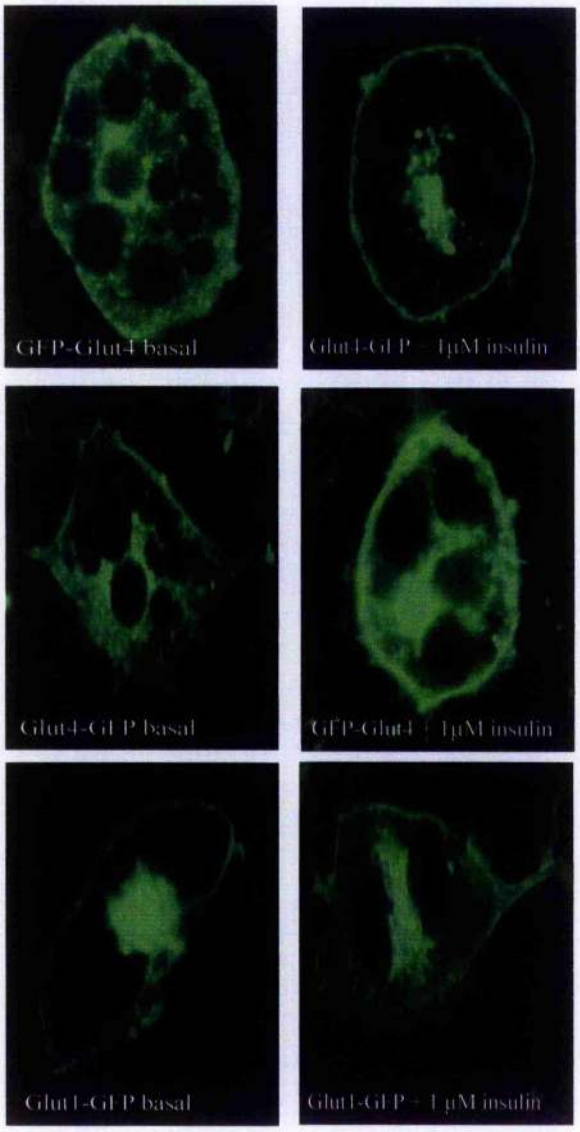

Panel B

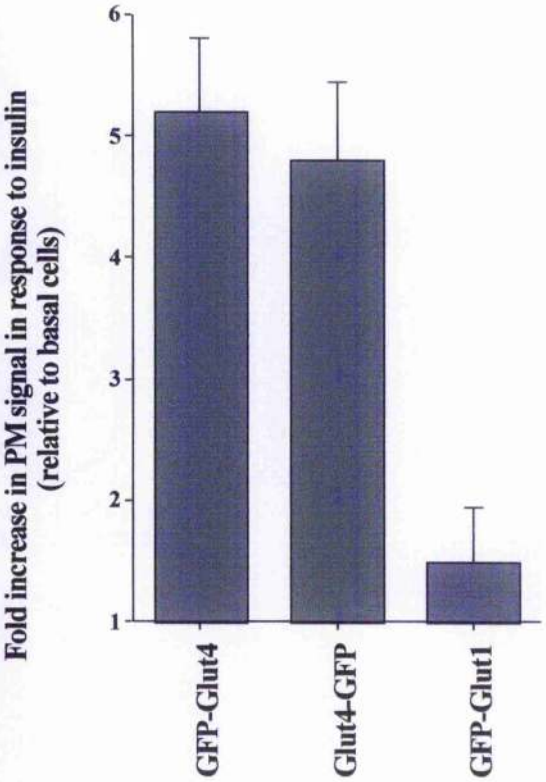

Figure 4.1 Expression of GFP-Glut4, Glut4-GFP and GFP-Glut1 in 3T3-L1 adipocytes and the effcets of insulin

3T3-L1 adipocytes were microinjected with plasmid DNA encoding the GFP-chimera indicated on the figures. After 24 h incubation in DMEM containing 10% foetal bovine serum, cells were incubated in serum-free DMEM for 2h. Insulin or vehicle were added directly to the DMEM in a CO_2 incubator for times from 5 to 60 minutes. The microinjected cells were then washed into KRP buffer containing 10 mM glucose and imaged by confocal microscopy as described using the 488 nm laser for excitation of the GFP. Shown in Figure *Panel A* are representative cells expressing the different GFP-chimeras incubated +\- insulin for 30 min. Quantification of several experiments of this type to determine the fold increase in plasms membrane associated GFP-Glut4 is shown in *Panel B.* In these experiments, the amount of GFP-Glut at the plasma membrane is expressed as a percentage of the total cellular GFP-Glut, calculated as outlined in *Materials and Methods.* The modest increase in plasma membrane-associated GFP-Glut1 was not statistically significant. For both GFP-Glut4 and Glut4-GFP, in the absence of insulin, only ~10% of the total cellular GFP signal was localised to the plasma membrane. In contrast, for GFP-Glut1, ~40% of the total cellular GFP signal was plasma membrane localises in the basal state.

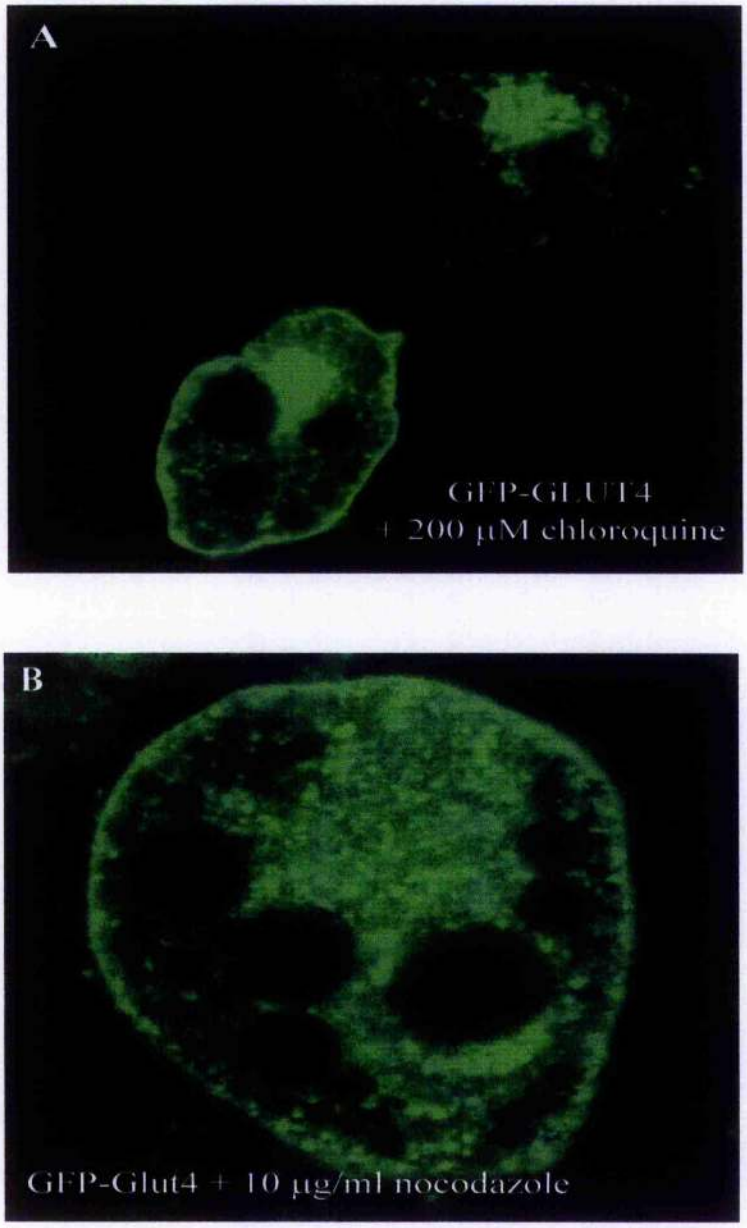

Figure 4.2 Disruption of GFP-Glut4 distribution by chloroquine or nocodazole

GFP-Glut4-injected 3T3-L1 adipocytes were treated with either 200 μM of the acidotrophic agent Chloroquine (A) or 10 μg/ml of the microtubule-disrupting drug nocodazole (B) prior to analysis by confocal microscopy.

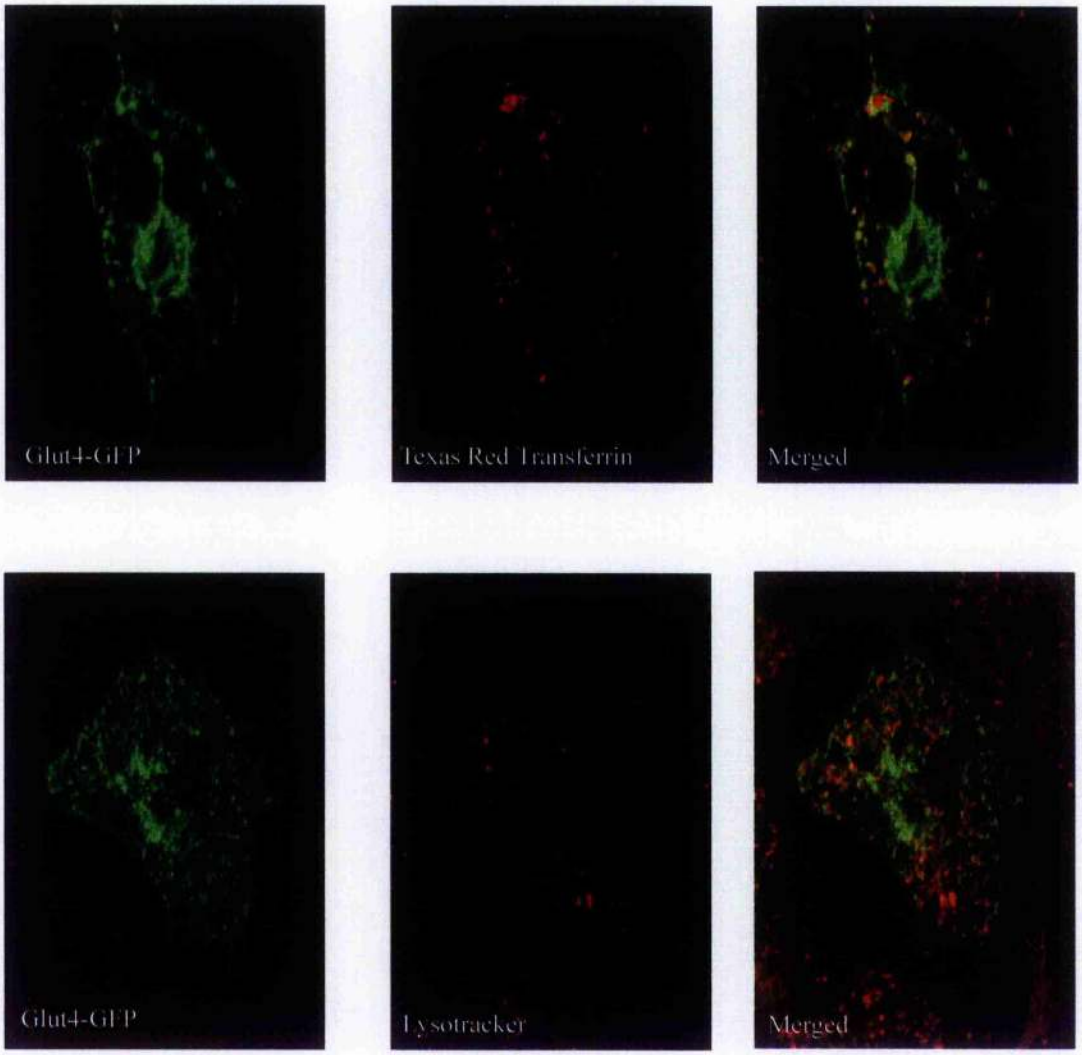

Figure 4.3 Colocalisation of GFP-Glut4 with Texas Red Transferrin or Lysotracker

After a 2 h incubation in serum-free DMEM, 3T3-L1 adipocytes expressing GFP-Glut4 were further incubated in serum-free DMEM containing either Texas Red Transferrin (20μg/ml) or Lysotracker-Red (50 nM) for 30 minutes at 37°C in a CO_2 incubator. Thereafter, cells were gently washed in KRP/glucose, transferred to the heat microscope stage at 37°C and images collected using confocal microscopy as outlined. (Figure 2) Shown in the left panel is the GFP-Glut4 signal (excitation 488 nm laser, filter 505-520 nm band pass), the middle panel is the corresponding signal from the Texas Red Transferrin or Lysotracker-Red® (excitation using 545 nm laser, long-pass 590 nm filter). The right hand panel is the merged image. The cells shown are representative of at least 5 experiments of this type. Areas of the cell where there is pronounced overlap between the GFP and Teaxs Red signals are indicated by yellow in the merged images.

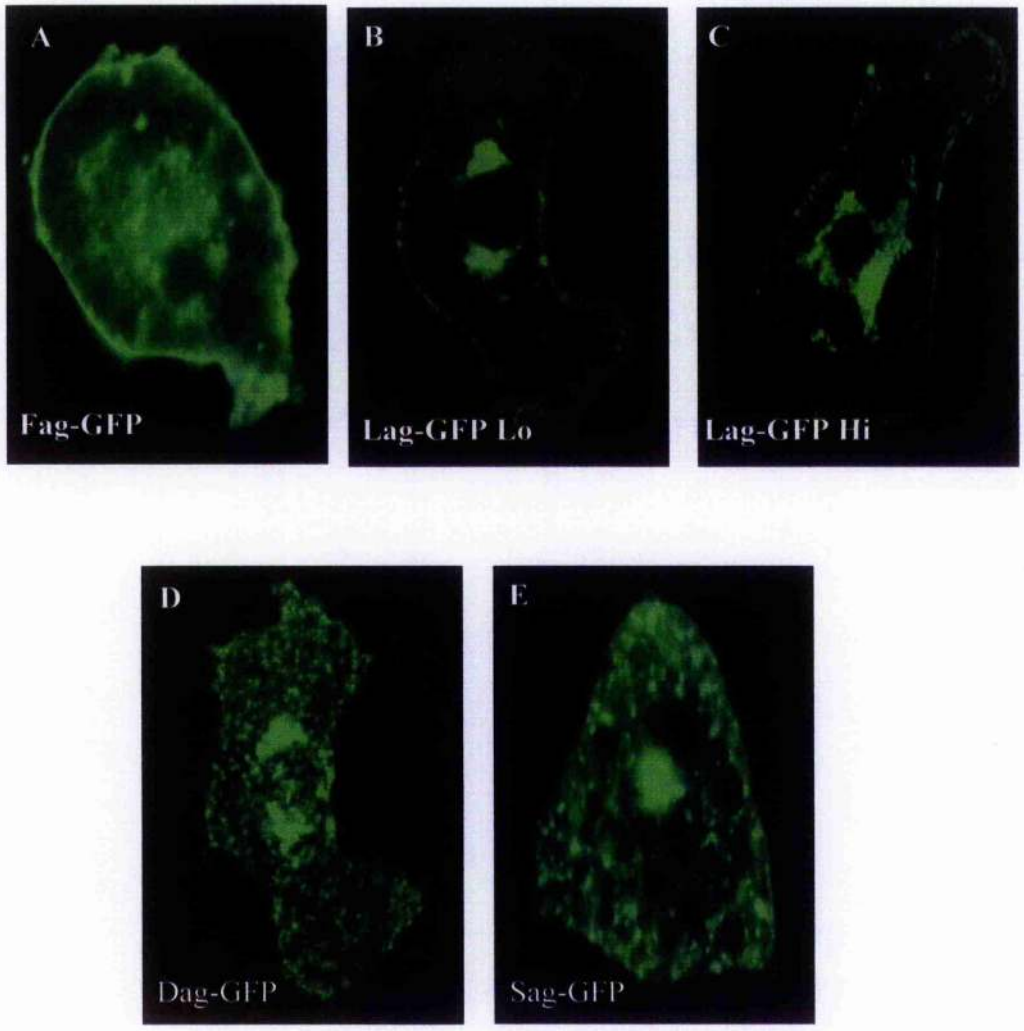

Figure 4.4.1 Distribution of FAG-, LAG-, DAG- and SAG-GFP in 3T3-L1 adipocytes

The GFP-tagged Glut4 cDNA mutants FAG (F5A, panel A), LAG (L489A, L490A, panel B), DAG (S488D, panel C), and SAG (S488A, panel D) were microinjected into the nucleus of 3T3-L1 adipocytes and anaysed 24 hours later by confocal microscopy LAG-GFP Hi and LAG-GFP Lo were cells judged to express high and low levels of LAG-GFP protein respectively.

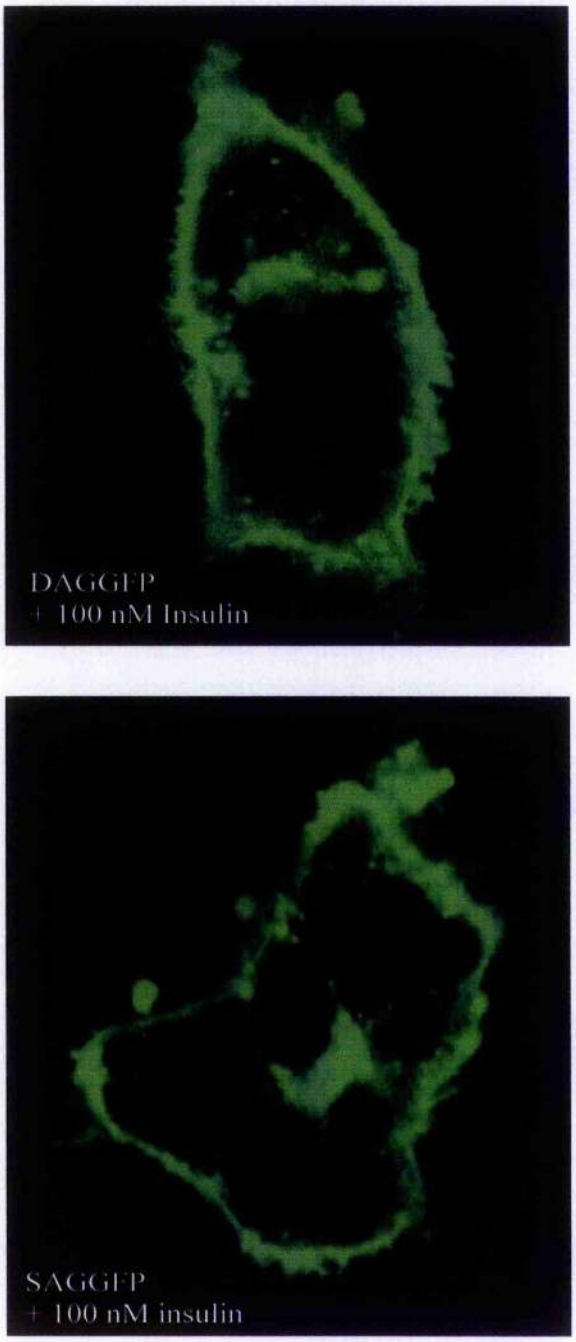

Figure 4.4.2 DAG-GFP and SAG-GFP tranaslocate to the plasma membrane in response to insulin

DAG-GFP and SAG-GFP were microinjected into 3T3-L1 adipocytes and treated with 100 nM insulin. Cells were then analysed by confocal microscopy. Both DAG-GFP and SAG-GFP displayed insulin-induced movement to the plasma membrane. This data suggests that Ser 488 is not critical for the translocation process.

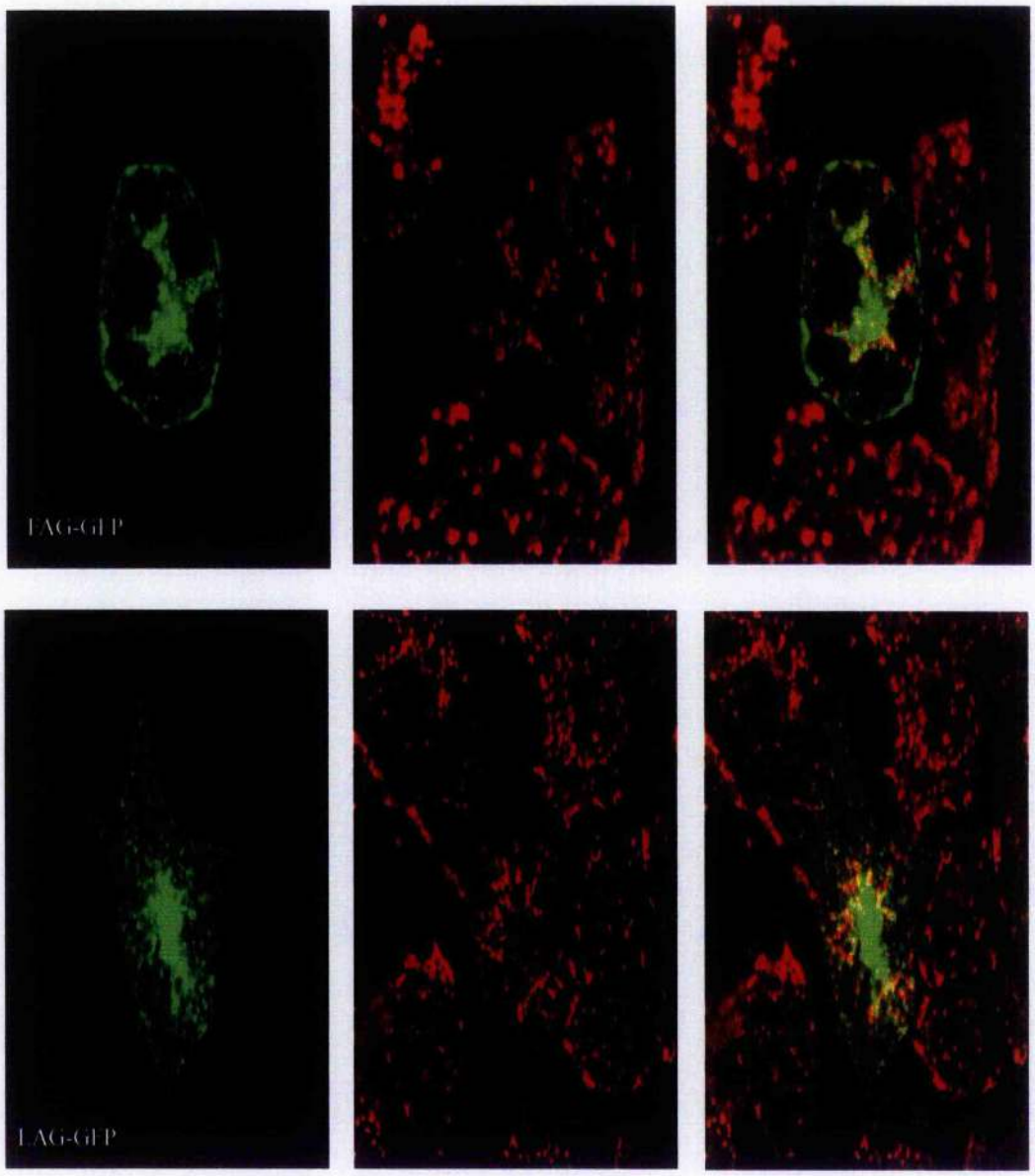

Figure 4.5 FAG-GFP and LAGGFP colocalise with Texas Red Transferrin to different extents

FAG-GFP (A) and LAG-GFP (B) were microinjected into 3T3-L1 adipocytes and their subcellular distributions compared with the early endosomal marker Texas Red Transferrin (TRT). The green left hand panel represents GFP-associated fluorescence, while the red centre panel shows the TRT marker. The merged right hand panel shows the overlap between GFP and TRT in the same cell. Regions where the colocalisation between GFP and TRT are greatest show as yellow on the merged image. The overlap between FAG-GFP and TRT was considerable, suggesting that FAG-GFP is distributed to early endosomes. However, the degree of colocalisation between LAG-GFP and TRT was judged to be even less than between Glut4-GFP and TRT.

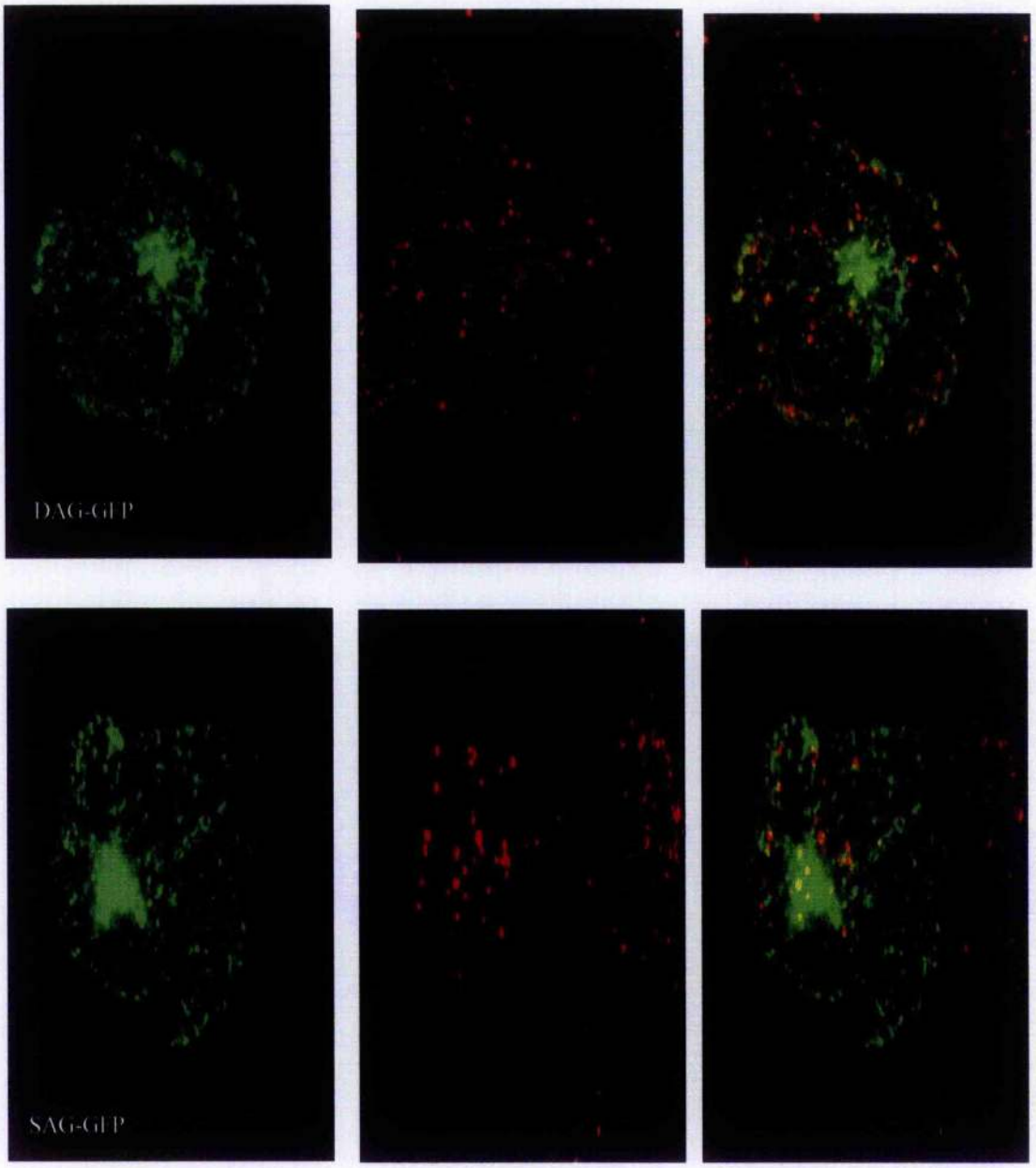

Figure 4.6 The degree of colocalisation between DAG- or SAG- GFP and Texas Red Transferrin is the same as between Glut4-GFP and TRT

DAG-GFP (A) and SAG-GFP (B) were microinjected into 3T3-L1 adipocytes and their subcellular distributions compared with the early endosomal marker Texas Red Transferrin (TRT). The green left hand panel represents GFP-associated fluorescence, while the red centre panel shows the TRT marker. The merged right hand panel shows the overlap between GFP and TRT in the same cell. Regions where the colocalisation between GFP and TRT are greatest show as yellow on the merged image. When compared to the overlap between Glut4-GFP and TRT (Figure 4.3), an equivalent degree of colocalisation is observed between DAG- or SAG-GFP and TRT in 3T3-L1 adipocytes.

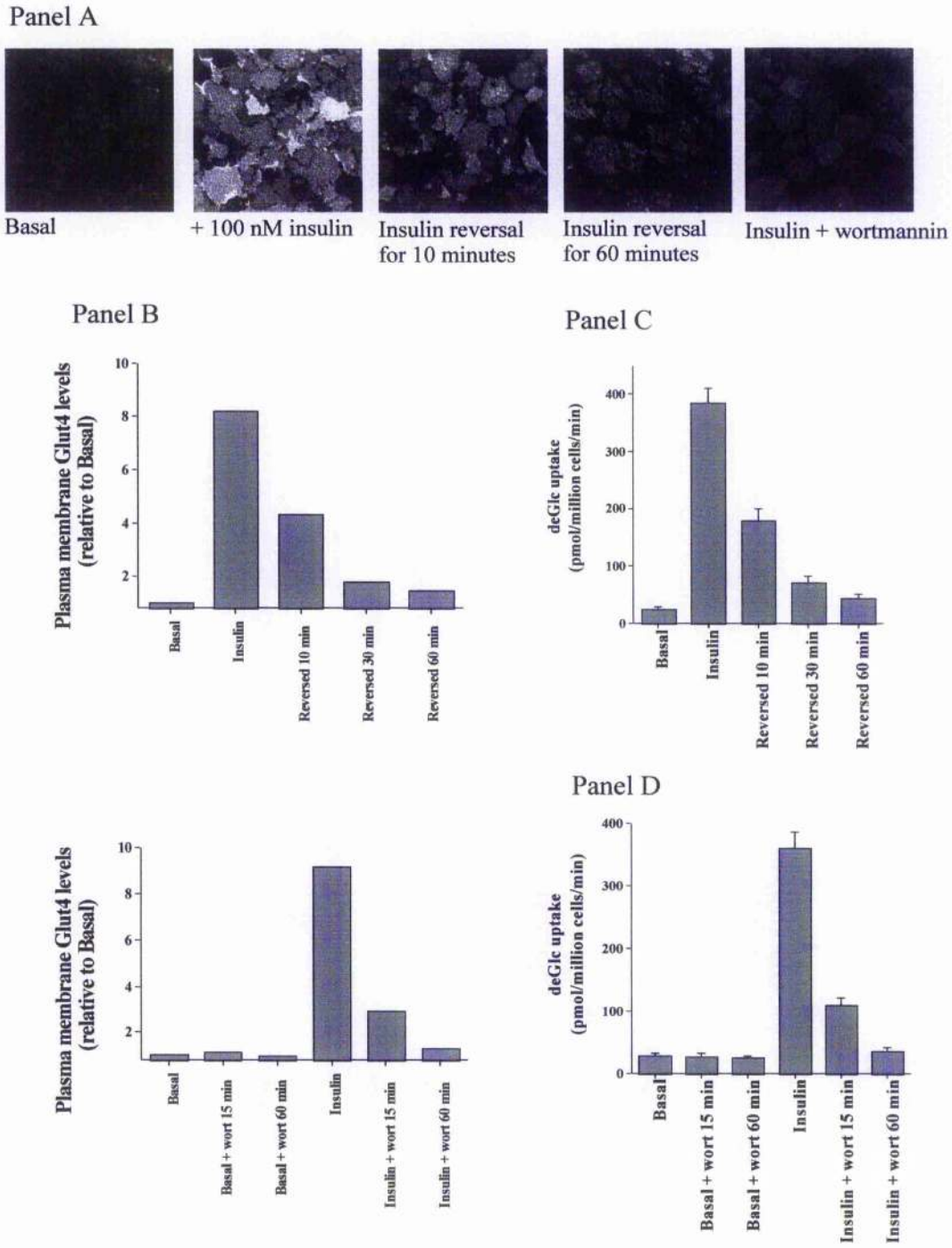

Figure 4.7 Reversal of insulin-stimulated glucose transport and Glut4 translocation in 3T3-L1 adipocyte by low pH washing or wortmannin treatemnt

3T3-L1 adipocytes were incubated in serum-free DMEM for 2h, then insulin was added (100nM) for a further 30 minutes. After this time, cells were transferred to a hot-plate at 37°C and rapidly washed in KRM buffer, pH 6 for the times shown then plasma membrane lawn assays for Glut4 were performed, presented in *panel A* Quantification of the data in *panel A is* shown in panel B. Cells were assayed for glucose uptake (*panel C*) under similar conditions. In *panel D,* the effect of addition of 50 nM wortmannin for the times indicated on basal and insulin-stimulated deoxyglucose transport is shown. (Note that the work shown in this diagram was performed by Dr. Kate Powell).

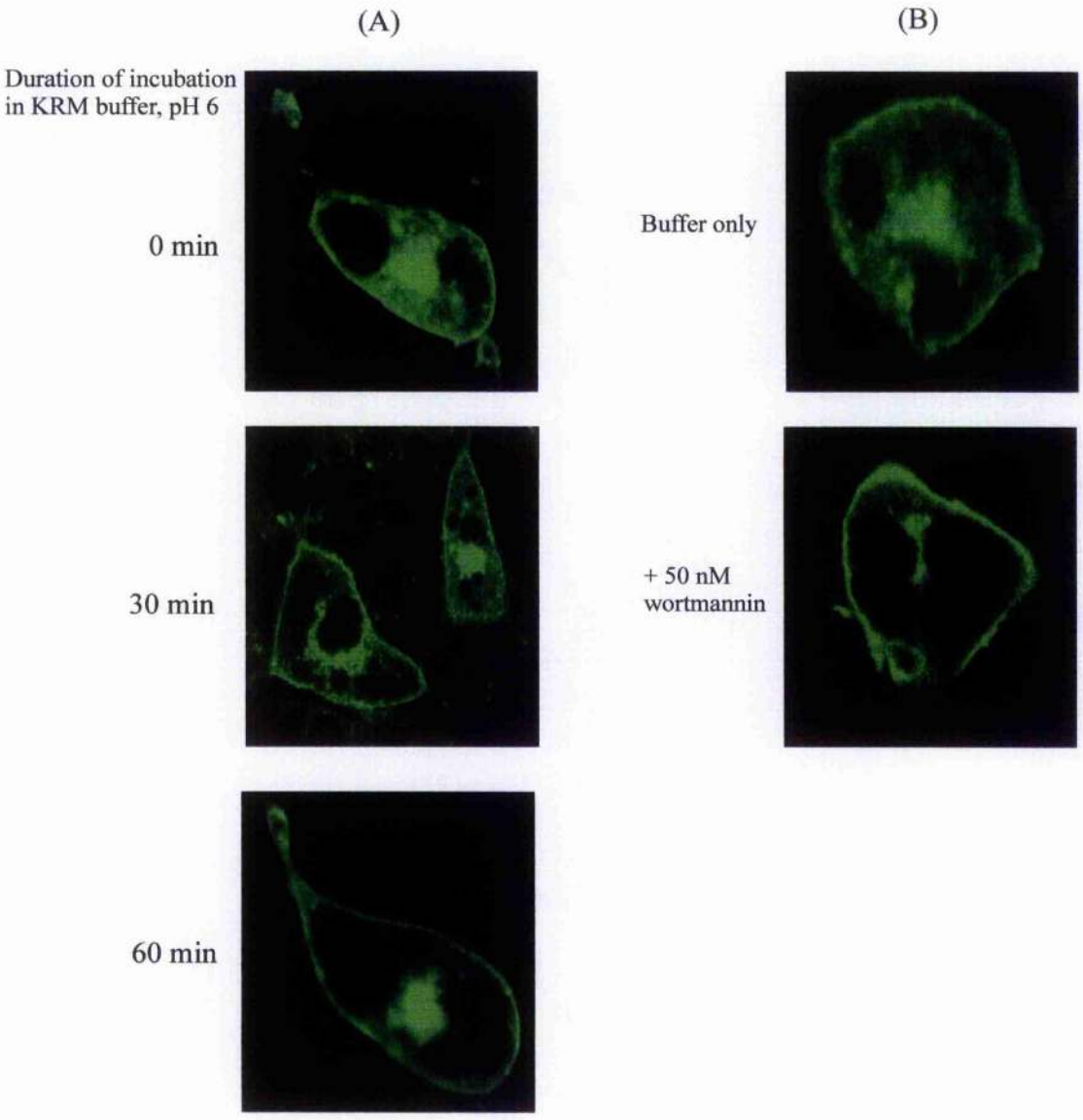

Figure 4.8 GFP-Glut4 is not internalised after insulin withdrawal.
3T3-L1 adipocytes were microinjected with DNA encoding GFP-Glut4 and incubated for 24 h. Cells were then incubated in serum-free DMEM for 2h, then insulin was added (100 nM) for a further 30 minutes. After this time, cells were *either* (a) transferred to a hot-plate at 37°C and rapidly washed in KRM buffer, pH 6 for 0, 30 or 60 min as indicated on the figures *or* (b) transferred to a hot plate and washed into KRP buffer ± 50 nM wortmannin and incubated for 60 min prior to image analysis. The cells shown are representative of three (low pH wash) or four (wortmannin) experiments of this type, in each experiment >10 injected cells were examined. Quantification of the fluorescence signal in defined areas of plasma membrane as a fraction of the total cellular fluorescence of many experiments of this type revealed that there was no significant loss of GFP-Glut4 fluorescence signal during the internalisation experiments (i.e. the plasma membrane/total cellular fluorescence signal was unaffected by the experimental manipulations shown).

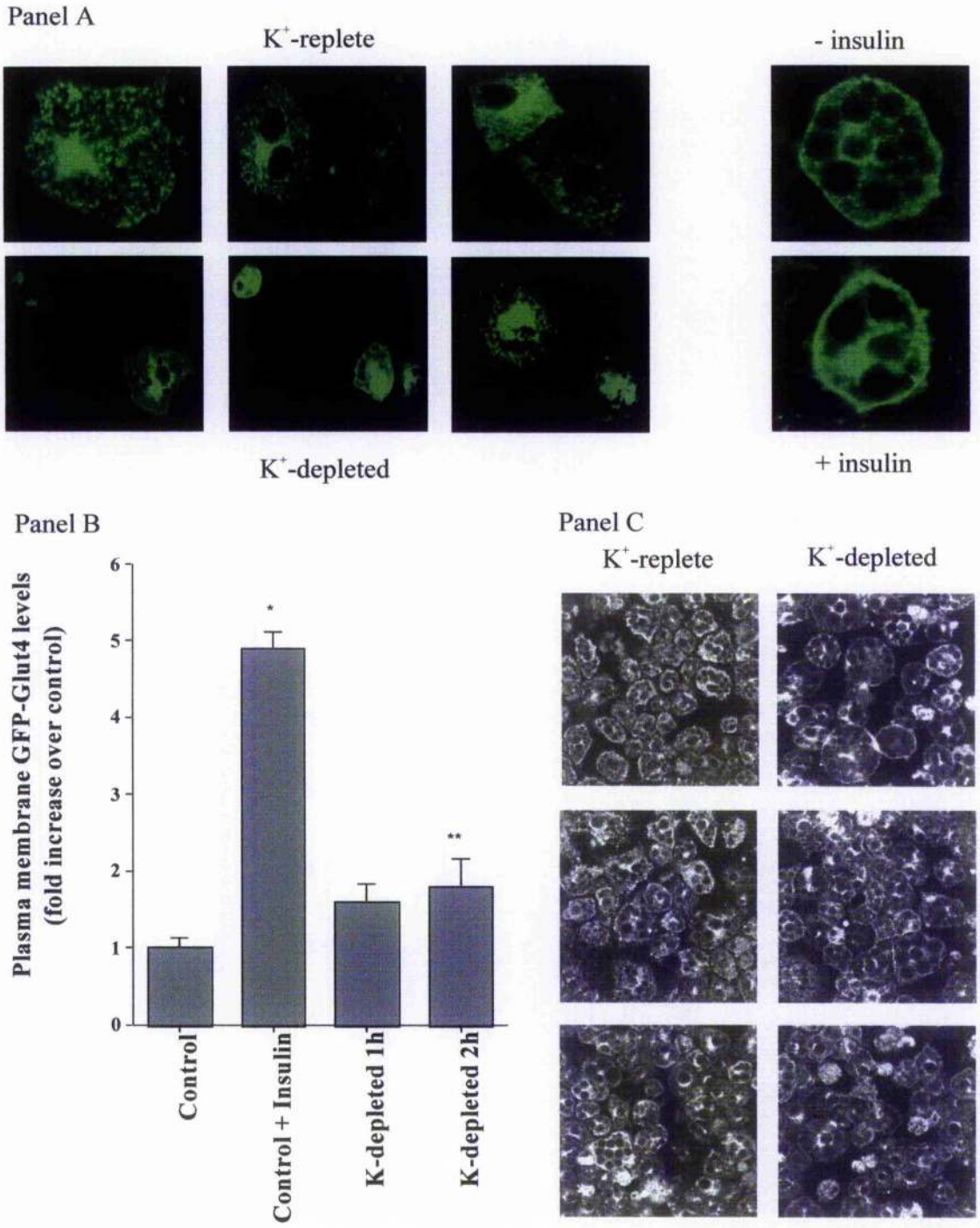

Figure 4.9 Potassium-depletion results in the accumulation of GFP-Glut4 at the plasma membrane. 3T3-L1 adipocytes expressing GFP-Glut4 were washed into KRP either with or without K^+. After 2 h incubation in this buffer on a hot-plate, cells were imaged by confocal microscopy in the same buffer using the 488 nm laser for excitation of the GFP (figure 6). Shown in *Panel A* are representative cells from each of the two conditions. In the cells incubated in K^+-depleted buffer, we observed increased GFP-Glut4 at the plasma membrane in 92% of the cells examined (n=76 cells in three experiments). *Panel B* shows the results of quantification of the level of GFP-Glut4 at the plasma membrane after either 1 or 2 h incubation in potassium-depleted buffer, expressed as a fold increase over the levels of GFP-Glut4 at the plasma membrane in control cells incubated in the same buffer with potassium. For comparison, the level of GFP-Glut4 at the plasma membrane in insulin-stimulated cells is also shown. * indicates a significant increase over Control cells ($p=0.005$), and **$p<0.05$. *Panel C* shows the accumulation of endogenous Glut4 at the cell surface in 3T3-L1 adipocytes treated exactly as outlined above for GFP-Glut4 injected cells (data from a representative experiment, repeated with similar results, is shown).

4.5.0 Discussion.

Insulin stimulates glucose disposal in peripheral tissues by virtue of the expression of the Glut4 glucose transporter isoform [151, 152, 225]. In the absence of insulin, this transporter is intracellularly sequestered within the elements of the endosomal system, the *trans* Golgi network and a specialised storage compartment [94, 95, 220, 221]. Glut4 is re-distributed from these intracellular locations to the plasma membrane in response to insulin [94, 95, 220, 221]. This paradigm of regulated membrane trafficking has been investigated using a range of methodologies, including transporter-specific photolabels, which have established that Glut4 undergoes continuous recycling between the plasma membrane and intracellular locations, even in the presence of insulin [26, 29, 32, 86, 87, 89, 129]. Upon removal of the insulin signal, Glut4 is effectively sequestered within the cell, and leaves the plasma membrane with a half-time of about 6 to 7 min. However, the mechanism(s) of this trafficking event remain poorly understood.

With the aim of addressing this, we have engineered two chimeric species between Glut4 and GFP. In the first, GFP is fused in frame at the N-terminus of Glut4 (termed GFP-Glut4) and a second with GFP fused in frame at the C-terminus of the protein (termed Glut4-GFP). These cDNAs were expressed in fully differentiated 3T3-L1 adipocytes by microinjection and exhibited similar patterns of intracellular expression in the absence of insulin (figure 4.1). As shown, fluorescence was observed in a perinuclear compartment and also in multiple punctate structures throughout the cytosol in a pattern reminiscent of native Glut4 identified in these cells. In response to insulin, both of these species exhibited extensive redistribution to the plasma membrane resulting in a continuous ring of fluorescence around the perimeter of the cell (figure 4.1). In our hands, translocation of both GFP-Glut4 and Glut4-GFP to the plasma membrane in response to insulin was consistently observed after stimulation of cells with insulin in a CO_2 incubator (figure 4.1). This translocation was rapid, maximal redistribution was achieved within 15 minutes of exposure to insulin (data not shown), consistent with studies of the endogenous Glut4 protein in these cells [226]. Under these conditions, we routinely observed insulin-stimulated translocation in >95% of cells expressing GFP-tagged Glut4.

This pattern of intracellular localisation and insulin-dependent re-distribution is specific for GFP-tagged Glut4. A chimeric Glut1-GFP species was found to distribute

between the plasma membrane and intracellular membranes in the absence of insulin, a distribution well characterised for this isoform, and did not exhibit extensive translocation to the plasma membrane (figure 4.1), consistent with studies of the endogenous isoforms in 3T3-L1 adipocytes [226]. Quantification of the extent of insulin-stimulated translocation of GFP-Glut4, Glut4-GFP and GFP-Glut1 is presented in figure 4.1. In our hands, GFP-Glut4 and Glut4-GFP behave identically. Therefore, in all that follows, we show data using GFP-Glut4, but note that all experiments have been replicated using Glut4-GFP with identical results. Collectively, this data argues that the trafficking signals dictating the specific sorting of Glut4 and Glut1 are recognised in the context of these chimeras.

Following on from our experiments in 3T3-L1 fibroblasts (Chapter 3) we examined the extent of the relationship between Glut4-GFP and microtubules in adipocyes. To this end we employed the microtubule depolymerising agent nocodazole (figure 3.6). Similar to the results in fibroblasts (Chapter 3, figure 3.7), we found that incubation of 3T3-L1 adipocytes in media containing 10 μg/ml nocodazole caused dispersion of the distinctive Glut4-GFP-containing perinuclear compartment and vesicles throughout the cytoplasm (figure 4.2). Furthermore, we saw evidence of increased levels of GFP-Glut4 at the plasma membrane. This evidence suggests that microtubules play at least some part in the basal distribution of Glut4-GFP in both 3T3-L1 adipocytes and fibroblasts. Furthermore, our data suggests that microtubules may be involved in the basal recycling of GFP-Glut4 in adipocytes since nocodazole causes GFP-Glut4 to accumulate at the plasma membrane. The involvement of microtubules in Glut4-GFP targeting is paralleled by work studying adenosine receptor and transferrin receptor distribution.[209, 227]. Saunders *et al.* observed a relocalisation of the adenosine receptor in reponse to nocodazole. Interestingly, Saunders *et al.* also found that adenosine receptor distribution was selective for microtubule-disrupting agents, since cytochalasin D, which disrupts actin polymerisation, did not alter adenosine receptor targeting. When examining transferrin receptor (TfR) trafficking, Jin *et al.* noted that nocodazole caused a 50% increase in the level of surface TfR, which was due to a change in receptor dynamics [209]. The endocytosis rate in treated cells was 20% of control, indicating that TfR endocytosis via clathrin-coated vesicles was slowed, whereas the recycling of internalised receptors to the cell surface was unaffected. We know that Glut4 is also endocytosed via clathrin-coated pits [131, 228] and from our

own data appears to partially colocalise with the TfR. Therefore, if disruption of microtubules also slows Glut4-GFP endocytosis in 3T3-L1 adipocytes it would readily explain the accumulation of Glut4-GFP at the plasma membrane in response to nocodazole.

In order to study the effect of endosomal pH. neutralisation on Glut4-GFP distribution, cultured 3T3-L1 adipocytes were treated with the acidotrophic agent chloroquine (figure 4.2) [204]. Similar to results obtained in 3T3-L1 fibroblasts, (Chapter 3, figure 3.9) we observed that the intracellular Glut-GFP-containing vesicles appeared swollen and in the majority of cells a portion of the total Glut4-GFP population was displaced to the plasma membrane following chloroquine treatment. This further supports the suggestion that at least some of the intracellular Glut4-GFP pool resides within acidic endosomes. From studies by Holman *et al.* using a bismannose photolabel to elucidate insulin-regulated Glut4 subcellular trafficking kinetics, we know that Glut4 undergoes continuous recycling between the plasma membrane and the cell interior in both the presence and absence of insulin [29]. Therefore, we speculate that Glut4-GFP may accumulate at the cell surface in chloroquine treated cells when recycling through the acidic endosomes is compromised.

In an effort to glean further insight into the relationship of the Glut4 storage compartment(s) and other membrane compartments, we used a series of fluorescence dyes to identify other subcellular compartments in GFP-Glut4 expressing cells. Specifically, we employed Texas red-labelled transferrin to identify the TfR itinerary and Lysotracker-red to identify acidic compartments (late endosomes/lysosomes). As shown in figure 4.3, these compounds are effectively internalised into cells expressing GFP-Glut4. Previous research suggests that a significant proportion of the intracellular Glut4 resides in a spatially distinct compartment from TfR in both adipocytes and muscle [97-99, 151, 220]. The only partial colocalisation of GFP-Glut4 or Glut4-GFP with Texas-Red Tf (figure 4.3) provides support for these observations, and further suggests that the localisation of the GFP-Glut4 chimeras studied here is accurately reflecting the localisation of the endogenous protein. The data of figure 4.3 further extends our understanding of Glut4 localisation in that there is no significant overlap between either GFP-Glut4 construct and Lysotracker-Red®, strongly implying that Glut4 is not significantly localised within the late endosomal/pre-lysosomal network.

We also studied mutant Glut4 species using this approach (figure 4.4.1) [219, 229, 230]. FAG-GFP was observed to localise predominantly to the plasma membrane, in

agreement with studies of epitope tagged FAG stably expressed in these cells [229]. LAG-GFP expression was observed both intracellularly and in part at the plasma membrane (figure 4.4.1). In contrast, the DAG-GFP and SAG-GFP mutants primarily displayed an intracellular distribution within punctate vesicles similar to the wild type Glut4-GFP construct (figure 4.4.1). Furthermore, DAG-GFP and SAG-GFP moved to the plasma membrane in response to insulin (figure 4.4.2), indicating that the Glut4 serine 488 phosphorylation site is not essential to the translocation process. These results are in good agreement with a range of studies which have examined the subcellular distribution of similar Glut4 mutants [229-231]. Collectively, these data argue strongly that the intracellular localisation of GFP-Glut4 faithfully replicates the distribution of the endogenous protein, and that the targeting signals within Glut4 are similarly recognised within the context of the GFP-Glut4 species.

The overlap between the mutant Glut4-GFP species and the TfR itinerary was also examined by dual wavelength confocal microscopy (figures 4.5 and 4.6). Reminiscent of the findings in 3T3-L1 fibroblasts described in chapter 3 (figure 3.5), the degree of overlap between FAG-GFP and TfR was considerable, whereas the overlap between LAG-GFP and TfR appeared negligible (figure 4.5). This result is in good agreement with work by Melvin *et al.* [219] using the Transferrin-HRP endosomal ablation technique to study FAG and LAG distribution in 3T3-L1 adipocytes. Melvin *et al.* found that in basal adipocytes 40% of Glut4 is ablated following Tf-HRP loading. In contrast, they found that in stable cell lines expressing FAG or LAG that almost all or virtually none respectively of the mutated Glut4 was localised to the ablated endosomal compartment. In the context of this additional biochemical data, our results imply that the amino terminal FQQI motif functions in trafficking Glut4 from early endosomes whereas the di-leucine motif is involved in sorting Glut4 from a separate intracellular compartment such as the TGN.

Colocalisation of DAG or SAG-GFP with TfR revealed that the extent of overlap was very similar to that observed between Glut4-GFP and TfR (figure 4.6). Again this is very similar to the observed distribution of SAG and DAG-GFP in fibroblasts (Chapter 3, figure 3.4) and largely agrees with another study that has characterised SAG in 3T3-L1 adipocytes [230]. In stably transfected adipocytes Marsh et *al.* showed that SAG trafficking was not significantly different from that of Glut4. In the basal state SAG displayed an intracellular distribution, translocated to the plasma membrane in response to insulin and was only partially ablated when cells were loaded

with Tf-HRP. All of these results are confirmed in our own studies using SAG-GFP and the endosomal marker Texas Red Transferrin. In addition, using immunoelectron microscopy, Marsh *et al.* showed that Glut4 is localised to intracellular vesicles containing the Golgi-derived g-adaptin subunit of AP-1 [232] and that this localisation is enhanced when Ser-488 is mutated to alanine. This result would prove difficult to corroborate in our own system due to the limits of resolution allowed by GFP and confocal microscopy.

Using this system, we have demonstrated insulin-dependent translocation of GFP-Glut4 to the plasma membrane when cells were treated with insulin in an incubator prior to image analysis (figure 4.1). We therefore set out to examine the ability of GFP-Glut4 and Glut4-GFP to re-internalise from the plasma membrane after withdrawal of the insulin-stimulus (either by low pH washes, anti-insulin antibodies, or both) or in response to addition of inhibitors of PI3K, under similar conditions. In a previous study [224], Dobson *et al.* showed that a chimera similar to GFP-Glut4 did not re-internalise from the plasma membrane after removal of the insulin stimulus, but that Glut4-GFP did. However, these data were collected using CHO cells which are not a *bona-fide* insulin-responsive cell line, and moreover the kinetics of internalisation observed did not parallel those reported for endogenous Glut4. Therefore, we decided to revisit these observations, this time in a more appropriate cellular context.

In order to remove the insulin signal, we employed either or both of two distinct approaches: washing in low pH buffer, or the use of anti-insulin antibodies [29, 33, 224]. Both of these methods were shown to reverse insulin-stimulated glucose transport and Glut4 translocation in wild-type 3T3-L1 adipocytes with the expected half-times (figure 4.7). Identical conditions were employed for cover-slips of cells expressing GFP-Glut4. Strikingly, we were unable to observe internalisation of either GFP-Glut4 or Glut4-GFP using any of these approaches alone or in combination (figure 4.8); quantification of the level of GFP-Glut4 at the plasma membrane of these cells after such treatments did not reveal any significant reduction in signal, expressed as a percentage of the total cellular GFP-Glut4 level (data not shown). Inhibition of PI3K using wortmannin or LY294002 also functions to reverse insulin-stimulated glucose transport and Glut4 translocation (see figure 4.7). However, incubation of cells with up to 250 nM wortmannin for up to 3 hours did not result in appreciable internalisation of GFP-tagged Glut4 from the plasma membrane (figure 4.8). Quantification of this data by measurement of GFP-Glut4 fluorescence at the plasma membrane as a percentage of

the total cellular GFP-Glut4 fluorescence further demonstrated no significant internalisation of GFP-Glut4 under any of the conditions employed (data not shown). These data strongly imply that the internalisation of Glut4 from the cell surface after withdrawal of the insulin-stimulus (or by inhibition of PI3K) has been perturbed by the presence of the GFP in the cytosolic domain of Glut4, either at the N- or C- terminus.

In order to examine the ability of GFP-Glut4 expressing cells to internalise other proteins from the cell surface, we examined the internalisation of Texas-Red transferrin and Lysotracker-Red® into cells expressing GFP-Glut4 in the presence of insulin. These ligands were effectively internalised by cells in the presence of insulin (data not shown), arguing that these cells do express a functional recycling pathway capable of internalising proteins from the plasma membrane to intracellular compartments in the presence of insulin.

We next sought to determine whether GFP-tagged Glut4 species were, like endogenous Glut4, undergoing recycling between the plasma membrane and intracellular compartments. The small number of injected cells on a coverslip precludes direct biochemical analysis of this, therefore we adopted a more indirect approach. Studies have shown that depletion of K^+ results in the accumulation of Glut4 at the plasma membrane, probably as a consequence of interruption of the recycling pathway [132]. We therefore incubated coverslips of cells expressing GFP-Glut4 in potassium-depleted buffer or control buffer, and examined the levels of GFP-Glut4 associated with the plasma membrane under these conditions (figure 4.9). As illustrated, cells incubated in potassium-depleted media exhibited consistently increased levels of GFP-Glut4 at the plasma membrane than control cells as evidenced by the clear definition of the plasma membrane in such cells which is not apparent in control cells. Quantification of the accumulation of GFP-Glut4 at the plasma membrane in these cells is shown in figure 4.9; a statistically significant increase is observed by 2 h of incubation in K^+-depleted buffer. Such experiments are suggestive of recycling of GFP-Glut4 in the absence of insulin. Using the same experimental conditions, we examined the distribution of endogenous Glut4 in 3T3-L1 adipocytes by whole cell immunofluorescence (figure 4.9). As shown, potassium depletion resulted in the accumulation of endogenous Glut4 at the cell surface, validating the concept that the morphological assay of GFP-Glut4 accumulation at the cell surface is reflecting the behaviour of the endogenous protein. Although we interpret these data to imply that low potassium levels are disrupting endosomal recycling, it is possible that these effects arise as a consequence of cellular

stress induced by changes in membrane potential, sodium-gradients and the activity of membrane transporters that utilise the sodium gradient. However, studies in primary rat adipocytes have strongly argued that the effect of potassium is to modulate recycling of Glut4 through the endosomal system, hence we argue that the responses observed here of GFP-Glut4 to potassium-depletion reflect the ability of this protein to recycle in the absence of insulin.

It has been shown that Glut4 undergoes constitutive recycling between the plasma membrane and intracellular compartments in the basal state [29, 32, 86]. The partial overlap between GFP-Glut4 and TfR positive intracellular membranes (figure 4.3) and the observation that K^+-depletion results in the accumulation of GFP-Glut4 at the cell surface (figure 4.9) support the notion that GFP-Glut4 is undergoing constitutive recycling between the plasma membrane and intracellular membranes in the absence of insulin. If the mechanism of GFP-Glut4 internalisation in the basal state were the same as that employed to internalise GFP-Glut4 after withdrawal of the insulin signal, then the data of figure 4.8 would imply that GFP-Glut4 should accumulate at the plasma membrane in the basal state. The data of figure 4.1 (obtained >24 h after microinjection) shows that this is not observed. Hence in the absence of insulin GFP-Glut4 appears to traffic like the endogenous protein and, also like the endogenous protein, exhibits insulin-stimulated translocation to the plasma membrane (figure 4.1). In contrast, after insulin withdrawal or inhibition of PI3K, GFP-Glut4 does not exhibit appreciable internalisation up to 6 hours after removal of the insulin stimulus, or up to 3 hours after addition of wortmannin (figure 4.8). These observations are not a function of laser toxicity, as the insulin withdrawal or wortmannin additions were made to cells either in a CO_2 incubator or on a 37°C hot-plate, and the cells were not exposed to laser illumination until the times indicated in the figures. Nor is this phenomenon restricted to GFP appended to the N-terminus of Glut4, as we observe similar phenomena with Glut4-GFP (not shown). It has also been suggested that GFP expression may be toxic to certain cells [128]. The fact that in all other respects GFP-Glut4 traffics apparantly normally and repsonds well to insulin would appear to mitigate against this being an issue in this system. Rather we argue that these observations imply distinct mechanisms of GFP-Glut4 internalisation in the basal state compared to post-insulin withdrawal.

Such a conclusion pre-supposes that GFP-Glut4/Glut4-GFP are faithfully mimicking the trafficking of the endogenous Glut4 protein in the basal state. Clearly, we cannot definitively demonstrate this, as we are limited by the very small numbers of cells

expressing the protein after microinjection. However, we argue that the following data support the notion that GFP-Glut4 is a reasonable model for endogenous Glut4 trafficking: (i) GFP-Glut4 exhibits significant insulin-stimulated translocation to the plasma membrane; Others have argued that newly synthesised Glut4 traffics from the TGN to the plasma membrane and is then sorted into an insulin-responsive compartment [135]. The fact that GFP-tagged Glut4 is capable of marked insulin-stimulated translocation strongly implies that this trafficking is operating correctly for the GFP-tagged species. (ii) Glut1-GFP in contrast is differentially distributed between the plasma membrane and intracellular membranes; (iii) mutations in the Glut4 primary sequence perturb targeting in a fashion similar to that reported for epitope-tagged Glut4; (iv) GFP-Glut4 exhibits partial overlap with the TfR, and almost no overlap with lysosomal markers; (v) potassium-depletion results in the accumulation of GFP-Glut4 at the plasma membrane, suggesting that GFP-Glut4 is recycling in the absence of insulin. Furthermore, GFP-Glut4 exhibits extensive overlap with the aminopeptidase, vp165/IRAP [101, 233], also arguing strongly for a close relationship between the trafficking of GFP-Glut4 and endogenous Glut4.

We argue that the mechanism of GFP-Glut4 internalisation in the basal state is distinct from that employed after insulin withdrawal, as we observe no GFP-Glut4 or Glut4-GFP at the plasma membrane in the basal state. Rather, we suggest that our data are consistent with a mechanistic distinction between GFP-Glut4 internalisation from the plasma membrane in the basal state and GFP-Glut4 internalisation after insulin withdrawal. We suggest that such mechanistic distinctions may also be operating for the endogenous protein, implying that distinct mechanisms for Glut4 internalisation may exist in peripheral tissues. In further support of this hypothesis, we note that the IC_{50} for wortmannin inhibition of basal and insulin-stimulated deGlc transport are distinct, and also that the inhibition of insulin-stimulated glucose transport observed in response to wortmannin does not fall appreciably below the basal rate [31, 89, 234] (see also figure 4.7). We argue that studies using GFP-tagged Glut4 can reveal hitherto unsuspected subtleties of Glut4 trafficking which may be of relevance to endogenous Glut4 cell biology.

Chapter 5

5.0.0 Switching the nucleotide specificity of ARFs 5 and 6 by site directed mutagenesis

5.1.0 Introduction

ADP-ribosylation factors (ARFs) represent a family of small molecular weight GTP-binding proteins that are believed to play a crucial role in the control of membrane traffic within the cell [235]. ARFs were originally recognised in the 1980s because of their ability to enhance the cholera toxin-catalysed ADP ribosylation of $G_{s\alpha}$ [236]. However, under normal physiological circumstances, the cellular roles of ARF proteins are much different. A whole family of ARF proteins have since been described [237] that represent critical components of vesicular trafficking pathways and activators of specific phospholipase Ds (PLDs) [235]. Similar to other guanine nucleotide binding proteins, ARFs with GDP bound are inactive, whereas ARFs with GTP bound are active and can associate with membranes [238]. The substitution of GDP with GTP is catalysed by guanine nucleotide exchange factors (GEFs) [127, 238]. Conversely, GTPase-activating proteins (GAPs) enhance the hydrolysis of bound GTP to inactivate ARFs [238, 239]. Therefore ARFs fulfill a critical role within the cell, translating the effects of upstream signalling proteins into membrane fusion events along the vesicular transport pathway.

5.1.1 *The ARF protein family*

The six ARF proteins are assigned to three classes based on sequence homology: class I, ARF1, ARF2, and ARF3; class II, ARF4 and ARF5; class III, ARF6 [237]. Hosaka *et al.* transfected HA epitope tagged Arf cDNAs into monkey kidney Vero cells to examine the subcellular localisation of each of the six ARF proteins by immunofluorescence. In this study the class I ARFs showed a perinuclear distribution while the class II and class III ARFs were localised in punctate structures throughout the cytoplasm and at the cell periphery. Fluorescence associated with ARFs 3-6 was also observed in the cell nucleus.

5.1.2 The *role of ARFs in trafficking*

The membrane trafficking pathway between the cell interior and the extracellular environment ensures that proteins and lipids can move dynamically through the cell as required. By this mechanism the cell can maintain the integrity of its membranes and synthesise new subcellular organelles [218]. The initial evidence that ARF may be involved in the trafficking pathway came from a genetic study in the yeast *Saccharomyces cerevisiae*, where deletion of the ARF gene resulted in a secretory defect [240]. Subsequently, ARF1 was found to be required for the recruitment of COPI to vesicles budding from the endoplasmic reticulum [241]. Since then a number of studies have implicated the importance of ARF proteins in eukaryotic cells at distinct points along the membrane trafficking pathway [242-245].

5.1.3 *ARFs and secretory vesicle formation*

The most studied of the ARF proteins, ARF1, is localised to the Golgi complex and recruits the coat proteins COP I and AP1-clathrin complex to Golgi membranes prior to vesicle budding and transport along the secretory pathway [235]. The mechanism by which active GTP-bound ARF gains the specificity to dock with the correct membrane site prior to vesicle formation is unclear. However, Galas *et al.* found evidence of ARF binding to the βγ subunits of heterotrimeric G proteins [243], an interaction that could provide a degree of specificity to ARF function at target membranes.

Xu *et al.* established a permeabilised cell system that supports prohormone processing and secretory vesicle formation from rat anterior pituitary growth hormone and prolactin secreting GH_3 cells [246]. Using this cell system, Chen *et al.* 1996 reported that recombinant human ARF-1 stimulates the release of nascent secretory vesicles from the TGN [247]. In contrast, mutant forms of ARF unable to exchange GDP for GTP or missing a portion of their N-terminal domain were unable to stimulate secretory vesicle formation. The binding of ARF to Golgi membranes and the formation of coatamer-coated vesicles is also associated with PLD activation [245]. The role of ARF-activated PLD in secretory vesicle release was examined by Chen *et al.* 1997 [248] Again using the permeabilised GH_3 cell system, they showed that the addition of recombinant PLD also stimulates secretory vesicle budding from the TGN. Furthermore, Chen *et al.* 1997 also showed that the addition of ARF-1 polypeptide, but not mutant ARF-1 unable to exchange GDP for GTP, increases PLD activity under the

same conditions where ARF-1 enhances vesicle budding from the TGN [247, 248]. These data demonstrate a clear link between ARF-1 and PLD activity leading to vesicle budding in the secretory pathway

Inhibition of PLD-derived phosphatidic acid (PA) formation using ethanol prevents coated vesicle formation budding from the Golgi membranes [245]. This result implies that PA is involved in the formation of secretory vesicles. However, whether PA accumulation itself or metabolites of PA, for example DAG, enhanced vesicle release remained unknown until the question was addressed by Siddhanta *et al.* [249]. Using the permeabilised GH_3 cell system, Siddhanta *et al.* added phospholipid-hydrolysing enzymes to generate either DAG or PA independently of PLD activity and then analysed their effects on the budding of nascent secretory vesicles. They found that the addition of a combination of enzymes expected to generate significant levels of PA rather than DAG gave the most significant increase in secretory vesicle budding from the TGN.

The stimulatory effect of PA may be a consequence of signalling events downstream of PA formation or a result of its effects as a fusogenic lipid [250]. In support of the latter hypotheses Ktistakis *et al.* observed that the β-COP subunit of the coatamer complex binds more effectively to PA-containing liposomes [245]. In addition, the transient, localised accumulation of negatively charged PA in the TGN membrane could promote changes in the lipid bilayer curvature, further contributing to vesicle formation.

Evidence that GTP-binding proteins may also be involved in the formation of neuroendocrine synaptic vesicles (SV) came form the observation that the non-hydrolysable GTP analogue GTPγS inhibited the production of properly sized SVs in PC12 cell extracts [251]. In the same cell type a peptide corresponding to ARF1 was shown to inhibit the formation of SVs, an effect that could be rescued by the addition of recombinant myristoylated native ARF1 [244]. Thus, in addition to a general house-keeping role in membrane transport, ARF proteins are also intimately tied to the formation of specialised vesicles.

5.1.4 *ARF 6*

ARF 6 displays a different cellular distribution to ARF 1 [237] and therefore may be expected to fulfill a slightly different role in membrane trafficking. In CHO cells, ARF6

exhibits a peripheral distribution localising mainly to the plasma membrane and some internal punctate structures [242]. Furthermore, ARF6 colocalises with endosomal transferrin receptors and cellubrevin [242], an endosomal v-SNARE [252].

This characteristic distribution suggests that ARF6 may be involved in membrane transport in recycling endosomes in CHO cells. D'Souza-Schorey *et al.* 1995, transiently expressed ARF6 in CHO cells that overexpressed the human transferrin receptor [253]. In these cells the researchers monitored receptor-mediated endocytosis by following transferrin receptor (TfR) recycling. Overexpression of ARF6 resulted in a significant increase in binding of Tfn when compared to control cells. Similarly, the mutant ARF6(Q67L) that is defective in GTP hydrolysis, and is therefore locked in the activated state, also increased cell surface-bound Tfn. In contrast, cells that overexpressed then mutant ARF6(T27N) that is defective in GTP binding, and therefore inactivated, showed a 70% decrease in cell surface-bound Tfn. This data suggests that these changes in Tfn binding probably reflect a redistribution of the TfR. The redistribution of TfR from punctate vesicles to the plasma membrane when ARF6 or ARF6(Q67L) is expressed was confirmed by confocal microscopy. In contrast, cells that overexpressed ARF6(T27N) showed little TfR at the plasma membrane but prominent fluorescent staining of intracellular compartments. Double labeling experiments revealed that ARF6(Q67L)) colocalised with TfR at the plasma membrane, while ARF6(T27N) colocalised with TfR in intracellular compartments.

The kinetics of Tfn internalisation and release was also examined in CHO cells overexpressing ARF6 or the ARF6 mutants. Tfn release was decreased by the overexpression of ARF6, ARF6(Q67L) and ARF6(T27N). Tfn internalisation was reduced in cells that expressed ARF6(Q67L), whereas the Tfn recycling rate was dramatically reduced in cells that expressed ARF6(T27N) and as a consequence internalised Tfn was trapped within the cells. Taken together, these data suggest overexpression of ARF6 results in significant changes in endocytic traffic in CHO cells. The colocalisation of the ARF6 mutants with TfR also suggests that the nucleotide status of ARF6 plays an important role in TfR progression through the recycling endosomes.

ARF6 has also been implicated in the exocytotic pathway in cultured chromaffin cells due to the inhibition of calcium-evoked catecholamine secretion by a myristoylated ARF6 peptide [243]. Therefore the involvement of ARF proteins in glucose transporter trafficking remains an intriguing possibility.

5.1.5 *GEFs and GAPs*

Under physiological conditions the release of GDP from ARF and GDP/GTP exchange is very slow but is greatly enhanced by the presence of guanine nucleotide exchange proteins (GEFs) [238] (figure 5.1). Similarly, the inactivation of ARF by the removal of GTP is very inefficient in the absence of GTPase activating proteins (GAPs) [238] (Fig 5.1).Clearly this added level of complexity provides mechanisms whereby extracellular factors could stimulate cell signalling pathways that have GEFs and GAPs as downstream targets, thus modulating the rates of membrane fusion events.

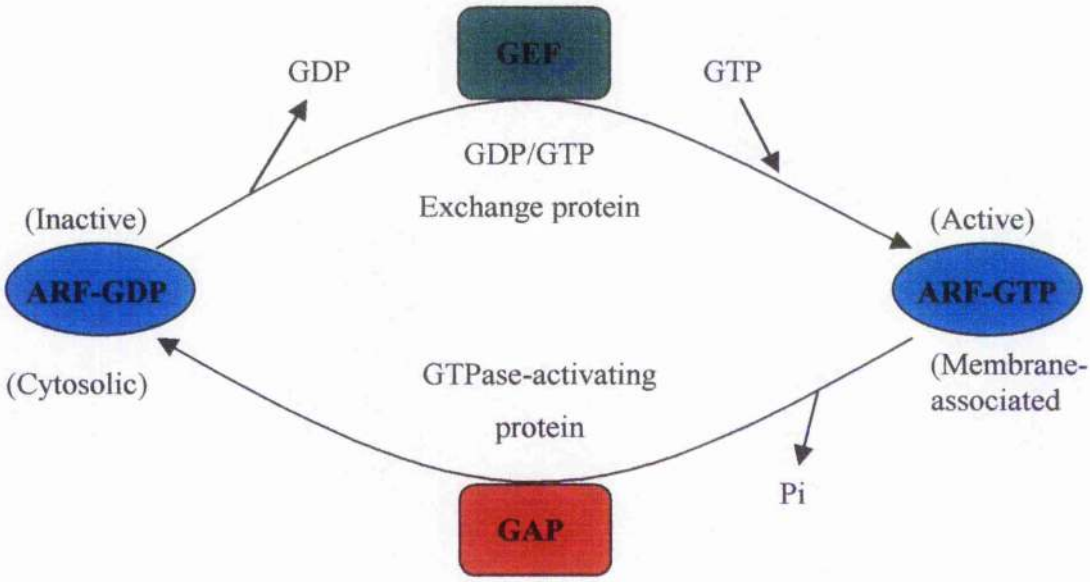

Figure 5.1 The relationship between ARFs GEFs and GAPs

Guanine Nucleotide ExchangeFactors (GEFs) catalyse the exchange of GDP for GTP to activate ARF proteins, whereas GTPase Activating Proteins (GAPs) enhance the hydrolysis of ARF-bound GTP to GDP rendering the ARF inactive.

ARNO (ARF nucleotide binding site opener) is a GEF for ARF6 [127]. ARNO also catalyses the exchange of GDP for GTP on ARF1 [254]. However, based on subcellular fractionation and immunolocalisation experiments the distribution of ARNO more closely resembles that of ARF6 than ARF I [127]. Therefore, it is more likely that ARNO affects vesicular trafficking by modulating the activity of ARF6. Whereas ARNO is ubiquitously expressed, the GEF cytohesin-1 is present in relatively few cells

[128]. The closely related cytohesin-3 (GRP-1) was isolated from a mouse adipocyte expression library in a search for proteins that bind 3'-phosphoinositides [255]. Therefore, cytohesin-3 provides an attractive theoretical means by which insulin induced PI3K activity could be translated into ARF activation, increased membrane fusion events and Glut4 movement to the plasma membrane in adipocytes.

To date more ARF GEFs than ARF GAPs have been discovered and characterised [238]. Ding *et al.* characterised an ARF GAP purified from rat spleen cytosol [239]. The purified GAP accelerated the hydrolysis of GTP bound to recombinant ARF1, ARF3, ARF5 and ARF6. This broad substrate specificity may indeed represent a less specialised function of ARF GAP. However, a more detailed study may reveal that the subcellular distribution of ARF GAP is tightly controlled and therefore inaccessible to ARF proteins of different classes.

5.1.6 *ARFs and Glut4*

Given the wide variety of cell types in which ARF proteins are expressed, their pivotal role in vesicular transport, and their involvement in the formation of specialised organelles, it is reasonable to hypothesise that ARF proteins may play a part Glut4 trafficking. This hypothesis was tested by Millar *et al.* in 3T3-L1 adipocytes [56]. This study found that 3T3-L1 adipocytes express ARF5 and ARF6 protein and that the former relocates to the plasma membrane in response to insulin. Permeabilised cells were then treated with myristoylated ARF5 and ARF6 peptides to investigate the function of these proteins. The ARF6 peptide caused an approximately 50% reduction in Glut4 translocation in response to insulin, whereas ARF5 and ARF1 peptides were without effect. Both, the ARF5 and ARF6 peptides inhibited cell surface levels of Glut1 and transferrin receptor (TfR) in response to insulin. However, the ARF6 peptide did not inhibit the fold increase in Glut1 and TfR at the plasma membrane in response to insulin. In light of this data, Millar *et al.* suggested that in 3T3-L1 adipocytes ARF5 controls membrane protein transport through the recycling endosomes where Glut1 and TfR are primarily located. In addition there is growing evidence the Glut4 populates two distinct intracellular compartments in 3T3-L1 adipocytes [98] whereas Glut1 is located within the endosomal system and the plasma membrane. One of the Glut4 intracellular compartments corresponds to the recycling endosomal system, the other a specialised Glut4 storage vesicle. The mechanism whereby ARF6 peptides reduce the degree of

Glut4 translocation by 50% and the cell surface levels of endosomaly derived Glut1 is unclear. Millar/Powell *et al.* speculate that ARF6 peptides may inhibit translocation from one of the two proposed Glut4 pools in 3T3-L1 adipocytes. Alternatively, ARF6 may function in constitutive membrane protein recycling hence causing the observed decrease in surface levels of Glut1 in the basal and insulin-stimulated state. In this model ARF6 peptides could also decrease cell surface Glut4 levels following insulin stimulation since Glut4 is known to recycle with intracellular compartments even in the presence of insulin [86]. Whether ARF6 is involved in the exocytosis of Glut4 storage vesicles in insulin-responsive cells, analogous to ARF6 function in the secretory granules of chromaffin cells [243], or plays a part in the recycling endosomal system as suggested by D'Souza-Schorey *et al.*, remains to be firmly established. The contribution of GEFs and GAPs to the control of Glut4 translocation remains unexplored.

5.1.7 *ARF XTPases*

In an effort to more clearly define the mechanism of Glut4 translocation we sought to make ARF5 and ARF6 XTPase mutants. A conserved NKXD motif is found in the GTP-binding site of the GTPase superfamily. It has been shown that the hydrogen bond formed with the aspartate residue belonging this motif determines the specificity of guanine nucleotide binding [256]. GTP-binding proteins carrying an aspartate to asparagine mutation at this position are characteristically regulated by xanthine nucleotides rather than guanine nucleotides [257-261]. Furthermore, Zhong *et al.* showed that GAP also accelerates the hydrolysis of XTP bound to a mutant Ras G protein. Examination of the amino acid sequence of ARF5 and ARF6 reveals that both proteins contain an NKXD motif towards the carboxyl terminus.

Aspartate to asparagine mutations were made within the NKXD motifs of ARF5 and ARF6 by site directed mutagenesis. Using PCR we subcloned the Arf cDNAs into a eukaryotic expression vector and added a FLAG epitope tag to the C-terminus of the ARF proteins. The addition of a FLAG epitope tag would allow for the efficient purification and immunolocalisation of wild type and mutant ARF proteins. Prior to any future experiments we must first verify the phenotype of the ARF5 and 6 XTPases. Subsequently we plan to make 3T3-L1 adipocyte cell lines that stably express both wild type and XTPase mutant ARF5 and 6. These stable cell lines will then be used to assay the contribution of ARF to Glut4 translocation in Glut4-GFP injected 3T3-L1 ARF5/6XTPase stable cell lines. Any effect detrimental to the action of insulin in such

cell lines should in theory be rescued by the addition of XTP to permeabilised cells. In this chapter we describe the molecular biological approach to the generation of ARF5 and ARF6 XTPases.

5.2.0 Materials and Methods

5.2.1.0 Site directed mutagenesis of Arf5FLAG/pBluescript

In order to change the nucleotide specificity of the ARF5 GTPase to an XTPase, we needed to make an aspartate to asparigine mutation at position 129 within an NKXD motif towards the C-terminus of ARF5. This D129N mutation was achieved using the Clontech Transformer™ Site-Directed Mutagenesis Kit. Arf5 cDNA subcloned into the Not I-Xba I site of the pBluescript II KS(+) vector was kindly supplied by Dr Kazuhisa Nakayama. The strategy for generating specific base changes using the Transformer Site-Directed Mutagenesis Kit is outlined below:

1. Denature dsDNA
2. Anneal Primers
3. Synthesise second strand with T4 DNA polymerse and seal gaps with T4 DNA ligase; primary digestion with restriction enzyme.
4. Transform mutS E. coli, first transformation
5. Isolate DNA from transformant pool
6. Secondary digestion with selection enzyme
7. Transform E. coli second (final) transformation
8. Isolate DNA from individual transformants to confirm presence of desired mutation

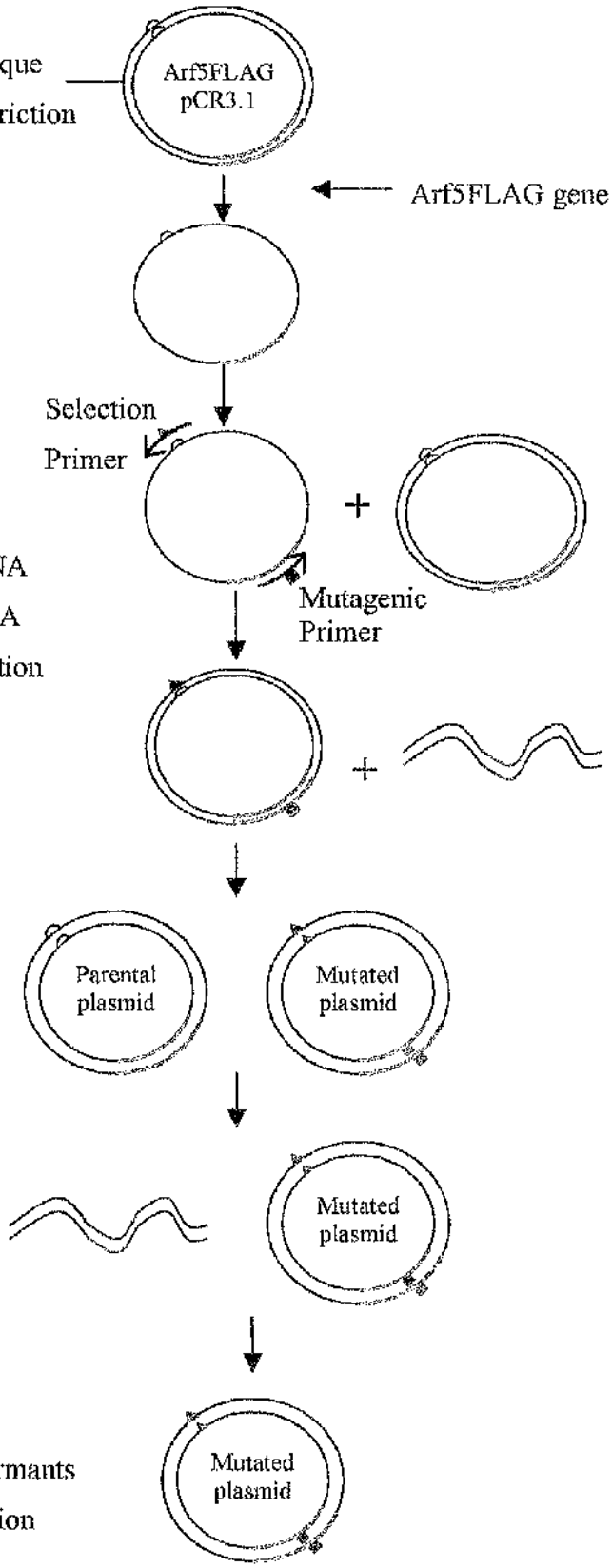

Figure 5.2 Diagramatical outline of site directed mutagenesis strategy

5.2.1.1 *Denaturing of plasmid DNA and annealing of primers to the DNA template*

Two primers were required for the mutagenesis reactions. The first primer, ARF5MUT, was designed to introduce the aspartate to asparagine mutation at position 129 of the ARF5 primary amino acid sequence. The second primer, XHOIMUTX, was designed to introduce a mutation into a unique Xho I restriction site within the Arf5/pBluescript vector.

Sequence of Arf5 site-directed mutagenesis oligonucleotide primers

Mutagenic Primer ARF5MUT

The oligonucleotide sequence is shown, with the corresponding ARF5 amino acid sequence written below. A red star highlights the G to A nucleotide mutation introduced, which alters the coding sequence such that an aspartate to asparagine substitution within the amino acid sequence of ARF5 results. Both the mutagenic and selection primers were 5′ phosphorylated so that they could be ligated to the 3′ end of the newly synthsised strand. The primers were purified by polyacrylamide gel electrophoresis (PAGE). 5′ Phosphorylation and PAGE purification of the primers was carried out by Genosys prior to delivery.

ARF5MUT sequence

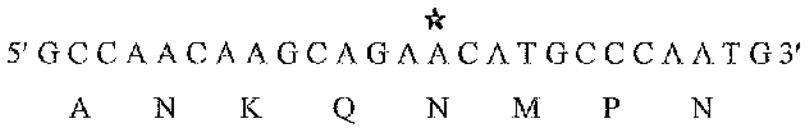

Selection Primer XHOIMUTX

The Clontech Transformer™ Site-Directed Mutagenesis Kit requires that one unique restriction site within the gene/vector DNA sequence is also mutated in order to select for mutant plasmids. Therefore, unique restriction sites within the Arf5/pBluescript DNA sequence were identified. We chose to mutate a unique Xho I restriction site within the multiple cloning region of the pBluescript backbone. Sequence analysis using Gene Jockey software showed that there were no Xho I sites within the cDNA sequence

of Arf5. Hence a selection primer carrying a mutation in the Xho I site was designed. A red star highlights the A to G nucleotide mutation introduced.

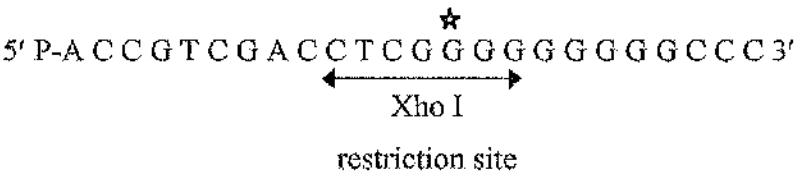

5.2.1.2 *Denaturation of plasmid DNA and annealing of primers to the DNA template*

The following reagents were pipetted into a 0.5 ml Eppendorf tube:

10x Annealing buffer	2.0 µl
Plasmid DNA	(0.05 µg/µl) 2.0 µl
Selection primer (XHOIMUTX)	(0.05 µg/µl) 2.0 µl
Mutagenic primer (ARF5MUT)	(0.05 µg/µl) 2.0 µl
H_2O	12.0 µl

The DNA was denatured by incubating the tube at 100°C for 3 minutes. Immediately thereafter, the sample was chilled in an ice water bath (0°C) for 5 minutes to anneal the primers to the Arf5/pBluescript template DNA.

5.2.1.3 *Synthesis of mutant DNA strand*

The following reagents were added to the primer/plasmid annealing reaction described above:

10x Synthesis buffer	3.0 µl
T4 DNA polymerase (2 units/µl)	1.0 µl
T4 DNA ligase (4 units/µl)	1.0 µl
H_20	5.0 µl

The sample was incubated at 37°C for 2 hours and then the reaction stopped by heating the mixture at 70°C for 5 minutes to inactivate the enzymes.

5.2.1.4 *Primary selection by restriction digestion*

The purpose of the primary restriction digestion is to selectively linearise the parental DNA. This step renders the parental DNA incapable of transforming the repair-deficient E. coli., thus greatly increasing the proportion of mutant plasmids present in the bacterial culture from the first transformation. The reagents for the restriction digestion were added to a 0.5 ml Eppendorf tube:

30 µl synthesis/ligation mix

3.25 µl 10x restriction enzyme buffer (added to optimise NaCl concentration)

1.5 µl Xho I restriction enzyme

5.25 µl H_2O

10x restriction buffer was added to the reaction in order to optimise the NaCl concentration for digestion by Xho I. The sample was incubated at 37°C for 2 hours and then at 70°C for 5 minutes to inactivate the restriction enzyme.

5.2.1.5 *First transformation*

The purpose of the first transformation is to amplify the mutated, Xho I-resistant strand of Arf5/pBlusescript into competent mutS (repair-deficient) E. coli. Repair-deficient bacteria are used so that any linearised parental Arf5/pBluescript DNA that is taken up by the mutS E. coli is not repaired and amplified by the bacterial cells. 10 µl of the plasmid/primer DNA solution from the previous step was added to 100 µl of competent BMH 71-18 mutS cells in a 15 ml Falcon tube and incubated on ice for 20 minutes. The cells were then heat shocked in a 42°C water bath for 1 minute. 1 ml of LB media was added to the tube and the sample placed in an incubator at 37°C for 1 hour with shaking at 225 r.p.m. Following the recovery step, 4 ml of LB containing 50 µg/ml ampicillin selection antibiotic was added to the mix. The culture was then incubated overnight at 37°C with shaking at 225 r.p.m. to amplify the transformants carrying the mutated Arf5/pBluescript plasmid. The following morning the mixed plasmid pool was isolated from 1.5 ml culture volume using the alkaline-lysis mini-prep method outlined in Chapter 2.

5.2.1.6 *Selection of the mutant plasmid*

The purpose of this second digestion is to select for the mutant Arf5/pBluescript plasmid by complete digestion of the parental unmutated plasmids. 5 µl of the purified mixed plasmid DNA from the previous step was digested with 10 units of Xho I as previously described and incubated at 37°C for 2 hours. Next, another 10 units of Xho I was added to the mix and the incubation continued for 1 hour to ensure that as much of the unmutated parental DNA plasmid as possible was linearised. As a control 100 ng of unmutated Arf5/pBluescript maxi-prep DNA was also digested with Xho I prior to the final transformation.

5.2.1.7 *Final transformation and analysis of putative Arf5XTPase/pBluescript clones*

5 µl of the digested plasmid DNA (approximately 25 ng) and 5 µl of the digested parental control DNA were transformed into Invitrogen One-Shot Top10F' competent cells as previously described in Chapter 3. Transformed cells at concentrations of 1x, 0.1x and 0.01x were then plated out onto agar plates containing 50 µg/ml ampicillin. Following an overnight incubation at 37°C there were approximately 10 fold more ampicillin-resistant colonies on the plates containing cells transformed with the mutated Arf5/pBluescript than on the control plates. Colonies were then picked from the plate containing mutant Arf5/Bluescript transformed cells and grown overnight in LB plus 50 µg/ml ampicillin. DNA was extracted from the overnight cultures using the alkaline-lysis mini-prep protocol as outlined before. 5 µl of the putative Arf5XTPase/pBluescript DNAs were then digested with Xho I and analysed by TBE agarose gel electrophoresis as previosly described. Mutant Arf5/pBluescript plasmids should be resistant to Xho I digestion and therefore migrate at a different rate from linearised parental DNA when analysed by agarose gel electrophoresis (figure 5.3).

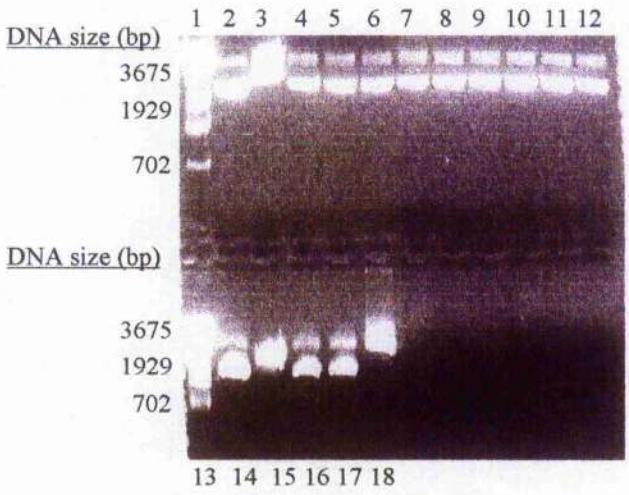

Figure 5.3 TBE agarose gel electrophoresis analysis of putative Arf5XTPase/pBluescript DNA clones

Putative Arf5XTPase/pBluescript DNA clones (lanes 4-12 and 16-18) were digested with Xho I and analysed by TBE agarose gel electrophoresis. A DNA molecular weight marker (lanes 1 and 13), uncut parental Arf5/pBluescript DNA (lanes 2 and 14) and parental Arf5/pBluescript DNA digested with Xho I were also run through the gel. The Successfully mutated Arf5XTPase/pBluescript clones were resistant to Xho I digestion and therefore migrated through the agarose gel at the same rate as the uncut parental Arf5/pBluescript DNA.

Figure 5.3 shows that the DNA from the putative Arf5XTPase/pBluescript clones 1-11 is resistant to Xho I digestion and migrates at a different rate from the linearised parental DNA. Therefore we would expect that the putative Arf5XTPase/pBluescript DNAs carry the desired mutations in the unique Xho I restriction site and in the codon encoding the aspartate residue at position 129. Automated sequencing confirmed that Arf5XTPase/pBluescript Clone1 did indeed contain the desired G to A nucleotide mutation within the codon encoding aspartate 129. Thus Arf5XTPase/pBluescript Clone 1 contained an aspartate to asparagine mutation at position 129 of the amino acid sequence, a mutation hypothesised to change the nucleotide specificty of Arf5 from GTP to XTP.

5.2.2 *Addition of a FLAG epitope tag to the C-terminus of wild-type ARF 5 and ARF5XTPase by PCR*

To allow for the efficient immunodetection or purification of wild type ARF 5 and ARF5XTPase we wanted to tag the ARF5 proteins with a FLAG epitope that has the amino acid sequence DYKDDDDK. The wild type and mutant ARF5s were tagged with the FLAG epitope by PCR. Two oligonucleotide PCR primers (ARFFLAGA and ARFFLAGC) were designed corresponding to the 5′ and 3′ ends of the Arf5 cDNA. The ARFFLAGC primer was designed to introduce a FLAG epitope to the C-terminus of Arf5. Furthermore a unique Sal I restriction site was added to the extreme 3′ end of the ARFFLAGC primer to allow for the positive identification of cDNA clones at a later date. Primers were synthesised and supplied by Genosys.

F1 and F2 oligonucleotide sequences

Sense primer ARFFLAGA

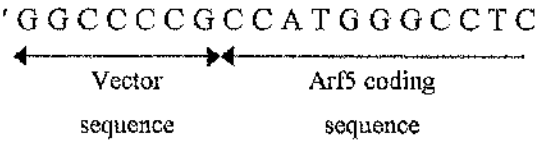

Anti-sense primer ARFFLAGC

5′ G T C G A C C T A C T T G T C G T C G T C G T C C T T A T A G T C C G C G C G C T T T G A C A G C T C G T G G G A C 3′

ARFFLAGC Sense

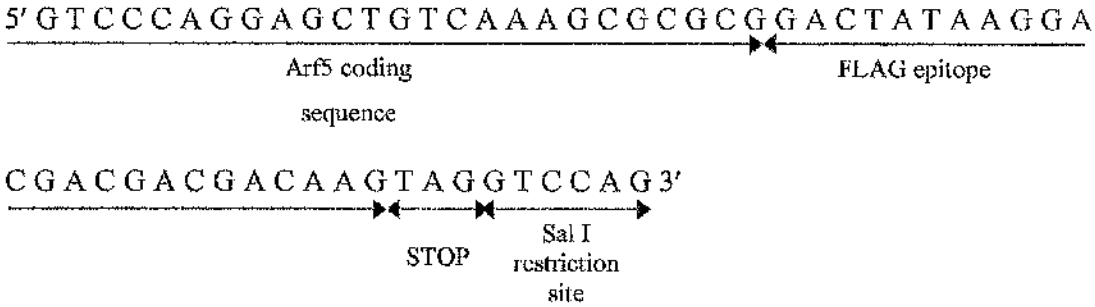

The wild type Arf5 cDNA was then amplified by PCR using the ARFFLAGA and ARFFLAGC primers. The mutant Arf5XTPase cDNA was amplified and epitope tagged in exactly the same way described for the wild type Arf5 cDNA.

PCR Protocol

1.0 µl Arf5/pBluescript template DNA (100 ng/µl)
1.0 µl ARFFLAGA primer (50 µM)
1.0 µl ARFFLAGC primer (50 µM)
5.0 µl 10x PCR buffer, Mg^{2+}-free
2.0 µl 25 mM $MgCl_2$
0.5 µl 100 mM dNTPs
38.5 of sterile H_2O
1.0 µl Taq DNA polymerase

PCR cycle parameters

10 minutes 94°C
1 minute 95°C
1 minute 78°C — 25 cycles
7 minutes 72°C
10 minutes 72°C

Following completion of the PCR reactions, the resultant DNA was purified using the Promega Wizard PCR clean-up kit, and the size of the DNA product checked by agarose gel electrophoresis as described in Chapter 2. The Taq-amplified DNA PCR product was then quantified by measuring its absorbance at 260 nm and then A-tail ligated into the Invitrogen pCR3.1 expression vector as described in Chapter 2. Ligation reactions were carried out overnight at 14°C, the ligated DNA transformed into One Shot™ TOP10F′ competent cells and DNA extracted from bacterial cultures, again as described in Chapter 2. Each of the putative Arf5FLAG cDNA clones was then restriction digested with Eco RI. The multiple cloning region (MCR) of the pCR3.1 vector contains two Eco RI restriction sites either side of the A-tailed PCR fragment

insertion point. Therefore, digestion with Eco RI would yield a DNA fragment approximately 600 base pairs in length indicating that the Arf5FLAG cDNA had been successfully subcloned into pCR3.1. Figure 5.4 shows that of the 18 putative Arf5FLAG/pCR3.1 clones, all but one yielded a DNA fragment of the expected size.

Figure 5.4 Putative Arf5FLAG/pCR3.1 DNA clones analysed by TBE agarose gel electrophoresis
18 Putative Arf5FLAG/pCR3.1 DNA clones (lanes 4-16 and 20-24) were digested with EcoR I and analysed by TBE agarose gel electrophoresis. Clones that contained the correct Arf5FLAG insert yielded a 600 base pair fragment (lanes 4-16 and 21-24). For comparison, a DNA molecular weight marker was included in lanes 1 and 17, uncut pCR3.1 plasmid DNA in lanes 2 and 18, and pCR3.1 plasmid DNA digested with EcoR I in Lanes 3 and 19.

The orientation of the Arf5FLAG cDNA inserts in the pCR3.1 vector was then checked using the Bam HI restriction enzyme:

Correct orientation

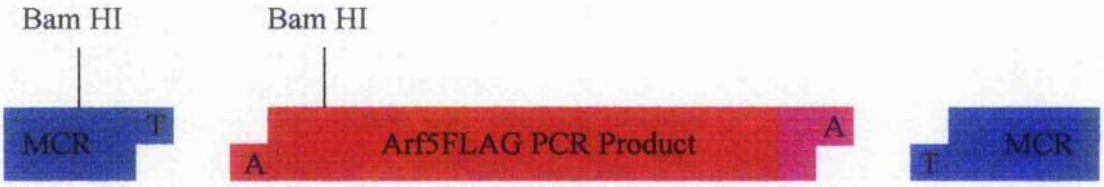

Figure 5.5 Relative position of Bam HI restriction sites within Arf5FLAG and pCR3.1

As well as a Bam HI site in the upstream MCR of pCR3.1, there is also a Bam HI site at position 105 of the Arf5FLAG PCR product (figure 5.5). Therefore, if the Arf5FLAG cDNA is inserted into the pCR3.1 vector in the correct orientation, a restriction digest with Bam HI will yield only a very small DNA fragment of about 140 base pairs. However, if Arf5FLAG is inserted in the antisense orientation, a restriction digest with Bam HI will yield a larger DNA fragment about 500 base pairs in length.

Following a Bam HI digest, putative Arf5FLAG/pCR3.1 cDNA clones were analysed by electrophoresis on a 1% agarose TBE gel. Four of the ten putative Arf5FLAG/pCR3.1 clones contained the Arf5FLAG cDNA inserted into the vector in the correct orientation. The DNA sequence of these four DNA clones was then verified by automated sequencing, and the corresponding clonal bacterial cultures made into frozen glycerol stocks as described.

5.2.3.0 *Addition of a FLAG epitope tag to the C-terminus of ARF6G2A by PCR*

Arf6 cDNA carrying a glycine to alanine mutation at position 2 and inserted into a pXS vector (Takebe *et al.*, 1988, MCB 8: 466-472) was kindly supplied by Dr. J. Donaldson, NIH, Bethesda, Maryland. Therefore, two oligonucleotide primers were designed, ARF6FLAGA and ARF6FLAGB. These primers encoded the addition of a FLAG epitope tag to the C-terminus of ARF6 and mutate the glycine residue at position 2 back to alanine.

ARF6FLAGA and ARFFLAGB oligonucleotide sequences

Sense primer ARF6FLAGA

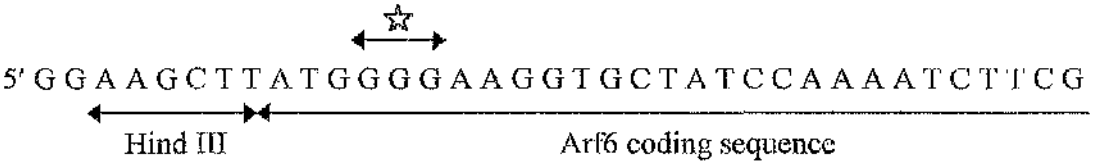

G G A A C 3'

☆= Alanine to glycine mutation codon

Antisense primer ARF6FLAGB

5' G G C T C G A G C T A C T T G T C G T C G T C G T C C T T G T A G T C C

G C A G A T T T G T A G T T A G A G G T C A A C 3'

ARF6FLAGB sense

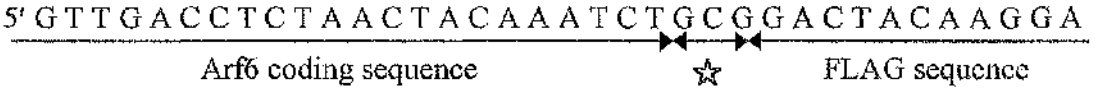

☆ = Stop codon to alanine mutation

5.2.3.1 *Arf6FLAG PCR and sub-cloning protocol*

Arf6FLAG was amplified by PCR and subcloned into the pCR3.1 expression vector in exactly the same way described for Arf5FLAG. Orientation of the Arf6FLAG cDNA fragment in the pCR3.1 vector was established by restriction digestion at a unique Bam HI site 44 base pairs downstream of the Arf6 start codon. Purified DNA stocks of

Arf6FLAG/pCR3.1 were then made using the Qiagen Maxi-Prep kit. The predicted DNA sequence of Arf6FLAG/pCR3.1 was confirmed by automated sequencing.

5.2.4 *Mutagenesis of wild-type ARF6FLAG to ARF6XTPaseFLAG*

To change the nucleotide specificity of the wild type ARF6FLAG GTPase to an XTPase we wanted to make an aspartate to asparagine mutation within the NKXD motif of ARF6, analogous to the D129N mutation described for the ARF5XTPase. The required mutation was achieved using the Clontech Transformer™ Site-Directed Mutagenesis Kit exactly as described previously when making the same mutation in ARF5. Two Arf6FLAG/pCR3.1-specific primers were designed to make the required aspartate to asaparagine mutation. The selection primer ARF6KPNMUT introduced a G to A mutation into a unique Kpn I restriction site within the mutiple cloning region of pCR3.1. The mutagenic primer ARF6XTP introduced a G to A mutation into the first position of the codon encoding aspartate 125 thus introducing the required D to N substitution.

ARF6XTP mutagenic primer sequence

ARF6KPNMUT selection primer sequence

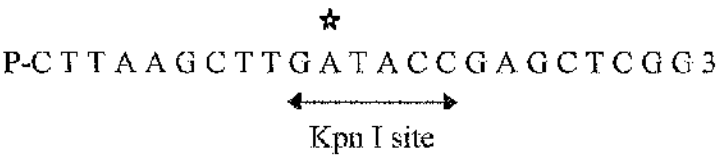

Both the ARF6XTP and ARF6KPNMUT primers were PAGE purified and 5' phosphorylated by Genosys prior to delivery. Red stars denote the mutation points.

5.2.5 *Transfection of HEK293 cells with wild-type Arf5FLAG/pCR3.1 and Arf5XTPaseFLAG/pCR3.1*

HEK293 cells were maintained in DMEM containing 10% calf serum and 1% penicillin/streptomycin antibiotic. Cells were trypsinised into 10 cm plates and grown to

50% confluency prior to transfection. The HEK293s were transfected with 10 μg of DNA mixed with 60 μl of Superfectin reagent per 10 cm plate as described in the Qiagen Superfect protocol.

5.2.6 *Lysis of transfected HEK 293 cells*

4x Lysis Buffer Recipe

1.9 ml 2M Tris pH 6.8

4 ml 20% SDS

4 ml glycerol

0.2 ml 0.2 M EDTA

0.1 ml Bromphenol Blue

Transfected cell were washed twice in cold PBS. 2 ml of 1x lysis buffer supplemented with 1:1000 dilutions of the proteases Aproptinin, Pepstatin A and DFP was added to each 10 cm plate and the cells scraped from the surface of the tissue culture dish. Nuclear DNA was sheered by passing the lysate through progressively smaller syringe needles. The lysates were then divided into 400 μl aliquots and snap frozen in liquid nitrogen prior to storage at -80°C.

5.2.7 SDS-PAGE and immunoblotting of transfected HEK293 cell lysates with an anti-FLAG antibody

Proteins within the transfected HEK293 cell lysates were separated by SDS-PAGE on a 15% acrylamide gel.

Resolving gel recipe for mini-gel	Stacking gel recipe
1.1 ml H_2O	1.4 ml H_2O
2.5 ml 30% acrylamide mix	0.33 ml 30% acrylamide mix
1.3 ml 1.5M Tris pH 8.8	0.25 ml 0.5 M Tris pH 6.8
0.05 ml 10% SDS	0.02 ml 10% SDS
0.05 ml 10% APS	0.02 ml 10% APS
0.02 ml TEMED	0.02 ml TEMED

SDS-PAGE running buffer recipe

14.43 g glycine

3 g Tris

1 g SDS

Made up to 1 L with H_2O

20 µl of lysate per lane was loaded onto the gel and polyacrylamide gel electrophoresis and transfer of lysate proteins onto nitrocellulose membranes carried out as described by Sambrook et al. 1989. The nitocellulose membrane was then incubated overnight at 4°C in a solution of TBST (150 mM NaCl, 150 mM Tris, 0.02% Tween 20, pH. 7.4) supplemented with 5% Marvel to block any non-specific interactions when immunoblotting with the anti-FLAG antibody. The following day the membrane was twice washed in room temperature TBST for 2 minutes. The membrane was then incubated in room temperature TBST containing 10 µg/ml anti-FLAG M2 (Sigma) primary antibody for 30 minutes in a heat-sealed plastic bag. Next the membrane was washed 3x for 2 minutes in TBST and then incubated with anti-mouse IgG peroxidase conjugated secondary antibody diluted 1:1000 for 30 minutes in a sealed bag. The membrane was then washed 3x in TBST with 15 minutes per wash. Finally, the

membrane was treated with ECL reagent and exposed for 5 seconds onto Kodak X-OMAT film.

5.3.0 Results

5.3.1 *Immunoblot of HEK293 cells transfected with wild-type Arf5FLAG and Arf5XTPaseFLAG cDNA*

In order to verify that the wild type Arf5FLAG and Arf5XTPaseFLAG constructs were correctly expressed in eukaryotic cells and that the FLAG epitope-tagged proteins could be detected by the anti-FLAG M2 antibody we transfected HEK 293 cells with Arf5FLAG/pCR3.1 or Arf5XTPaseFLAG/pCR3 DNA. The HEK 293 fibroblast cell line was chosen because HEK 293 cells have high transfection efficiency and are easily grown in culture. Lysates from control and Arf5FLAG –transfected cells were analysed by SDS-PAGE and immunoblotted with the anti-FLAG M2 antibody (figure 5.6).

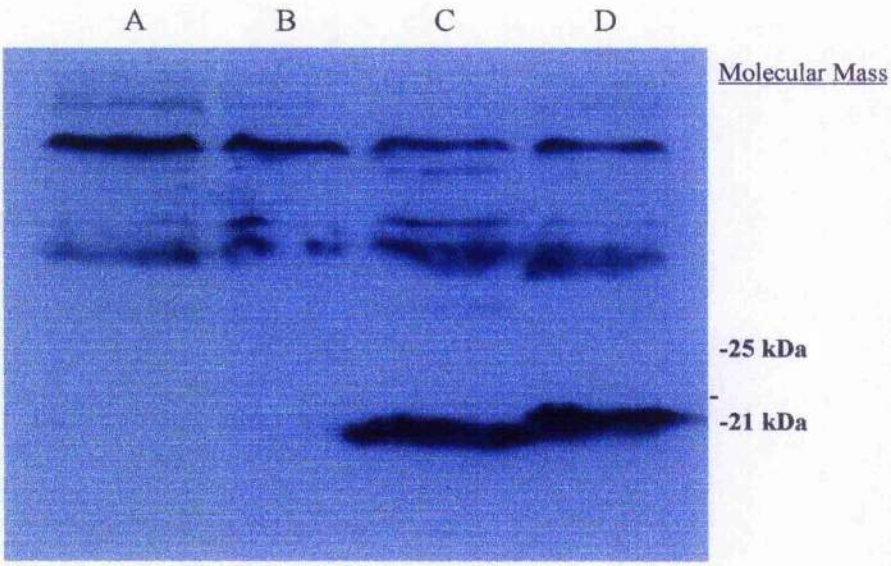

Figure 5.6 SDS-PAGE verification of ARFFLAG expression in Hek 293 cells

Lysates from transfected Hek 293 cells were analysed by SDS-PAGE and the gel loaded as described in the table below. Proteins were then transferred to a nitrocellulose membrane and immunoblotted with an anti-FLAG primary antibody. Following treatment with an HRP-conjugated anti-mouse secondary antibody, addition of ECL reagent and exposure to X-OMAT film, bands corresponding to FLAG-tagged ARF5 proteins were visible at the predicted molecular mass of 21 kDa.

Lane A	Lysate from **untransfected** Hek 293 cells
Lane B	Lysate from Hek 293 cells transfected with **Glut4-GFP** cDNA
Lane C	Lysate from Hek 293 cells transfected with wild type **ARF5FLAG** cDNA
Lane D	Lysate from Hek 293 cells transfected with **ARF5XTPaseFLAG** cDNA

The above figure shows that in cells transfected with the wild-type and mutant Arf5FLAG constructs there is a band corresponding to the predicted molecular mass of Arf5FLAG, approximately 21 kDa. This band is not found in the lysate from mock-transfected cells or HEK293s transfected with Glut4-GFP. Therefore we suggest that this band represents FLAG epitope-tagged wild type and XTPase mutant ARF5 and that the cDNA constructs are correctly expressed by eukaryotic cells.

5.4.0 Discussion

Using molecular biological techniques we successfully epitope tagged wild type Arf5 and Arf6 cDNA. Then by site directed mutagenesis we made an aspartate to asparagine mutation in the GTP-binding NKXD motif of both proteins. Automated sequencing showed that the Arf5XTPaseFLAG cDNA contained no mutations other than the desired G to A substitution within the aspartate codon of the NKXD motif. However, we were not so fortunate in the generation of the Arf6XTPaseFLAG mutant. The sequence of the mutated cDNA did not match with the known sequence of the wild type Arf6 cDNA. This suggests that during the site directed mutagenesis protocol either one or both of the selection and mutagenic oligonucleotides did not anneal correctly to the template DNA. Therefore, replication of the parental DNA strand by DNA polymerase was misprimed. In an attempt to circumvent this problem a variety of selection primers were designed corresponding to different unique restriction sites within the Arf6FLAG/pCR3.1 vector DNA. Unfortunately, regardless of selection primer used, very few mutant colonies were obtained. Furthermore, the cDNA retrieved from these colonies did not match the sequence of Arf6. This suggests that the problem may lie within the crucial mutagenic primer. The sequence of the mutagenic primer is evidently defined by the DNA sequence surrounding the desired mutation point. Therefore, if the mutagenic primer misprimes due to secondary structures within the oligonucleotide itself or within the template plasmid DNA there is little we can do to rectify this problem other than adopt a different site-directed mutagenesis protocol.

Upon completion of site directed mutagenesis and the addition of an epitope tag and DNA sequencing, wild type and mutant Arf5FLAG/pCR3.1 were transfected into HEK293 cells. Western blot analysis of transfected cell lysates gave a clear band at 20 kDa, not present in the control cells, that corresponds to the predicted molecular mass of ARF5FLAG (figure 5.6). This result suggests that the ARF5FLAG protein is correctly expressed in a eukaryotic cell background. Once the phenotype of the ARF5XTPase has been verified we will endeavour to make 3T3-L1 cell lines that stably express wild type or mutant ARF5FLAG. Our success in generating stable cell lines may depend upon how critical ARF5 is for normal cell function. Studies have already demonstrated the importance of ARFs 5 [56] and 6 [56, 243, 253] in endosomal transport. Hosaka *et al* found mRNA corresponding to each of the ARF family members in all mouse tissues

examined [237]. In addition Millar *et al.* showed that ARFs 5 and 6 are expressed in mouse 3T3-L1 adipocytes [56]. Assuming that ARFs 5 and 6 do play a critical a role in 3T3-L1 cells, then the generation of stable transfectants carrying ARF5/6XTPase mutations may prove difficult since cells carrying a mutation in such a critical component of the endosomal system may not prove viable. If this is the case, then the effect of a mutation in ARF5 or ARF6 on Glut4 trafficking could be examined by the coinjection of Arf5/6XTPase and Glut4-GFP cDNA into adipocytes. The effects of an ARF5 GTP-binding site mutation on Glut4 translocation could then be examined by confocal microscopy and any detrimental effects rescued by the addition of XTP.

Whatever the outcome, the continued study of ARF proteins in relation to Glut4 trafficking is important. ARFs may hold the crucial key to unlocking Glut4 translocation in response to insulin-induced signalling pathways. Under such circumstances, ARF proteins may provide a future target for the development of antidiabetic therapeutic agents.

Chapter 6

6.0.0 An investigation of nitric oxide signalling and Glut4 trafficking in L6 cells

6.1.0 Introduction

Skeletal muscle is the principal tissue of glucose utilisation by the body during exercise and of insulin-stimulated post-prandial glucose disposal. Therefore control of glucose transport into muscle is vital for glucose homeostasis. Two distinct mechanism mediate glucose uptake into skeletal muscle, the insulin-stimulated and the contraction-dependent signalling cascades [262, 263]. Whereas insulin stimulates increased glucose transport into skeletal muscle through a Phosphatidylinositol-3-Kinase (PI3K)-dependent pathway [189], there is growing evidence that contraction-stimulated glucose uptake is Nitric Oxide (NO)-dependent [75]. It is established that NO synthase (NOS) is expressed in skeletal muscle and NO is released from incubated skeletal muscle preparations [72, 264]. The downstream result of both the insulin and exercise-mediated signalling pathways is the recruitment of glucose transporter 4 (Glut4) from an intracellular location to the plasma membrane in a process called 'translocation' [262, 263] and hence increase glucose transport into the cell. Once the key components of the signalling pathways leading to translocation are identified, novel therapeutic agents could be designed as possible anti-diabetic compounds.

In the absence of a contraction stimulus a NO-donor alone can stimulate glucose transport and metabolism in rat skeletal muscle [74]. However, there is conflicting evidence regarding the effect of NO on insulin-stimulated glucose transport. Work by Balon *et al.* [264] shows that the effects of the NO-donor sodium nitroprusside (SNP) and insulin on 2-deoxyglucose transport are additive in skeletal muscle, whereas Kapur *et al.*[265] suggest that the NO-donor, GEA5024, blunts insulin-stimulated glucose transport. It is of some importance that this ambiguity be resolved since there is evidence that altered sensitivity of the NO/cGMP signalling cascade contributes to skeletal muscle insulin resistance [266] and therefore may play a part in non-insulin-dependent diabetes mellitus [267].

NO interacts with the haem group bound to a soluble form of guanylate cyclase expressed in a variety of tissues [73]. This interaction catalyses the formation of the intracellular signal molecule cGMP from GTP by guanylate cyclase. The NO-donor

SNP causes a rise in both cGMP concentrations and 2-deoxyglucose transport in rat skeletal muscle, increases that are diminished by the guanylate cyclase inhibitor LY-83583 [74]. However, the downstream intracellular target of cGMP in muscle cells that leads to increased glucose utilisation has not yet been identified. It is now recognised that cGMP targets in a variety of cell types include the Protein Kinase G family (PKG's), the cGMP-stimulated/cGMP-inhibited phosphodiesterases and cGMP-gated cation channels [268]. Young *et al.* have demonstrated that Zaprinast, considered to be a selective inhibitor of cGMP-specific PDE's [269], increases cGMP levels and glucose oxidation in incubated soleus muscle from rats [74].

The link between exercise and skeletal muscle Glut4 translocation is well established [262, 263]. Furthermore, the nitric oxide synthase inhibitor L-NAME inhibits both exercise-stimulated glucose transport in rats and Glut4 translocation [264]. This data therefore suggests that exercise-induced Glut4 translocation is mediated by NO. GFP-tagged Glut4 provides an attractive means by which to test this hypothesis.

L6 is a skeletal muscle cell line that has been used to investigate the effects of insulin and serotonin [270, 271]. L6 cells also provide a suitable method to study NO-signalling pathways in cultured muscle cells, without the added complication of diffusion of NO gas into cells of the muscle tissue vasculature, which can lead to difficulty in data interpretation. L6 cells have no detectable endogenous NOS activity in the resting state, but express inducible NOS (iNOS) upon exposure to cytokines and endotoxin [272]. Therefore, L6 myotubes can be used as a model to investigate the action of NO on glucose uptake in muscle cells.

In this study we used cultured L6 muscle cells to investigate the effect of NO-donors on both basal and insulin-stimulated 2-deoxyglucose transport. We hypothesised that the effects of NO-donors on glucose transport in L6 cells were mediated by cGMP and therefore, we measured cGMP levels in cells exposed to the NO-donor SNP. We also investigated whether manipulation of endogenous cGMP levels within the cell by inhibitors of soluble guanylate cyclase (ODQ) or cGMP-specific PDE's (Zaprinast) could affect a change in 2-deoxyglucose uptake. Finally, we microinjected L6 myotubes with GFP-tagged Glut4 cDNA to examine the effect of NO and insulin on Glut4-GFP translocation. A clearly demonstrated link between NO, cGMP, Glut4-GFP translocation and glucose transport within muscle cells would present a range of targets for future therapeutic intervention and treatment of diabetes.

6.2.0 Materials and Methods

6.2.1 *L6 cell culture*

Monolayers of L6 muscle cells were grown to the stage of myotubes in α-minimum essential medium containing ribonucleosides, 2% foetal calf serum and 1% antimicotic/antibiotic solution at 37° C in an atmosphere of 5% CO_2 , 95% air. Muscle cells were grown in 6-well plates for transport measurements and cGMP concentration studies.

6.2.2 *2-Deoxyglucose uptake assay*

All uptake assays were performed in triplicate on fully differentiated L6 myotubes grown in 6-well tissue culture plates. Cells were assayed 5-10 days post confluency. Following drug treatment, cells were washed once with 2 ml of Krebs Ringer Phosphate (KRP) buffer pH.7.4, then incubated for 20 minutes in radioactive 50 μM 2-deoxyglucose (14C 2-deoxyglucose 0.1 μCi/ml). Uptake was stopped by three washes with ice cold phosphate buffered saline (PBS) pH. 7.4 and the plates left to air dry. Thereafter, cells were lysed by a 20 minute incubation in 1% Triton X-100 on an orbital shaker and the radioactivity associated with the cells determined by scintillation counting. Non-carrier-mediated uptake was checked by incubation in the presence of 5 μM-cytochalasin B and it amounted to no more than ~1% of the total uptake.

6.2.3.0 *Cyclic GMP Assay*

6.2.3.1 *Sample preparation*

All cGMP assays were performed on fully differentiated L6 myotubes grown in 6-well tissue culture plates. Cells were assayed 5-10 days post confluency. Following the appropriate drug treatment cells were washed once in ice cold PBS and placed on ice. The PBS was then aspirated away and 1 ml of 12.5% acetic acid added to the first well on the 6-well plate. The cells in this well were then scraped in the 12.5% acetic acid and transferred into the second well and scraped again. This process was repeated until the cells in each of the wells were combined into 1ml of 12.5% acetic acid, which was then transferred into a 1.5 ml Eppendorf tube. Next, cells sonicated briefly to brake down cell membranes and the cell lysates centrifuged for 15 minutes at 4°C. The supernatant

was then transferred to a fresh tube spun down over night in a 'speed-vac'. The dried-out samples were then resuspended in 250 µl phosphate buffer

6.2.3.2 *Cyclic GMP assay protocol*

The cyclic GMP assay was then performed as described in the Cayman Chemical Cyclic GMP Enzyme Immunoassay Kit protocol. Briefly, the assay is based on the competition between the free cGMP in a particular sample and a cGMP tracer linked to an acetylcholinesterase molecule, for a limited number of anti-cGMP binding sites on a cGMP-specific rabbit antiserum. As the concentration of tracer cGMP is constant, the amount of cGMP tracer able to bind the specific antiserum is inversely proportional to the amount of free cGMP in a particular sample. This competition for binding sites occurs in the individual wells of a 96-well plate pre-coated with a mouse anti-rabbit monoclonal antibody. The plate is washed to remove any unbound reagents and then Ellman's Reagent (which contains the substrate to acetylcholinesterase) is added to the well. The product of the enzymatic reaction catalysed by acetylcholinesterase absorbs at 412 nm. Therefore, the intensity of this yellow colour determined spectrophotometrically is inversely proportional to the amount of free cGMP present in the well.

6.2.3.3 *Acetylation of cGMP samples*

The cGMP enzyme immunoassay is able to detect lower concentrations of cGMP if the samples are first acetylated. In these cGMP assays all samples and standards were acetylated prior to performing the assay. To acetylate 150 µl of each sample, 30 µl of 4 M KOH and 25 µl Acetic Anhydride were added in quick succession. The sample was then vortexed for 15 seconds, 7.5 µl 4 M KOH added and then vortexed again. This process was repeated for all samples and standards.

6.2.3.4 *Performing the assay*

Each sample was assayed in duplicate at two dilutions (undiluted and a 1:10 dilution)

Plate design

Partial Plate Format

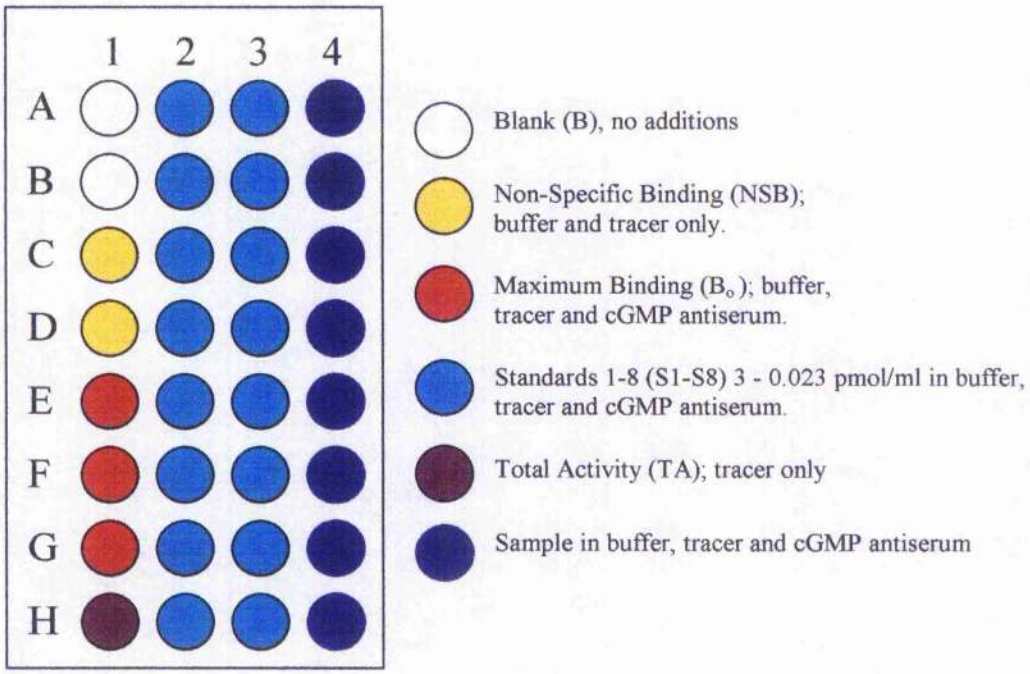

Figure 6.1.1 Plate design for cGMP assay

Immediately prior to use the plate was rinsed once with wash buffer. The samples and reagents were then pipetted into the wells and incubated for 18 hours at room temperature. Next all wells were emptied and rinsed 5 times with wash buffer, before adding 200 µl Ellman's Reagent to each well and 5 µl tracer to the total activity wells. The plate was then covered and developed in the dark for 90 minutes.

6.2.3.5 *Calculating the results*

The results were calculated as follows on a Macintosh computer using SOFTmax®PRO software.

-Absorbance readings averaged from the NSB wells.

-Absorbance readings averaged from the B_o wells.

-NSB average subtracted from the B_o average. This is the corrected B_o.

-%B/B_o calculated for the remaining wells, i.e. average NSB absorbance subtracted from the average S1 absorbance and divided by the corrected B_o. The result is then multiplied by 100 to obtain %B/B_o. This is repeated for S2-S8 and all sample wells.

6.2.3.6 *Standard curve*

%B/B_o for standards S1-S8 was plotted versus cGMP concentration (pmol/ml) on semi-log paper (figure 6.1.2)

6.2.3.7 *Determination of sample concentration*

The concentration of each sample was found by identifying its %B/B_o on the standard curve and reading the corresponding cGMP concentration values on the x-axis.

6.2.4 *L6 microinjection and confocal analysis*

L6 myotubes were grown on collagen-coated coverslips and microinjected with Glut4-GFP cDNA exactly as described in Chapter 2. Insulin- or NO-treated cells were than analysed by confocal microscopy, again as described in Chapter 2.

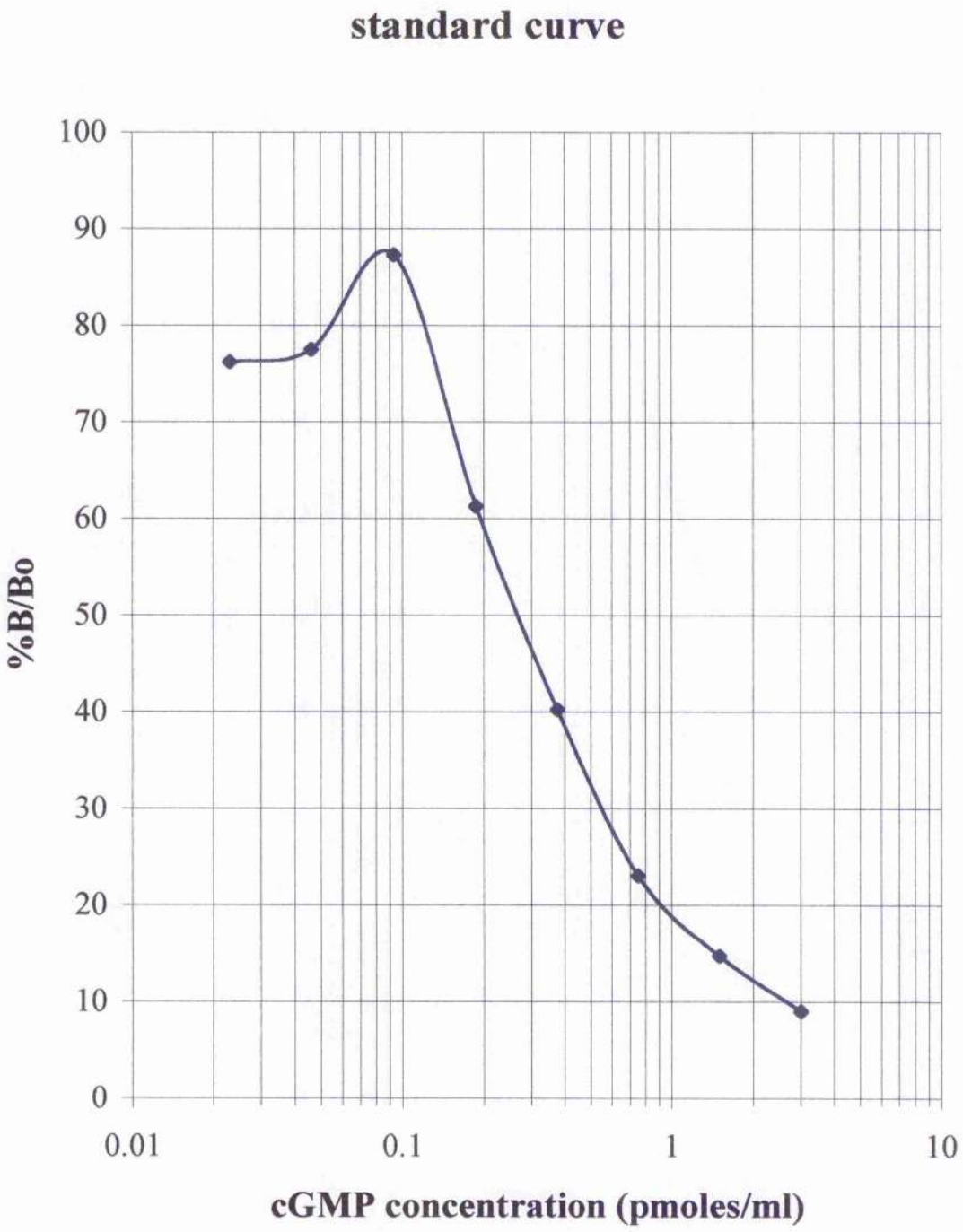

Figure 6.1.2 cGMP assay standard curve
The standard curve was prepared as described in materials and methods, section 6.2.3.6

6.3.0 Results

6.3.1 *Nitric Oxide donors stimulate 2-deoxyglucose uptake in L6 cells*

The nitric oxide donor sodium nitroprusside (SNP) was effective at stimulating uptake of the non-metabolisable glucose analogue 2-deoxyglucose into L6 myotubes. When added directly into the cell culture media for a period of 90 minutes, SNP at concentrations of 10 mM and above significantly increased 2-deoxyglucose uptake approximately 1.4 fold relative to basal (figure 6.2.1) in a time dependent manner. Similarly, SNP-stimulated 2-deoxyglucose uptake into L6 cells dose-dependently (figure 6.2.2). In response to both 1 and 10 mM SNP, 2-deoxyglucosse uptake was significantly elevated after a 90 minute incubation (figure 6.2.1).

To ensure that the increase in 2-deoxyglucose uptake seen in L6 cells in response to SNP was not an effect peculiar to the NO-donor SNP, two further NO-donors were tested, S-Nitroso-N-acetyl-D, L-penicillamine (SNAP) and [1,2,3,4-Oxatriazolium, 5-amino-3-(3-chloro-2-methylphenyl)-,chloride] (GEA5024) (Figure 6.2.3). SNAP caused a significant increase in 2-deoxyglucose uptake in L6 cells at concentrations of 100 μM and above. However, GEA5024 did not enhance 2-deoxyglucose uptake into L6 cells and proved toxic to the cells at concentrations over 100 μM.

6.3.2 *Effects of NO-donors and insulin on 2-deoxyglucose uptake*

Next the effect of insulin in combination with NO upon 2-deoxyglucose uptake was examined. When insulin alone at concentrations of 100 nM or 1 μM was added to L6 cells for 15 minutes, a 20-30 % increase in 2-deoxyglucose uptake was observed. However, when 1 μM insulin was added in the last fifteen minutes of a 90 minute incubation with SNP, no additional increase in 2-deoxyglucose uptake was found (figure 6.3.1). Similarly, insulin had no further effect upon 2-deoxyglucose uptake when combined with 100 μM SNAP (figure 6.3.2). Conversely, the effect of 1 μM insulin upon transport levels in cells preincubated with GEA5024 was additive, and GEA5024 at concentrations over 10 μM appeared to inhibit insulin-stimulated 2-deoxyglucose transport (figure 6.3.2). However, we propose that the inhibitory effect of GEA5024 on insulin stimulated transport is merely an artifact of GEA5024 toxicity at concentrations over 10 μM.

6.3.3 *Treatment with SNP causes cGMP levels to rise within the cell*

We hypothesised that the increase seen in 2-deoxyglucose uptake in response to NO-donors may be a cGMP-mediated effect. Therefore, we measured cGMP concentrations in L6 cells following a 90 minute incubation with 10 or 50 mM SNP or 1 μM insulin. 10 mM SNP produced a small yet significant increase (approximately 1.5 fold above basal) in cGMP concentrations within the L6 cells, while 50 mM SNP gave a roughly 5 fold increase in cGMP levels (figure 6.4.1). As expected, insulin produced no change in cGMP levels within the cell, probably as insulin acts via PI3K to increase glucose transport.

6.3.4 *The guanylate cyclase inhibitor ODQ inhibits the NO-induced increase in 2-deoxyglucose uptake and cGMP levels*

To further test the hypothesis that NO-stimulated 2-deoxyglucose uptake in L6 cells is a cGMP-mediated effect we used the potent and specific guanylate cyclase inhibitor 1H-[1,2,4]oxadiazolo[4,3,-α]quinoxalin-1-one, (ODQ). L6 cells treated with 200 μM ODQ for 90 minutes showed a small decrease in intracellular cGMP levels, as did cells coincubated with 10 mM SNP and 200 μM ODQ relative to 10 mM SNP only (figure 6.5.1). We therefore assayed whether an ODQ-induced decrease in endogenous cGMP levels within the cell also mediated a decrease in the rate of 2-deoxyglucose uptake (figure 6.5.2). ODQ alone had no significant effect on basal 2-deoxyglucose transport, however at concentrations over 100 μM, ODQ caused a decrease in NO-stimulated 2-deoxyglucose uptake into L6 cells.

6.3.5 *The phosphodiesterase inhibitor Zaprinast enhances the effects of SNP*

Free cGMP within the cell is broken down by cGMP -specific phosphodiesterases (PDE's), e.g. PDEV. Therefore, we treated L6 cells both in the presence and absence of 10 mM SNP with Zaprinast, a PDEV-specific inhibitor, with the hypothesis that by manipulating endogenous cGMP levels within the cell at the PDE level we could alter the rate of 2-deoxyglucose uptake (Figure 6.6.1). At the concentrations tested, Zaprinast had no stimulatory effect upon 2-deoxyglucose uptake into L6 cells and appeared somewhat toxic at concentrations much over 50 μM. However, 50 μM Zaprinast further enhanced NO-stimulated 2-deoxyglucose uptake, approximately 2-fold above SNP only. 50 μM Zaprinast also caused a concomitant rise in cGMP levels within L6 cells (Figure

6.6.2). A 90 minute incubation with 50 μM Zaprinast or 10 mM SNP alone caused a small increase in cGMP levels, whereas 50 μM Zaprinast in combination with 10 mM SNP caused a much larger increase in cGMP levels within L6 cells.

6.3.6 *cGMP analogues do not mimic the effects of SNP on 2-deoxyglucose transport*

Although manipulation of endogenous cGMP levels within L6 cells appeared to affect 2-deoxyglucose uptake levels, this effect was not replicated by incubation with exogenous cGMP analogues. Transport assays showed that following a 90 minute incubation with the cGMP analogue dibutyryl-cGMP (dbcGMP), no increase in 2-deoxyglucose transport was observed in L6 cells (Figure 6.7.1). Neither did the cGMP analogues 8-bromo-cGMP and 8-pCPT-cGMP cause any increase in 2-deoxyglucose transport (data not shown). However, the cAMP analogue dibutyryl-cAMP (dbcAMP) that was used as a control, consistently elevated 2-deoxyglucose uptake levels at concentrations of 100 μM and above (Figure 6.7.1). This suggests that the failure of db-cGMP to induce any increase in 2-deoxyglucose uptake is not a consequence of cell impermeability to this analogue (see discussion).

6.3.7 *Inhibition of protein kinase G does not block the effects of SNP*

We conjectured that any increase in endogenous intracellular cGMP levels that leads to a change in sugar transport levels may be mediated by protein kinase G (PKG). PKG is activated by cGMP and the cGMP analogue Rp-8-pCPT-cGMPS is known to be a specific inhibitor of PKG activity. Therefore, the ability of Rp-8-pCPT-cGMPS to inhibit NO-stimulated 2-deoxyglucose uptake was tested on L6 cells (Figure 6.8.1). Rp-8-pCPT-cGMPS failed to inhibit NO-stimulated 2-deoxyglucose transport at any of the concentrations tested. This result suggests that the increase in 2-deoxyglucose transport seen in cultured L6 cells is not mediated by PKG.

6.3.8 *Insulin but not a NO-donor stimulates Glut4-GFP translocation in L6 cells*

The effects of insulin and NO on Glut4 translocation were investigated using the GFP-Glut4 chimera (figure 6.9.1). L6 myotubes grown on glass coverslips were microinjected with GFP-Glut4 cDNA. The following day the injected cell were incubated in serum-free media for 2 hours, then treated with 1 μM insulin for 15 minutes (figure 6.9.1B) or 100 μM SNAP for 90 minutes (figure 6.9.1C). Basal cells

(figure 6.9.1A) are shown for comparison. Stimulation with 1 μM insulin caused significant translocation of GFP-Glut4, indicated by increased GFP-associated fluorescence at the plasma membrane. However, microinjected L6 cells treated with the NO-donor SNAP showed no evidence of GFP-Glut4 translocation.

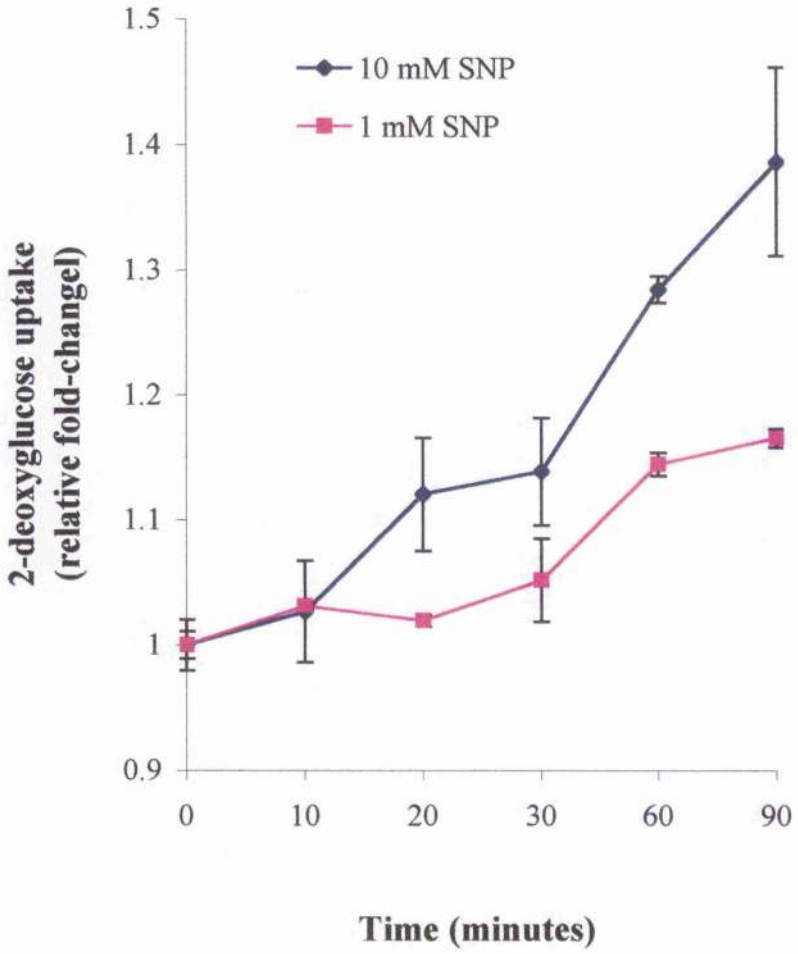

Figure 6.2.1 SNP stimulates 2-deoxglucose uptake into L6 cells in a time-dependent manner

L6 myotubes were grown in 6-well plates until fully differentiated. Prior to the assay, cells were incubated in serum-free a-Medium for 2 hours and then treated with either 1 mM or 10 mM SNP diluted in serum-free media for the times indicated at 37°C and 5% CO_2. The 2-deoxyglucose transport assay was performed as described in materials and methods. The graph shown is representative of a number of experiments. Results are expressed as mean values +/- standard errors of the mean.

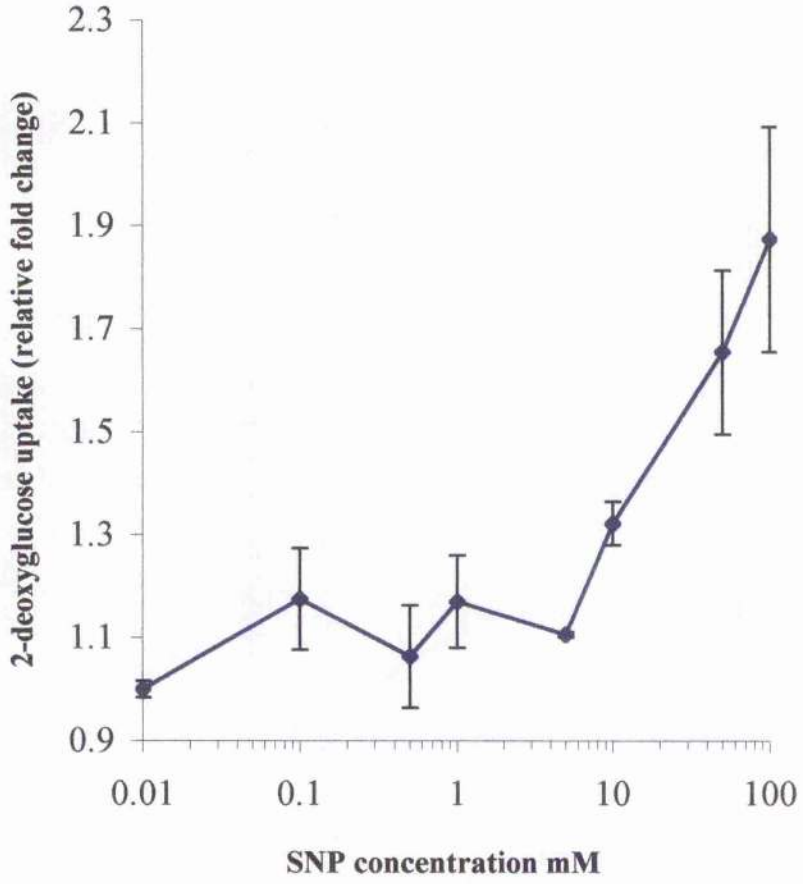

Figure 6.2.2 2-deoxyglucose uptake inreases in L6 myotubes in reponse to inreasing doses of SNP

Prior to the assay, cells were incubated in serum-free a-medium for 2 hours and then treated with 10 mM SNP diluted in serum-free media for 90 miutes at 37°C and 5% CO_2. The 2-deoxyglucose transport assay was performed as described in materials and methods. The graph shown is representative of a number of experiments. Results are expressed as mean values +/- standard errors of the mean.

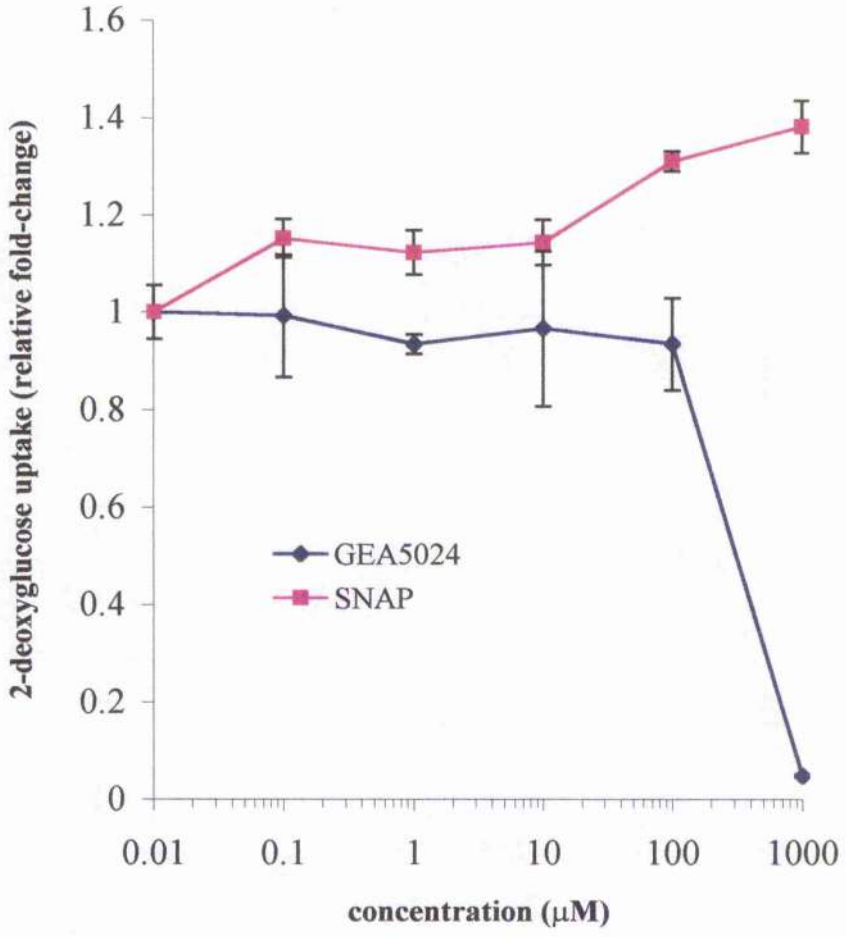

Figure 6.2.3 2-deoxyglucose uptake in L6 myotubes increases in reponse to inreasing doses of the nitric oxide donor SNAP but not GEA5024

Prior to the assay, cells were incubated in serum-free a-medium for 2 hours and then treated with SNAP or GEA5024 diluted in serum-free media for 60 miutes at 37 °C and 5% CO_2. The 2-deoxyglucose transport assay was performed as described in materials and methods. The graph shown is representative of a number of experiments. Results are expressed as mean values +/- standard errors of the mean.

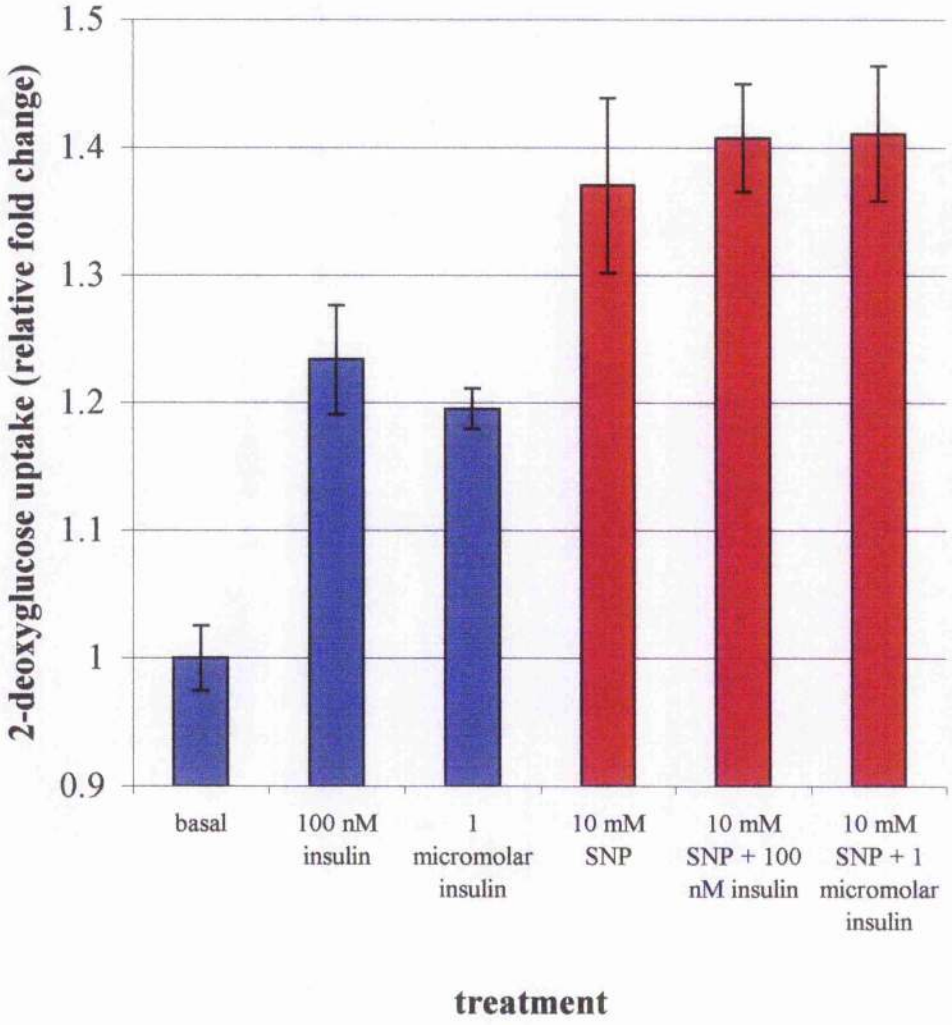

Figure 6.3.1 The effects of insulin and SNP on 2-deoxyglucose uptake in L6 cells are not additive

Prior to the assay, cells were incubated in serum-free a-medium for 2 hours and then treated with 10 mM SNP diluted in serum-free media for 90 miutes at 37°C and 5% CO_2 or insulin for 15 minutes. During the last 15 minutes of the SNP incubation 100 nM or 1 μM insulin was added to the media. The 2-deoxyglucose transport assay was performed as described in materials and methods. The graph shown is representative of a number of experiments. Results are expressed as mean values +/- standard errors of the mean.

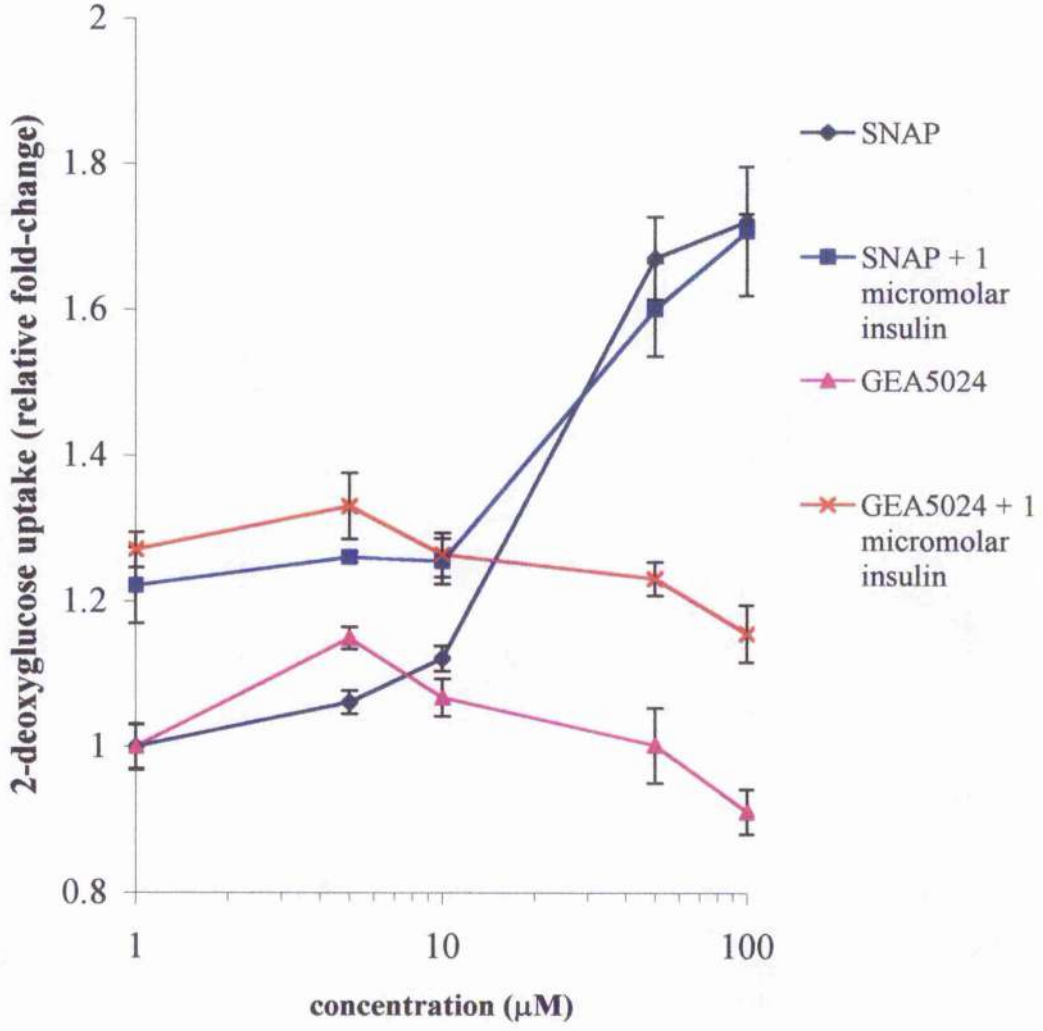

Figure 6.3.2 Effect of the NO-donors SNAP and GEA5024 on insulin-stimulated 2-deoxyglucose uptake

Prior to the assay, cells were incubated in serum-free a-medium for 2 hours and then treated for 90 minutes with SNAP or GEA5024 diluted in serum-free media to the concentations indicated at 37°C and 5% CO_2. During the last 15 minutes of the SNAP/GEA5024 incubation,1 μM insulin was added to the media of the appropriate wells. The 2-deoxyglucose transport assay was performed as described in materials and methods. The graph shown is representative of a number of experiments. Results are expressed as mean values +/- standard errors of the mean.

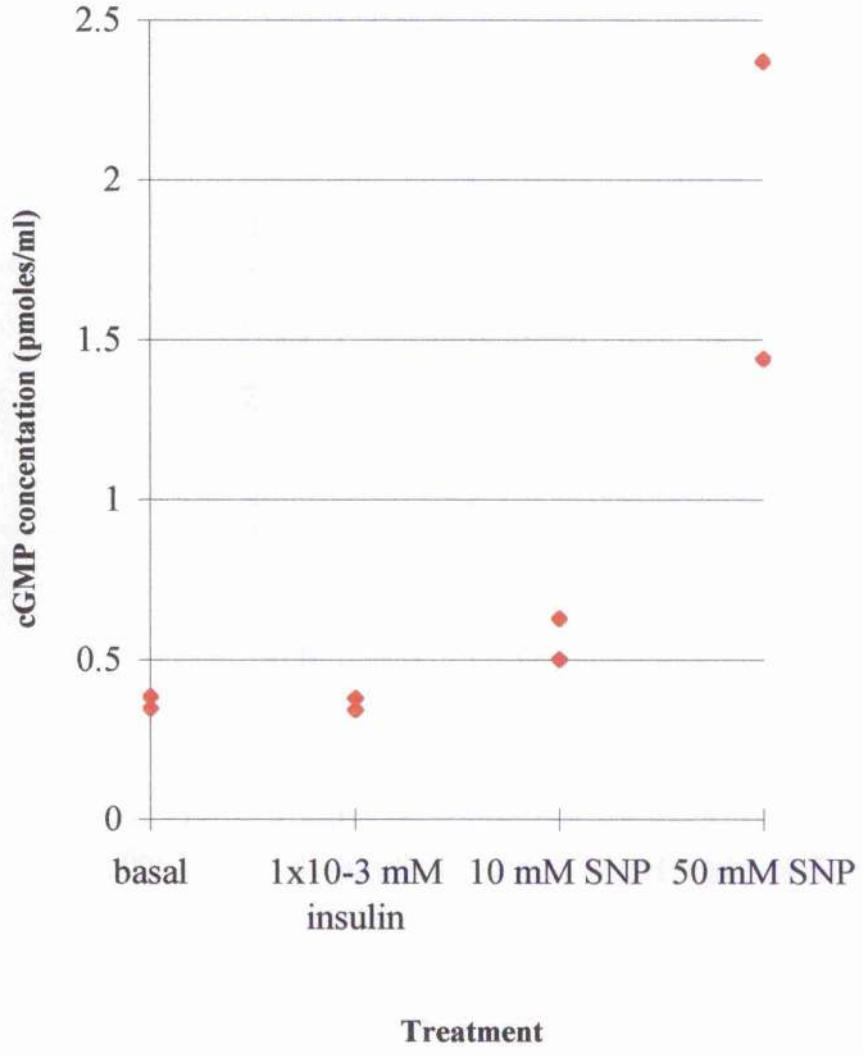

Figure 6.4.1 SNP but not insulin causes cGMP concentrations to rise in L6 cells

Effect of insulin or SNP on cGMP concentration in L6 cells. Prior to assay cells were serum starved in a-medium for 2 hours. Next, cells were treated with either insulin for 15 minutes or SNP for 90 minutes diluted to the appropriate concentration in a-medium at 37°C and 5% CO_2. The cGMPassay was then carried out exactly as described in the materials and methods. Results are presented in duplicate and the graph shown is typical of a number of like experiments.

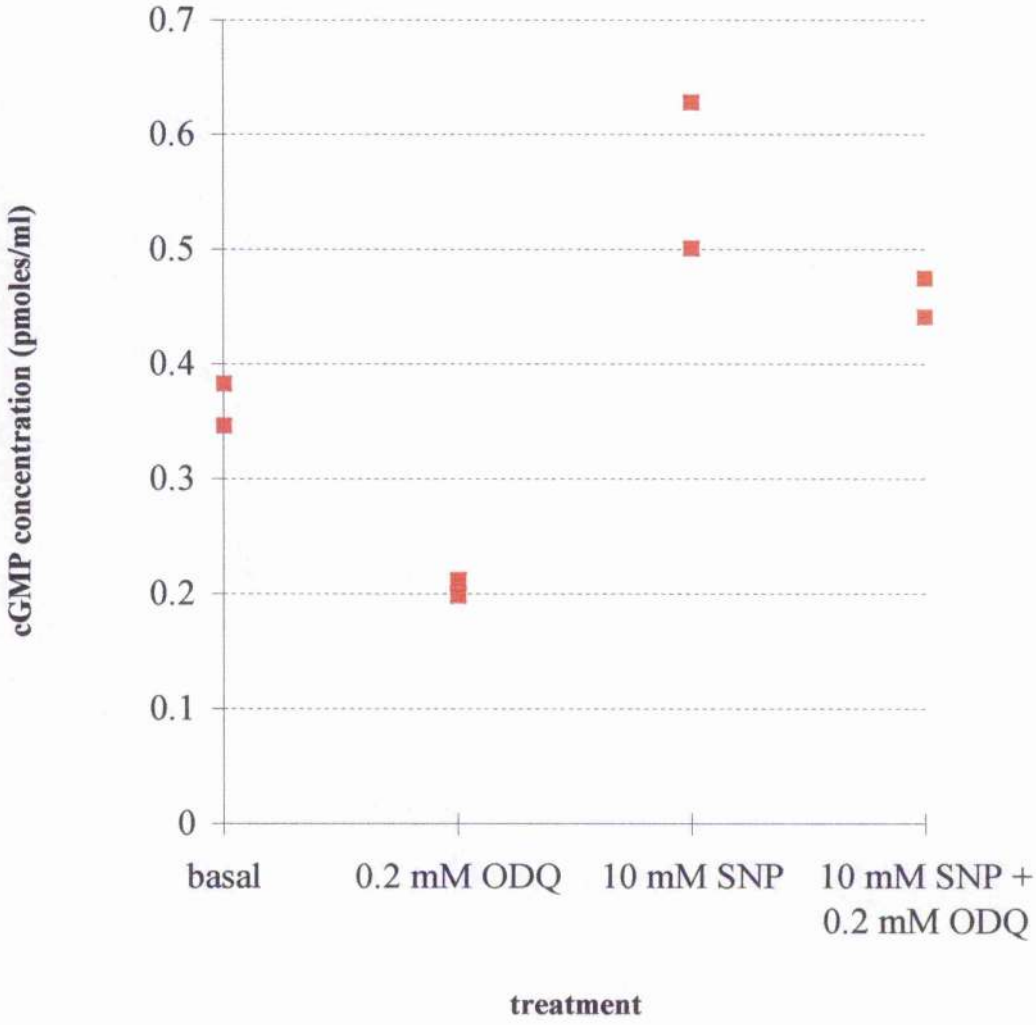

Figure 6.5.1 ODQ decreases the cGMP content of L6 cells

Effect of SNP and the guanylyl synthase inhibitor ODQ on cGMP concentration in L6 cells. Prior to assay cells were serum starved in a-medium for 2 hours. Next, cells were treated with either SNP, ODQ or SNP + ODQ for 90 minutes diluted to the appropriate concentration in a-medium at 37°C and 5% CO_2. The cGMP assay was then carried out exactly as described in the materials and methods. Results are presented in duplicate and the graph shown is typical of a number of like experiments.

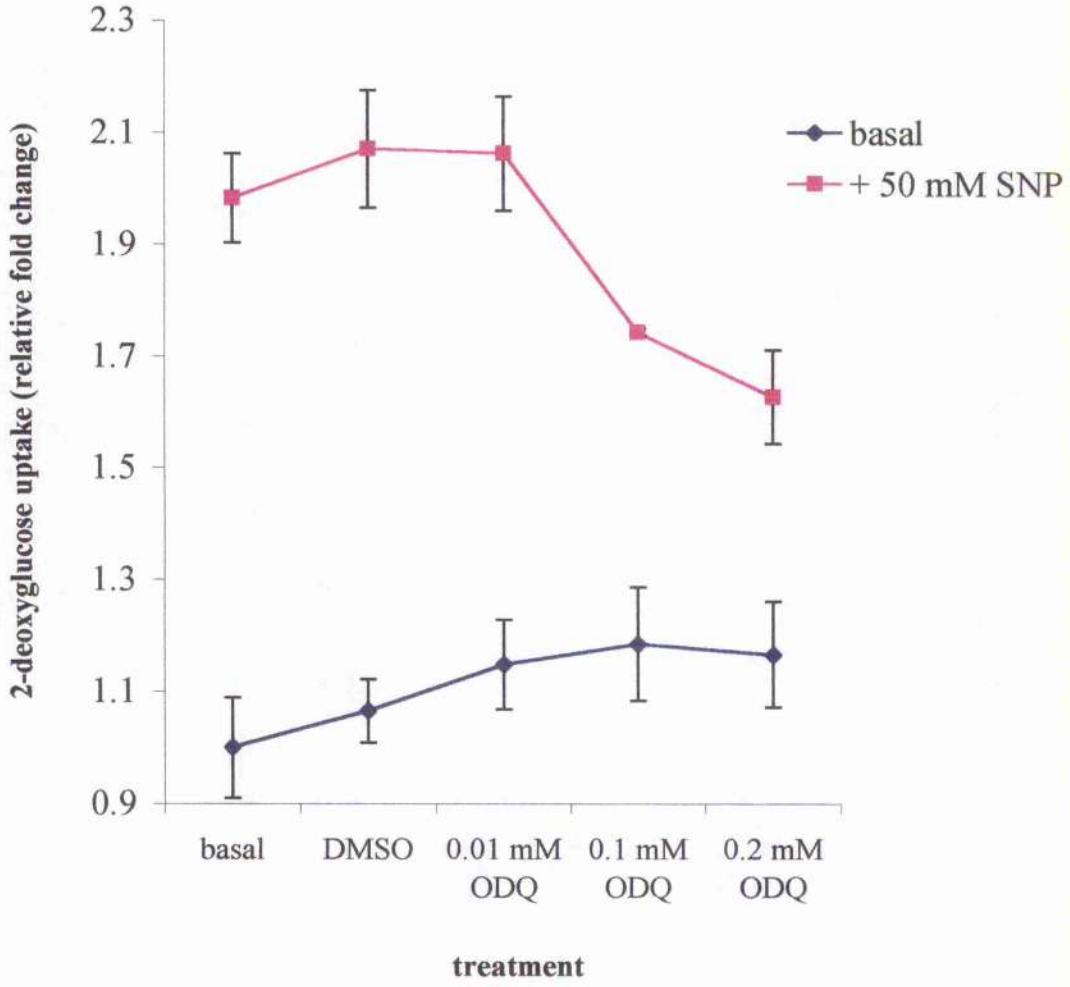

Figure 6.5.2 The guanylyl cyclase inhibitor ODQ decreases NO-stimulated 2-deoxyglucose uptake in L6 cells

Prior to the assay, cells were incubated in serum-free a-medium for 2 hours. Then cells were treated with 10 mM SNP +/- ODQ or vehicle (DMSO) diluted in serum-free media for 90 miutes at 37°C and 5% CO_2. The 2-deoxyglucose transport assay was performed as described in materials and methods. The graph shown is representative of a number of experiments. Results are expressed as mean values +/- standard errors of the mean.

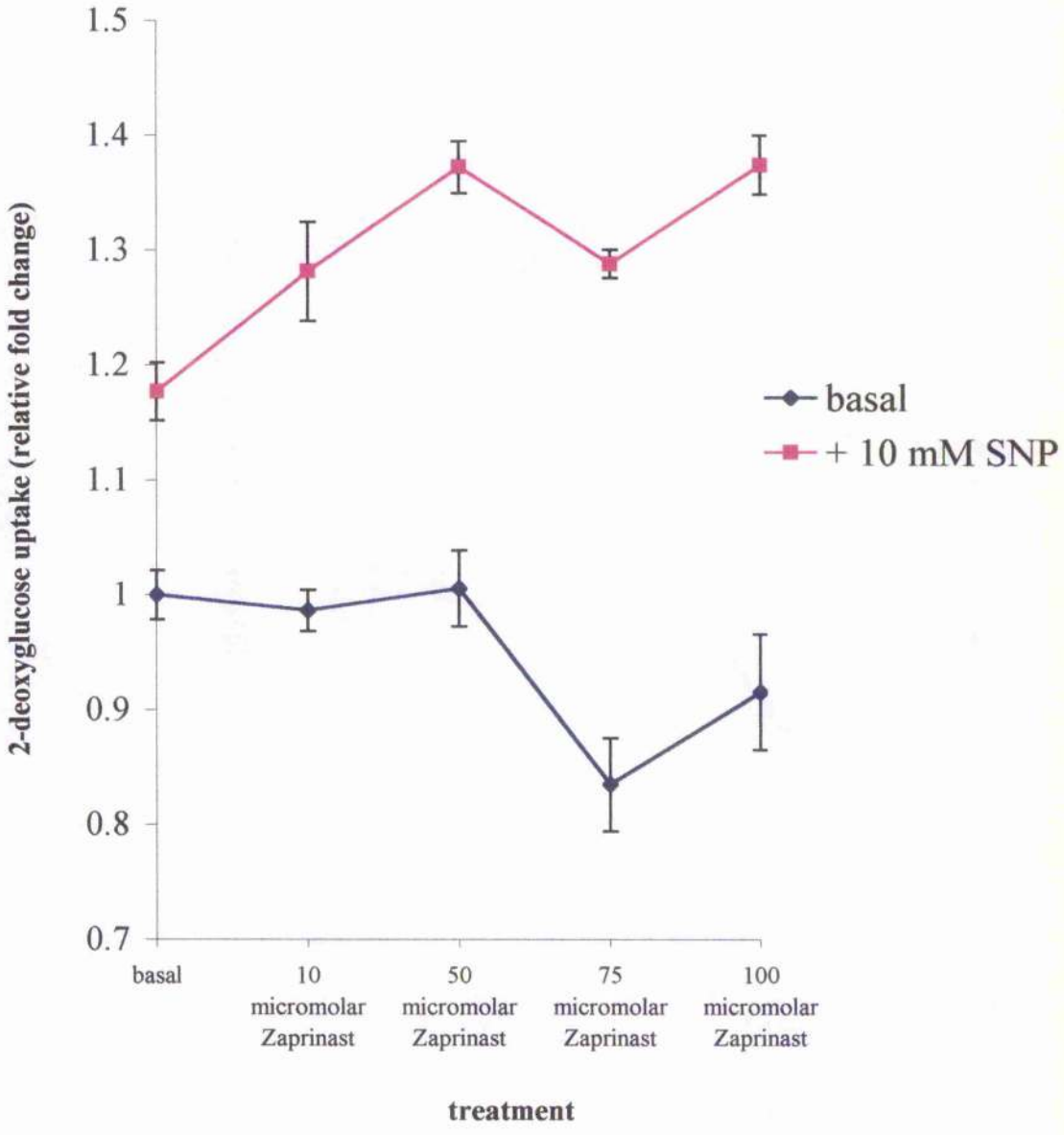

Figure 6.6.1 The PDE V inhibitor Zaprinast enhances SNP-stimulated 2-deoxyglucose uptake into L6 myotubes

Prior to the assay, cells were incubated in serum-free a-medium for 2 hours. Then cells were treated with 10 mM SNP +/- Zaprinast diluted in serum-free media for 90 miutes at 37°C and 5% CO_2. The 2-deoxyglucose transport assay was performed as described in materials and methods. The graph shown is representative of a number of experiments. Results are expressed as mean values +/- standard errors of the mean.

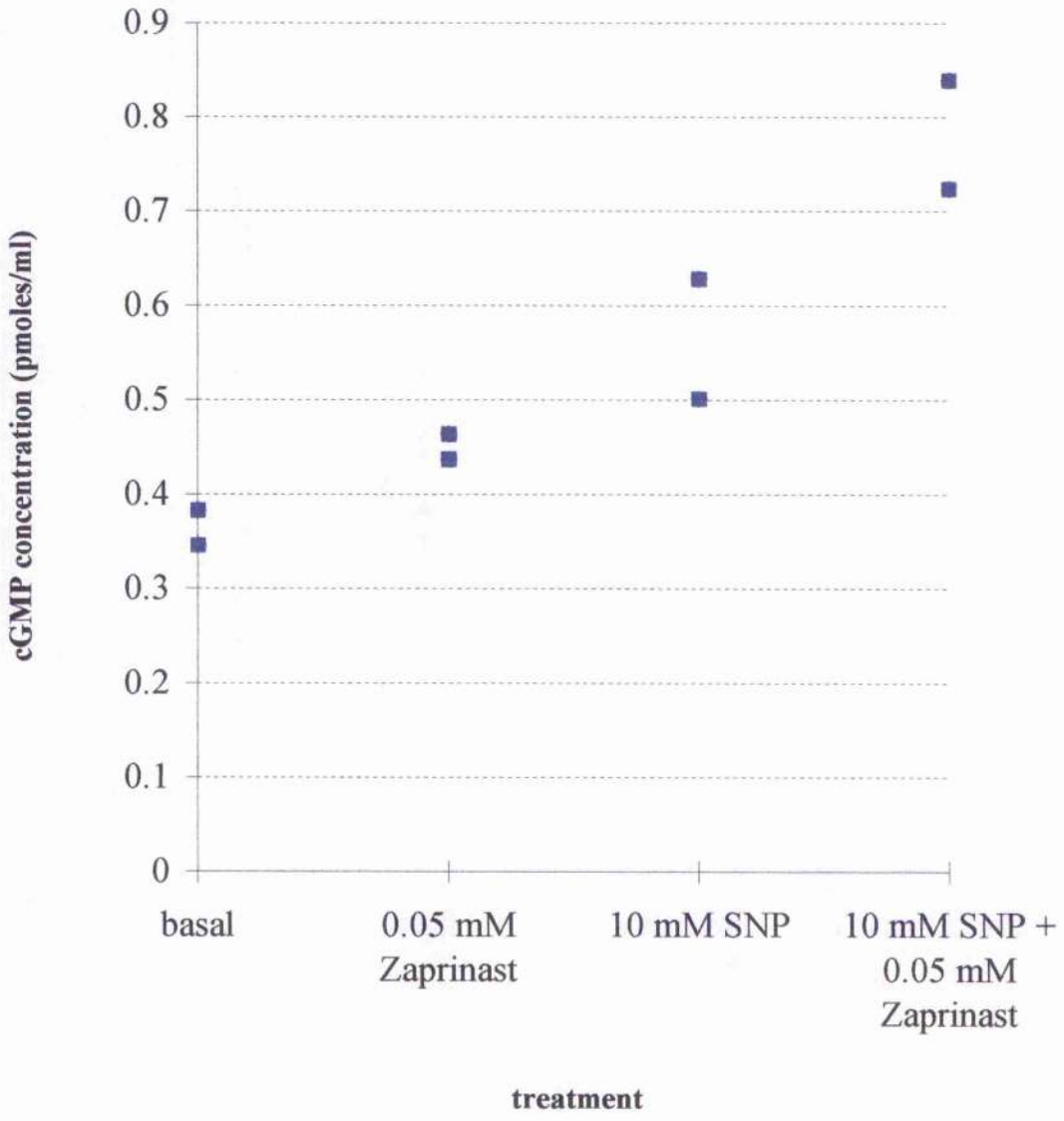

Figure 6.6.2 SNP and the PDE V inhibitor Zaprinast have an additive effect on cGMP concentration in L6 cells

Prior to assay cells were serum starved in a-medium for 2 hours. Next, cells were treated with SNPor Zaprinast or SNP + Zaprinas for 90 minutes diluted to the appropriate concentration in a-medium at 37°C and 5% CO_2. The cGMPassay was then carried out exactly as described in the materials and methods. Results are presented in duplicate and the graph shown is typical of a number of like experiments.

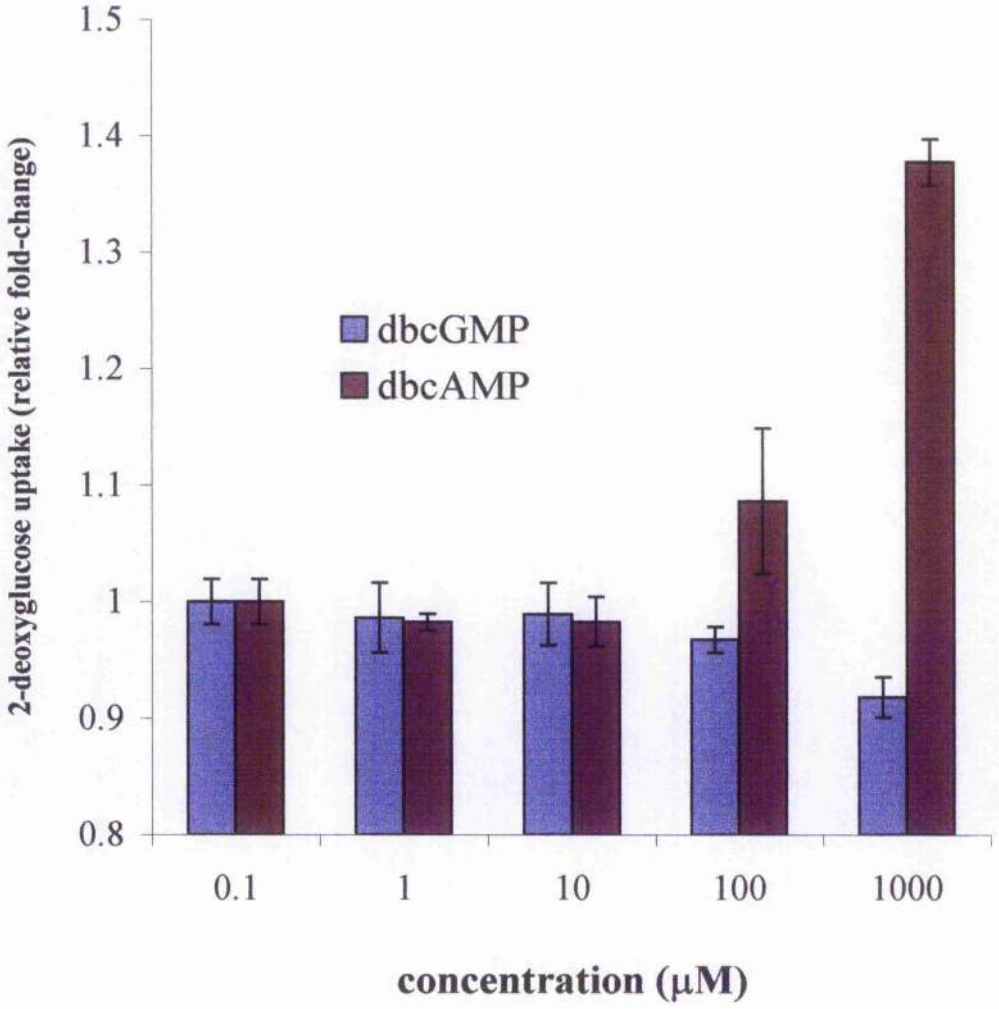

Figure 6.7.1 The cyclic nucleotide analogue dbcAMP but not dbcGMP increases 2-deoxyglucose uptake in L6 cells

Prior to the assay, cells were incubated in serum-free a-medium for 2 hours. Then cells were treated with cAMP or cGMP diluted in serum-free media for 90 miutes at 37°C and 5% CO_2. The 2-deoxyglucose transport assay was performed as described in materials and methods. The graph shown is representative of a number of experiments. Results are expressed as mean values +/- standard errors of the mean.

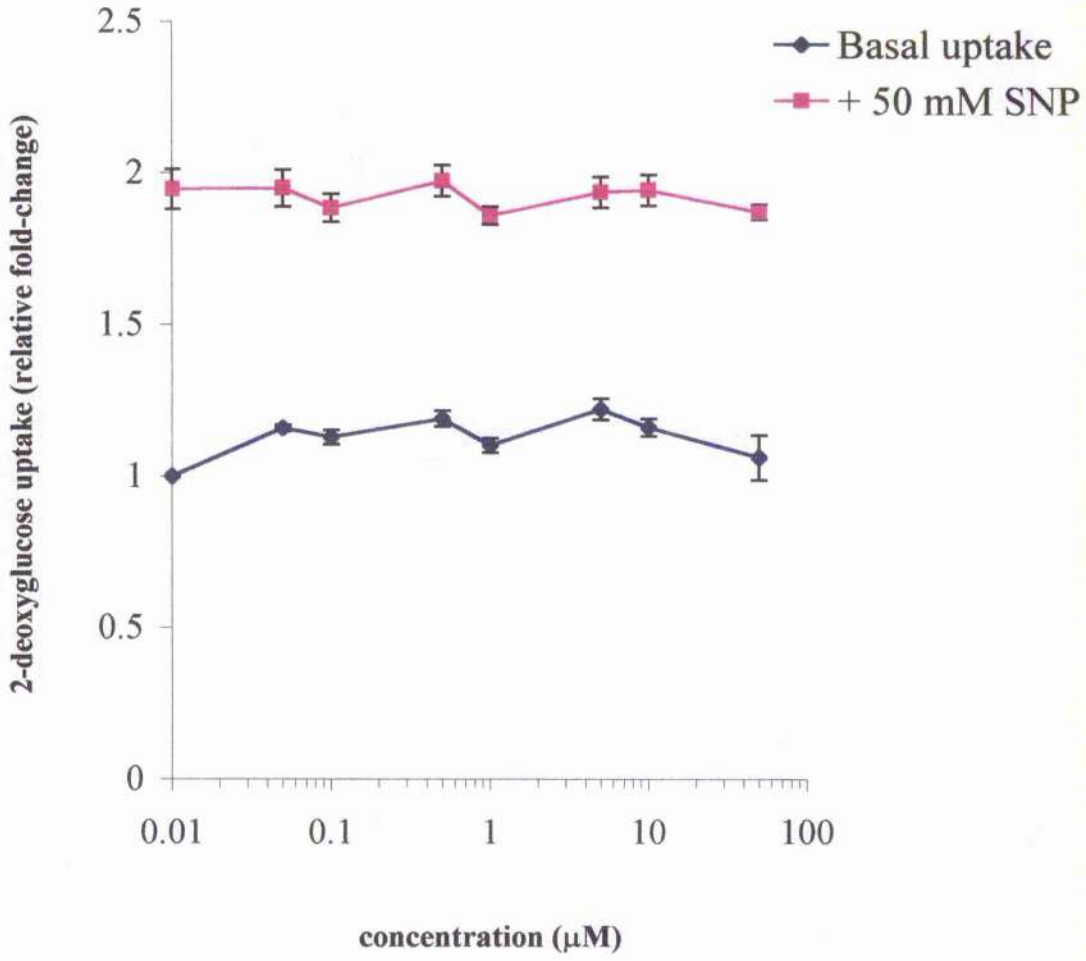

Figure 6.8.1 The PKG inhibitor Rp-8pCPT-cGMPs does not inhibit NO-stimulated 2-deoxyglucose uptake in L6 cells

2-deoxyglucose uptake in L6 myotubes in reponse to 50 mM SNP +/- the PKG inhibitor Rp-8pCPT-cGMPS. Prior to the assay, cells were incubated in serum-free a-medium for 2 hours. Then cells were treated with 10 mM SNP +/- Rp-8pCPT-cGMPS diluted in serum-free media for 90 miutes at 37°C and 5% CO_2. The 2-deoxyglucose transport assay was performed as described in materials and methods. The graph shown is representative of a number of experiments. Results are expressed as mean values +/- standard errors of the mean.

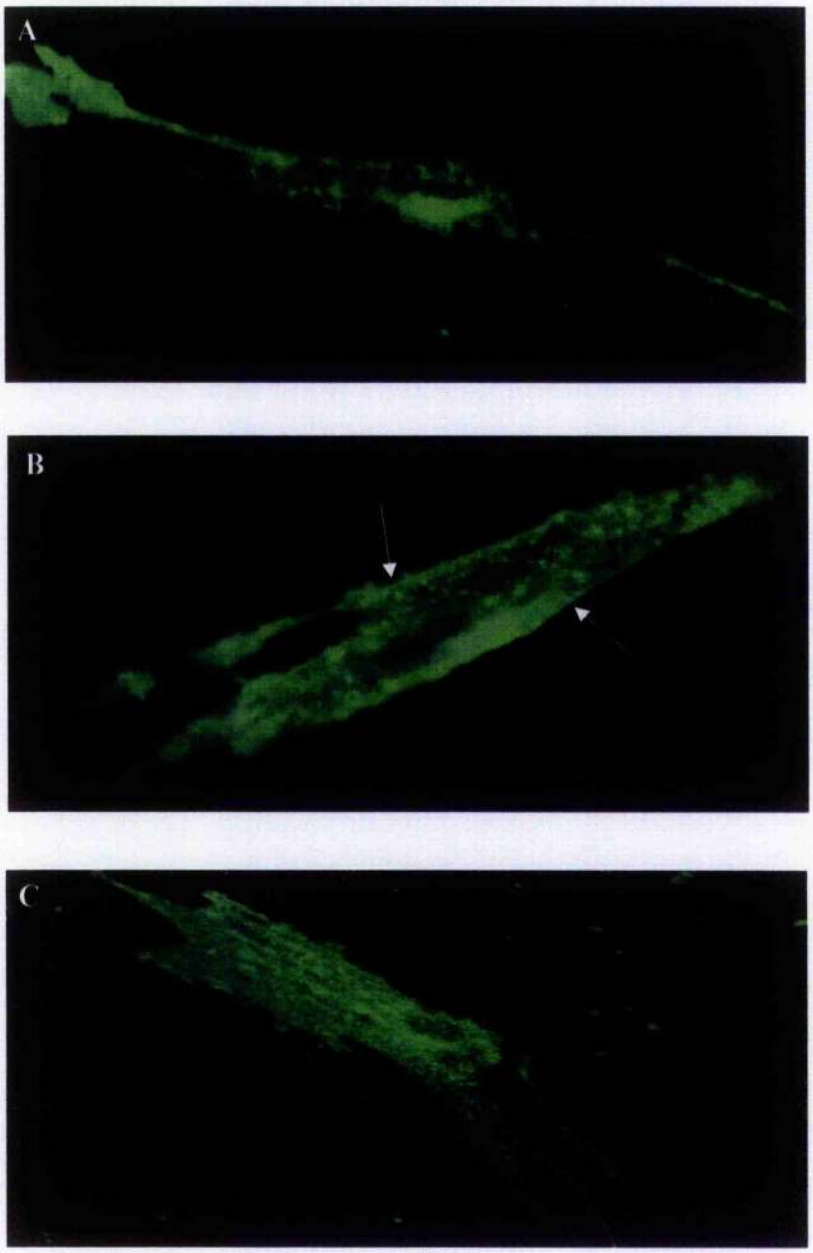

Figure 6.9.1 Insulin but not SNAP induces GFP-Glut4 translocation in L6 cells L6 cells were grown on collagen-coated coverslips and once fully differentiated injected with GFP-Glut4 cDNA as described in the materials and methods section of Chapter 3. The next day the injected cells were serum starved in DMEM for 2 hours and then treated with 1 μM insulin for 15 minutes (B), 100 μM SNAP for 90 minutes (C) or left untreated (A). The cells were then analysed by confocal microscopy, again as described in Chpater 3. Insulin was observed to cause an increase in GFP-Glut4 levels at the plasmsa membrane, see arrows.

6.4.0 Discussion

Previous work has shown that NO-donors can stimulate glucose transport in skeletal muscle tissue [72, 74]. In the present studies we show that NO-donors cause a similar increase in glucose transport in cultured L6 myotubes (figures 6.2.1, 6.2.2, 6.2.3) and that this increase is concomitant with a rise in cGMP levels within the cell (Fig 6.4.1).

We found no additive effect on glucose transport using NO-donors, either SNP or SNAP, in combination with maximal doses of insulin (figures 6.3.1, 6.3.2). Similarly, Balon *et al.* [264] showed that in rat skeletal muscle, when using a maximal stimulating concentration of insulin, SNP has no additional effect on the stimulation of 2-deoxyglucose transport. Although L6 cells in our hands yielded only small increase in glucose transport, about 30%, in response to maximal doses of insulin, these values are in line with those found by other groups using the same cell type [73, 270]. The lack of any additive effect upon glucose transport between NO-donors and maximal doses of insulin may suggest that the downstream signalling cascades triggered by each stimuli utilise the same pool of glucose transporters, at least in this cell system.

In agreement with the work of Balon *et al.* [264] in skeletal muscle tissue but in contrast with results obtained by Kapur *et al.* [265] in both skeletal muscle and L6 cells we found that NO-donors have no inhibitory effect on 2-deoxyglucose uptake in L6 cells. However, we found that the NO-donor GEA5024 used in some experiments by Kapur *et al.* was toxic to L6 cells at concentrations of 50-100 μM. Therefore, we suggest that the inhibitory effects of GEA5024 on insulin-stimulated glucose uptake are likely due to the toxic effects caused by this particular NO-donor.

We hypothesised that the messenger molecule cGMP affected the increase in glucose transport seen in response to NO-donors. Therefore, we investigated glucose transport rates and cGMP levels using inhibitors of soluble guanylate cyclase or cGMP-specific phosphodiesterases. ODQ is a potent and specific inhibitor of guanylate cyclase [273] and as such has been used in a number of studies to investigate the function of the cGMP pathway in NO signal transduction [274-276]. In Figures 6.5.1 and 6.5.2 we show that incubation of L6 cells with ODQ decreases cGMP levels within the cell and that this decrease in cGMP levels is reflected in a decreased rate of NO-stimulated 2-

deoxyglucose transport. This result suggests that guanylate cyclase is involved in mediating the effect of NO-donors on L6 cells.

Using RT-PCR we know that L6 myotubes express PDEV (results not shown). Zaprinast is a known inhibitor of cGMP-specific PDE's [70, 269]. Therefore we tested the ability of Zaprinast to elevate endogenous cGMP levels within L6 cells and to alter glucose transport. We show that incubation of L6 cells with 50 μM Zaprinast increases the cGMP content of L6 cells in both the basal and NO-stimulated states (figure 6.6.2). Furthermore, 50 μM Zaprinast caused a significant increase in NO-stimulated glucose transport (figure 6.6.1). This evidence gives further weight to the hypothesis that cGMP levels and rates of glucose transport are intimately linked in L6 cells and is in agreement with work published by Young *et al.* in rat skeletal muscle [74].

Although protein kinase G (PKG) mediates many of the downstream effects of cGMP in other cell types [268, 277], it is also known that skeletal muscle expresses little if any PKG [71]. That PKG is not the mediator of cGMP-induced increases in glucose uptake in L6 muscle cells is supported by the finding that the specific PKG inhibitor Rp-8-pCPT-cGMPS [278] has no effect on NO-stimulated glucose uptake (figure 6.8.1). The cGMP analogue dbcGMP is a known activator of PKG, whereas 8-bromo-cGMP and 8-pCPT-cGMP are more potent activators of the enzyme than the native nucleotide [279]. Nevertheless, neither dbcGMP (figure 6.7.1), 8-bromo-cGMP nor 8-pCPT-cGMP (data not shown) caused any increase in 2-deoxyglucose uptake in L6 cells. However, the cyclic AMP analogue dbcAMP consistently stimulated glucose uptake in L6 cells (figure 6.7.1).

This paradox between the apparent ability of endogenous cGMP and cAMP analogues, but not cGMP analogues, to cause an increase in glucose uptake may be explained in terms of the PDE's expressed in L6 cells. PDE3, often referred to as the cGMP-inhibited PDE, is expressed in a number of tissues [70]. Inhibition of PDE3, which results in increased cAMP and activation of cAMP-dependent protein kinase [70], may mediate some of the biological effects of endogenous cGMP. For example, in rat thymocytes NO-donors increased cAMP, and thereby cell proliferation, at least in part by increasing cGMP which inhibits PDE3 [280]. Furthermore, Marcoz *et al.* showed that 8-bromo-cGMP had only weak inhibitory effects on PDE3.

We tested the hypothesis that NO can increase Glut4 translocation by microinjecting L6 myotubes with GFP-Glut4 cDNA and then incubating the cells with

the NO donor SNAP. It is well established that insulin causes an increase in glucose transport in L6 cells from our own studies and the work of others [270, 271]. Research by Hajduch *et al.* suggests that this insulin-induced increase in glucose transport is at least partly mediated by Glut4 [271]. This finding is supported by our own experiments that show GFP-Glut4 translocation in L6 cells in response to insulin.

Exercise also induces Glut4 translocation in rat skeletal muscle [75, 262, 281]. In light of the proposed links between exercise, NO generation, and glucose uptake [72, 75, 264], we may also expect that like insulin, NO induces Glut4 translocation. However, figure 6.9.1 shows no evidence of GFP-Glut4 translocation in L6 cells in response to treatment with 100 μM SNAP, a concentration shown to increase glucose transport (figure 6.2.3). GFP-Glut4 translocation was also absent in cells treated with 200 μM SNAP (data not shown). The implication of this finding is that the increase in glucose transport in response to the NO donor SNAP is not mediated by Glut4 and instead may be attributable to translocation by Glut1 or Glut3, glucose transporters that are also expressed in L6 cells [271]. Induction of glucose transport and GFP-Glut4 translocation by insulin is rapid, around 15 minutes. However, appreciable increases in glucose transport by NO-donors in both skeletal muscle and L6 cells are much slower, usually 60 minutes or more [74, 264]. This difference in time course of action between insulin and NO may reflect the utilisation of different glucose transporters in response to these two stimuli. For example, while insulin-stimulated glucose uptake is mediated by Glut4, Glut1 or Glut3 may mediate NO stimulated glucose uptake. Alternatively, the increase in glucose transport seen in L6 cells in response to NO may not be due to Glut translocation, but instead reflects an increase in the intrinsic transporter activity of Gluts already present at the plasma membrane. Such an increase in the intrinsic catalytic activity Glut1 is proposed to mediate noradrenaline-induced glucose transport in brown adipocytes [82]. Regarding the results of Roberts *et al.*, we suggest that signalling events upstream of NO generation must contribute to nitric oxide dependent exercise stimulated glucose transport and Glut4 translocation in rat skeletal muscle, since in our hands, NO alone is not sufficient to stimulate GFP-Glut4 translocation in L6 cells.

This study clearly demonstrates that by manipulation of the NO-signalling pathway it is possible to enhance glucose uptake into muscle cells. Furthermore, we show that this increase in glucose transport is mediated by cGMP. The mechanism by which NO and cGMP induce an increase in glucose transport in L6 cells requires further

investigation. Nevertheless, we propose that components of the NO-signalling pathway in skeletal muscle present potential targets for therapeutic intervention in the treatment of diabetes. The precise mechanism by which cGMP mediates an increase in glucose transport remains an important challenge for future studies.

7.0.0 Conclusion

To date, the majority of research investigating Glut4 distribution and trafficking has used immunofluorescence or electron microscope-based techniques [96, 101, 193]. These strategies involve a fixation process prior to image analysis, and are therefore unsuitable methods for examining Glut4 trafficking in live cells in real time. To circumvent the shortcomings of conventional imaging methods we tagged Glut4 with GFP. The native fluorescence of Glut4-GFP allowed us to monitor Glut4-GFP trafficking in real time by confocal microscopy when expressed in a variety of cell types.

When expressed in 3T3-L1 fibroblasts we found that Glut4-GFP exhibited an intracellular distribution principally within a distinct perinuclear compartment and discrete punctate vesicles throughout the cytoplasm (figure 3.2.2). Glut4-GFP displayed a very similar distribution when expressed in 3T3-L1 adipocytes (figure 4.1) and L6 cells (figure 6.9.1), suggesting that the Glut4-GFP intracellular compartment is a feature of a variety of cell types [193]. In order to further characterise this compartment we compared the distribution of Glut4-GFP with established markers of the early endosomes (figures 3.3, 4.3) and late endosomes (lysotracker) (figure 4.3). We found that Glut4-GFP only partially overlaps with Texas Red Transferrin and displays very little colocalisation with Lysotracker in 3T3-L1 adipocytes, in good agreement with endosomal ablation studies [97, 98]. We also present evidence that the organisation of the Glut4-GFP-containing compartment is defined by elements of the cytoskeleton. Nocodazole, an inhibitor of microtubule formation, was found to disrupt the perinuclear distribution of Glut4-GFP when added to Glut4-GFP-expressing 3T3-L1 fibroblasts (figure 3.7) or adipocytes (figure 4.2)

Glut4 contains known targeting motifs with its N- and C-termini [198, 199, 231] that contribute to the intracellular localisation of Glut4. To further study these targeting motifs we made mutant Glut4-GFP constructs carrying a mutation in the N-terminus tyrosine motif (FAG) and double mutation in the C-terminus dileucine motif (LAG). In both 3T3-L1 fibroblasts and adipocytes, FAG-GFP accumulated at the plasma membrane and within an endosomal compartment as defined by TRT (figures 3.2.2, 4.4.1, 3.5A, 4.5A) LAG-GFP also accumulated at the plasma membrane when expressed at high levels (figures 3.2.2, 4.4.1). In addition, LAG-GFP accumulated within an enlarged perinuclear compartment, distinct from the TRT endosomal marker

(figures 3.5B,4.5B). Again these results are in good agreement with ablation analysis of FAG and LAG Glut4 mutants [219]. Together, these data suggest that the phenylalanine 5 residue is required for the efficient intracellular sequestration of Glut4 and targeting to a non-endosomal cellular compartment. Conversely, the Glut4 C-terminus dileucine motif may play a role in sorting Glut4 from a post-Golgi compartment into the recycling endosomes.

Multi-planar confocal analysis allows us to construct 3-dimensional representations of Glut4-GFP expressing cells in computer memory (see accompanying CD-ROM). Using this technique we examined the 3-D distribution of Glut4-GFP in a living adipocyte (z-section). These 3-D reconstructions give a more detailed picture of the Glut4-GFP containing compartments in relation to the other cellular compartments. In addition, we used time lapse confocal microscopy to investigate Glut4-GFP trafficking in basal 3T3-L1 fibroblasts and adipocytes (see accompanying CD-ROM). These time-lapse movies give us a new appreciation of the dynamics of Glut4-GFP movement in the context of the cell. Interactions between Glut4-GFP-containing vesicles, structural elements of the cell and other vesicles are clearly visible (movie).

From the outset we fully intended to make time-lapse movies of Glut4-GFP translocation in real time. However, we were unsuccessful in our attempts to induce Glut4-GFP translocation on the confocal microscope stage. This failure may be due to inappropriate buffer conditions or poor temperature management. Alternatively, elements within the translocation machinery may be sensitive to ultra-violet or laser light illumination, thus rendering Glut4-GFP translocation impossible. Nevertheless, Glut4-GFP expressed in 3T3-L1 adipocytes or L6 cells did translocate to the plasma membrane when placed in a CO_2 incubator following insulin addition to the media (figure 4.1). This suggests that Glut4-GFP is distributed to the correct insulin-sensitive compartment and is a functional protein in the context of translocation. Therefore, our inability to promote real time translocation of Glut4-GFP is more likely due to technical limitations within our system rather than the GFP tag disrupting the translocation machinery.

Although the exocytotic arm of Glut4-GFP translocation appears normal in our system, perhaps the most significant finding of this study is the observation that Glut4-GFP endocytosis following insulin stimulation is defective. Endogenous Glut4 is known to recycle in both the basal and insulin-stimulated states [26, 29, 86]. Glut4-GFP also appears to recycle normally in the basal state as evidenced by the basal time lapse

movies (CD-ROM) and Glut4-GFP accumulation at the plasma membrane when incubated in K^+ depleted media (figure 4.9) [132]. However, subsequent to insulin withdrawl, Glut4-GFP is not effectively endocytosed (figure 4.8), suggesting that the GFP tag may interfere with a unique rapid reinternalisation mechanism following insulin-induced Glut4 translocation. This hypothesis makes physiological sense since it would be undesirable to continue to have a large number of Glut4 glucose transporters at the plasma membrane in the absence of insulin, as such a situation would lead to hypoglycaemia.

We also briefly examined Glut4-GFP translocation in L6 cells in the context of nitric oxide (NO) signalling. Using inhibitors of the NO signalling pathway we established that the increase in glucose uptake seen in L6 muscle cells in response to NO-donors is likely mediated by gaunylyl cyclase and cGMP (figures 6.4.1, 6.5.1, 6.5.2). Although unable to identify the downstream target of cGMP in the NO signalling pathway, it is unlikely protein kinase G plays a role in NO-induced glucose uptake (figure 6.8.1). Although Glut4-GFP moved to the plasma membrane in L6 cells in response to insulin, we were unable to replicate Glut4-GFP translocation using a NO donor. This observation suggests that NO-induced glucose uptake is mediated by a glucose transporter isoform other than Glut4 in L6 cells. Whereas insulin-induced glucose uptake is rapid [151], reflecting Glut4 translocation, appreciable NO- donor-induced glucose uptake occurs more slowly (figure 6.2.1) [74, 264]. This further suggests that a glucose transporter other than Glut4 mediates NO donor-induced glucose transport in L6 cells.

Given more time we would address the question of the glucose transporter isoform that mediates NO-induced glucose uptake in L6 cells firstly by using a Glut1-GFP chimera. The downstream target of cGMP in the NO signalling pathway may be a phosphodiesterase. Therefore a more detailed analysis of the phosphodiesterase isoforms expressed in L6 cells is also desirable. NO-donors yield a pronounced increase in glucose uptake in muscle cells (figure 6.2.2) and tissue [74]. Therefore it is of some importance that the components of the NO-signalling pathway are resolved. This knowledge would enable the screening of small molecule inhibitors that could mimic the effects of NO donors on glucose uptake and would therefore hold potential as anti-diabetic agents.

Recent evidence suggests that ARF proteins play a crucial role in insulin-stimulated Glut4 translocation [56]. In Chapter 5 we describe the molecular biological steps

performed to create ARF5 and ARF6 XTPases. By mutating the ARF GTPase we hope to change the nucleotide specificity of ARF5 and ARF6 from GTP to XTP. Such a mutation would allow us to inhibit and then rescue ARF5 or ARF6 function by the addition of XTP to permeabilised cells, thus establishing the contribution of ARF5 and ARF6 to insulin stimulated Glut4 translocation. Now that the ARF5XTPase cDNA constructs is made, efforts are continuing within our laboratory to confirm its nucleotide-binding characteristics. Once the ARFXTPases are fully characterised their contribution to Glut4 trafficking will be analysed by establishing stable 3T3-L1 cell lines that overexpress ARFXTPase, or by ARFXTPase/Glut4-GFP cDNA coinjection into adipocytes, or by the addition of ARFXTPase protein directly to permeabilised cells.

In the final analysis, our inability to promote Glut4-GFP translocation in real time on the microscope stage was a disappointment. Furthermore, the labour intensive process of nuclear microinjection required to express the Glut4-GFP constructs in 3T3-L1 cells limited both the power of the system and our ability to perform a comprehensive biochemical analysis. Nevertheless, our studies with wild-type and mutant Glut4-GFP chimeras gave us a greater understanding of the intracellular Glut4 compartment in the basal state. The problems associated with the real time translocation of Glut4-GFP are most likely technical in nature. Perhaps a confocal microscope with more powerful optics, thus allowing us to decrease the intensity of the laser, would prove more amenable to the delicate translocation process. Even so, we have highlighted an inconsistency in Glut4-GFP trafficking as evidence for a novel Glut4 reinternalisation mechanism following insulin-induced translocation. Therefore a question remains over the continued use of Green Fluorescent Protein as an entirely valid method to study Glut4 trafficking.

8.0.0 References

1. Stryer, L., *Biochemistry.* W. H. Freeman and Company/ New York, 1988(3): p. 331-334.
2. Berne, R.M., and Levy, M. N., *Physiology.* Mosby-Year Book, Inc., 1993(3): p. 833-850.
3. Berne, R.M., and Levy, M. N., *Physiology.* Mosby-Year Book, Inc., 1993(3): p. 851-876.
4. Permutt, M.A., Chirgwin, J., Rotwein, P., and Giddings, S., *Insulin gene structure and function: a review of studies using recombinant DNA methodology.* Diabetes Care, 1984. **7**(4): p. 386-394.
5. Kahn, C.R., *Insulin action, diabetogenes, and the cause of type II diabetes.* Diabetes, 1994. **43**: p. 1066-1084.
6. James, D.E., and Piper, R., *Insulin resistance, diabetes and the insulin-regulated trafficking of GLUT4.* 1994.
7. Olefsky, J.M., *Insulin-stimulated glucose transport minireview series.* J. Biol. Chem., 1999. **274**(4): p. 1863.
8. Matchinsky, F.M., *Glucokinase as glucose sensor and metabolic signal generator in panreatic beta cells and hepatocytes.* Diabetes, 1990. **39**: p. 647.
9. Baldwin, S.A., Baldwin, J. A., and Lienhard, G. E., *Monosaccharide transporter of the human erythrocyte. Characterization of an improved preparation.* Biochemistry, 1982. **21**: p. 3836-3842.
10. Baldwin, S.A., Gorga, J. C. and Lienhard, G. E., *The monosaccharide transporter of the human erythrocyte. Transport activity upon reconstitution.* J. Biol. Chem., 1981. **256**: p. 3685-3689.
11. Lowe, A.G., and Walmsley, A. R., *The kinetics of glucose transport in human red blood cells.* Biochim, Biophys. Acta., 1986. **857**: p. 146-154.
12. Walmsley, A.R., *The dynamics of the glucose transporter.* Trends. Biochem. Sci., 1988. **13**: p. 226-231.
13. Davies, A., Meeram, K., Cairns, M. T., and Baldwin, S. A., *Peptide-specific antibodies as probes of the orientation of the glucose transporter in the human erythrocyte membrane.* J. Biol. Chem., 1987. **262**: p. 9347-9352.

14. Mueckler, M., Caruso, C., Baldwin, S. A., Panico, M., Blench, I., Morris, H. R., Allard, W. J., Lienhard, G. E., and Lodish, H. F., *Sequence and structure of a human glucose transporter.* Science, 1985. **229**: p. 941-945.
15. Birnbaum, M.J., Haspel, H. C., and Rosen, O. M., *Cloning and characterization of a cDNA encoding the rat brain glucose-transporter protein.* Proc. Natl. Acad. Sci. U.S.A., 1986. **83**: p. 5784-5788.
16. Thorens, B., Sarkhar, H. K., Kaback, H. R., and Lodish, H. F., *Cloning and functional expression in bacteria of a novel glucose transporter present in liver, intestine, kidney, and beta-pancreatic islet cells.* Cell, 1988. **55**: p. 281-290.
17. Gould, G.W., Thomas, H. M., Jess, T. J., and Bell, G. I., *Expression of human glucose transporters in Xenopus oocytes: kinetic characterization and substrate specificities of the erythrocyte, liver, and brain isoforms.* Biochemistry, 1991. **30**: p. 5139-5145.
18. Kayano, T., Kukumoto, H., Eddy, R. L., Fan, Y.-S., Byers, M. G., Shows, T. B., and Bell, G. I., *Evidence for a family of human glucose transporter-like proteins. Sequence and gene localization of a protein expressed in fetal skeletal muscle and other tissues.* J. Biol. Chem., 1988. **263**: p. 15245-15248.
19. Colville, C.A., Seatter, M. J., Jess, T. J., Gould, G. W., and Thomas, H. M., *kinetic analysis of the liver-type (GLUT2) and brain-type (GLUT3) glucose transporters in Xenopus oocytes: substrate specificities and effects of transport inhibitors.* Biochem. J., 1996. **290**: p. 701-706.
20. James, D.E., Strube, M. I., and Mueckler, M., *Molecular cloning and characterization of an insulin-regulatable glucose transporter.* Nature (London), 1989. **338**: p. 83-87.
21. Birnbaum, M.J., *Identification of a novel gene encoding an insulin-responsive glucose transporter protein.* Cell, 1989. **57**: p. 305-315.
22. Charron, M.J., Brosius, F. C., Alper, S. L., and Lodish, H. F., *A glucose transport protein expressed predominately in insulin-responsive tissues.* Proc. Natl. Acad. Sci. U.S.A., 1989. **86**: p. 2535-2539.
23. Kaestner, K.H., Christy, R. J., McLenithan, J. C., Briterman, L. T., Cornelius, P., Pekala, P. H., and Lane, M. D., *Sequence, tissue distribution, and differential expression of mRNA for a putative insulin-responsive glucose transporter in mouse 3T3-L1 adipocytes [published erratum appears in Proc Natl Acad Sci U S A 1989 Jul;86(13):4937].* Proc. Natl. Acad. Sci. U.S.A., 1989. **86**: p. 3150-3154.

24. Fukumoto, H., Kayano, T., Buse, J. B., Edwards, Y., Pilch, P. F., Bell, G. I., and Seino, S., *Cloning and characterization of the major insulin-responsive glucose transporter expressed in human skeletal muscle and other insulin- responsive tissues.* J. Biol. Chem., 1989. **264**: p. 7776-7779.

25. Waddell, I.D., Zomerschoe, A. G., Voice, M. W., and Burchell, A., *Cloning and expression of a hepatic microsomal glucose transport protein. Comparison with liver plasma-membrane glucose-transport protein 2.* Biochem. J., 1992. **286**: p. 173-177.

26. Holman, G.D., Kozka, I. J., Clark, A. E., Flower, A. F., Saltis, J., Habberfield, A. D., Simpson, I. A., and Cushman, S. W., *Cell surface labeling of glucose transporter isoform GLUT4 by bis- mannose photolabel. Correlation with stimulation of glucose transport in rat adipose cells by insulin and phorbol ester.* J. Biol. Chem., 1990. **265**: p. 18172-18179.

27. May, J.M., and Mikulecky, D. C., *The simple model of adipocyte hexose transport. Kinetic features, effect of insulin, and network thermodynamic computer simulations.* J. Biol. Chem., 1982. **257**: p. 11601-11608.

28. Holman, G.D., and Kasuga, M., *From receptor to transporter: insulin signalling to glucose transport.* Diabetologia, 1997. **40**(9): p. 991-1003.

29. Holman, G.D., Leggio, L. L., and Cushman, S. W., *Insulin-stimulated GLUT4 glucose transporter recycling. A problem in membrane protein subcellular trafficking through multiple pools.* J. Biol. Chem, 1994. **269**: p. 17516-17524.

30. Cushman, S.W., and Wardzala, L. J., *Potential mechanism of insulin action on glucose transport in the isolated rat adipose cell. Apparent translocation of intracellular transport systems to the plasma membrane.* J. Biol. Chem., 1980. **255**: p. 4758-4762.

31. Okada, T., Kawano, Y., Sakakibara, T., Kazeki, O., and Ui, M., *Essential role of phosphatidylinositol 3-kinase in insulin-induced glucose transport and antilipolysis in rat adipocytes. Studies with a selective inhibitor wortmannin.* J. Biol. Chem., 1994. **269**: p. 3568-3573.

32. Yang, J., Clark, A. E., Harrison, R., Kozka, I. J., and Holman, G. D., *Trafficking of glucose transporters in 3T3-L1 cells. Inhibition of trafficking by phenylarsine oxide implicates a slow dissociation of transporters from trafficking proteins.* Biochem. J., 1992. **281**: p. 809-817.

33. Gibbs, E.M., Lienhard, G. E., and Gould, G. W., *Insulin-induced translocation of glucose transporters to the plasma membrane precedes full stimulation of hexose transport.* Biochemistry, 1988. **27**: p. 6681-6685.

34. Hopfer, U., *Physiology of the gastrointestinal tract.* Raven Press, New York, 1987(2nd edn.): p. 1499-1526.

35. Burant, C.F., Takeda, J., Brot-Laroche, E., Bell, G. I., and Davidson, N. O., *Fructose transporter in human spermatozoa and small intestine is GLUT5.* J. Biol. Chem., 1992. **267**: p. 14523-14526.

36. Shepherd, P.R., Gibbs, E. M., Weslau, C., Gould, G. W., and Kahn, B. B., *Human small intestine facilitative fructose/glucose transporter (GLUT5) is also present in insulin-responsive tissues and brain. Investigation of biochemical characteristics and translocation.* Diabetes, 1992. **41**: p. 1360-1365.

37. Gould, G.W., and Holman, G. D., *The glucose transporter family: structure, function and tissue-specific expression.* Biochem. J., 1993. **295**: p. 329-341.

38. Cope, D.L., Holman, G. D., Baldwin, S. A., and Wolstenholme, A. J., *Domain assembly of the GLUT1 glucose transporter.* Biochem. J., 1994. **300**: p. 291-294.

39. Chin, J.J., Jung, E. K. Y., and Jung, C. Y., *Structural basis of human erythrocyte glucose transporter function in reconstituted vesicles.* J. Biol. Chem., 1986. **261**: p. 7101-7104.

40. Seatter, M.J., De La Rue, S. A., Porter, L. M., and Gould G. W., *QLS motif transmembrane helix VII of the glucose transporter family interacts with the C-1 position of D-Glucose and is involved in substrate selection at the exofacial binding site.* Biochemistry, 1998. **37**(5): p. 1322-1326.

41. Seatter, M.J., Kane, S., Porter, L. M., Arbuckle, M. I., Melvin, D. R., and Gould, G. W., *Structure-function studies of the brain-type glucose transporter GLUT3: alanine-scanning mutagenesis of putative transmembrane helix VIII and investigation of the role of proline residues in transport catalysis.* Biochemistry, 1997. **36**(21): p. 6401-6407.

42. Hashiramoto, M., Kadowaki, T., Clark, A. E., Muraoka, A., Momomura, K., Sakura, H., Tobe, K., Akamura, A., Yazaki, Y., Holman, G. D., and Kasuga, M., *Site-directed mutagenesis of GLUT1 in helix 7 residue 282 results in perturbation of exofacial ligand binding.* J. Biol. Chem., 1992. **267**: p. 17502-17507.

43. Holman, G.D., Rees, W. D., *Photolabelling of the hexose transporter at external and internal sites: fragmentation patterns and evidence for a conformational change.* Biochim. Biophys. Acta., 1987. **897**: p. 395-405.

44. Oka, Y., Asano, T., Shibasaki, Y., Lin, J-L., Tsukuda, K., Katagiri, H., Akanuma, Y., and Takaku, F., *C-terminal truncated glucose transporter is locked into an inward-facing form without transport activity.* Nature, 1990. **345**: p. 550-553.

45. Mori, H., Hashiramoto, M., Clark, A. E., Yang, J., Muraoka, A., Tamori, Y., Kasuga, M., and Holman, G. D., *Substitution of tyrosine 293 of GLUT1 locks the transporter into an outward facing conformation.* J. Biol. Chem., 1994. **269**(15): p. 11578-11583.

46. Massague, J., Pilch, P. F., Czech, M. P., *Electrophoretic resolution of three major insulin receptor structures with unique subunit stoichiometries.* Proc. Natl. Acad. Sci. U.S.A., 1981. **77**: p. 7137-7141.

47. Kasuga, M., Hedo, J. A., Yamada, K. M., and Kahn, C. R., *Structure of insulin receptor and its subunits.* J. Biol. Chem., 1982. **257**: p. 10392-10399.

48. Kasuga, M., Karlsson, F. A., and Kahn, C. R., *Insulin stimulates the phosphorylation of the 95,000-dalton subunit of its own receptor.* Science, 1982. **215**: p. 185-187.

49. Herrera, R., and Rosen, O. M., *Autophosphorylation of the insulin receptor in vitro: designation of phosphorylation sites and correlation with receptor kinase activation.* J. Biol. Chem., 1986. **261**: p. 11980-11985.

50. Rosen, O.M., *After insulin binds.* Science, 1987. **237**: p. 1452-1458.

51. White, M.F., *The IRS-signalling system: a network of docking proteins that mediate insulin action.* Mol. Cell. Biochem., 1998. **182**: p. 3-11.

52. Shepherd, P.R., Withers, D. J., and Siddle, K., *Phosphoinositide 3-kinase: the key switch mechanism in insulin signalling.* Biochem. J., 1998. **333**: p. 471-490.

53. Pawson, T., *Protein modules and signalling networks.* Nature, 1995. **373**: p. 573-580.

54. Medema, R.H., De Vries-Smits, A. M. M., van der Zon, G. C. M., Maassen, J. A., Bos, J. L., *Ras activation by insulin and epidermal growth factor through enhanced exchange of guanine nucleotides on p21ras.* Mol. Cell. Biol., 1993. **13**: p. 155-162.

55. Farah, S., Agazie, Y., Ohan, N., Ngsee, J. K., and Liu, X. J., *A Rho-associated protein kinase, ROKα, binds insulin receptor substrate-1 and modulates insuling signalling.* J. Biol. Chem., 1998. **273**(8): p. 4740-4746.

56. Millar, C.A., Powell, K. A., Hickson, G. R. X., Bader, M-F., and Gould. G., *Evidence for a role of ADP-ribosylation factor 6 in insulin-stimulated glucose transporter-4 (GLUT4) trafficking in 3T3-L1 adipocytes.* J. Biol. Chem., 1999. **274**(25): p. 17619-17625.

57. Simonsen, A., Lippe, R., Christoforidis, S., Gaullier, J-M., Brech, A., Callaghan, J., Toh, B-H., Murphy, C., Zerial, M., and Stenmark, H., *EEA1 links PI(3)K function to Rab5 regulation of endosome fusion.* Nature, 1998. **394**: p. 494-498.

58. Venkateswarlu, K., Oatey, P. B., Tavare, J. M., and Cullen, P. J., *Insulin-dependent translocation of ARNO to the plasma membrane of adipocytes requires phosphatidylinositol 3-kinase.* Curr. Biol., 1998. **8**: p. 463-466.

59. Fingar, D.C., and Birnbaum, M. J., *A role for Raf-1 in the divergent signalling pathways mediating insulin-stimulated glucose transport.* J. Biol. Chem., 1994. **269**(13): p. 10127-10132.

60. Haruta, T., Morris, A. J., Rose, D. W., Nelson, J. G., Mueckler, M., and Olefsky, J. M., *Insulin-stimulated GLUT4 translocation is mediated by a divergent intracellular signalling pathway.* J. Biol. Chem., 1995. **270**(47): p. 27991-27994.

61. Cheatham, B., Vlahos, C. J., Cheatham, L., Wang, L., Blenis, J., and Kahn, C. R., *Phosphatidylinositol 3-kinase activation is required for insulin stimulation of pp70 S6 kinase, DNA synthesis, and glucose transporter translocation.* Mol. Cell. Biol., 1994. **14**: p. 4902-4911.

62. Sharma, P.M., Egawa, K., Huang, Y., Martin, J. L., Huvar, I., Boss, G. R., and Olefsky, J. M., *Inhibition of phosphatidylinositol 3-kinase by adenovirus-mediated gene transfer and its effect on insulin action.* J. Biol. Chem., 1998. **273**(29): p. 18528-18537.

63. Martin, S.S., Haruta, T., Morris, A. J., Klippel, A., Williams, L. T., Olefsky, J. M., *Activated phoshpatidyl 3-kinase is sufficient to mediate actin rearrangement and GLUT4 translocation in 3T3-L1 adipocytes.* J. Biol. Chem., 1996. **271**(30): p. 17605-17608.

64. Jiang, T., Sweeney, G., Rudolf, M. T., Klip, A., Traynor-Kaplan, A., and Tsien, R. Y., *Membrane-permeant esters of phosphatidylinositol 3, 4, 5, -triphosphate.* J. Biol. Chem., 1998. **273**(18): p. 11017-11024.

65. Hayashi, T., Wojtaszewski, J. F., and Goodyear, L. J., *Exercise regulation of glucose transport in skeletal muscle.* Am. J. Physiol., 1997. **273**: p. E1039-E1051.

66. Cortright, R.N., and Dohm, G. L., *Mechanisms by which insulin and muscle contraction stimulate glucose transport.* Can. J. Appl. Physiol., 1997. **22**: p. 519-530.

67. Brozinick, J.T., and Birmbaum, M. J., *Insulin, but not contraction, activates Akt/PKB in isolated rat skeletal muscle.* J. Biol. Chem., 1998. **273**: p. 14679-14682.

68. Hayashi, T., Hirshman, M. F., Kurth, E. J., Winder, W. W., and Goodyear, L. J., *Evidence for 5'AMP-acivated protein kinase mediation of the effect of muscle contraction on glucose transport.* Diabetes, 1998. **47**: p. 1369-1373.

69. Bergeron, R., Russell III, R. R., Young, L. H., Ren, J-M., Marcucci, M., Lee, A., and Shulman, G. I., *Effect of AMPK activation on muscle glucose metabolism in concious rats.* Am. J. Physiol., 1999. **276**: p. E938-E944.

70. Beavo, J.A., *Cyclic nucleotide phosphodiesterases: functional implications of multiple isoforms.* Physiological Reviews, 1995. **75**(4): p. 725-748.

71. Lincoln, T.M.a.C., J. D., *Characterisation and biological role of the cGMP-dependent protein kinase.* Adv. Cyclic Nucleotide Res., 1983. **15**: p. 139-192.

72. Balon, T.W., and Nadler, J. L., *Nitric oxide is present from incubated skeletal muscle preparations.* J. Appl. Physiol., 1994. **77**: p. 2519-2521.

73. Lane, P., and Gross, S. S., *Cell signalling by nitric oxide.* Semin Nephrol, 1999. **19**(3): p. 215-229.

74. Young, M.E., Radda, G. K. and Leighton, B., *Nitric oxide stimulates glucose transport and metabolism in rat skeletal muscle in vitro.* Biochem J., 1997. **322**: p. 223-228.

75. Roberts, C.K., Barnard, R. J., Scheck, S. H., and Balon, T. W., *Exercise-stimulated glucose transport in skeletal muscle is nitric oxide dependent.* American Journal Physiology, 1997. **273**: p. E220-E225.

76. Chen, Z.-P., Mitchelhill, K. I., Michell, B. J., Stapleton, D., Rodriguez-Crespo, I., Witters, L. A., Power, D. A., Oritz de Montellano, P. R., and Kemp, B. E., *AMP-activated protein kinase phosphorylation of endothelial NO synthase.* FEBS Letters, 1999. **443**: p. 285-289.

77. Gether, U., and Kobilka, B. K., *G protein-coupled receptors.* J. Biol. Chem., 1998. **273**(29): p. 17979-17982.

78. Hurley, J.H., *Structure, mechanism, and regulation of mammalian adenyly cyclase.* J. Biol. Chem., 1999. **274**: p. 7599-7602.

79. Yan, X., Corbin, J. D., Francis, S. H., and Lawrence, D. S., *Precision targeting of protein kinases. An affinity label that inactivates the cGMP- but not the cAMP-dependent protein kinase.* J. Biol. Chem., 1996. **271**(4): p. 1845-1848.

80. Han, X.X., and Bonen, A., *Epinephrine translocates GLUT-4 but inhibits insulin-stimulated glucose transport in rat muscle.* Am. J. Physiol., 1998. **274**: p. E700-E704.

81. Kishi, K., Hayashi, H., Wang, L., Kamohara, S., Tamaoka, K., Shimizu, T., Ushikubi, F., Narumiya, S., and Ebina, Y., *Gq-coupled receptors transmit the signal for GLUT4 translocation via an insulin-independent pathway.* J. Biol. Chem., 1996. **271**(43): p. 26561-26568.

82. Shimizu, Y., Kielar, D., Minokoshi, Y., and Shimazu, T., *Noradrenaline increases glucose transport into brown adipocytes in culture by a mechanism different from that of insulin.* Biochem. J., 1996. **314**: p. 485-490.

83. Omatsu-Kambe, M., Zarnowski, M. J., and Cushman, S. W., *Glucose transport in rat brown adipose cells.* Biochem. J., 1996. **315**: p. 25-31.

84. Suzuki, K., and Kono, T., *Evidence that insulin causes translocation of glucose transport activity to the plasma membrane from an intracellular storage site.* Proc. Natl. Acad. Sci. U.S.A., 1980. **77**: p. 2542-2545.

85. Charron, M.J., Katz, E. B., and Olson, A. L., *GLUT4 gene regulation and manipulation.* J. Biol. Chem., 1999. **274**(6): p. 3523-3526.

86. Yang, J., and Holman, G. D., *Comparison of GLUT4 and GLUT1 subcellular trafficking in basal and insulin-stimulated 3T3-L1 cells.* J. Biol. Chem, 1993. **268**: p. 4600-4603.

87. Satoh, S., Nishimura, H., Clark, A. E., Kozka, I. J., Quon, M. J., Cushman, S. W., and Holman, G. D., *Use of bismannose photolabel to elucidate insulin-regulated GLUT4 subcellular trafficking kinetics in rat adipose cells. Evidence that exocytosis is a critical site of hormone action.* J. Biol. Chem., 1993. **268**: p. 17820-17829.

88. Kanai, F., Ito, K., Todaka, M., Hayashi, H., Kamohara, S., Ishii, K., Okada, T., Hazeki, O., Ui, M., and Ebina, Y., *Insulin-stimulated GLUT4 translocation is*

relevant to the phosphorylation of IRS-1 and the activity of PI3-kinase. Biochem. Biophys. Res. Commun., 1993. **195**: p. 762-768.

89. Clarke, J.F., Young, P. W., Yonezawa, K., Kasuga, M. and Holman, G. D., *Inhibition of the translocation of GLUT1 and GLUT4 in 3T3-L1 cells by the phosphatidylinositol 3-kinase inhibitor, wortmannin.* Biochem. J., 1994. **300**: p. 631-635.
90. Calera, M.R., Martinez, C., Liu, H., Jack, A. K. E., Birnbaum, M. J., and Pilch, P. F., *Insulin Increases the Association of Akt-2 with Glut4-containing Vesicles.* J. Biol. Chem., 1998. **273**: p. 7201-7204.
91. Kohn, A.D., Summers, S. A., Birnbaum, M. J., and Roth, R. A., *Expression of a constitutively active Akt Ser/Thr kinase in 3T3-L1 adipocytes stimulates glucose uptake and glucose transporter 4 translocation.* J. Biol. Chem., 1996. **271**: p. 31372-31378.
92. Bandyopadhyay, G., Standaert, M. L., Zhao, L., Yu, B., Avignon, A., Galloway, L., Karnam, P., Moscat, J., and Farese, R. V., *Activation of protein kinase C (α, β, and ζ) by insulin in 3T3/L1 cells.* J. Biol. Chem., 1997. **272**(4): p. 2551-2558.
93. Clague, M.J., *Molecular aspects of the endocytic pathway.* Biochem. J., 1998. **336**: p. 271-282.
94. Ploug, T., van Deurs, B., Ai, H., Cushman, S. W., and Ralston, E., *Analysis of GLUT4 distribution in whole skeletal muscle fibers: identification of distinct storage compartments that are recruited by insulin and muscle contractions.* J. Cell. Biol, 1998. **142**: p. 1429-1446.
95. Slot, J.W., Geuze, H. J., Gigengack, S., Lienhard, G. E., and James, D. E., *Immunolocalisation of the insulin regulatable glucose transporter in brown adipose tissue of the rat.* J. Cell. Biol, 1991. **113**: p. 123-135.
96. Rodnick, K.J., Slot. J. W., Studelska, D. R., Hanpeter, D. E., Robinson, L. J., Geuze, H. J., and James, D. E., *Immunocytochemical and biochemical studies of GLUT4 in rat skeletal muscle.* J. Biol. Chem, 1992(267): p. 6278-6285.
97. Martin, S., Tellam, J., Livingstone, C., Slot, J. W., Gould, G. W., and James, D. E., *The glucose transporter (GLUT-4) and vesicle-associated membrane protein-2 (VAMP-2) are segregated from recycling endosomes in insulin- sensitive cells.* J. Cell. Biol, 1996. **134**: p. 625-635.

98. Livingstone, C., James, D. E., Rice, J. E., Hanpeter, D., and Gould, G. W., *Compartment ablation analysis of the insulin-responsive glucose transporter GLUT4 in 3T3-L1 adipocytes.* Biochem. J., 1996. **315**: p. 487-495.

99. Ralston, E., and Ploug, T., *GLUT4 in cultured skeletal myotubes is segregated from the transferrin receptor and stored in vesicles associated with TGN.* J. Cell. Sci., 1996. **109**: p. 2967-2978.

100. Martin, S., Reaves, B., Banting, G., and Gould, G. W., *Analysis of the co-localization of the insulin-responsive glucose transporter (GLUT4) and the trans Golgi network marker TGN38 within 3T3-L1 adipocytes.* Biochem. J., 1994. **300**: p. 743-749.

101. Martin, S., Rice, J. E., Gould, J. W., Keller, S., Slot, J. W. and James, D. E., *The glucose transporter GLUT4 and the aminopeptidase vp165 colocalise in tubulo-vesicular elements in adipocytes and cardiomyocytes.* J. Cell. Sci., 1997. **110**: p. 2281-2291.

102. Waters, S.B., D'Auria, M., Martin, S. S., Nguyen, C., Kozma, L. M., and Luskey, K. L., *The amino terminus of insulin-responsive aminopeptidase causes Glut4 translocation in 3T3-L1 adipocytes.* J. Biol. Chem., 1997. **272**(37): p. 23323-23327.

103. Sollner, T., Whiteheart, S. W., Brunner, M., Erdjument-Bromage, H., Geromanos, S., Tempst, P., and Rothman, J. E., *SNAP receptors implicated in vesicle targeting and fusion.* Nature, 1993. **362**: p. 318-324.

104. Cain, C.C., Trimble, W. S., and Lienhard, G. E., *Members of the VAMP family of synaptic vesicle proteins are components of glucose transporter-containing vesicles from rat adipocytes.* J. Biol. Chem., 1992. **267**: p. 11681-11684.

105. Volchuk, A., Wang, Q., Ewart, S., Liu, Z., He, L., Bennet, M. K., and Klip, A., *Cellubrevin is a resident protein of insulin-sensitive GLUT4 glucose transporter vesicles in 3T3-L1 adipocytes.* J. Biol. Chem., 1995. **270**: p. 8233-8240.

106. Olson, A.L., Knight, J. B., and Pessin, J. E., *Syntaxin 4, VAMP2, and/or VAMP3/Cellubrevin are functional target membrane and vessicle SNAP receptors for insulin-stimulated GLUT4 translocation in adipocytes.* Mol. Cell. Biol., 1997. **17**(5): p. 2425-2435.

107. Martin, L., Shewan, A., Millar, C. A., Gould, G. W., and James, D. E., *Vesicle-associated Membrane Protein 2 plays a specific role in the insulin-dependent trafficking of the facilitative glucose transporter GLUT4 in 3T3-L1 adipovytes.* J Biol. Chem., 1998. **273**(3): p. 1444-1452.

108. Macaulay, S.L., Hewish, D. R., Gough, K. H., Stoichevska, V., Macpherson, S. F., Jagadish, M., and Ward, C. W., *Functional studies in 3T3-L1 cells support a role for SNARE proteins in insulin-stimulation of GLUT4 translocation.* Biochem. J., 1997. **324**: p. 217-224.

109. McMahon, H.T., Ushkaryov, Y. A., Edelman, L., Link, E., Binz, T., Niemann, H., Janh, R., and Sudof, T. C., *Cellubrevin is a ubiquitous tetanus-toxin substrate homologous to a putative synaptic vesicle fusion protein.* Nature, 1993. **364**: p. 346-349.

110. Millar, C.A., Shewan, A., Hickson, G. R. X., James, D. E., and Gould, G. W., *Differential regulation of secretory compartments containing the insulin-responsive glucose transporter 4 in 3T3-L1 adipocytes.* Mol. Biol. Cell, 1999. **10**: p. 3675-3688.

111. Rea, S., Martin, L. B., McIntosh, S., Macaulay, S. L., Ramsdale, T., Baldini, G., and James, D. E., *Syndet, an adipocytes target SNARE involved in the insulin-induced translocation of GLUT4 to the cell surface.* J. Biol. Cehm., 1998. **273**(30): p. 18784-18792.

112. Thurmond, D.C., Ceresa, B. P., Okada, S., Elmendorf, J. S., Coker, K., and Pessin, J. E., *Regulation of insulin-stimulated GLUT4 translocation by Munc18c in 3T3-L1 adipocytes.* J. Biol. Chem., 1998. **273**(50): p. 33876-33883.

113. Fujita, Y., Sasaki, T., Fukui, K,m Kotani, H., Kimura, T., Hata, Y., Sudhlof, T. C., Scheller, R. H., and Takai, Y., *Phosphorylation of Munc-18/n-Sec1/rbSec1 by Protein Kinase C.* J. Biol. Chem., 1996. **271**: p. 7265-7268.

114. Tellam, J.T., McIntosh, S., and James, D. E., *Molecular Identification of Two Novel Munc-18 Isoforms Expressed in Non-neuronal Tissues.* J. Biol. Chem., 1995. **270**: p. 5857-5863.

115. Colombo, M.L., Gelberman, S. C., Whiteheart, S. W., and Stahl, P. D., *N-Ethylmaleimide-sensitive factor-dependent α-SNAP release, an early event in the docking/fusion process, is not regulated by Rab GTPases.* J. Biol. Chem., 1998. **273**(3): p. 1334-1338.

116. Mayer, A., Wickner, W., and Haas, A., *Sec18p (NSF)-driven release of Sec17p (alpha-SNAP) can preced docking and fusion of yeast vacuoles.* Cell, 1996. **85**: p. 83-94.

117. Mayer, A., and Wickner, W., *Docking of yeast vacuoles is catalysed by the Ras-like GTPase Ypt7 after symmetric priming by Sec18 (NSF).* J. Cell. Biol., 1997. **136**: p. 307-317.

118. Pfeffer, S.R., *Rab GTPases; master regulators of membrane trafficking.* Current Opinion in Cell Biology, 1994. **6**: p. 511-526.

119. Cormont, M., Tanti, J. F.,Zahraoui, A., Van Obberghen, E., Tavtian, A., and Le Marchand-Brustel, Y., *Insulin and okadaic acid induce Rab4 redistribution in adipocytes.* J. Biol. Chem., 1993. **268**: p. 19491-19497.

120. Shibata, H., Omata, W., Suzuki, Y., Tanaka, S., and Kojima, I., *A synthetic peptide corresponding to the Rab4 hypervariable carboxyl-terminal domain inhibits insulin action on glucose transport in Rat adipocytes.* J. Biol. Chem., 1996. **271**: p. 9704-9709.

121. Shibata, H., Omata, W., and Kojima, I., *Insulin stimulates guanine nucleotide exchange on Rab4 via a wortmannin-sensitive signalling pathway in rat adipocytes.* J. Biol. Chem., 1997. **272**(23): p. 14542-14546.

122. Stenmark, H., Vitale, G., Ullrich, O., and Zerial,M., *Rabaptin-5 is a direct effector of the small GTPase Rab5 in endocytic membrane fusion.* Cell, 1995. **83**: p. 423-432.

123. Horiuchi, H., Lippe, R., McBride, H. M., Rubino, M., Woodman, P., Stenmark, H., Rybin, V., Wilm, M., Ashman, K., Mann, M., and Zerial, M., *A novel Rab5 GDP/GTP exchange factor complexed to Rabaptin-5 links nucleotide exchange to effector recruitment and function.* Cell, 1997. **90**: p. 1149-1159.

124. Vitale, G., Rybin, V., Christofordis, S., Thornqvist, P., McCaffrey, M., Stenmark, H., and Zerial M., *Distinct Rab-binding domains mediate the interaction of Rabaptin-5 with GTP-bound Rab4 and Rab5.* EMBO Journal, 1998. **17**(7): p. 1941-1951.

125. Novick, P., and Zerial, M., *The diversity of Rab proteins in vesicle transport.* Current Opinion in Cell Biology, 1997. **9**: p. 496-504.

126. Klarlund, J.K., Rameh, L. E., Cantley, L. C., Buxton, J. M., Holik, J. J., Sakelis, C., Patki, V., Corvera, S., and Czech, M. P., *Regulation of GRP1-catalysed ADP ribosylation factor guanine nucleotide exchange by phosphatidylinositol 3,4,5-triphosphate.* J. Biol. Chem., 1998. **273**(4): p. 1859-1862.

127. Frank, S., Upender, S., Hansen, S. H., and Cassanova, J. E., *ARNO is a guanine nucleotide exchange factor for ADP-ribosylation factor 6.* J. Biol. Chem., 1998. **273**(1): p. 23-27.

128. Liu, L., and Pohajdak, B., *Cloning and sequencing of a human cDNA from cytolytic NK/T cells with homology to yeast SEC7.* Biochim. Biophys. Acta., 1992. **1132**: p. 75-78.

129. Clark, A.E., Holman, G. D., and Kozka, I. J., *Determination of the rates of appearance and loss of glucose transporters at the cell surface of rat adipose cells.* Biochem. J., 1991. **278**: p. 235-241.

130. Yang, J., Clarke, J. F., Ester, C., Young, P. W., Kasuga, M., and Holman, G. D., *Phosphatidylinositol 3-kinase acts at an intracellular membrane site to enhance GLUT4 exocytosis in 3T3-L1 cells.* Biochem. J., 1996. **313**: p. 125-131.

131. Robinson, L., J., Pang, S., Harris, D. S., Heuser, J., and James, D. E., *Translocation of the glucose transporter (GLUT4) to the cell surface in permeabilized 3T3-L1 adipocytes: effects of ATP insulin, and GTP gamma S and localization of GLUT4 to clathrin lattices.* J. Cell. Biol., 1992. **117**: p. 1181-1196.

132. Nishimura, H., Zarnnowski, M. J., and Simpson, I. A., *Glucose transporter recycling in rat adipose cells. Effects of potassium depletion.* J. Biol. Chem., 1993. **268**: p. 19246-19253.

133. Marks, M.S., Ohno, H., Kirchhausen, T., and Bonifacino, J. S., *Protein sorting by tyrosine-based signals: adapting to the Y's and wherefores.* Trends Cell Bio., 1997. **7**: p. 124-128.

134. Zhang, J.Z., Davletov, B. A., Sudhof, T. C., and Anderson, R. G. W., *Synaptotagmin I is a high affinity receptor for clathrin AP-2: implications for membrane recycling.* Cell, 1994. **78**: p. 739-750.

135. Al-Hasani, H., Hinck, C. S., and Cushman, S. W., *Endocytosis of the glucose transporter GLUT4 is mediated by the GTPase Dynamin.* J. Biol. Chem., 1998. **273**: p. 17504-17510.

136. Schmid, S.L., *Clathrin-coated vesicle formation and protein sorting: an integrated process.* Annu. Rev. Biochem., 1997. **66**: p. 511-548.

137. David, C., McPherson, P. S., Mundigl, O., and De Camilli, P., *A role of amphiphysin in synaptic vesicle endocytosis suggested by its binding to dynamin in nerve terminals.* Proc. Natl. Acad. Sci. USA., 1996. **93**: p. 331-335.

138. Baron, V., Alengrin, F., and Van Obberghen, E., *Dynamin associates with Src-Homology Collagen (Shc) and becomes tyrosine phosphorylated in response to insulin.* Endocrinology, 1998. **139**: p. 3034-3037.

139. Volchuk, A., Narine, S., Foster, L. J., Grabs, D., De Camilli, P, and Klip, A., *Perturbation of Dynamin II with an Amphiphysin SH3 Domain Increases GLUT4 Glucose Transporters at the Plasma Membrane in 3T3-L1 Adipocytes. DYNAMIN II PARTICIPATES IN GLUT4 ENDOCYTOSIS.* J. Biol. Chem, 1998. **273**: p. 8169-8176.

140. Wang, L.H., Sudhof, T. C., and Anderson, R. G. W., *The Appendage Domain of -Adaptin Is a High Affinity Binding Site for Dynamin.* J. Biol. Chem., 1995. **270**: p. 10079-10083.

141. Moller, D.E., *Transgenic approaches to the pathogenesis of NIDDM.* Diabetes, 1994. **43**: p. 1394-1401.

142. Duvillie, B., Cordonnier, N., Deltour, L., Dandoy-Dron, F., Itier, J. -M., Monthioux, E., Jami, J., Joshi, R. L. and Bucchini, D., *Phenotypic alterations in insulin-deficient mutant mice.* Proc. Natl. Acad. Sci. U.S.A., 1997. **94**: p. 5137-5140.

143. Joshi, R.L., Lamonthe, B., Cordonnier, N., Mesbah, K., Monthioux, E., Jami, J., and Bucchini, D., *Targeted disruption of the insulin receptor gene in the mouse results in neonatal lethality.* EMBO, 1996. **15**: p. 1542-1547.

144. Tamemoto, H., Kadowaki, T., Tobe, K., Yagi, T., Sakura, H., Hayakawa, T., Terauchi, Y., Ueki, K., Kaburagi, Y., Satoh, S., Sekihara, H., Yoshioka, S., Horikoshi, H., Furuta, Y., Ikawa, Y., Kasuga, M., Yazaki, Y., and Aizawa, S., *Insulin resistance and growth retardation in mice lacking insulin receptor substrate-1.* Nature, 1994. **372**: p. 182-190.

145. Withers, D.J., Gutierrez, J. S., Towery, H., Burks, D. J., Ren, J-M., Previs, S., Zhang, Y., Bernal, D., Pons, S., Shulman, G. I., Bonner-Weir, S., and White, M. F., *Disruption of IRS-2 causes type 2 diabetes in mice.* Nature, 1998. **391**: p. 900-904.

146. Katz, E.B., Stenbit, A. E., Hatton, K., DePinho, R., and Charron, M. J., *Cardiac and adipose tissue abnormalities but not diabetes in mice deficient in GLUT4.* Nature, 1995. **377**: p. 151-155.

147. Terauchi, Y., Tsuji, Y., Satoh, S., Minoura, H., Murakami, K.,Okuno, A., Inukai, K., Asano, T., Kaburagi, Y., Uek,i K., Nakajima, H., Hanafusa, T.,Matsuzawa, Y., Sekihara, H., Yin, Y., Barrett, J. C., Oda, H., Ishikawa, T., Akanuma, Y., Komuro,

I., Suzuki, M. , Yamamur, *Increased insulin sensitivity and hypoglycaemia in mice lacking the p85 alpha subunit of phosphoinositide 3-kinase.* Nat. Gen., 1999. **21**(2): p. 230-235.

148. Bruning, J.C., Michael, M. D., Winnay, J. N., Hayashi, T., Horsch, D., Accili, D., Goodyear, L. J., and Kahn, C. R., *A muscle-specific insulin receptor knockout exhibits features of the metabolic syndrome of NIDDM without altering glucose tolerance.* Mol. Cell, 1998. **2**(5): p. 559-569.

149. Araki, E., Lipes, M. A., Patti, M-E., Bruning, J. C., Haag III, B., Johnson, R. S., and Kahn, R., *Alternative pathway of insulin signalling in mice with targeted disruption or the IRS-1 gene.* Nature, 1994. **372**: p. 186-190.

150. DeFonzo, R.A., *Pathogenesis of type 2 (non-insulin dependent) diabetes mellitus: a balanced overview.* Diabetologia, 1992. **35**: p. 389-397.

151. Rea, S., and James, D. E., *Moving GLUT4: the biogenesis and trafficking of GLUT4 storage vesicles.* Diabetes, 1997. **46**: p. 1667-1677.

152. Zorzano, A., Munoz, P., Camps, M., Mora, C., Testar, X., and Palacin, M., *Insulin-induced redistribution of GLUT4 glucose carriers in the muscle fiber. In search of GLUT4 trafficking pathways.* Diabetes, 1996. **45**: p. S70-S81.

153. Liu, M.-L., Gibbs, E. M., McCoid, S. C., Milici, A. J., Stukenbrok, H. A., McPherson, R. K., Treadway, J. L., Pessin, J. E., *Transgenic mice expressing the human GLUT4/muscle-fat facilitative glucose transporter protein exhibit efficient glycemic control.* Proc. Natl. Acad. Sci. U.S.A., 1993. **90**: p. 11346-11350.

154. Guillam, M.T., Schaerer, E., Wu, J. Y., Birnbaum, M., Beerman, F., Schmidt, A., Deriaz, N. and Thorens, B., *Early diabetes and abnormal postnatal pancreatic islet development in mice lacking Glut-2.* Nat. Genet., 1997. **17**: p. 327-330.

155. Taylor, S.I., Cama, A., and Accili, D, et al., *Mutations in the insulin receptor gene.* Endocr. Rev., 1992. **13**: p. 566-595.

156. Steiner, D.F., Tager, H. S., and Chan, S. J., *Lessons learned from the molecular biology of insulin-gene mutations.* Diabetes Care, 1990. **13**: p. 600-609.

157. Bell, G.I., Froguel, P., and Hishi, S., *Mutations of the human glucokinase gene and diabetes mellitus.* Trends Endocrinol. Metab., 1993. **4**: p. 86-90.

158. Laakso, M., Malkki, M., and Kekalinen P., *Insulin receptor substrate-1 variants in non-insulin-dependent diabetes.* J. Clin. Invest., 1994. **94**: p. 1141-1146.

159. Hitman, G.A., Hawrami, K., McCarthy, M. I., *Insulin receptor substrate-1 gene mutations in NIDDM; implications for the study of polygenic disease.* Diabetologia, 1995. **38**: p. 481-486.

160. Imai, Y., Philippe, N., Sesti, G., Accili, D., and Taylor, S. I., *Expression of variant forms of insulin receptor substrate-1 identified in patients with noninsulin-dependent diabetes mellitus.* J. Clin. Endocrinal. Metab., 1997. **82**(12): p. 4201-4207.

161. Bektas, A., Warram, J. H., White, M. F., Krolewski, A. S., and Doria, A., *Exclusion of insulin receptor substrate 2 (IRS-2) as a major locus for early-onset autosomal dominant type 2 diabetes.* Diabetes, 1999. **48**(3): p. 640-642.

162. Hansen, T., Andersen, C. B., Echwald, S. M., Urhammer, S. A., Clausen, J. O., Vestergaard, H., Owens, D., Hansen, L., and Pedersen, O., *Identification of a common amino acid polymorphism in the p85alpha regulatory subunit of phosphatidylinositol 3-kinase: effects on glucose disappearance constant, glucose effectiveness, and the insulin sensitivity index.* Diabetes, 1997. **46**: p. 494-501.

163. Dib, K., Whitehead, J. P., Humphreys, P. J., Soos, M. A., Baynes, K. C., Kumar, S., Harvey, T., and O'Rahilly, S., *Impaired activation ofphosphoinositide 3-kinase by insulin in fibroblasts from patients with severe insulin resistance and pseudoacromegaly. A disorder characterized by selective postreceptor insulin resistance.* J. Clin. Invest., 1998. **105**(5): p. 1111-1120.

164. Choi, W.-H., O'Rahilly, S., and Buse, J. B., *Molecular scanning of the insulin responsive glucose transporter (GLUT4) in patients with non-insulin dependent diabetes mellitus.* Diabetes, 1991. **40**: p. 1712-1718.

165. Kusari, J., Varma, U. S., Buse, J. B., Henry, R. R., and Olefsky, J. M., *Analysis of the gene sequence of the insulin receptor and insulin-sensitive glucose transporter GLUT4 in patients with common type NIDDM.* J. Clin. Invest., 1991. **88**: p. 1323-1330.

166. Garvey, W.T., Maianu, L., Huecksteadt, T. P., Birnbaum, M. J., Molina, J. M., and Ciaraldi, T. P., *Pretranslational suppression of a glucose transporter protein causes insulin resistance in adipocytes from patients with NIDDM and obesity.* J. Clin. Invest., 1991. **87**: p. 1072-1081.

167. Ciaraldi, T.P., Molina, J. M., and Olefsky, J. M., *Insulin action kinetics in adipocytes from obese and non-insulin dependent diabetes mellitus subjects:*

identification of multiple cellular defects in glucose transport. J. Clin. Endocrinol. Metab., 1991. **72**: p. 876-882.

168. Marshall, B., A., Ren, J. M., Johnson, D. W., Gibbs, E. M., Lilliquist, J. S., Soeller, W. C., Holloszy, J. O., and Mueckler, M., *Germline manipulation of glucose homeostasis via alteration of glucose transporter levels in skeletal muscle.* J. Biol. Chem., 1993. **268**: p. 18442-18445.

169. Pedersen, O., Bak, J. F., Anderson, P. H., Lund, S., Moller, D. E., Flier, J. S., and Kahn, B. B., *Evidence against altered expression of GLUT1 or GLUT4 in skeletal muscle of patients with obesity or NIDDM.* Diabetes, 1990. **398**: p. 865-870.

170. Handberg, A., Vaag, A., Damsbo, P., Beck-Nielsen, H., and Vinten, J., *Expression of insulin-regulatable glucose transporters in skeletal muscle from type 2 (NIDDM) diabetic patients.* Diabetologia, 1990. **33**: p. 625-627.

171. Leturque, A., Loizeau, M., Vaulont, S., Salminen, M., and Girard, J., *Improvement of insulin action in diabetic transgenic mice selectively overexpressing GLUT4 in skeletal muscle.* Diabetes, 1996. **45**(1): p. 23-27.

172. Houmard, J.A., Egan, P. C., and Neuffer, P. D., *Elevated skeletal muscle glucose transporter levels in exercise-trained, middle aged men.* Am. J. Physiol., 1991. **261**: p. E437-443.

173. Dela, F., Ploug, T., and Handberg, A., *Physical training increases muscle GLUT4 protein and messenger RNA in patients with NIDDM.* Diabetes, 1994. **43**: p. 862-865.

174. Thai, M.V., Guruswamy, S., Cao, K. T., Pessin, J. E., and Olson, A. L., *Myocyte enhancer factor 2 (MEF2)-binding site is required for GLUT4 gene expression in transgenic mice.* J. Biol. Chem., 1998. **273**(23): p. 14285-14292.

175. Olson, A.L., and Pessin, J. E., *Transcriptional regulation of the human GLUT4 gene promoter in diabetic transgenic mice.* J. Biol. Chem., 1995. **270**(40): p. 23491-23495.

176. Shimomura, O., Johnson, F. H., and Saiga, Y, *Extraction, purification, and properties of Aequorin, a bioluminescent protein from the luminous hydromedusan, Aequorea.* J. Cell. Comp. Physiol., 1962. **59**: p. 223-239.

177. Johnson, F.H., Shimomura, O., Saiga, Y., Gershman, L. C., Reynolds, G. T., and Waters, J. R., *Quantum efficiency of Cypridinaluminescence, with a note on that of Aequorea.* J. Cell. Comp. Physiol., 1962. **60**: p. 85-103.

178. Shimomura, O., *Structure of the chromophore of Aequorea green fluorescent protein.* FEBS Lett., 1979. **104**: p. 220-222.

179. Prasher, D.C., Eckenrode, V. K., Ward, W. W., Prendergas, F. G., and Cormier, M. J., *Primary structure of the Aequorea victoria green-fluorescent protein.* Gene, 1992. **111**.

180. Chalfie, M., Tu, Y., Euskichen, G., Ward, W. W., and Prasher, D. C., *Green fluorescent protein as a marker for gene expression.* Science, 1994. **263**: p. 802-805.

181. Ormo, M., Cubitt, A. B., Kallio, K., Gross, L. A., Tsien, R. Y., and Remington, S. J., *Crystal structure of the Aequorea victoria green fluorescent protein.* Science, 1996. **273**: p. 1392-1395.

182. Tsien, R.Y., *The green fluorescent protein.* Annu. Rev. Biochem., 1998. **67**: p. 509-544.

183. Yokoe, H., and Meyer, T., *Spatial dynamics of GFP-tagged proteins investigated by local fluorescence enhancement.* Nat. Biotechnol., 1996. **14**: p. 1252-1256.

184. Heim, R., Cubitt, A. B., and Tsien R. Y., *Improved green fluorescence.* Nature, 1995(373): p. 663-664.

185. Girotti, M., and Banting, G., *Girotti M. Banting G. TGN38-green fluorescent protein hybrid proteins expressed in stably transfected eukaryotic cells provide a tool for the real-time, in vivo study of membrane traffic pathways and suggest a possible role for rat TGN38.* J. Cell. Science, 1996. **109**: p. 2915-2826.

186. Kaether, C., and Gerdes, H-H., *Visualization of protein transport along the secretory pathway using green fluorescent protein.* FEBS letts., 1995. **369**: p. 267-271.

187. Drmota, T., Gould, G. W., and Milligan, G., *Real time visualization of agonist-mediated redistribution and internalization of a green fluorescent protein-tagged form of the thyrotropin-releasing hormone receptor.* J. Biol. Chem., 1998. **273**: p. 24000-24008.

188. Sambrook, J., Fritsch, E.F. and Maniatis, T., *Molecular Cloning. A Laboratory Manual (2nd Ed.).* Cold Spring Harbor Laboratory Press, New York., 1989.

189. Klip, A., and Marette, A., *Acute and chronic signals controlling glucose transport in skeletal muscle.* J. Cell. Biochem., 1992. **48**: p. 51-60.

190. Wei, M.L., Bonzelius, F., Scully, R. M., Kelly, R. B., and Herman G. A., *GLUT4 and transferrin receptor are differentially sorted along the endocytic pathway in CHO cells.* The Journal of Cell Biology, 1998. **140**(3): p. 565-575.

191. Verhey, K.J., and Birnnbaum M. J., *A Leu-Leu sequence is essential for COOH-terminal targeting signal of GLUT4 glucose transporter in fibroblasts.* The J. Biol. Chem., 1994. **269**(4): p. 2353-2356.

192. Piper, R.C., Tai, C., Slot, J. W., Hahn, C. S., Rice, C. M., Huang, H., and James, D. E., *The efficient intracellular sequestration of the insulin-regulatable glucose transporter (GLUT-4) is conferred by the NH_2 terminus.* J. Cell Biol., 1992. **117**: p. 729-743.

193. Haney, P.M., Slot, J. W., Piper, R. C., James, D. E., and Mueckler, M., *Intracellular targeting of the insulin-regulatable glucose transporter (GLUT4) is isoform specific and independent of cell type.* J. Cell. Biol., 1991. **114**: p. 689-699.

194. Piper, R.C., Hess, L. J., and James, D. E., *Differential sorting of two glucose transporters expressed in insulin-sensitive cells.* A. J. Physiol, 1991. **260**: p. C570-C580.

195. Thorens, B., Cheng, Z. -Q., Brown, D., and Lodish, H. F., *Liver glucose transporter: a basolateral protein inn hepatocytes and intestine and kidney cells.* A. J. Physiol., 1990. **259**: p. C279-C285.

196. Harris, D.S., Slot, J. W., Geuze, H. J., and James, D. E., *Polarized distribution of glucose transporter isoforms in Caco-2 cells.* Proc. Natl. Acad. Sci. USA, 1992. **89**: p. 7556-7560.

197. Herman, G.A., Bonzelius, F., Cieutat, A., and Kelly, R. B., *Adistinct class of intracellular storage vesicles, identified by expression of the glucose transporter GLUT4.* Proc. Natl. Acad. Sci. USA, 1994. **91**: p. 12750-12754.

198. Piper, R.C., Tai, C., Kulesza, P., Pang, S., Warnock, D., Baenziger, J., Slot, J. W., Geuze, H. J., Puri, C., and James, D. E., *GLUT-4 NH_2 terminus contains a phenylalanine-based targeting motif that regulates intracellular sequestration.* The Journal of Cell Bilogy, 1993. **121**(6): p. 1221-1232.

199. Garippa, R.J., Johnson, A., Park, J., Petrush, R. L., and McGraw, T. E., *The carboxyl terminus of GLUT4 contains a serine-leucine-leucine sequence that functions as a potent internalization motif in chinese hamster ovary cells.* The J. Biol. Chem., 1996. **271**(34): p. 20660-20668.

200. Araki, S., Yang, J., Hashiramoto, M., Tamori, Y., Kasuga, M., and Holman, G. D., *Subcellular trafficking kinetics of GLUT4 mutated at the N- and C-termini.* Biochem. J., 1996. **315**: p. 153-159.

201. Shin, J., Dunbrack, R. J., Lee, S., and Strominger, J. L., *Phosphorylation-dependent down-modulation of CD4 requires a specific structure within the cytoplasmic domain of CD4.* J. Biol. Chem., 1991. **266**: p. 10658-10665.

202. Johnson, K.F., and Kornfield, S., *The cytoplasmic tail of the mannose 6-phosphate/insulin-like growth factor-II receptor has two signals for lysosomal enzyme sorting in the Golgi.* J. Cell. Biol., 1992. **119**: p. 249-257.

203. James, D.E., Hiken J., and Lawrence, J. C., *Isoproterenol stimulates phosphorylation of the insulin-regulatable glucose transporter in rat adipocytes.* Proc. Natl. Acad. Sci., 1989. **86**: p. 8368-8372.

204. De Duve, C.C., De Barsy, T., Poole, B., Trouet, A., Tulkens, P., and Van Hoof, F., *Commentary. Lysosomotropic agents.* Biochem. Pharmacol., 1974. **23**: p. 2495-2531.

205. Bevan, A.P., Krook, A., Tikerpae, K., Seabright, P. J., Siddle, K., and Smith, G. D., *Chloroquine extends the lifetime of the activated insulin receptor complex in endosomes.* J. Biol. Chem., 1997. **272**(43): p. 26833-26840.

206. Blazar, B.R., Whitlet, C. B., Kitabchi, A. E., Tsai, M. Y., Santiago, J., White, N., Stentz, F. B., and Brown, D. M., *In vivo chloroquine-induced inhibition of insulin degradation in a diabetic patient with severe insulin resistance.* Diabetes, 1984. **33**: p. 1133-1137.

207. Geiger, B., and Karsent, E., *Cytoskeleton.* Current Opinion in Cell Biology, 1997. **9**: p. 1-3.

208. Maples, C., Ruiz, W. G., and Apodaca, G., *Both microtubules and actin filaments are required for efficient postendocytotic traffic of the polymeric immunoglobulin receptor in polarised Madin-Darby Canine Kidney cells.* J. Biol. Chem, 1997. **272**(10): p. 6741-6751.

209. Jin, M.a.S., M. D., *Role of microtubules in transferrin receptor transport from the cell surface to endosomes and the Golgi complex.* J. Biol. Chem, 1993. **268**(24): p. 18390-18397.

210. Cooper, J.A., *Effects of cytochalasin and phalloidin on actin.* J. Cell. Biol, 1987. **105**: p. 1473-1478.

211. Tsakiridis, T., Vranic, M., and Klip, A., *Disassembly of the actin network inhibits insulin-dependent stimulation of glucose transport and prevents recruitment of glucose transporters to the plasma membrane.* J. Biol. Chem., 1994. **269**(47): p. 29934-29942.

212. Wang, Q., Bilan, P. J., Tsakiridis, T., Hinek, A., and Klip, A., *Actin filaments participate in the relocalisation of phosphotidylinsositol 3-kinase to glucose transporter-containing compartments and in the stimulation of glucose uptake in 3T3-L1 adipocytes.* Biochem. J., 1998. **331**: p. 918-928.

213. Jarett, L., and Smith, R., *Effect of cytochalasin B and D on groups of insulin receptors and on insulin action in rat adipocytes. Possible evidence for a structural relationship of the insulin receptor to the glucose transport system.* J. Clin. Invest., 1979. **63**: p. 571-579.

214. Reed, B.C., Kaufmann, J. C., Mackall, A. K., Student, A. K., and Lane, M. D., *Alterations in insulin binding accompanying differentiation of 3T3-L1 preadipocytes.* Proc. Natl. Acad. Sci. USA., 1976. **74**: p. 4876-4880.

215. El-Jack, A.K., Hamm, J. K., Pilch, P. F., and Farmer, S. R., *Reconstitution of insulin-sensitive glucose transport in fibroblasts requires expression of both PPARγ and C/EBPα.* J. Biol. Chem., 1999. **274**(12): p. 7946-7951.

216. Corvera, S., Chawla, A., Chakrabarti, R., Marguerite, Buxton, J., and Czech, M. P., *A double leucine within the GLUT4 glucose transporter COOH-terminal domain functions as an endocytosis signal.* J. Cell. Biol, 1994. **126**(4): p. 979-989.

217. Kornfeld, S., and Mellman, I., *The biogenesis of lysosomes.* Annu. Rev. Cell Biol., 1989. **7**: p. 124-128.

218. Mellman, I., *Endocytosis and molecular sorting.* Annu. Rev. Cell. Dev. Biol., 1996. **12**: p. 575-625.

219. Melvin, D.R., Marsh, B. J., Walmsley, A. R., James, D. E., and Gould, G. W., *Analysis of amino and carboxyl terminal GLUT-4 targeting motifs in 3T3-L1 adipocytes using an endosomal ablation technique.* Biochemistry, 1999. **38**(5): p. 1456-62.

220. Slot, J.W., Geuze, H. J., Gigengack, S., James, D. E., and Lienhard, G. E., *Translocation of the glucose transporter GLUT4 in cardiac myocytes of the rat.* Proc. Natl. Acad. Sci. USA, 1991. **88**: p. 7815-7819.

221. Slot, J.W., Garruti, G., Martins, S., Oorschot, V., Posthuma, G., Kraegen, E. W., Laybutt, R., Thibault, G., and James, D. E., *Glucose transporter (GLUT-4) is targeted to secretory granules in rat atrial cardiomyocytes.* J. Cell. Biol, 1997. **137**: p. 1243-1254.

222. Gerdes, H.-H., and Kaether, C., *Green fluorescent protein: applications in cell biology.* FEBS Lett, 1996. **389**: p. 44-47.

223. Tarasova, N., I., Stauber, R. H., Choi, J. K., Hudson, E. A., Czerwinski, G., Miller, J. L., Pavlakis, G. N., Michejda, C. J., and Wank, S. A., *Visualization of G Protein-coupled Receptor Trafficking with the Aid of the Green Fluorescent Protein. ENDOCYTOSIS AND RECYCLING OF CHOLECYSTOKININ RECEPTOR TYPE A.* J. Biol. Chem., 1997. **272**: p. 14817-14824.

224. Dobson, S., Livingstone, C., Gould, G. W., and Tavare, J. M., *Dynamics of insulin-stimulated translocation of GLUT4 in single living cells visualised using green fluorescent protein.* FEBS Lett., 1996. **393**: p. 179-184.

225. Holman, G.D., and Kasuga, M., *From receptor to transporter: insulin signalling to glucose transport.* Diabetelogia, 1997. **40**: p. 991-1003.

226. Calderhead, D.M., Kitagawa, K., Tanner, L. I., Holman, G. D., and Lienhard, G. E., *Insulin regulation of the two glucose transporters in 3T3-L1 adipocytes.* J. Biol. Chem., 1990. **265**: p. 13801-13808.

227. Saunders, C., and Limbird, L. E., *Disruption of microtubules reveals two independent apical targeting mechanisms for G-protein-coupled receptors in polarized renal epithelial cells.* J. Biol. Chem., 1997. **272**(30): p. 19035-19045.

228. Chakrabarti, R., Buxtin, J., Joly, M., and Corbera, S., *Insulin-sensitive association of GLUT-4 with endocytic clathrin-coated vesicles revealed with the use of brefeldin A.* J. Biol. Chem, 1994. **269**: p. 7926-7933.

229. Marsh, B.J., Alm, R. A., McIntosh, S. R. and James, D. E., *Molecular regulation of GLUT-4 targeting in 3T3-L1 adipocytes.* J. Cell. Biol, 1995. **130**: p. 1081-1091.

230. Marsh, B.J., Martin, S., Melvin, D., Martin, L. B., Alm, R. A., Gould, G. W., and James, D. E., *Mutational analysis of the carboxy-terminal phosphorylation site of GLUT-4 in 3T3-L1 adipocytes.* Am. J. Physiol., 1998. **275**: p. E418-E422.

231. Verhey, K.J., Yeh, J. I., and Birnbaum, M. J., *Distinct signals in the GLUT4 glucose transporter for internalization and for targeting to an insulin-responsive compartment.* J. Cell. Biol., 1995. **130**: p. 1071-1079.

232. Seaman, M.N.J., Sowerby, P. J., and Robinson, M. S., *Cytosolic and membrane-associated proteins invilved in the recruitment of Ap-1 adaptors onto the Trans-Golgi Network.* J. Biol. Chem., 1996. **271**(41): p. 25446-25451.

233. Kandror, K.V., Yu, L., and Pilch, P. F., *The major protein of GLUT4-containing vesicles, gp160, has aminopeptidase activity.* J. Biol. Chem., 1994. **269**: p. 30777-30780.

234. Jess, T.J., Belham, C. M., Thomson, F. J., Scott, P. H., Plevin, R. J., and Gould, G. W., *Phosphatidylinositol 3'-kinase, but not p70 ribosomal S6 kinase, is involved in membrane protein recycling: wortmannin inhibits glucose transport and downregulates cell-surface transferrin receptor numbers independently of any effect on fluid-phase endocytosis in fibroblasts.* Cell. Sig., 1996. **8**: p. 297-304.

235. Moss, J., and Vaughan, M., *Structure and function of ARF proteins: activators of cholera toxin and critical components of intracellular vesicular transport processes.* J. Biol. Chem., 1995. **270**(21): p. 12327-12330.

236. Kahn, R.A., and Gilman, A. G., *Purification of a protein cofactor required for ADP-ribosylation of the stimulatory regulatory component of adenylate cyclase by cholera toxin.* J. Biol. Chem., 1984. **259**: p. 6228-6234.

237. Hosaka, M., Toda, K., Takatsu, H., Torii, S., Murakami, K., and Nakayama, K., *Structure and intracellular localisation of mouse ADP-ribosylation factors type 1 to type 6 (ARF1-ARF6).* J. Biochem., 1996. **120**: p. 813-819.

238. Moss, J.a.V., M., *Molecules in the ARF orbit.* J. Biol. Chem., 1998. **273**(34): p. 21431-21434.

239. Ding, M., Vitale, N., Tsai, S-C, Adamik, R., Moss, J., and Vaughan, M., *Characterisation of a GTPase-activating protein that stimulates GTP hydrolysis by both ADP-ribosylation factor (ARF) and ARF-like proteins.* J. Biol. Chem., 1996. **271**(39): p. 24005-24009.

240. Stearns, T., Kahn, R. A., Botstein, D. and Hoyt, M. A., *ADP ribosylation factor is an essentila protein in Saccharomyces cerevisiae and is encoded by two genes.* Mol. Cell. Biol., 1990. **10**(12): p. 6690-6699.

241. Bednarek, S.Y., Ravazzola, M., Hosobuchi, M., Amherdt, M., Perrelet, A., Schekman, R., and Orci, L., *COPI- and COPII-coated vesicles bud directly from the endoplasmic reticulum in yeast.* Cell, 1995. **83**: p. 1183-1195.

242. D'Souza-Schorey, C., Donselaar, E., Hsu, V. W., Yang, C., Stahl, P., and Peters, P. J., *ARF6 targets recycling vesicles to the plasma membrane: insights from an ultrastructural investigation.* J. Cell. Biol., 1998. **140**(3): p. 603-616.

243. Galas, M.-C., Helms, J. B., Vitale, N., Thierse, D., Aunis, D., and Bader, M-F., *Regulated exocytosis in chromaffin cells.* J. Biol. Chem., 1997. **272**(5): p. 2788-2793.

244. Faundez, V., Horng, J-T., and Kelly, R. B., *ADP ribosylation factor 1 is required for synaptic vesicle budding in PC12 cells.* J. Cell. Biol., 1997. **138**(3): p. 505-515.

245. Ktistakis, N.T., Brown, H. A., Waters, M. G., Sternweis, P. C., and M. G. Roth, *Evidence that phospholipase D mediates ADP ribosylation factor-dependent formation of Golgi coated vesicles.* J. Cell. Biol., 1996. **1334**: p. 295-306.

246. Xu, H., and Shields, D., *Prohormone processing in the trans-Golgi network; endoproteolytic cleavage of prosomatostatin and formation of nascent secretory vesicles in permeabilised cells.* J. Cell. Biol., 1993. **122**: p. 1169-1184.

247. Chen, Y.-G.a.S., D., *ADP-ribosylation factor-1 stimulates formation of nascent secretory vesicles from the trans-Golgi network of endocrine cells.* J. Biol. Chem., 1996. **271**(10): p. 5297-5300.

248. Chen, Y.-G., Siddhanta, A., Austin, D. D., Hammond, S. M., Sung, T-C., Frohman, M. A., Morris, A. J., and Shields, D., *Phospholipase D stimulates release of nascent secretory vesicles from the trans-Golgi network.* J. Cell. Biol., 1997. **138**(3): p. 495-504.

249. Siddhanta, A., and Shields, D., *Secretory vesicle budding from the Trans-Golgi Network is mediated by phosphatidic acid levels.* J. Biol. Chem., 1998. **273**(29): p. 17995-17998.

250. Singer, W.D., Brown, H. A., and Sternweis, P. C., *Regulation of eukaryotic phosphatidylinositol specific phospholipase C and phospholipase D.* Annu. Rev. Biochem., 1997. **66**: p. 475-509.

251. Desnos, C., Clift-O'Grady, L., and Tooze, S. A., *Biogenesis of synaptic vesicles in vitro.* J. Cell. Biol., 1996. **130**: p. 1041-1049.

252. Galli, T., Chilcote, T., Mundgil, O., Binz, T., Nieman, H., and Camilli, P., *Tetanus-toxin-mediated cleavage of cellubrevin impairs exocytosis of transferrin receptor-containing vesicles in CHO cells.* J. Cell. Biol, 1994. **125**: p. 1015-1024.

253. D'Souza-Schorey, C., Li, G., Colombo, M. I., Stahl, P. D., *A regulatory role for ARF6 in receptor-mediated endocytosis.* Science, 1995. **267**: p. 1175-1178.

254. Chardin, P., Paris, S., Antonny, B., Robineau, S., Beraud-Dufour, S., Jackson, C., and Chabre, M., *A human exchange factor for ARF contains Sec7- and pleckstrin-homology domains.* Nature, 1996. **384**: p. 481-484.

255. Klarlund, J., Guilherme, A., Holik, J. J., Virbasius, J. V., Chawla, A., and Czech, P. M., *Signalling by phosphoinositide-3,4,5-trisphosphate through proteins containing pleckstrin and Sec7 homology domains.* Science, 1997. **275**: p. 1927-1930.

256. Der, C.J., Pan, B.-T., and Cooper, G. M., *rasH mutants deficient in GTP binding.* Mol. Cell. Biol., 1986. **6**: p. 3291-3294.

257. Kang, C., Sun, N., Honzatko, R. B., and Fromm, H. J., *Replacement of Asp^{333} with Asn by site-directed mutagenesis changes the substrate specificity of Escherichia coli adenylosuccinate synthetase from guanosine 5'-triphosphate to xanthosine 5'-triphosphate.* J. Biol. Chem., 1994. **269**(39): p. 24046-24049.

258. Rybin, V., Ullrich, O., Rubino, M., Alexandrov, K., Simon, I., Seabra, M. C., Goody, R., and Zerial, M., *GTPase activity of Rab5 acts as a timer for endocytic membrane fusion.* Nature, 1996. **383**: p. 266-269.

259. Yu, B., Slepak, V. Z., and Simon, M. I., *Characterisation of a Goα mutant that binds xanthine nucleotides.* J. Biol. Chem., 1997. **272**(29): p. 18015-18019.

260. Powers, T., and Wolter, P., *Reciprocal stimulation of GTP hydrolysis by two directly interacting GTPases.* Science, 1995. **269**: p. 1422-1424.

261. Zhong, J.-M., Chen-Hwang, M-C., and Hwang, Y-W., *Switching nucleotide specificity of Ha-Ras p21 by a single amino acid substitution at aspartate 119.* J. Biol. Chem., 1995. **270**(17): p. 10002-10007.

262. Douen, A.G., T. Ramlal, S. Rastogi, P. J. Bilan, G. D. Cartee, M. Vranic, Holloszy, J. O., and Klip, A., *Exercise induces recruitment of the "insulin-responsive glucose transporter". Evidence for distinct intracellular insulin- and exercise- recruitable transporter pools in skeletal muscle.* J. Bio. Chem., 1990. **265**(23): p. 13427-13430.

263. Lund, S., G. D. Holman, O. Schmitz, and Pedersen, O., *Contraction stimulates translocation of glucose transporter GLUT4 in skeletal muscle through a mechanism distinct from that of insulin.* Proc. Natl. Acad. Sci. USA, 1995. **92**: p. 5817-5821.

264. Balon, T.W., and Nadler, J. L., *Evidence that nitric oxide increases glucose transport in skeletal muscle.* J. Appl. Physiol., 1997. **82**: p. 359-363.

265. Kapur, S., Bedard, S., Marcotte, B., Cote, C .and Marette, A., *A novel role for nitric oxide as a modulator of insulin action.* Diabetes, 1997. **46**: p. 1691-1700.

266. Young, M.E., and Leighton, B., *Evidence for altered sensitivity of the nitric oxide/cGMP signalling cascade in insulin-resistant skeletal muscle.* Biochem. J., 1998. **329**: p. 73-79.

267. Reaven, G.M., *Role of insulin resistance in human disease.* Diabetes, 1988. **37**(12): p. 1595-1607.

268. Lincoln, T.M., and Cornwell, T., *Intracellular cyclic GMP receptor proteins.* FASEB J., 1993. 7: p. 328-338.

269. Gillespie, P.G., and Beavo, J. A., *Inhibition and stimulation of photoreceptor phosphodiesterases by dipyridamole and M&B 22,948.* Mol Pharm, 1989. **36**(5): p. 773-781.

270. Klip, A., Ramlal, T., Douen, A., Bilan, P., and Skoreck, K., *Inhibition by forskolin of insulin-stimulated glucose transport in L6 muscle cells.* Biochem. J., 1988. **255**: p. 1023-1029.

271. Hajduch, E., Rencurel, F., Balendran, A., Batty, I., Downess, P., and Hundal, H., *Serotonin (5-hydroxytryptamine), a novel regulator of glucose transport in rat skeletal muscle.* The J. Biol. Chem., 1999. **274**(19): p. 13563-13568.

272. Bedard, S., Marcotte, B. and Marette, A., *Cytokines modulate glucose transport in skeletal muscle by inducing the expression of inducible nitric oxide synthase.* Biochem. J., 1997. **325**: p. 487-493.

273. Garthwaite, J., Southam, E., Boulton, C. L., Nielsen, E. B., Schmidt, K., and Mayer, B., *Potent and selective inhibition of nitric oxide-sensitive guanylyl cyclase by 1H-[1,2,4]oxadiazolo[4,3-a]quinoxalin-1-one.* Mol Pharmacol, 1995. **48**: p. 184-188.

274. Kim, Y., Talanian, R., and Billiar, T., *Nitric Oxide inhibits apoptosis by preventing increases in caspase-3-like activity via two distinct mechanisms.* The J. Biol. Chem., 1997. **272**(49): p. 31138-31148.

275. Bouchie, L., Hansen, H., and Feener, E., *Natriuretic factors and nitric oxide suppress plasminogen activator inhibitor-1 expression in vascular smooth muscle cells.* Arterioscler. Thromb. Vasc. Biol., 1998. **18**: p. 1771-1779.

276. Guh, J.-H., Hwang, T.-L., Ko, F.-N., Chueh, S.-C., Lai, M.-K., and Teng, C.-M., *Antoproliferative effect in human prostatic smooth muscle cells by nitric oxide donor.* Mol. Pharmacol., 1997. **53**: p. 467-474.

277. Hood, J.a.G., H., *Protein Kinase G mediates vascular endothelial growth factor-induced Raf-1 activation and proliferation in human endothelial cells.* J. Biol. Chem., 1998. **273**(36): p. 23504-23508.

278. Amir, A., Willmott, J., Brickley, K., Dolphin, A. C., Galione, A., and Hunt, S. V., *AntiIg-induced calcium influx in rat B lymphocytes mediated by cGMP through a dihydropyridine-sensitive channel.* J. Biol. Chem., 1996. **271**(13): p. 7287-7300.

279. Wolfe, L., Corbin, J. D., and Francis, S. H., *Characterisation of a novel isoenzyme of cGMP-dependent protein kinase from bovine aorta.* J. Biol. Chem., 1989. **264**: p. 7734-7741.

280. Marcoz, P., Prigent, A. F., Lagarde, M. and Nemoz, G., *Modulaion of rat thymocyte proliferative response through the inhibition of different cyclic nucleotide phosphodiesterase isoforms by means of selective inhibitors and cGMP-elevating agents.* Mol. Pharmacol., 1993. **44**(5): p. 1027-1035.

281. Kandror, K.V., Coderre, L., Pushkin, A. V., and Pilch, P. F., *Comparison of glucose-transporter-containing vesicles from rat fat and muscle tissues: evidence for a unique endosomal compartment.* Biochem. J., 1995. **307**: p. 383-390.